IMPLEMENTATION OF A FLOOD MANAGEMENT SYSTEM FOR NICOSIA

A THESIS SUBMITTED TO
THE GRADUATE SCHOOL OF NATURAL AND APPLIED SCIENCES
OF
MIDDLE EAST TECHNICAL UNIVERSITY

BY

HASAN ZAİFOĞLU

IN PARTIAL FULFILLMENT OF THE REQUIREMENTS
FOR
THE DEGREE OF DOCTOR OF PHILOSOPHY
IN
CIVIL ENGINEERING

OCTOBER 2018

Approval of the thesis:

IMPLEMENTATION OF A FLOOD MANAGEMENT SYSTEM FOR NICOSIA

submitted by **HASAN ZAİFOĞLU** in partial fulfillment of the requirements for the degree of **Doctor of Philosophy in Civil Engineering Department, Middle East Technical University** by,

Prof. Dr. Halil Kalıpçılar
Dean, Graduate School of **Natural and Applied Sciences** _____

Prof. Dr. İ. Özgür Yaman
Head of Department, **Civil Engineering** _____

Prof. Dr. A. Melih Yanmaz
Supervisor, **Civil Engineering Dept., METU** _____

Assist. Prof. Dr. Bertuğ Akıntuğ
Co-Supervisor, **Civil Engineering Prog., METU NCC** _____

Examining Committee Members:

Assoc. Prof. Dr. Nuri Merzi
Civil Engineering Dept., METU _____

Prof. Dr. A. Melih Yanmaz
Civil Engineering Dept., METU _____

Prof. Dr. İsmail Yücel
Civil Engineering Dept., METU _____

Assist. Prof. Dr. Müsteyde Baduna Koçyiğit
Civil Engineering Dept., Gazi University _____

Assist. Prof. Dr. Aslı Numanoğlu Genç
Civil Engineering Dept., Atılım University _____

Date: 02.10.2018

I hereby declare that all information in this document has been obtained and presented in accordance with academic rules and ethical conduct. I also declare that, as required by these rules and conduct, I have fully cited and referenced all material and results that are not original to this work.

Name, Surname: Hasan Zaifoğlu

Signature:

ABSTRACT

IMPLEMENTATION OF A FLOOD MANAGEMENT SYSTEM FOR NICOSIA

Zaifoğlu, Hasan
Doctor of Philosophy, Civil Engineering
Supervisor: Prof. Dr. A. Melih Yanmaz
Co-Supervisor: Assist. Prof. Dr. Bertuğ Akıntuğ

October 2018, 222 pages

The implementation of effective flood management particularly in ungauged basins requires regional frequency analysis (RFA) to determine the occurrence probabilities of extreme precipitation events. In this context, the quality control and homogeneity analysis of daily precipitation series of 37 stations in Northern Cyprus are carried out and trend analyses are employed to assess the variability of extreme precipitation indices. The increasing trends especially in winter period are dominated the northern part of the island. Then, identification of homogeneous regions is performed by utilizing the time series clustering approaches as a new perspective in RFA and the quantile estimates for different return periods are obtained. The flood hydrographs generated from the SCS Unit Hydrograph approach are provided to the outlet of Kanlıköy and Gönyeli ponds which are the boundary conditions for the river model. Moreover, 1D model MIKE 11 for the Kanlıdere River's tributaries is developed to simulate the flow in main channel. Besides, the flow depths, velocities, and flood inundation extent on floodplain is detected by 2D MIKE 21 model. MIKE FLOOD coupling of MIKE 11 and MIKE 21 is used to simulate the flood event in 2010 and the flood inundation maps are generated based on the different scenarios. Flood mitigation alternatives, such as dredging and increasing crest elevations of dam and spillway for Gönyeli Pond, and implementation of a new upstream detention facility

for Kanlıköy Pond were proposed. The proposed structural measure shows that Nicosia can be protected from flooding up to approximately 500-year return period.

Keywords: Regional Frequency Analysis, Hydrological Modelling, Hydraulic Modelling, MIKE FLOOD, Flood Inundation Map

ÖZ

LEFKOŞA İÇİN BİR TAŞKIN YÖNETİM SİSTEMİ GELİŞTİRİLMESİ

Zaifoğlu, Hasan
Doktora, İnşaat Mühendisliği
Tez Danışmanı: Prof. Dr. A. Melih Yanmaz
Ortak Tez Danışmanı: Dr. Öğr. Üyesi Bertuğ Akıntuğ

Ekim 2018, 222 sayfa

Etkin bir taşkın yönetim uygulaması için ekstrem yağışların meydana gelme olasılıklarının belirlenmesi gerekir ve özellikle ölçüm yapılmamış havzalarda bölgesel frekans analizine (BFA) ihtiyaç duyulmaktadır. Bu bağlamda Kuzey Kıbrıs'ta yer alan 37 yağış istasyonunun günlük verilerine kalite kontrol ve homojenlik analizi uygulanmış ve trend analizi ile ekstrem yağış indislerinin değişkenliği değerlendirilmiştir. Özellikle kış mevsiminde artan trendlerin adanın kuzeyine hakim olduğu görülmüştür. Daha sonra, homojen bölgelerin belirlenmesinde yeni bir yaklaşım olarak zaman serilerinin kümeleme yöntemleri BFA içerisinde kullanılmıştır. Böylelikle çeşitli dönüş aralıklarına karşılık gelen günlük yağış tahminleri yapılmıştır. Kanlıköy ve Gönyeli göletlerinin çıkış noktalarında hesaplanan akış hidrografları SCS Birim Hidrograf yöntemi ile üretilmiş ve akarsu modelinde memba sınır koşulu olarak tanımlanmıştır. Buna ek olarak, Kanlı Dere için 1Boyutlu MIKE 11 modeli kullanılarak ana kanal içerisindeki akımın simülasyonu gerçekleştirilmiştir. Bunun yanında, taşkın yatağı üzerindeki akım derinliği, hızı ve taşkın yayılım alanı 2 Boyutlu olarak MIKE 21 ile saptanmıştır. MIKE FLOOD yazılımı ile MIKE 11 ve MIKE 21 birlikte çalıştırılarak 2010 yılında meydana gelen taşkın simüle edilmiş ve çeşitli senaryolar üzerinde çalışılarak su basma haritaları oluşturulmuştur. Gönyeli Göleti'nin kazılması ve baraj ve dolusavak kret kotlarının yükseltilmesi ve Kanlıköy Göleti memba kısmına yapılacak yeni bir sel kapanı tesisi

uygulaması gibi çeşitli önlemler geliştirilmiştir. Önerilen yapısal önlemle Lefkoşa'nın yaklaşık olarak 500 yıl dönüş aralığındaki yağışa kadar taşkından korunabileceği görülmüştür.

Anahtar Kelimeler: Bölgesel Frekans Analizi, Hidrolojik Modelleme, Hidrolik Modelleme, MIKE FLOOD, Su Basma Haritası

To My Family and My Lovely Wife Begüm

ACKNOWLEDGMENTS

Foremost, I would like to express my sincere thanks to my supervisor Prof. Dr. A. Melih Yanmaz for his continuous support, encouragement, enthusiasm, and motivation. His guidance and immense knowledge have helped me to widen my research and improve both my personal and professional skills. He has taught me various aspects of hydraulics and water resources engineering and the passion he has for his work deserves great respect. I could not have thought a better mentor for my doctoral thesis and planning of my career.

I would like to thank my co-supervisor Assist. Prof. Dr. Bertuğ Akıntuğ for his advices and huge help throughout my doctoral research. Particularly without his precious support it would not be possible to conduct this research. Also, his support was valuable to ease my pressure especially during my research and teaching assistantship duty and his mentorship and experience have contributed to improve my teaching skills as well as the quality of the study.

I gratefully acknowledge support from Middle East Technical University Northern Cyprus Campus Research Fund (BAP FEN-15-D-2) and Co-Supervisor Funding for supporting this project. Besides, I appreciate with gratitude the support of METU Northern Cyprus Campus Civil Engineering Program for 4-year teaching assistantship duty. It is always honor to be the member of such prestigious family of METU Northern Cyprus Campus.

For the measurements and the data support of this research, I would like to thank the Meteorological Office, Mapping Office, Land Registry Office of Northern Cyprus, Nicosia Turkish Municipality, Gönyeli Municipality, and Civil Defense of TRNC.

Finally, I have my special regards to my family: my mother Tuncel, my father Ekman, and my sibling Peyman for their unconditional and huge support during the thesis process. And most of all, a very special gratitude goes to my dearest wife Begüm for her endless love, encourage, understanding, and patience throughout my life. I consider myself the luckiest in the world to have such a lovely wife.

TABLE OF CONTENTS

LIST OF TABLES

TABLES

LIST OF FIGURES

FIGURES

LIST OF ABBREVIATIONS

ABBREVIATIONS	
1D	One dimensional
2D	Two dimensional
AB	Absolute bias
ADI	Alternating Direction Implicit
AR	Autoregressive
AR.MAH	Maharaj similarity measure
AR.PIC	Piccolo similarity measure
ARMA	Autoregressive moving average
CCl	Climatology of the World Meteorological Organization's World Climate Data and Monitoring Programme
CCW	Coefficient of correlation weighting
CLIVAR	Climate Variability and Predictability Programme of the World Climate Research Programme
COR	Correlation-based approach
DEM	Digital elevation model
DS	Double sweep
DTM	Digital terrain model
DTW	Dynamic time warping
DWT	Discrete wavelet transform
ECA&D	European Climate Assessment and Dataset
EFAS	European flood alert system
EM-DAT	International Disaster Database
EPA	The U. S. Environmental Protection Agency
ETCCDI	Expert Team on Climate Change Detection and Indices
EUCL	Euclidean distance
F	F-statistic
GEV	Generalized extreme value
GIS	Geographical information system
GLO	Generalized logistic

GNO	Generalized normal
GNSS	Global navigation satellite system
GPA	Generalized Pareto
HEC	Hydrologic Engineering Center
IDF	Intensity-duration-frequency
IDW	Inverse distance weighting
IOC	Intergovernmental Oceanographic Commission
JCOMM	Technical Commission on Oceanography and Marine Meteorology
LPC	Linear predictive coding
LPC.CEP	Cepstral-based distance
MAE	Mean absolute error
MAN	Manhattan distance
MAP	Mean annual precipitation
MAPE	Mean absolute percentage error
MNR-T	Modified normal ratio based on square root distance
MSE	Mean square error
NASH	Nash criterion
NN	Nearest neighbor
NN	Normal ratio method
PAA	Piecewise aggregate approximation
PE3	Pearson type III
PRCPTOT	Total precipitation in wet days
R20mm	Number of very heavy precipitation days
R95p	Total precipitation depth in very wet days
R95Ptot	Precipitation fraction due to very wet days
RB	Relative bias
RE	Relative error
RFA	Regional frequency analysis
RMSE	Root mean square error
RR1	Number of wet days in a year

RRMSE	Relative root mean square error
RTK	Real time kinematics
Rx1day	Annual maximum daily precipitation
SAX	Symbolic aggregate approximation
SCS	Soil conservation service
SDII	Simple daily intensity index
SNHT	Standard normal homogeneity test
SWMM	Storm water management model
TIN	Triangulated Irregular Network
TRNC	Turkish Republic of Northern Cyprus
UH	Unit hydrograph
WMO	World Meteorological Organization

LIST OF SYMBOLS

SYMBOLS

A	Water surface area
A_{CS}	Cross-sectional flow area
A_c	Catchment area
A_{cov}	Covariance matrix
A_{est}	Estimated flood inundation area of MIKE FLOOD
A_i	Area of subdivision i.
$\boldsymbol{A}_j^{(i)}$	Approximation coefficients of DWT
A_{obs}	Inundated area of observed flood extent map of 2010 event
$A_{overlap}$	Overlapping areas of observed and modelled flood extent maps
B	Break points in SAX
B_4	Bias of L-kurtosis of the regional weighted average
C	Chezy's resistance coefficient
CFL	Courant-Friedrichs-Lewy number
CN	Curve number
$CN_{composite}$	Composite curve number
C_α	Test statistic for significance assessment of Sen's slopes
D_{cr}	Critical value for discordancy measure
D_i	Discordancy measure for station i
$\boldsymbol{D}_j^{(i)}$	Detail coefficients of DWT
E	Total error sum of square
$E[X]$	Expected value of data
H	Heterogeneity measure
$\boldsymbol{H}_j$	Matrix including approximation and detail coefficients of DWT
$I(t)$	Inflow hydrograph
IQR	Interquartile range of data
I_a	Initial abstraction
J	Scale of time series

K_d	Crest elevation of embankment of pond
K_s	Crest elevation of spillway of pond
L	Length of main stream channel
L_{CV}	L-moment coefficient of variation
L_{CV}^{R}	Average regional coefficient of L-variation
$L_{kur}^{[m]}$	Regional average L-kurtosis for the m-th simulated region
L_{kur}	L-moment coefficient of kurtosis
L_{kur}^{DIST}	L-kurtosis of the candidate distribution
L_{kur}^{R}	L-kurtosis of the regional weighted average
L_{skew}	L-moment coefficient of skewness
M	Number of repetitions in Monte Carlo simulation
M_1	Lower boundary of confidence interval of Sen's slopes
M_2	Upper boundary of confidence interval of Sen's slopes
N	Number of observations
N_{VN}	Test statistic of the Von Neumann test
N_i	Normal annual precipitation values of neighboring stations
N_{sim}	Number of simulated regions
N_t	Normal annual precipitation values of target station
P	Accumulated rainfall depth at time t
P_e	Accumulated precipitation excess at time t
P_{est}	Estimated values in a certain period
P_i	Corresponding observed values of neighboring stations
P_{obs}	Observed values in a certain period
P_{out}	Threshold value using for substituting precipitation outliers
P_t	Estimated missing value at the target station t
$\boldsymbol{R}_{X_T}$	Sample covariance matrices of time series
$\boldsymbol{R}_{Y_T}$	Sample covariance matrices of time series
$Q(t)$	Outflow hydrograph
Q_i	Linear assumed slope in Sen's slope estimator
$Q_i(F)$	Quantile of non-exceedance probability F at station-i

$Q_i(t)$	Local (at-site) estimate
Q_{ij}	Observed data at station-i with sample size of nj
Q_{med}	Sen's slope
Q_p	Peak discharge
Qpeak	Peak discharge of the hydrograph
$\bar{Q}(t)$	Mean of local estimates of the N stations
$\hat{Q}_i(t)$	Regional estimate at the non-exceedance probability t for station-i
Q100	Hydrographs of events with 500-year return period
Q200	Hydrographs of events with 200-year return period
Q500	Hydrographs of events with 500-year return period
R	Rescaled adjusted range in the Buishand range test
R^2	Determination coefficient
R_h	Hydraulic radius
S	Potential maximum retention
S_0	Channel bed slope
S_h	Average catchment slope
S_{MK}	Test statistic of the Mann-Kendall
S_f	Friction slope
S_k^*	Test statistic of the Buishand range test for k year period
$T(k)$	Test statistic of standard normal homogeneity test for k year period
T_0	Test statistic of standard normal homogeneity test for a certain period
T_{xx}	Depth-averaged turbulent stress
T_{xy}	Depth-averaged turbulent stress
T_{yy}	Depth-averaged turbulent stress
U	Depth-averaged velocity components in the *x* direction
V	Wind velocity
$\boldsymbol{V}$	Matrix of variance and covariance of time series
$\widehat{\boldsymbol{V}}$	Estimator of *V* matrix

Var	Variance operator
V_x	Wind velocity in x-direction
V_y	Wind velocity in y-direction
X_{a_i}	i-th value of time series having observation period of *a*
X_E	Maximum of test statistics of the Pettitt test
X_T	Time series having observation period of *T*
X_k	Test statistic of the Pettitt test for k year period
X_t	t-th values of time series
$\overline{\boldsymbol{X}}_T$	Mean of time series having observation period of *T*
$\overline{\boldsymbol{X}}_{wi}$	Vector of average values of each segment in PAA
$\widehat{\boldsymbol{X}}_\alpha$	SAX representation of time series
Y	Depth-averaged velocity components in the *y* direction
Y_{b_i}	i-th value of time series having observation period of *b*
Y_T	Time series having observation period of *T*
Y_i	Annual series of homogeneity testing variables
Y_t	t-th values of time series
$\bar{Y}$	Mean of annual series of homogeneity testing variables
$\overline{\boldsymbol{Y}}_T$	Mean of time series having observation period of *T*
Z^{DIST}	Goodness-of-fit measure
Z_S	Standardized test statistic of the Mann-Kendall
Z_{data}	Actual surface elevations
Z_{est}	Estimated surface elevation
a_{k,j^*}	Elements of j^* scaled approximation coefficients of DWT
c	Celerity
d	Time varying depth
d_{L_q}	Minkowski distance
$d_{AR.MAH}$	Maharaj distance
$d_{AR.PIC}$	Piccolo distance
d_{COR}	Correlation-based distance
d_{DTW}	Dynamic time warping distance

d_{DWT}	Discrete wavelet transform distance
d_{it}	Weight factor implies the Euclidean distance between the *i*-th neighboring station and the target station
$d_{LPC.Cep}$	Ceptral-based distance
$d_{MINDIST.SAX}$	Distance between the series represented by symbols in SAX
dS/dt	Rate of storage change
$d_{\alpha}(l_i, l_j)$	Distance between two symbols in SAX
$f(V)$	Wind friction factor
g	Gravitational acceleration
h	Water depth measured from thalveg of reservoir bed
h_c	Number of coefficient in AR model
h_n	Known beginning water surface level
h_{n+1}	Water surface level at the following time level of $t_n + \Delta t$
l_i	Symbols of SAX
m	Manning's number correction factor for meandering channels
n	Manning's roughness coefficient
n_1	Manning's number modification factor for channel irregularity
n_2	Manning's number modification factor for channel variations
n_3	Manning's number modification factor for obstructions in cross-sections
n_4	Manning's number modification factor for vegetation type and density
n_b	Base value for material type or the grain size
p	Fluid pressure
p_a	Atmospheric pressure
q	Flux density
$q(F)$	Dimensionless regional quantile function
$q_{0.75}$	Third quartile of data
r	Superscript value to adjust the influence of the distances
r_1	Coefficient of lag-1 serial correlation
r_i	Ranks of the testing variables

r_{it}	Correlation coefficient
s	Standard deviation
t	Time
$t^{(i)}$	Coefficient of L-variation
t_i	Number of ties of extent i
t_l	Lag time
t_p	Time to peak
t_r	Duration of excess rainfall
${t_3}^{(i)}$	Coefficient of L-skewness
${t_4}^{(i)}$	Coefficient of L-kurtosis
u	Depth-averaged velocity components in x-direction
$\bar{u}$	Unweighted regional average of stations
u_i	Vector of L-moment ratios
v	Depth-averaged velocity components in y-direction
w	Depth-averaged velocity components in z-direction
x	Axis Cartesian coordinates
x_i	Sample data series
$\bar{x}_{m,k}$	Mean of the m-th cluster for the kth variable
$x_{ml,k}$	Score on the k-th variable for the l-th object in the m-th cluster
y	Axis Cartesian coordinates
z	Axis Cartesian coordinates
z	Water surface elevation
$\bar{z}_1$	Standardized test statistic of standard normal homogeneity test for k year period
$\bar{z}_2$	Standardized test statistic of standard normal homogeneity test for n-k year
Δt	Time interval
Δx	Grid space
$\widehat{\mathbf{\Pi}}'_{X_T}$	Estimated model parameter of fitted time series
$\widehat{\mathbf{\Pi}}'_{Y_T}$	Estimated model parameter of fitted time series period
$\widehat{\mathbf{\Pi}}_{X_T}$	Parameter of AR model

$\widehat{\mathbf{\Pi}}_{Y_T}$	Parameter of AR model
$\emptyset_r$	Autoregression coefficients
Ω	Coriolis parameter
α	Significance level
β_k	Probability weighted moments
ε_t	White noise
ζ	Surface elevation
λ_{r+1}	$(r+1)$th L-moment
μ	Dynamic viscosity
$\mu(X)$	Mean of data
μ_i	Index-flood
ρ	Density of fluid
σ	Normal stress
σ^2	Variance of data
$\sigma_{X_T}^2$	Variances of the white noise processes of time series
$\sigma_{Y_T}^2$	Variances of the white noise processes of time series
σ_4	Standard deviation of L_{kur}^R
τ	Shear stress
τ_{hx}	Bed shear stress
τ_{hy}	Bed shear stress
τ_3	L-moment coefficient of skewness
τ_4	L-moment coefficient of kurtosis
ψ	Cepstral coefficients
w	Segment of the piecewise aggregate approximation

CHAPTER 1

INTRODUCTION

This chapter points out the background of the study, statement of the problem, significance of the study, and scope and objective of the study.

1.1. Background of the Study

Flooding is one of the most common natural disasters in recent years due to several reasons, such as unplanned urbanization, improperly designed infrastructure, effects of climate change, etc. On the other hand, the water shortages and droughts are mainly tackled problems in arid and semi-arid regions predominated by the Mediterranean climate. However, in the capital city of Cyprus, Nicosia (Lefkoşa), the flooding of Kanlıdere (Pedieos) Creek is recursive event that has been happening since the 14th century (Charalambous et al., 2016). Particularly last one decade, drastically increased extreme precipitation events lead to cause flash floods across Northern Cyprus which resulted in adverse socio-economic impacts including loss of properties, psychosocial effects, economic damages, and loss of trust in the authorities.

The historical flood events have been of great importance to clarify the varying characteristics of local extreme precipitation events, record inundation extents, and understand the financial and environmental risk of flooding. In recent years, especially two floods stand out as the most dramatic events in Northern Nicosia. On February 26, 2010, a long-lasting heavy precipitation caused the Kanlıköy and Gönyeli ponds to nearly overtop and the evacuated water damaged the spillways. The Öksüzdere (Almyros) Creek at the downstream of the Gönyeli Pond overflowed and the main road from Nicosia to Kyrenia was closed off and some settlement areas of Gönyeli and the main hospital of the country (Burhan Nalbantoğlu Hospital) inundated. On

December 9, 2014, due to a short duration and high intensity precipitation, Çınarderesi (Jinar) Creek overflowed onto the main roads and some houses in the town of Gönyeli and Yenikent were affected adversely. Additionally, the great volume of water flooded the city of Nicosia, some parts of the main hospital, and caused the students and teachers trapped in a private high school.

Despite of the risk of flooding, many settlements are still located near to the frequently flooded rivers. Therefore, people should be adapted to live with rivers considering the guidelines and regulations of holistic flood risk management approaches (Fleming, 2002). Similarly, the Kanlıdere Creek which played crucial role in order to setting and growing of the city of Nicosia in the past (Leventis, 2005) assessed by the authority in Southern Cyprus and the flood hazard and risk maps were produced in compliance with the Flood Directive of the European Union. However, unfortunately, there is no any study related to flood management for Northern Cyprus.

1.2. Statement of the Problem

Natural disasters including floods, droughts, earthquakes, epidemics, storms, etc., are uncontrollable catastrophic events that cause physical damages to the environment and man-made structures, a number of deaths and injuries for people, economic damages, and movement of populations. According to the International Disaster Database (EM-DAT), the total number of reported natural disasters throughout the world have gradually increased since 1900s as shown in Figure 1.1.

Flooding events stand out as the most widespread natural disaster type across the globe with the highest number of occurrence. Particularly in the last four decades, the reported flooding events in EM-DAT have dramatically increased and reached the highest level in 2006 with 226 recorded events across the globe. In 2017, floods are still one of the most observed disasters in the world with 126 events. These events costed almost US$ 20.3 billion and affected 55.5 million people living in different parts of the world. Moreover, the number of people affected from the floods have indicated upward trend during the period 1978-2017 and in the last decade,

approximately 1.3 billion people have suffered from the negative impacts of overflowing of the vast volume of water (Table 1.1). Besides, economic damages from floods have drastically increased and almost US$ 362.9 billion losses in the period of 2008-2017 are calculated as a most recent and top record.

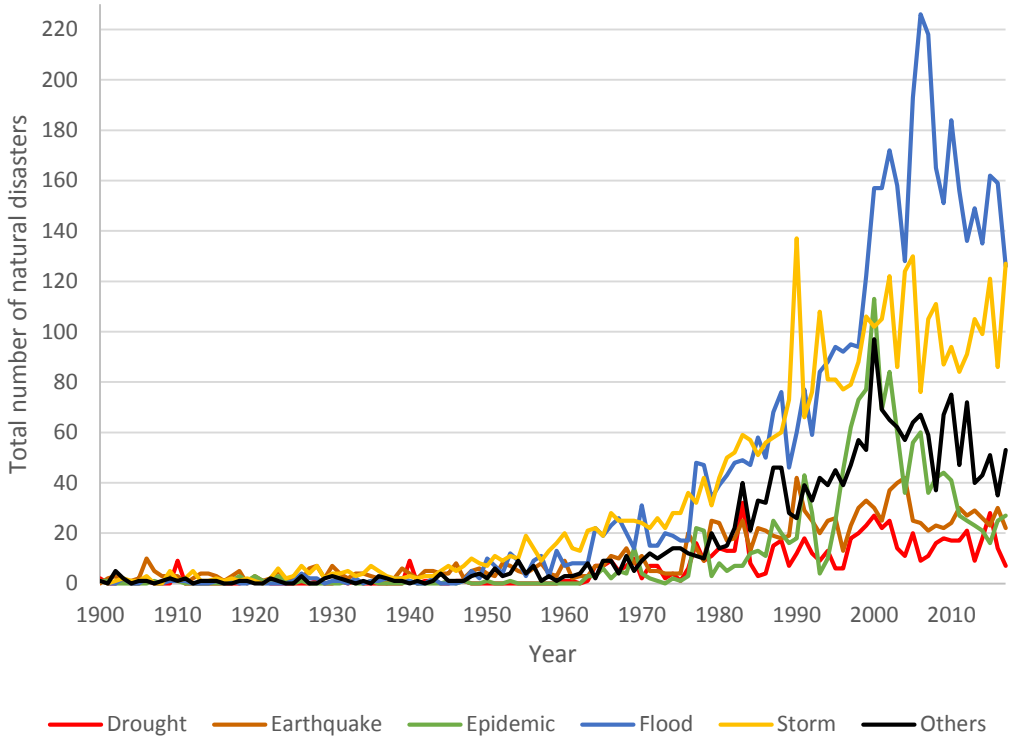

Figure 1.1. Total number of reported natural disasters between years 1900-2017 (EM-DAT, 2017)

Table 1.1. Total Number of Affected People and Economic Damage by the Floods in the World (EM-DAT, 2017)

Time Interval	Number of Occurence	Number of Affected People	Total Damage in US$ (Billion)
1978-1987	483	329209289	32.4
1988-1997	771	1206116728	163.8
1998-2007	1625	1289627394	198.5
2008-2017	1523	729800753	362.9

In Europe, the number of reported flood disasters by EM-DAT have indicated an increasing trend until the 1998-2007 period and then, a slight decrease is detected in the last decade as illustrated in Table 1.2. Additionally, the number of affected people and total damage costs of this type of disaster have the similar drop compared to the previous decade. Nevertheless, nearly 3.5 million people have faced the flood inundation problem and the estimated cost of 171 events is US$ 46.5 billion. In 2017, eight flood events affected 44877 people and caused US$ 134 million total damage.

Table 1.2. Total Number of Affected People and Economic Damage by the Floods in Europe (EM-DAT, 2017)

Time Interval	Number of Occurence	Number of Affected People	Total Damage in US$ (Billion)
1978-1987	53	875347	8.4
1988-1997	93	3898580	26.7
1998-2007	243	3723663	55.6
2008-2017	171	3531387	46.5

The floods in Northern Cyprus, which are observed more frequently since the last one decade, has mainly triggered by extreme precipitation events, land cover changes, and a lack of storm water storage facilities and drainage network. In 2010, a flash flood occurred at the town of Güzelyurt which is located at the west side of Northern Cyprus and about five million TL economic loss was detected by the district governorship including the repair and renewal costs for the houses, cars, work places, industrial places, animals, etc. (Şahin, 2012).

According to Savvidou et al. (2008), 43 floods were recorded in Cyprus during 1994-2006 and the majority of the events were observed in Nicosia district, generally in urbanized areas. Likewise, the overflowing of two branches of Kanlıdere Creek, Çınarderesi Creek starting from Kanlıköy Pond and flows through Yenikent and Nicosia and Öksüzdere Creek starting from Gönyeli Pond and passes through Gönyeli and joining to the main channel of Asidere Creek in Nicosia, caused flooding problems typically in metropolitan part of Nicosia. Moreover, according to the audit report of

Nicosia Turkish Municipality covering the period of 2008-2011, totally 214,350 TL was paid to compensate the local damage caused by the flood on February 26th, 2010, involving invoices of 143,000 TL for cleaning and disinfection of 859 houses, 53,250 TL for cleaning of 196 streets, and 18,100 TL for disinfection of 89 workplaces. However, it is clear that the economic loss of this flood is much greater even if only the damaged spillways, bridges, hospital, and schools are considered.

Besides, Nicosia Industrial Area which is the center of the light industry and shares considerable amount of economic activities of the country have experienced many inundation problems for a long time. In order to mitigate the flood effects and prevent people's production services, the stormwater management model was developed and a set of remedial measures were proposed by Zaifoğlu and Akıntuğ (2016). Nowadays, this study is considered one of the pioneering projects to be implemented by the government of Northern Cyprus.

The flood inundation mapping is a primary step for planning the cities and developing flood management strategies by determining the regions under risk. In this context, city planners can strengthen the link between flood planning and land-use planning to reach sustainable flood management (Howe and White, 2004). Therefore, these maps for Nicosia would enable to assess the regions under risk and develop a sustainable flood management model. It could lead to take a step for integrated water resources management which is a must for the countries especially with the limited water resources.

1.3. Significance of the Study

The main reason of the flood events in the Mediterranean region is mainly short duration and high intensity of precipitation events (Charalambous, 2016). Thus, precipitation data sets become the unique source while executing the flood management studies. For this reason, a procedure of quality checks is carried out as a preliminary scope of this study. Due to the lack of analysis of precipitation data sets in Northern Cyprus, reconstruction of data series including missing data computation,

quality control methods, and assessment of the homogeneity are executed. Reliable and questionable data series are exhibited and lead to further researches to work with quality-controlled, completed, and homogeneous data sets for their subsequent studies about climate variability, water resources management, and hydrological analysis.

The trend analysis of extreme precipitation indices in this study is necessary to assess the variability and characteristics of local precipitation regimes and contribute to the climate change studies in the Mediterranean region. Besides, annual and seasonal trends of extreme indices will enhance the knowledge for drought and flood management studies in Northern Cyprus in terms of developing strategies, determining the priorities, and planning the water resources management strategies including long and short term actions.

In most developing countries as well as in Northern Cyprus, the long term precipitation records are generally limited in quantity. For this reason, the regional frequency analysis is employed in this study to overcome this limitation and obtain reliable estimates. At this point, identification of homogeneous regions step becomes the crucial one which directly affects the quantile estimates. Due to the complex topography of the island, delineation of Northern Cyprus needs to be clearly handled. Therefore, time series clustering approach is proposed as a new perspective in RFA to determine the homogeneous hydrological regions of Northern Cyprus and for the larger return periods, daily precipitation estimates declare as more accurate. Achieved results could be useful for engineers and researchers in climate studies, water management issues, and hydraulic structure designs at ungauged sites in particular.

This study develops 1D-2D coupled hydrodynamic model of the Çınarderesi Creek, Öksüzdere Creek, and Asidere Creek passing through the town of Gönyeli and the capital city of Nicosia. The flood inundation maps based on different scenarios for various storms are generated to reveal the regions at risk. This data will be valuable especially for city planners, municipalities, and relevant government offices. Besides, it will be helpful to see the consequences of the floods based on several storms with

different return periods. Therefore, new hydraulic structures or modification of the existing ones could be proposed to the authorities and contribute to reduce negative impacts of floods.

1.4. Scope and Objective

The main objective of this study is to determine the parts of city under the risk of flooding and propose safe and economic flood protection measures to mitigate the inundation problem of Nicosia region.

Within the scope, the specific aims of this study are outlined as follows:

- To apply a set of quality check procedures to create quality-controlled, complete, and homogeneous daily precipitation data sets.
- To investigate the local effects of climate change and the annual and seasonal variability of extreme precipitation events in Northern Cyprus.
- To identify the hydrologically homogeneous regions of Northern Cyprus.
- To apply regional frequency analysis to obtain reliable precipitation estimates for larger return periods.
- To develop the rainfall-runoff models and the coupling of 1D-2D hydrodynamic model for the study area.
- To generate flood inundation maps by considering a set of scenarios for storm events with larger return periods.
- To propose a number of structural measures to protect the capital city of Nicosia and other certain areas from the effects of floods relied on the generated flood inundation maps.
- To recommend implementation of early warning systems to ensure earliest warning of local people and if necessary, provide adequate time for evacuation.

CHAPTER 2

LITERATURE REVIEW

This chapter points out the related studies, applied methods and approaches, and proposed solutions to the problems of data reliability, quantile estimates by frequency analysis, and flood inundation and management measures from allover the world.

2.1. Quality Control and Trend Analysis of Precipitation Data

Recently, many studies have evaluated climate change effects by analyzing the results of past, present, and future projections in variation of climate in the world (e.g. Marengo et al., 2017; Bonsal et al., 2017; Pechlivanidis et al., 2017). According to the report of the Intergovernmental Panel on Climate Change (IPCC) (2014), there is an increasing trend in the frequency and intensity of the extreme precipitation incidents and this leads to enhance the flooding risks as well as the amounts and quality of the water bodies throughout the world. In the following decades, increment in risk of flooding is still going to upwards because of the development of socio-economic structure and climate change (Visser et al., 2014; IPCC, 2014). In order to estimate the occurrence probabilities of extreme precipitation correctly, reliable and long-term data sets are required (Vicente-Serrano et al., 2010).

As the missing record periods in climatic data sets are commonly a striking issue in the literature, several methods and approaches are proposed to complete the series. For instance, the Inverse Distance Weighting method (IDW) and Normal Ratio method (NR) are the commonly used methods suggested by ASCE (1996). Revised and different versions of these methods are also derived to overcome their limitations (Tang et al., 1996; Suhaila et al., 2008). Besides, other representative studies referring to missing data estimation are as follows: artificial neural networks (Kim and

Pachepsky, 2010), linear and nonlinear multiple regression (Ulke et al., 2009), co-kriging (Seo et al., 1990), nearest neighbor (Teegavarapu and Chandramouli, 2005), copula-based method (Bardossy and Pegram, 2014), thin plate splines (Jarvis and Stuart, 2001). Moreover, when estimation methods using the information of neighboring stations are applied, the reliability of the data series with completed periods strongly depend on the number of neighboring stations and their record lengths (Eischeid et al. 2000). For instance, in Eischeid et al. (2000) to fill the missing data series, the chosen number of neighboring stations are varying from one to four with at least 0.35 correlation between the series. In another example, the nearest neighbor estimation method utilizes the neighboring stations within a radial distance of 15 km away, minimum correlation coefficient of 0.5, and minimum common record length of three years (Vicente-Serrano et al., 2010).

The records of meteorological stations may have some discontinuities which cause poor quality of series (Reek et al., 1992; Wallis et al., 1991) due to the effects of non-climatic conditions, such as type of instrument, location of instrument, observation methods, environment of station, calculation methods (Heino, 1994; Gullett et al., 1990). For these reasons, assessing the quality of data sets by applying manual (e.g., Griffiths et al. 2003) and automatic (Kunkel et al. 2005; Durre et al. 2010) approaches is a must. Mainly such procedures consist of completion of missing series, detection of gross errors and outliers, and checking of spatial consistence of neighboring stations. On the other hand, the detected outliers must be treated carefully. Because they could have valuable information about the extreme events in some cases. Instead of completely taking them out of the series, such outliers should be changed by their threshold values. Therefore, this information is kept in the series and the negative effects on the analyses are prevented.

While conducting the climate related studies, using homogeneous data sets is crucial to reach correct results. Homogeneous series are the one that are only affected by the weather and climate based variations (Conrad and Pollak, 1950). In this context, various methods are proposed to analyze and detect the inhomogeneties in series. They

could be categorized into two methodologies: direct methodologies based on the availability of metadata files (history of data) and changes in instrument, and indirect methodologies including the absolute tests which are applied to the individual station without reliable and sufficient number of neighboring stations and relative tests which are employed to generate reference series to compare the candidate station with reference series (Peterson et al., 1998).

Nowadays, the index-based methods have been used to check and analyze the variability of climatic events (e.g. Wang et al., 2013; Dookie et al., 2018). Due to the simplicity and practicality of the calculation of the indices of daily series, several studies are widely carried out to evaluate the climate change and their effects on agriculture and economy in terms of adaptation facilities (Zhao et al., 2018). For instance, changes in extreme precipitation indices have been studied for the different parts of the world on local or regional scale (Klein Tank and Können 2003; Vincent and Mekis 2006; Bothale and Katpatal 2015). On global scale, the similar researches have been conducted to indicate the changes in extreme climatic events in terms of amount, frequency, and intensity (e.g., Alexander et al., 2006; Donat et al., 2013). Moreover, some studies have used the climate models and made the projections to assess the extreme precipitation events (e.g. Kysely et al., 2011; Hadjinicolaou et al., 2011; Arnbjerg-Nielsen, 2012).

2.2. Regional Frequency Analysis

Knowing the characteristics of precipitation is very important for the design of hydraulic structures and water resources management (Chebana et al., 2014) where the variability of precipitation events is under the effect of climate change in terms of increased number of extreme events and natural disasters (IPCC, 2014). For these reasons, there is a widespread interest in determining the occurrence frequency of such extreme events by executing an extreme value analysis (e.g. Katz, 1999; Renard and Lang, 2007; Um et al., 2017). Besides, where there is no or limited amount of records available, the probability estimates, particularly for larger return periods are not

reliable. Therefore, applying regional frequency analysis (RFA) enable to utilize from the data of the other sites in a region and lead to reduce the estimation of uncertainty of the data (e.g. Kyselý et al., 2011; Burn, 2014). In this context, the index-flood approach of Dalrymple (1960) which collects the data of different sites are properly used in RFA (Hosking and Wallis, 2005). According to this approach, the frequency distribution of the sites in the same homogeneous region is identical and differ only in a specific scale factor, known as index-flood. Generally, this factor is the mean of the data series sample. But, it could be obtained by using different approaches in ungauged sites or limited series, such as derivation of regression equation (Alobaidi et al. 2015). In addition, in index-flood method, rather than using the conventional moments for estimation of parameters of distributions and quantiles, L-moments are typically chosen due to their robustness.

Regional frequency analysis using L-moments has been widely applied in the different parts of the world on various topics, such as analyzing the flooding events (e.g. Kjeldsen et al., 2002), spatiotemporal variability of extreme rainfall (e.g. Yang et al., 2010), rainfall intensity-duration-frequency (IDF) relationships (e.g. Hailegeorgis et al., 2013), the potential of satellite-based precipitation estimates at ungauged sites (e.g. Gao et al., 2017). To give the examples from different regions, Guse et al. (2010) revealed the effects of two pooling methods on quantile estimates in Germany. Hailegeorgis et al. (2013) utilized the RFA to update the existing IDF curves in Norway and obtain more reliable ones. Kumar et al. (2015) aim to compare the L-moments with soft computing methods in RFA using the annual streamflow data in India. Liu et al. (2015) estimated the return period of one of the most destructive events in Jakarta. Bezak et al. (2016) developed intensity-duration-frequency curves using the copula based methods. Wang et al. (2017) carried out RFA using L-moments, fuzzy c-means, and other statistical methods to deeply analyze the regional and spatial variations of extreme precipitation events in China.

Generally, the regional frequency analysis can be divided into four parts: preliminary analysis of data (validation of assumptions and data screening), formation of homogeneous regions, determination of frequency distribution, and estimation and evaluation of estimated quantiles (Hosking and Wallis, 2005). Herein, formation of the homogeneous region differs as a crucial and subjective step which seriously affect the results. Moreover, several approaches and frameworks have been discussed across the globe in order to reach the best regionalization for the hydrological data sets. As representative examples, Burn (1989) presented cluster analysis to group similar basins and used in RFA. Ouarda et al. (2008) carried out a comparison of approaches, known as hierarchical clustering, the type of canonical correlation analysis, and the canonical kriging approach for delineation purposes. Di Prinzio et al. (2011) applied self-organizing map to reduce the uncertainity and classify the watersheds. Kileshye et al. (2012) used principal component analysis to detect the similarities of catchments in the equatorial Nile region. Sivakumar and Singh (2012) used nonlinear dynamic method to determine the complexity level of streamflow data sets for classifying the stations in western United States.

According to Hosking and Wallis (2005), the most practical method to identify the homogeneous regions is the clustering analysis using the features of the stations from great amount of data sets. Since the selected features highly affect the formation of homogeneous regions (Oudin et al., 2010), a set of features, such as latitude, longitude, elevation, catchment area, mean annual precipitation, mean annual temperature, humidity, slope, basin lag time, statistical measures are mainly preferred in conventional approach (Potter and Faulkner, 1987; Malekinezhad and Zare-Garizi, 2014; Satyanarayana and Srinivas, 2008; Castellarin et al., 2001). Furthermore, clustering algorithms are classified into two categories: hierarchical and partitional clustering methods (Kaufman and Rousseeuw, 2009). The most common types of hierarchical methods are single linkage, maximum linkage, average linkage and Ward's minimum variance method (e.g. Bhaskar and O'Connor, 1989; Santos et al., 2015; Rahman et al., 2017). In partitional clustering methods, k-means or k-medoids

and fuzzy c-means are widely applied (e.g. Ngongondo et al., 2011; Bharath and Srinivas, 2015). Since the hierarchical Ward's method tends to form almost equal-sized clusters, Hosking and Wallis (2005) recommended to use this method in the studies of regional frequency analysis to identify homogeneous regions.

According to Chiang et al. (2002), during the delineation process, using the characteristics of stations may keep some information, but the nature of the series may be negatively affected. Direct usage of time series preserves the sequential and stochastic structure of the series. In the study of Liao (2005), time series clustering methods are reviewed and can be grouped under three approaches as follows: directly using the raw data, using some features of raw data, and model developing from raw data. A comprehensive review study about the time series clustering can be found in Aghabozorgi et al. (2015). From the stand point of regionalization by using the time series in hydrology, a framework on hydrological regionalization by using the time series of monthly flow data was recommended by Chiang et al. (2002). It was the first attempt to group series by utilizing the autoregressive moving average (ARMA) model parameters as clustering variables. Corduas (2011) proposed a model-based approach to form groups based on the similarity of the modelling of streamflow time series. In order to check the similarities, the parameters of regression and autoregressive models were analyzed in terms of calculated proximity distances, named as the Mahalanobis and the Euclidean distances. By applying the wavelet analysis to hydrological data series, the high dimensionality of data is reduced and the formation of groups are executed based on the features of new transformed data sets (e.g. Smith et al. 1998; Hong-Fa 2012).

2.3. Flood Management

Upward trend of population growth leads to increase in urbanization or in other words, increasing of impervious areas. Therefore, decreasing percent of soil and vegetation cover severely damage the hydrologic cycle in terms of enhancing the amount of runoff and contracting amount of evapotranspiration and interception (Jacobson,

2011). Recently, in order to manage the flooding risks and conduct a sustainable floodplain protection to prevent people and economical damages, integrated flood management is required (Di Baldassarre, 2012).

In this context, improving the knowledge of river network hydraulics and responses of floodplains are necessary. Hydrological models are important tools to closely mimic the behaviors of real world with the simulated models to get the responses of urban catchments in particular (Koriche et al., 2012). Various studies have been executed to examine the role of the hydrological processes and characteristics of catchments in the flood inundation problems (e.g. Nied et al., 2013; Prosdocimi et al., 2015; Karamage et al., 2017).

In ungauged study regions developing a rainfall-runoff models still remains a tough task in hydrology (Sivapalan et al., 2003) due to the lack of runoff data using in parameter calibration purposes (Blöschl, 2006). A less number of parameters using to describe the characteristics of catchments under the condition of scared data is preferable (Ahmad et al., 2009).

The most popular and useful software in hydrological modelling are developed across the world: HEC-HMS developed by the Hydrologic Engineering Center within the U.S. Army Corps of Engineers (USACE, 2000), the U. S. Environmental Protection Agency's (EPA) storm water management model, SWMM (Rossman, 2010), and MIKE SHE (Abbott et al., 1986) developed by Danish Hydraulic Institute. For example, Sampath et.al (2015) used HEC-HMS to execute hydrological model of the Deduru Oya River basin and make runoff estimation. In Northern Cyprus, for the industrial region, Zaifoğlu and Akıntuğ (2016) developed SWMM model to analyze the responses of the catchment and proposed a set of structural measures to mitigate the inundation problem. Paparrizos and Maris (2017) revealed that hydrological model of Sperchios River basin in Greece successfully simulated the water balance by using MIKE SHE.

Flood modelling has been carried out since the 1970s (Teng et al, 2017) for different objectives, such as flood inundation mapping (e.g. Bhandari et al., 2017; Afshari et al., 2018), flood risk assessment (e.g. Budiyono et al., 2015; Vojinovic et al., 2016), flood real-time forecasting (e.g. Arduino et al., 2005), water management (e.g. Vaze et al., 2013), bridge scour analysis (e.g. Lu et al., 2008), and sediment transport modelling (e.g. Hu et al., 2009). In order to simulate the fluid motion in a model, mathematical hydrodynamic models based on the principles of conservation of mass and momentum are used by solving the continuity and the Navier Stokes equations.

The simplest and the most commonly used approach for modeling the river is the one dimensional (1D) flow models which assume that the flow velocity distribution is perpendicular to the cross-sections. In several conditions, the flow can be adequately represented by 1D modelling, such as channel flow and pipe flow (Teng et al, 2017). Moreover, while solving the 1D Saint-Venant equations to conserve the mass and momentum balance among the successive cross-sections, 1D models perform computationally efficient (Ali et al., 2015). However, they generally fail to simulate lateral diffusion of water onto the floodplains (Hunter et al., 2007). MIKE 11 developed by the Danish Hydraulic Institute, Denmark (DHI, 1997) and HEC-RAS from the US Army Corps of Engineer's Hydrologic Engineering Center (Brunner, 2002), have been widely preferred software using 1D modelling of rivers. For representative examples, Chatterjee et al. (2008) employed MIKE 11 for setting up the 1D model of the Elbe River in order to compare the capabilities of different models in terms of computation time, DEM resolutions, number of cross-sections, etc. Mishra et al. (2001) indicated that MIKE 11 performed well in the large and complex irrigation system and helped the improvement of irrigation management plans. Timbadiya et al. (2014) developed unsteady 1D model of MIKE 11 to obtain rating curves in Lower Tapi River. 1D hydrodynamic model of HEC-RAS was formed to analyze the water levels in Kalu River under the steady and unsteady flow conditions (Nandalal, 2009). In Northern Cyprus, Sahin et al. (2013) developed a 1D HEC-RAS model to assess the Güzelyurt Flooding and proposed remedial measures.

When the water level reaches its maximum point in a main channel, it starts to overflow into the floodplains and since the assumptions of 1D flow is no longer available, 2D flow modelling provides better results (e.g. Cobby et al., 2003; Tayefi et al., 2007). Therefore, 2D modelling becomes more suitable in determination of inundation area by considering topographic features (Cook and Merwade, 2009), especially while modelling the urban regions (Syme et al., 2004). However, increasing computation time and data requirements are the main disadvantages of 2D modelling (Abderrezzak et al., 2009; Yoon and Kang, 2004). Also, ability of 2D models to efficiently simulate the flow through the hydraulic structures is limited (Frank et al., 2001).

Majority of the 2D flow models uses shallow water equations and applies the conservation of mass and momentum equations to solve the 2D flow phenomena. The floodplains are modelled by applying different discretization approaches, known as finite element, finite difference, and finite volume methods, where each element in solution domain is represented by structured, unstructured, and flexible meshes (Teng et al., 2017). In order to solve these numerical schemes and simulate 2D flow, several software are available, such as MIKE 21 (DHI, 2000), TELEMAC 2D (Bates and De Roo, 2000), DELFT-FLS (Hesselink et al., 2003), HEC-RAS-v5 (Brunner, 2014), SOBEK (WL, 2005).

2D hydrodynamic models have been commonly applied for determining the flood inundation extents and assessing the results of flooding events. For instances, according to Fernandes et al. (2001), who showed that the calibrated and validated TELEMAC 2D model could give promising results despite of the lack of data and space discretization in the Patos Lagoon. Hesselink et al. (2003) used Delft-FLS 2D modelling software to simulate the overland flow and discussed the sensitivity of flood inundation extent from the viewpoint of topography and hydraulic friction. David et al. (2009) presented a comparison of six 2D models to simulate flood events in a dense urban area in the city of Glasgow. Tarekegn et al. (2010) proposed a 2D model of SOBEK with remote sensing, GIS procedure to analyze the flood features of the Lake

Tana basin. Singh et al. (2018) assessed the vulnerability of the road network in flood events simulated by 2D hydrodynamics model developed in MIKE 21. Ballesteros et al. (2011) employed 2D model in MIKE 21 to estimate the discharge of flash flood in an ungauged region. Quirogaa et al. (2016) demonstrated the capabilities of newly released HEC-RAS-v5 2D modelling tool by simulating the flood event in the Bolivian Amazonia.

As mentioned before, 1D modeling has drawbacks to simulate the flow on complex floodplains, while 2D modelling is challengeable due to restricted ability to accurately simulate supercritical or pressurized flow conditions particularly near hydraulic structures (Gilles and Moore, 2010). Therefore, integrated 1D/2D hydrodynamic modelling is used to overcome such limitations (Patro, et al. 2009) by developing the 1D model for river flow and 2D model for the floodplains to obtain efficient model in the way of computation time and hydraulic phenomena (Gilles, 2010). Within this context, the area occupied by the geometry of cross-sections along the river can be excluded from the solution domain and this reduces the number of grid cells involved in 2D model and save a great amount of time and memory. Besides, when the uncertainty of boundary conditions exists, coupled 1D/2D modelling approach offers a solution to extend the domain. Additionally, since the time step is under the control of the Courant number for stability purposes, using the integrated modelling of a river and floodplain comparing to 2D modeling enable to choose greater time steps (Blade et al., 2012).

In order to combine a 1D model with a 2D model, different linking options, such as standard link, lateral link, urban link, river-urban link, and structural link are available. However, the technique of lateral link is the commonly used one which allows water to laterally discharge from a river model to a floodplain. This flow exchange is controlled by using the weir equations or depth-discharge curves depending on the markers of channel geometry in 1D model, bed levels of cells in 2D model, and the combination of these. Due to the limitation of 1D model to simulate overbanking

channel flow, lateral links do not ensure to the conservation of momentum (DHI, 2009).

Since the coupled 1D/2D modelling offers an optimal satisfactory among the type and number of input data, simulation cost, and promising results (Apel et al., 2007), several integrated models have begun to be proposed, such as MIKE FLOOD, which combines the 1D model MIKE 11 with the 2D model MIKE 21 (DHI, 2009), Sobek Urban, which links 1D flow model of SOBEK with 2D Delft FLS (Deltares, 2017), 1D/2D TUFLOW (WBM Oceanics, 2003) and HEC-RAS-v5 (Brunner, 2014). For example, Syme et al. (2004) used 1D/2D TUFLOW model to simulate the flooding event in urban area of Bristol, UK. Phillips et al. (2005) used calibrated 1D/2D TUFLOW and presented the interaction between the drainage system and 2D flow model. Bolle et al. (2006) carried out a number of simulations to compare the performance of a sewer system and river model separately with the integrated model. By using the MIKE FLOOD, the flood inundation extent and flow depths of Mahanadi River Basin in India were analyzed (Patro et al., 2009). Timbadiya et al. (2014) made a comparison between the 1D, 2D, and 1D/2D models and MIKE FLOOD coupled model performed the best estimations in flood prediction. Patel et al. (2017) executed to analyze the flood inundation map and tested the capabilities of new 1D/2D model of HEC-RAS-v5.

The hydrological and hydraulic models are tools to widen the perspective of flood events in terms of identifying flow depths, velocities, flood extends, etc., and enable to conduct a sustainable flood management system. Flood management is essential to reduce the probability of damages and contribute to sustainable development in a country. Therefore, the measures in flood management could be divided into two typical categories (Li et al., 2016): structural measures which modify the physical characteristics of floods and non-structural measures which regulate the exposure of human life and properties to floods (Casale and Margottini, 1999).

Nowadays, such measures have been widely applied to flood control and mitigation purposes, such as levees and floodwalls (e.g. Ganoulis, 2003; Dijkman, 2007), channels and diversion structures (e.g. Smith and Winkley, 1996; Rasekh et al. 2010), retention and detention basins (e.g. Ngo et al. 2007; Yazdi and Neyshabouri, 2012), sediment management (e.g. Schick et al., 1997; Sequeiros et al., 2009), floodplain management (e.g. Sadeghi et al. 2009; Kiedrzyńska et al., 2015), flood warning systems (e.g. Golian et al. 2011; Daupras et al., 2015), flood insurance (e.g. Burby, 2001; Kousky and Kunreuther, 2014) etc. While examining the worldwide examples, flood mitigation measures in Pakistan which are mainly structural measures consisting of construction of embankments along the main rivers and their branches to prevent overflowing, spurs to guard these embankments, dikes to regulate water level, bunds to protect settlement and agricultural areas, and dams to store vast amount of flood water. Besides, there exist flood forecast and early warning systems as non-structural measures (Tariq and Van de Giesen, 2012). In Slovakia, the structural measures including levees, flood walls, dams, and other mobile elements were completed in 2010 (Kryžanowski et al., 2014). Detention dams and floodwalls as structural measures and watershed management, waterproofing, and flood warning as non-structural measures were applied within the integrated flood management project for Kan basin in Iran (Yazdi and Neyshabouri, 2012). Thielen et al. (2009) presented the European Flood Alert System (EFAS) which was developed to provide preparedness to the local authorities about floods in transnational river basins of Europe.

Moreover, as a new perspective, 'Natural Flood Management' offers to reduce the velocity or volume of water in a catchment by conducting river and land use management, such as creation of wetland and ponds, restoration of rivers, and formation of woodlands, etc. (Rouillard et al., 2015; Waylen et al., 2018). For example, as a part of the Eddleston Water Project in Scotland, the implemented measures are: planting of woodlands to decrease the flow rates, protect the erosion, and strengthen bank stability; restoration of rivers and floodplains (SEPA, 2016).

CHAPTER 3

HYDROLOGICAL METHODOLOGY

This chapter explains the methodologies used in quality control of data sets, regional frequency analysis, and hydrological modelling of the study area used in this thesis.

3.1. Quality Control

3.1.1. Missing Data Estimation

In order to estimate the missing periods in daily precipitation records, the methods which utilize the information of neighboring stations are chosen instead of data-driven methods which use only one series. At this point, the selected neighboring stations play crucial role on the estimated values (Eischeid et al., 2000). As shown in Figure 3.1, the box plot which shows the number of neighboring stations falling within certain ranges in Northern Cyprus is plotted for the stations with missing data. The 50% of the number of the neighboring stations within a radius of 5 and 7.5 km are zero, even increasing the radius to 12.5 km some stations still do not have neighboring stations around. Moreover, it is clear that the average correlations (r) between daily precipitation series decreased as a function of distance (Figure 3.2) and the average correlation is found as 0.45 with a range from 0.26 to 0.70. This range was getting narrower from lower to greater distances and the weak correlations can be observed at close stations due to the complex orography of Northern Cyprus.

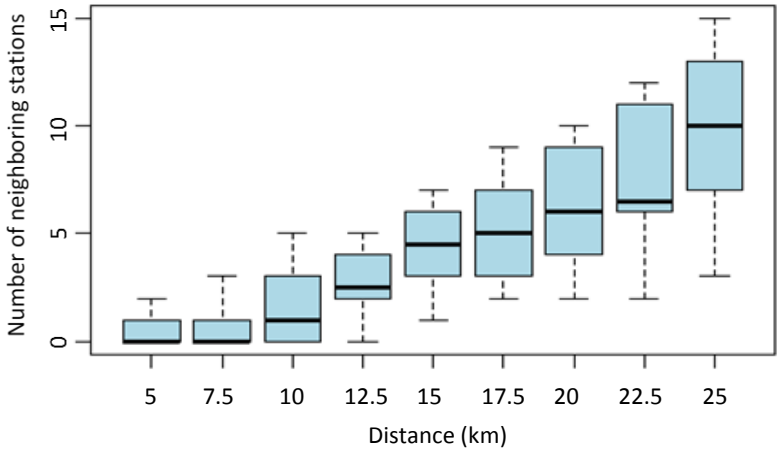

Figure 3.1. Box plots of the ranges of distances and corresponding number of neighboring stations

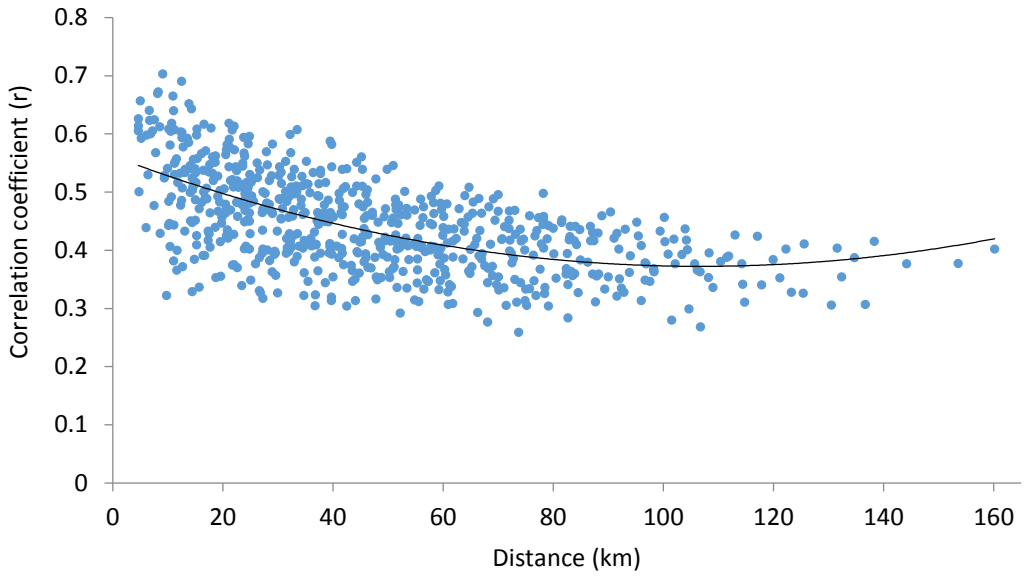

Figure 3.2. Correlation coefficients between the daily precipitation series at different distances

In order to determine the best number of neighboring stations and the best method for the estimation of missing values, the following procedure is decided. As a first step, several intervals are tried from a range of 5 km to 25 km by increasing the radius as 2.5 km at each trial. The station located in a selected radius is marked as neighboring station. Then, the common and complete periods of the target and neighboring stations are assumed as incomplete to test the performance of the data estimation methods. In this study, five different methods are considered appropriate: nearest neighbor with the highest correlation (NN), inverse distance weighting (IDW) (Isaaks and Srivastava, 1989), normal ratio (NR) (Paulhus and Kohler, 1952), modified normal ratio based on square root distance (MNR-T) (Tang et al., 1996), and coefficient of correlation weighting (CCW) (Teegavarapu and Chandramouli, 2005). For various radius and method combinations, these steps are repeated and finally, the estimation of the missing values is executed according to the optimum radius and appropriate method with the lowest root mean square error (RMSE). The RMSE is calculated as follows (Gaile and Willmott, 2013):

$$RMSE = \sqrt{\frac{1}{N}\sum(P_{obs} - P_{est})^2} \tag{3.1}$$

where P_{obs} is the observed values in a common period and P_{est} is the corresponding estimated values for N number of observations.

In the nearest neighbor with the highest correlation method, the missing values are filled by directly copying values from the nearest neighboring station. Definition of the nearest neighboring station in this study is the station that has the highest correlation coefficient between daily precipitation series of common observation period instead of selecting a station with geometrically close to the target station.

Inverse distance weighting method is based on weighting the neighboring stations inversely proportional to the target station by their distances. IDW is given by (Isaaks and Srivastava, 1989):

$$P_t = \frac{\sum_{i=1}^{n} P_i {d_{it}}^{-r}}{\sum_{i=1}^{n} {d_{it}}^{-r}} \tag{3.2}$$

where P_t is the estimated missing value at the target station *t*, P_i is the corresponding observed values of neighboring stations, and d_{it} is the weight factor implying the Euclidean distance between the *i*-th neighboring station and the target station. The influence of the distances can be adjusted by the value of *r* and in this study it is selected as 2 which is the most commonly used value (Tang et al., 1996).

In the normal ratio method, the missing values of the target stations are estimated by utilizing the ratio of the normal annual precipitation of the target station to the neighboring stations as a weighting factor (Paulhus and Kohler, 1952).

$$P_t = \frac{1}{N} \sum_{i=1}^{N} \frac{N_t}{N_i} P_i \tag{3.3}$$

where P_t is the estimated value of target station and P_i is the values at the neighboring stations. N_t and N_i are the normal annual precipitation values of target and neighboring stations, respectively. For using this method, the normal annual precipitation data of at least one neighboring station needs to be exceeding 10% of the target station's value (McCuen, 1998).

Modified normal ratio based on square root distance method is proposed by Tang et al. (1996) for filling the gaps in Malaysian rainfall data. It can be defined as the combination of the impact of distance with the normal ratio method and given as (Tang et al., 1996):

$$P_t = \frac{\sum_{i=1}^{N} P_i \frac{N_t}{N_i} {d_{it}}^{-r}}{\sum_{i=1}^{n} {d_{it}}^{-r}} \tag{3.4}$$

where P_t, P_i, N_t, N_i, and d_{it} are the same parameters described above. Likewise, inverse distance weighting method, *r* is taken as a value of 2 for calculations.

The coefficient of correlation weighting method relies on the existence of strong positive spatial autocorrelation among the target and neighboring stations that leads to the IDW method to be used successfully. By replacing weighting factors of distance by correlation coefficient, the results of estimations are improved compared to the IDW and some other methods as shown by Teegavarapu and Chandramouli (2005). The expression of the CCW method with r_{it} which is the correlation coefficient calculated by using the available historical data of the target station and the corresponding values of the neighboring stations is given by (Teegavarapu and Chandramouli, 2005):

$$P_t = \frac{\sum_{i=1}^{n} P_i r_{it}}{\sum_{i=1}^{n} r_{it}} \tag{3.5}$$

3.1.2. Detection of Unreasonable Values and Outliers

By using the completed data sets, the following step is to detect the erroneous values in precipitation series. Therefore, physically impossible values particularly occur in duplication or collection processes are analyzed for each station separately. Priorly, a range of limits must be determined for checking the values out of this interval. Some of the studies (e.g. Feng et al., 2004; Durre et al., 2010) constructed these limits relied on the historical information of the World Meteorological Organization World Weather/ Climate Extremes Archive (2017). For minimum and maximum values of this interval, the global minimum daily precipitation value of 0 mm and the global maximum precipitation value of 1,828.8 mm are selected. But, on the other hand, the limits of 0 mm and 508 mm are considered as more suitable in some other studies (e.g. Wallis et al., 1991; Shafer et al. 2000) as well as for this study. This approach is known as a fixed range test. Subsequently, as detailed in Reek et al. (1992), the repeating precipitation values except zero values in a period of at least seven days or more are also marked as erroneous.

The presence of outliers, especially due to the extreme precipitation events, should be checked while executing quality control checks. Therefore, detected outliers which are absolutely inaccurate records should be kept out of the analysis or modified (González-Rouco et al., 2001). However, some of them could represent some rare extreme climatological events which are actually so meaningful and valuable for climatic studies. For this reason, replacement of outliers with their unique threshold values rather than removing them from data sets would be a better application (Barnett and Lewis, 1994). Therefore, outliers both conserve the effect of extreme precipitation events and do not show negative impact on the results of some methods, such as homogeneity tests (González-Rouco et al., 2001).

A threshold value using for substituting an outlier is calculated as follows (González-Rouco et al., 2001):

$$P_{out} = q_{0.75} + 3IQR \tag{3.6}$$

where $q_{0.75}$ is the third quartile and IQR (interquartile range) is the difference between the third and the first quartiles. In this study, when the outliers are greater than the P_{out} values, they are substituted. This procedure is applied to the monthly precipitation data sets aggregated by the daily series for each month separately.

Additionally, in some cases instead of detecting the outliers for each series individually, the procedure utilizing the information of the other neighboring stations could be more convenient. In this respect, discordancy measure of Hosking and Wallis (2005) is applied to reveal the stations which are grossly discordant with the group as a whole. Discordancy measure is calculated based on the sample L-moment ratios, known as L-variation, the L-skewness, and the L-kurtosis. If there is any problem in data series due to inaccurate records, presence of outliers, trends, or shifts, the L-moments of such data series become noticeable different than other stations in a region. Also, this measure is generally used in data screening step of regional frequency analysis studies (e.g. Liu et al., 2015; Hailegeorgis and Alfredsen, 2017).

In discordancy measure, let $u_i = \left[t^{(i)}\ {t_3}^{(i)}\ {t_4}^{(i)}\right]^T$ be the vector involving L-moment ratios, named as the coefficient of L-variation ($t^{(i)}$), L-skewness (${t_3}^{(i)}$), and L-kurtosis (${t_4}^{(i)}$) for station i. Hosking and Wallis (2005) define the following statistical terms.

Let $\bar{u}$ be the unweighted regional average of stations:

$$\bar{u} = N^{-1}\sum_{i=1}^{N} u_i \tag{3.7}$$

Let define covariance matrix, A_{cov} as:

$$A_{cov} = \sum_{i=1}^{N}(u_i - \bar{u})(u_i - \bar{u})^T \tag{3.8}$$

and the discordancy measure for station i is given as follows:

$$D_i = \frac{1}{3}N(u_i - \bar{u})^T A_{cov}^{-1}(u_i - \bar{u}) \tag{3.9}$$

In order to detect discordant stations in a region, Hosking and Wallis (2005) recommend some critical limits based on the number of stations in a region. Therefore, when a station's D_i value exceeds the critical limit, this station is marked as a discordant station and further analysis of sample L-moments is needed to detect erroneous value(s) based on the comparison to other stations in a region. In this study, this application is employed for the annual maximum daily precipitation and annual total precipitation series.

3.1.3. Homogeneity Analysis

3.1.3.1. Procedure of Homogeneity Analysis

Inhomogeneous climatic data series are typical problems in climate studies (Vicente-Serrano et al., 2010) which lead to biased data sets and wrong assessment of results in climate research (Peterson et al., 1998). Therefore, relative and absolute homogeneity

analysis methods have been yielded to find the significant inhomogeneties and adjust them to compensate for the biases. As outlined in Wijngaard et al. (2003), the main difference of these methods is in the relative methods, the data of neighboring stations are assisted for the analysis. However, in absolute methods, only the data of a target station is considered. When neighboring stations and target station show significantly high correlation, the relative homogeneity analysis methods are more suitable (Peterson et al., 1998). On the other hand, if the homogeneity of neighboring stations is doubtful or some external physical modifications of target station and neighboring stations occur simultaneously, the relative methods may be incapable of determining the inhomogeneous series (Tayanç et al., 1998; Karabörk et al., 2007). In such cases, absolute homogeneity analysis methods stand out to overcome these limitations and do not need historical metadata. In this study, these methods are considered to investigate the homogeneity of the records of precipitation stations. A comprehensive review about the procedure and methods for the homogeneity analysis can be found in Peterson et al. (1998) and Ribeiro et al. (2016).

As detailed in Wijngaard et al. (2003), the two-step approach is employed to control the homogeneity of the precipitation stations. As a first step, four homogeneity tests, known as the standard normal homogeneity test (SNHT) for a single break (Alexandersson 1986), the Buishand range test (Buishand 1982), the Pettitt test (Pettitt 1979), and the Von Neumann ratio test (Von Neumann 1941) are conducted. While applying these tests, testing variable of Y is used and according to the constructed null hypothesis, annual values of Y_i are assumed to be independent and identically distributed. On the other hand, according to the alternative hypothesis, the SNHT, the Buishand range test, and the Pettitt test are assumed that there is a stepwise shift in the mean or in other words, a break exists. These three homogeneity tests are also known as location-specific tests which can enable one to detect the exact location of the shift in a series. However, by using the Von Neumann ratio test, it is not possible to determine a break in series. The alternative hypothesis of this test represents that data set is not randomly distributed.

As a second step, the assessment and classification of the precipitation stations are carried out based on the results of four tests. According to the number of the rejected null hypothesis, the stations are defined as follows: if one or zero tests reject the null hypothesis, Class 1 or useful; if two tests reject the null hypothesis, Class 2 or doubtful; if three or four tests reject the null hypothesis, Class 3 or suspect. Different from Wijngaard et al. (2003), instead of a significance level of $\alpha = 0.01$, $\alpha = 0.05$ is considered for safety reasons to remove a station from the analysis if little doubt exists. Moreover, daily precipitation series are tested in terms of four testing variables. Total annual precipitation, monthly maximum precipitation, seasonal total precipitation, and annual wet days are used in the two-step approach to ensure the homogeneity of the series.

3.1.3.2. Absolute Homogeneity Tests

Let the annual data of testing variables is Y_i, $\bar{Y}$ is the average and *s* is the standard deviation of the series. Alexandersson (1986) derived a statistic $T(k)$ for the standard normal homogeneity test in order to compare the average of the first *k* years and the average of the last $n - k$ years during the recording period. This statistic is calculated as follows (Alexandersson, 1986):

$$T(k) = k\bar{z}_1^2 + (n-k)\bar{z}_2^2 \qquad k = 1, \dots, n \tag{3.10}$$

where

$$\bar{z}_1 = \frac{1}{k}\sum_{i=1}^{k}\frac{(Y_i - \bar{Y})}{s} \tag{3.11}$$

and

$$\bar{z}_2 = \frac{1}{n-k}\sum_{i=k+1}^{k}\frac{(Y_i - \bar{Y})}{s} \tag{3.12}$$

When the peak value of $T(k)$ is observed at K year, this implies that a break or shift is detected at the year $k = K$. Therefore, the test statistics of T_0 is found as greater than its critical value and the null hypothesis is rejected. T_0 is computed as:

$$T_0 = \max_{1 \le k \le n} T(k) \tag{3.13}$$

In the Buishand range test, the rescaled adjusted range (R) is used to assess the significance of the break as given (Buishand, 1982):

$$R = \frac{\left(\max_{1 \le k \le n} S_k^* - \max_{1 \le k \le n} S_k^*\right)}{s} \tag{3.14}$$

Here, adjusted partial sums are calculated as follows:

$$S_0^* = 0 \text{ and } S_k^* = \sum_{i=1}^{k} (Y_i - \bar{Y}) \quad k = 1, \dots, n \tag{3.15}$$

If the series are homogeneous, a set of values of S_k^* will be around zero. Otherwise, S_k^* get its maximum value due to negative shift or minimum value due to positive shift at the year of break. Here, the critical values for $R/\sqrt{n}$ is found in Buishand (1982).

In the Pettitt test, test statistic is calculated as follows (Pettitt, 1979):

$$X_k = 2\sum_{i=1}^{k} r_i - k(n+1) \quad k = 1, \dots, n \tag{3.16}$$

where r_i is the ranks $(r_1, \dots, r_n)$ of the testing variables Y_i. When a break exists in year E, X_k becomes maximum or minimum in year $k = E$. Pettitt (1979) provides the critical values for X_E to test the null hypothesis and X_E is calculated as follows:

$$X_E = \max_{1 \le k \le n} |X_k| \tag{3.17}$$

In the Von Neumann test, the test statistics (N_{VN}) is proposed as follows (Bingham and Nelson, 1981):

$$N_{VN} = \frac{\sum_{i=1}^{n-1} (Y_i - Y_{i+1})^2}{\sum_{i=1}^{n} (Y_i - \bar{Y})^2} \tag{3.18}$$

When there is a break in series, the value of N_{VN} has a falling tendency under the expected value which is $N_{VN} = 2$ in homogeneous series. Due to the rapid variations of the mean, N_{VN} values may increase above 2 (Bingham and Nelson, 1981) as well. As mentioned before, the Von Neumann ratio test does not provide the location of the break year. Buishand (1982) suggested the critical values for N_{VN} statistics.

3.2. Trend Analysis

After applying the quality checks, the quality-controlled, complete, and homogeneous precipitation series are employed to analyze the extreme precipitation events by using the indices. The presence and changes of the annual and seasonal extreme precipitation indices are investigated via conducting nonparametric trend analysis test, Mann-Kendall and trend's magnitude is determined by using Sen's slope estimator. Priorly, the existence of serial correlation (autocorrelation) in series should be checked to avoid the negative impact on the results of trend tests.

3.2.1. Extreme Precipitation Indices

Recently, trend analysis of extreme precipitation indices is widely applied allover the world to assess the changes in extreme events (Zhang et al., 2005; Alexander et al., 2006; Teegavarapu, 2012; Donat et al., 2013; Panda et al. 2016). The joint Commission for Climatology of the World Meteorological Organization's World Climate Data and Monitoring Programme (CCl)/Climate Variability and Predictability Programme of the World Climate Research Programme (CLIVAR)/Joint World Meteorological Organization (WMO)-Intergovernmental Oceanographic Commission (IOC) Technical Commission on Oceanography and Marine Meteorology (JCOMM) Expert Team on Climate Change Detection and Indices (ETCCDI) provides 27 extreme precipitation and temperature indices. Moreover, 72 indices related with pressure, sunshine, wind, cloudiness, etc. (European Climate Assessment and Dataset, 2017) and involving aforementioned indices of ETCCDI are presented in the project of the European Climate Assessment and Dataset (ECA&D) (Klok and Klein Tank, 2009). Within the scope of this study, seven precipitation

indices reflecting the different features, e.g. intensity, amount, and frequency of extreme precipitation events are chosen to interpret the reasons of increased flood inundation problems. As shown in Table 3.1, the definitions of the listed indices are as follows: RR1 is the number of wet days in a year; PRCPTOT implies the total precipitation in wet days; SDII refers to the simple daily intensity index; R20mm is the number of very heavy precipitation days; Rx1day means the annual maximum daily precipitation; R95p is the total precipitation depth in very wet days, and R95pTOT is the precipitation fraction due to very wet days.

Table 3.1. Description of Precipitation Indices (European Climate Assessment and Dataset, 2017)

Index	Description	Unit
RR1	Number of days when daily precipitation ≥ 1 mm	days
PRCPTOT	Total precipitation in days when daily precipitation ≥ 1 mm	mm
SDII	The ratio of annual total precipitation to the number of wet days	mm/day
R20mm	Number of days when daily precipitation ≥ 20 mm	days
Rx1day	Maximum one-day precipitation amount	mm
R95p	Total precipitation amount in days > the 95th percentile of precipitation	mm
R95pTOT	Ratio of R95p to PRCPTOT.	%

3.2.2. Serial Correlation

The existence of positive serial correlation in time series could lead to obtain inaccurate results of trend tests, such as increasing the probability of rejecting the null hypothesis constructed as there is no trend (Bayazıt and Önöz, 2007) and incorrect assessment in determination of the significance of trends (von Storch and Navarra, 1995). For this reason, in such cases, prewhitening the series prior to using the Mann-Kendall trend test is recommended by von Storch and Navarra (1995) in order to form series of no autocorrelation or reduce the impact of lag-1 autocorrelation [AR(1)] component on tests. Pre-whitening application is executed as follows (von Storch and Navarra, 1995):

$$Y_t = X_t - r_1 X_{t-1} \tag{3.19}$$

where r_1 is the coefficient of lag-1 serial correlation of data sample and calculated as (Salas et al., 1980):

$$r_1 = \frac{\frac{1}{N-1}\sum_{i=1}^{N-1}(x_i - \mu(x_i))(x_{i+1} - \mu(x_i))}{\frac{1}{N}\sum_{i=1}^{N}(x_i - \mu(x_i))^2} \tag{3.20}$$

where $\mu(x_i)$ is the mean of the sample data series (x_i) whose length is n. Moreover, in order to assess whether or not the data sets are serially correlated, the confidence interval of the lag-1 autocorrelation coefficient at the significance level of α=0.05 can be expressed by (Salas et al., 1980):

$$\frac{-1 - 1.96\sqrt{N-2}}{N-1} \leq r_1 \leq \frac{-1 + 1.96\sqrt{N-2}}{N-1} \tag{3.21}$$

If the defined confidence interval involves r_1 within its range, the sample series are accepted as the serially independent. In the contrary case, they are assumed to be significantly serially correlated.

3.2.3. Mann-Kendall Trend Test

In the Mann-Kendall trend test, the test statistics (S_{MK}) is calculated as follows (Mann, 1945; Kendall, 1975):

$$S_{MK} = \sum_{i=1}^{N-1}\sum_{j=i+1}^{N} \text{sgn}(x_j - x_i) \tag{3.22}$$

where x_i and x_j are the consecutive values of sample data where ($j > i$), *n* is the length of data sample, and the sign function of $\text{sgn}(x_j - x_i)$ is defined as:

$$\text{sgn}(x_j - x_i) = \begin{cases} +1, & \text{if} \quad x_j - x_i > 0 \\ 0, & \text{if} \quad x_j - x_i = 0 \\ -1, & \text{if} \quad x_j - x_i < 0 \end{cases} \tag{3.23}$$

Mann (1945) and Kendall (1975) presented when the sample size is $N \geq 8$, test statistic *S* is distributed nearly normally with mean and the variance as follows:

$$E[S_{MK}] = 0 \tag{3.24}$$

$$\sigma^2(S_{MK}) = \frac{N(N-1)(2N+5) - \sum_{i=1}^{N} t_i i(i-1)(2i+5)}{18} \tag{3.25}$$

where t_i is the number of ties of extent i. If no ties exist between the series, $t_i = 0$ in the equation and becomes as:

$$\sigma^2(S_{MK}) = \frac{N(N-1)(2N+5)}{18} \tag{3.26}$$

The standardized test statistic Z_S is computed by:

$$Z_S = \begin{cases} \dfrac{S_{MK}-1}{\sqrt{\sigma^2(S_{MK})}}, & \text{if} \quad S_{MK} > 0 \\ 0, & \text{if} \quad S_{MK} = 0 \\ \dfrac{S_{MK}+1}{\sqrt{\sigma^2(S_{MK})}} & \text{if} \quad S_{MK} < 0 \end{cases} \tag{3.27}$$

where Z_S is normally distributed with zero mean and variance of one. Positive value of Z_S indicates an increasing trend, however, negative value of Z_S implies a decreasing trend. Moreover, when $|Z_S| > 1.96$, the null hypothesis constructed as no trend is rejected at the significance level of $\alpha = 0.05$. If the significance level of $\alpha = 0.01$ is selected, rejection criterion becomes as $|Z_S| > 2.576$ for two-sided trend test.

3.2.4. Sen's Slope Estimator

The non-parametric method of Sen (1968) is used to estimate the slope of trend and a set of slopes (Q_i) is calculated as follows:

$$Q_i = \frac{x_j - x_k}{j - k} \tag{3.28}$$

where x_j and x_k are the data values at the specific time steps of *j* and *k*, respectively, for $k < j$.

Let the sample size of data set is *n*, then $N = \frac{n(n-1)}{2}$ possible slopes that can be calculated and ranked from minimum to maximum. Ultimately, Sen's slope (Q_{med}) is calculated as follows:

$$Q_{med} = \begin{cases} Q_{[(N+1)/2]}, & \text{if } N \text{ is odd} \\ \dfrac{Q_{[N/2]} + Q_{[(N+2)/2]}}{2}, & \text{if } N \text{ is even} \end{cases} \quad (3.29)$$

Significance of the median slope is checked by determining the $100(1-\alpha)\%$ two-sided confidence interval as follows (Gilbert, 1987):

$$C_\alpha = Z_{1-\alpha}\sqrt{Var(S_{MK})} \quad (3.30)$$

where $Var(S_{MK})$ is expressed under the Mann-Kendall test and $Z_{1-\alpha}$ is taken from the table of standard normal distribution.

As detailed by Gilbert (1987), $M_1 = (N - C_\alpha)/2$ and $M_2 = (N + C_\alpha)/2$ are calculated to define Q_{min} and Q_{max} values which are the lower and the upper boundary of the confidence interval, respectively. They are obtained from the M_1th largest and the $(M_2 + 1)$th largest of the *N* ordered slope estimates. Herein, both Q_{min} and Q_{max} having the same sign implies the significance of the Q_{med} at $\alpha = 0.01$ and $\alpha = 0.05$ significance levels, respectively.

3.3. Regional Frequency Analysis

3.3.1. L-moments

L-moments can be described as the linear modification of probability weighted moments. Hosking and Wallis (2005) recommended L-moments as an alternative approach to summarize the probability distributions. The advantages of using L-moments instead of conventional moments are to characterize a wider range of distributions and whenever estimated from a sample, they are less sensitive to outliers in series (Hosking and Wallis, 2005). Therefore, more robust estimates of parameters of probability distribution are obtained. As shown by Hosking (1990), the $(r+1)$th L-moment (λ_{r+1}) is defined as follows:

$$\lambda_{r+1} = \sum_{k=0}^{r} \beta_k (-1)^{r-k} \binom{r}{k} \binom{r+k}{k} \quad (3.31)$$

where β_k is the probability weighted moments. For instance, the first four L-moments in terms of the probability weighted moments are:

$$\lambda_1 = \beta_0 \tag{3.32}$$

$$\lambda_2 = 2\beta_1 - \beta_0 \tag{3.33}$$

$$\lambda_3 = 6\beta_2 - 6\beta_1 + \beta_0 \tag{3.34}$$

$$\lambda_4 = 20\beta_3 - 30\beta_2 + 12\beta_1 - \beta_0 \tag{3.35}$$

L-moment ratios are represented as follows (Hosking, 1990):

$$L_{CV} = \tau = \lambda_2/\lambda_1 \tag{3.36}$$

$$L_{skew} = \tau_3 = \lambda_3/\lambda_2 \tag{3.37}$$

$$L_{kur} = \tau_4 = \lambda_4/\lambda_2 \tag{3.38}$$

where L_{CV} is the L-moment coefficient of variation, L_{skew} is the L-moment coefficient of skewness, and L_{kur} is the L-moment coefficient of kurtosis.

3.3.2. Data Screening

3.3.2.1. Validation of Assumptions

The two main assumptions of frequency analyses are the serial independence and the stationarity of data sets. Therefore, the validation of these assumptions are essential. In order to confirm the serial independence of series which otherwise causes bias in series and enhances the error probability in estimations for different return periods (Landwehr et al. 1979; Srikanthan and MacMahon, 1981), lag-1 autocorrelation coefficients are calculated by using the annual maximum precipitation series of each precipitation station as given in Section 3.2.2. The results of autocorrelation analysis are checked by constructing a null hypothesis that the series are serially independent and a significance level of $\alpha = 0.05$ is determined for rejecting the null hypothesis in this study.

The stationarity assumption could be validated based on a trend analysis of annual maximum precipitation series. Because, if the series are stationary, this implies that they are free from trends. Particularly, the external effects damage the homogeneity of series and trigger the formation of trends. Therefore, a widely used trend test of Mann-Kendall is chosen for the assessment of series as given in Section 3.2.3. In this study, a significance level of $\alpha = 0.05$ is considered for checking the null hypothesis which claims there is no trend in series.

3.3.2.2. Discordancy Measure

In regional frequency analysis, the discordancy measure is typically used for a data screening procedure as a first step. The application of this measure can be divided in two steps. First, the Northern Cyprus is assumed to be one homogeneous region involving all precipitation stations and the discordancy measure is calculated to mark the station which is grossly different than the others in a whole region. Secondly, the measure is applied to each homogeneous region after delineation of the region into sub-regions. Therefore, the discordant station is locally investigated in the meaning of having physical ground and from major to minor scales, the inconsistencies could be better assessed. The detailed information about the calculation of discordancy measure and its equations are given in Section 3.1.2.

3.3.3. Identification of Homogeneous Regions

3.3.3.1. Conventional Cluster Analysis

As a conventional clustering approach in regional frequency analysis, the homogeneous regions are delineated based on physical and meteorological features of the stations. In this study, latitude, longitude, elevation, and mean annual precipitation (MAP) are selected as clustering variables. Since the clustering variables have differences in magnitudes and variances, standardization of the data is required which scale to have zero mean and one standard deviation. Therefore, this make them comparable by assigning equal weights to variables before calculating the similarity measures which are sensitive to differences in scales.

3.3.3.2. Time Series Clustering

The clustering of time series data is a challenging attempt in different aspects like high dimensionality, length of time series, noise, outliers and shifts in datasets (Aghabozorgi, 2015). Therefore, time series clustering approaches are developed as follows: shaped-based approach directly deals with raw time series, the feature-based approach converts time series data into feature vector of lower dimensions, and in the model-based approach, extracted model parameters are clustered (Liao, 2005; Aghabozorgi, 2015).

3.3.3.2.1. Shape-based Approach

The most commonly used similarity measure for this type of approach is Minkowski distance (d_{L_q}) and it is calculated as follows (Charrad et al., 2014):

$$d_{L_q}(\boldsymbol{X}_T, \boldsymbol{Y}_T) = \left(\sum_{t=1}^{T} (X_t - Y_t)^q \right)^{1/q} \tag{3.39}$$

where T is the observation period and X_t and Y_t represent t-th values of time series of $\boldsymbol{X}_T$ and $\boldsymbol{Y}_T$, respectively. When $q = 1$, L_q distance is named as Manhattan distance (MAN) and when $q = 2$, L_q distance is named as Euclidean distance (EUCL). The main limitations of these methods are directly affected by the existance of noise and shifts in series and unavailable for time series with different length. Therefore, in order to remove such problems and help a time series to be warped in time for obtaining the best match, dynamic time warping (DTW) method is proposed by Berndt and Clifford, 1994. It also works for the time series in different length. In addition, DTW is employed to detect a mapping r between the time series $\boldsymbol{X}_T$ and $\boldsymbol{Y}_T$ to reduce the distance to the lowest level between the paired values, X_{a_i} and Y_{b_i}. DTW distance is given as follows (Berndt and Clifford, 1994):

$$d_{DTW}(\boldsymbol{X}_T, \boldsymbol{Y}_T) = \min_{r \in M} \left(\sum_{i=1,\dots,m} \left| X_{a_i} - Y_{b_i} \right| \right) \tag{3.40}$$

where M is a group of all possible sequences of m pairs and $a_i, b_i \in \{1, \dots, T\}$. Mainly, the shape-based approaches perform better for short time series without noise, shift or outliers.

3.3.3.2.2. Feature-based Approach

The feature-based similarity measures generally help dimension reduction of time series and reduce the processing time in analyses. In correlation-based measure, the distance between the time series of $\boldsymbol{X}_T$ and $\boldsymbol{Y}_T$ could be assumed in terms of Pearson's correlation as follows (Golay et al. 1998):

$$COR(\boldsymbol{X}_T, \boldsymbol{Y}_T) = \frac{\sum_{t=1}^{T}(X_t - \overline{\boldsymbol{X}}_T)(Y_t - \overline{\boldsymbol{Y}}_T)}{\sqrt{\sum_{t=1}^{T}(X_t - \overline{\boldsymbol{X}}_T)^2}\sqrt{\sum_{t=1}^{T}(Y_t - \overline{\boldsymbol{Y}}_T)^2}} \tag{3.41}$$

where $\overline{\boldsymbol{X}}_T$ and $\overline{\boldsymbol{Y}}_T$ are the average of time series and the similarity measure of correlation-based approach (COR) becomes:

$$d_{COR}(\boldsymbol{X}_T, \boldsymbol{Y}_T) = \sqrt{2\left(1 - COR(\boldsymbol{X}_T, \boldsymbol{Y}_T)\right)} \tag{3.42}$$

In discrete wavelet transform (DWT) distance, according to Zhang et al. (2006), a time series $\left(\boldsymbol{X}_T^{(1)}, \dots, \boldsymbol{X}_T^{(m)}\right)$ with the scale of $J = log_2(T)$ is transformed to $\boldsymbol{H}_j\left(\boldsymbol{X}_T^{(i)}\right) = \left(\boldsymbol{A}_j^{(i)}, \boldsymbol{D}_j^{(i)}, \boldsymbol{D}_{j+1}^{(i)}, \dots, \boldsymbol{D}_{j-1}^{(i)}\right)$, where $\boldsymbol{A}_j^{(i)}$ is the approximation coefficients and $\boldsymbol{D}_j^{(i)}$ is the detail coefficients of DWT. Herein, the DWT similarity measure among the series of $\boldsymbol{X}_T^{(u)}$ and $\boldsymbol{X}_T^{(v)}$ at the scale of j^* is computed as follows (Zhang et al., 2006):

$$d_{DWT}\left(\boldsymbol{X}_T^{(u)}, \boldsymbol{X}_T^{(v)}\right) = \sqrt{\sum_{k} \left(a_{k,j^*}^{(u)} - a_{k,j^*}^{(v)}\right)^2} \tag{3.43}$$

in which $u, v \epsilon (1, \dots, m)$ and, $a_{k,j^*}^{(u)}$ and $a_{k,j^*}^{(v)}$ are the elements of $A_{j^*}^{(u)}$ and $A_{j^*}^{(v)}$, respectively. As recommended by Zhang et al. (2006), the Haar wavelet transform is employed due to efficiency reasons like using the fastest transform algorithm widely applied.

According to the procedure of symbolic aggregate approximation (SAX) given in Lin et al. (2007), the data series are normalized to mean of zero and variance of unity and the piecewise aggregate approximation (PAA) is applied to transform them into *w* segments. A vector, $\overline{\boldsymbol{X}}_{wi} = (\bar{X}_{w1}, \dots, \bar{X}_{wn})$, is created which consists of the average values of each segment. Later on, discretization is applied to the time series to define symbols to each PAA segment based on the break points ($B = \beta_1, \dots, \beta_{\alpha-1}$). These points cover equal-sized areas under the Gaussian curve. Ultimately, the SAX words are formed by the combination of defined symbols and $\widehat{\boldsymbol{X}}_\alpha$ becomes the SAX representation of time series. For instance, the distance between two symbols of l_i and l_j is calculated as follows (Montero and Vilar, 2014):

$$d_\alpha(l_i, l_j) = \begin{cases} 0 & \text{if } |i-j| \leq 1 \\ z_{(\max(i,j)-1)/\alpha} - z_{\min(i,j)/\alpha} & \text{otherwise} \end{cases} \tag{3.44}$$

The similarity measure of two series represented by symbols is computed as given in (Montero and Vilar, 2014):

$$d_{MINDIST.SAX}(\widehat{\boldsymbol{X}}_\alpha, \widehat{\boldsymbol{Y}}_\alpha) = \sqrt{\frac{T}{w}} \sqrt{\sum_{i=1}^{w} \left[d_\alpha(\hat{X}_i, \hat{Y}_i)\right]^2} \tag{3.45}$$

3.3.3.2.3. Model-based Approach

In model-based approach, the model parameters are fitted to the time series and the similarity measure is used to calculate the distances between the parameters. First of all, the piccolo similarity measure (AR.PIC) presented by Piccolo (1990) employs to calculate the Euclidean distance between the parameters of the AR(∞) models with the orders of k_1 and k_2. Here, $\boldsymbol{X}_T$ and $\boldsymbol{Y}_T$ are the time series and

$\widehat{\boldsymbol{\Pi}}_{X_T} = \left(\hat{\pi}_{1,X_T}, \dots, \hat{\pi}_{k_1,X_T}\right)^T$ and $\widehat{\boldsymbol{\Pi}}_{Y_T} = \left(\hat{\pi}_{1,Y_T}, \dots, \hat{\pi}_{k_1,Y_T}\right)^T$ are the parameters of AR(k_1) and AR(k_2), respectively. AR.PIC is calculated as follows (Piccolo, 1990):

$$d_{AR.PIC}(\boldsymbol{X}_T, \boldsymbol{Y}_T) = \sqrt{\sum_{j=1}^{k} \left(\hat{\pi}'_{j,X_T} - \hat{\pi}'_{j,Y_T}\right)^2} \tag{3.46}$$

where $k = \max(k_1, k_2)$, $\hat{\pi}'_{j,X_T} = \hat{\pi}_{j,X_T}$ for $j \leq k_1$, otherwise $\hat{\pi}'_{j,X_T} = 0$. For $\boldsymbol{Y}_T$, the same conditions are valid.

Maharaj (2000) proposed a similarity distance for invertible and stationary autoregressive moving average models (ARMA). The Maharaj distance is given as follows (Maharaj, 2000):

$$d_{AR.MAH}(\boldsymbol{X}_T, \boldsymbol{Y}_T) = \sqrt{T}\left(\widehat{\boldsymbol{\Pi}}'_{X_T} - \widehat{\boldsymbol{\Pi}}'_{Y_T}\right)^T \widehat{\boldsymbol{V}}^{-1} \left(\widehat{\boldsymbol{\Pi}}'_{X_T} - \widehat{\boldsymbol{\Pi}}'_{Y_T}\right) \tag{3.47}$$

where $\widehat{\boldsymbol{\Pi}}'_{X_T}$ and $\widehat{\boldsymbol{\Pi}}'_{Y_T}$ are the estimated model parameters of fitted time series of $\boldsymbol{X}_T$ and $\boldsymbol{Y}_T$. $\widehat{\boldsymbol{V}}$ is the estimator of

$$\boldsymbol{V} = \sigma^2_{X_T} \boldsymbol{R}^{-1}_{X_T}(k) + \sigma^2_{Y_T} \boldsymbol{R}^{-1}_{Y_T}(k) \tag{3.48}$$

where $\sigma^2_{X_T}$ and $\sigma^2_{Y_T}$ are the variances of the white noise processes, and $\boldsymbol{R}_{X_T}$ and $\boldsymbol{R}_{Y_T}$ are the sample covariance matrices of the time series of $\boldsymbol{X}_T$ and $\boldsymbol{Y}_T$, respectively.

In Kalpakis et al. (2001), the linear predictive coding (LPC) cepstrum of time series is used to get clusters of ARIMA models. Therefore, the significant features of time series could be extracted. The similarity measure of cepstral-based distance is conducted to calculate the Euclidean distances between the LPC cepstral coefficients of time series, $\boldsymbol{X}_T$ and $\boldsymbol{Y}_T$. For instance, when $\boldsymbol{X}_T$ is fitted to AR(p) model, $X_t = \sum_{r=1}^{p} \emptyset_r X_{t-r} + \varepsilon_t$, $\emptyset_r$ is the autoregression coefficients and ε_t is white noise with mean zero and non-zero variance. By using the autoregression coefficients, the cepstral coefficients (ψ) are computed as follows (Kalpakis et al., 2001):

$$\psi_{h_c} = \begin{cases} \emptyset_1 & \text{if } h_c = 1 \\ \emptyset_{h_c} + \sum_{m=1}^{h_c-1} \left(\emptyset_m - \psi_{h_c-m}\right) & \text{if } 1 < h_c \leq p \\ \sum_{m=1}^{p} \left(1 - \frac{m}{h_c}\right) \emptyset_m \psi_{h_c-m} & \text{if } p < h_c \end{cases} \tag{3.49}$$

where h_c is the number of coefficients, and p represents the order of AR(p) model. Regarding this, the cepstral-based distance (LPC.CEP) is obtained as follows:

$$d_{LPC.Cep}(\boldsymbol{X}_T, \boldsymbol{Y}_T) = \sqrt{\sum_{i=1}^{T} \left(\psi_{i,X_T} - \psi_{1,Y_T}\right)^2} \tag{3.50}$$

3.3.3.3. Clustering Algorithm of Hierarchical Ward's Method

As outlined in Ward (1963), the hierarchical Ward's method is a member of agglomerative hierarchical clustering algorithm which follows steps of clustering procedure that, firstly, *n* number of single-membered clusters are formed which means that each precipitation station is located separately in one cluster and finally, one cluster including all station is created based on the hierarchical structure. While applying this procedure, the similarity measures are used to calculate distances between stations to form a matrix, called distance matrix. During the agglomerative hierarchical clustering, the stations which are close to each other are merged based on the values in distance matrix and step by step, new clusters are produced. At each step, distance matrices are recomputed by using the new cluster and the other clusters and merging process is executed up to reach the largest cluster of involving all stations.

This procedure aims to minimize the increment in the total error sum of square (*E*) within each cluster. This increment is the squared Euclidean distance between cluster centers and *E* is calculated as follow (Ward, 1963):

$$E = \sum_{m=1}^{g} E_m \tag{3.51}$$

where

$$E_m = \sum_{l=1}^{n_m} \sum_{k=1}^{p_k} \left(x_{ml,k} - \bar{x}_{m,k}\right)^2 \tag{3.52}$$

in which $\bar{x}_{m,k}$ is the mean of the *m*-th cluster for the *k*-th variable, $x_{ml,k}$ is the score on the *k*-th variable for the *l*-th object in the *m*-th cluster, where $k = 1, \ldots, p$; $l = 1, \ldots, n_m$; and $m = 1, \ldots, g$. Generally, the results of hierarchical clustering are presented in a dendrogram or a tree diagram which illustrates the clustering process of how the clusters are merged. The clustering of the stations is carried out by cutting the dendrogram at the desired height and separate from the nodes to form clusters.

Hosking and Wallis (2005) recommended to use Ward's agglomerative hierarchical clustering method while identifying the homogeneous regions in RFA in order to utilize its property to create equal-sized clusters as much as possible. Moreover, since the dendrograms give opinion about the number of clusters, there is no common approach for this issue. Therefore, in this study, R package *NbClust* (Charrad et al., 2014) which employs 30 different indices is preferred to determine the optimum number of clusters according to the majority rule based on the results of indices.

3.3.3.4. Heterogeneity Measure

Heterogeneity measure is used to assess the homogeneity degree of sub-regions after the delineation of homogeneous regions by the clustering analysis. This measure conducts Monte Carlo simulation processes to create numerous simulations of homogeneous regions consisting of the precipitation stations with the same number of observation records as the real stations. Then, the four-parameter Kappa distribution is fitted to the series in terms of the regional average L-moment ratios and N_{sim}

number of simulated regions are generated. The *V*-statistic is computed for each region as follows (Hosking and Wallis, 2005):

$$V = \left\{ \frac{\sum_{i=1}^{N} n_i (L_{CV}^{(i)} - L_{CV}^{R})^2}{\sum_{i=1}^{N} n_i} \right\}^{1/2} \tag{3.53}$$

in which *N* is the number of stations in the region, n_i is the length of observation records in station *i*, $L_{CV}^{(i)}$ is the sample coefficient of L-variation for station *i* and L_{CV}^{R} is the average regional coefficient of L-variation.

Let μ_V and σ_V are the mean and standard deviation of *V*-statistics, respectively, the heterogeneity measure is calculated from N_{sim} number of simulations:

$$H = \frac{(V - \mu_V)}{\sigma_V} \tag{3.54}$$

As given in Hosking and Wallis (2005), the assessment of the homogeneity of a region is depended on the *H*-statistic. When $H < 1$, the region is called "acceptably homogeneous"; when $1 \leq H < 2$, the region becomes "possibly heterogeneous"; and finally, when $H \geq 2$, the region is accepted to be "definitely heterogeneous".

3.3.4. Comparison of Clustering Approaches

Since there exist several clustering approaches based on different assumptions with several limitations, the final clusters to be determined could differ. For this reason, applying the uncertainty analysis and comparison of clustering approaches are vital issue and necessary to reach the best clustering. In this context, a jackknife validation procedure (Miller, 1964; Shao and Tu, 1995) is applied to evaluate the performance of the previously mentioned clustering approaches. According to the procedure, each station is assumed as ungauged and excluded from the analysis instantaneously. Next, the quantiles for different return periods are estimated by using the regional frequency analysis regarding the different alternatives of homogeneous regions. Finally, the RFA results of different clustering approaches are assessed by using the five different performance evaluation statistics: absolute bias (AB), relative bias (RB), root mean

square error (RMSE), relative root mean square error (RRMSE), and Nash criterion (NASH). The equations of these statistics are presented as follows:

$$AB = \frac{1}{N}\sum_{i=1}^{N}\left|Q_i(t) - \hat{Q}_i(t)\right| \tag{3.55}$$

$$RB = \frac{1}{N}\sum_{i=1}^{N}\frac{Q_i(t) - \hat{Q}_i(t)}{Q_i(t)} \times 100\% \tag{3.56}$$

$$RMSE = \sqrt{\frac{1}{N}\sum_{i=1}^{N}\left(Q_i(t) - \hat{Q}_i(t)\right)^2} \tag{3.57}$$

$$RRMSE = \sqrt{\frac{1}{N}\sum_{i=1}^{N}\left(\frac{Q_i(t) - \hat{Q}_i(t)}{Q_i(t)}\right)^2} \times 100\% \tag{3.58}$$

$$NASH = 1 - \frac{\sum_{i=1}^{N}\left(Q_i(t) - \hat{Q}_i(t)\right)^2}{\sum_{i=1}^{N}(Q_i(t) - \bar{Q}(t))^2} \tag{3.59}$$

where *N* is the total number of stations, $Q_i(t)$ is the local (at-site) estimate, $\hat{Q}_i(t)$ is the regional estimate at the non-exceedance probability *t* for station-*i*, and $\bar{Q}(t)$ is the mean of local estimates of the *N* stations. Therefore, the comparison of the quantile estimates in regional frequency analysis and local frequency analysis is carried out. In the local frequency analysis, only the Log-Pearson Type III distribution is fitted to the data sets of all stations relying on the same parameter estimation method. This decision is made to eliminate the effects of using different local frequency distributions and ensure that the possible errors are due to the regionalization only (Merz and Blöschl, 2005).

As applied in Wazneh et al. (2015), there are some assumptions for the jackknife validation procedure which are also valid for this study. For instance, the observation length of the stations is adequate to make reliable quantile estimates for the larger

return periods. The data series are independent, stationary, and homogeneous and can be employed for comparison purposes in performance assessment of RFA. Also, if any precipitation station has an observation period of more than 15 years, it could verify the assumptions (Wazneh et al., 2015). At the end, the best clustering is decided and the homogeneous sub-regions are formed based on the results of jackknife procedure. The remaining steps in RFA, e.g. determination of frequency distribution for each homogeneous sub-region, quantile estimates for different return periods, and assessment of the estimates are executed according to the best clustering approach.

3.3.5. Goodness-of-fit and Growth Curves

In order to choose the most suitable frequency distribution i.e. growth curve for each homogeneous region, a goodness-of-fit measure and L-moment ratio diagram are required. In this context, three-parameter frequency distributions, such as generalized logistic (GLO), generalized extreme value (GEV), generalized normal (GNO), generalized Pareto (GPA), and Pearson type III (PE3), are among the alternatives. Hosking and Wallis (2005) do not recommend the use of two-parameter distributions in RFA due to the increasing probability of estimating biased quantiles. Besides, the four-parameter Kappa and five-parameter Wakeby distributions could be used in some cases where three-parameter distributions are not appropriate.

Hosking and Wallis (2005) presented a goodness-of-fit measure (Z^{DIST}) relied on the difference among the L-kurtosis of the candidate distribution (L_{kur}^{DIST}) and L-kurtosis of the regional weighted average (L_{kur}^{R}). The goodness-of-fit measure is calculated from:

$$Z^{DIST} = \frac{(L_{kur}^{DIST} - L_{kur}^{R} + B_4)}{\sigma_4} \tag{3.60}$$

where B_4 is the bias of L_{kur}^{R} and computed from:

$$B_4 = N_{sim}^{-1} \sum_{m=1}^{N_{sim}} (L_{kur}^{[m]} - L_{kur}^{R}) \tag{3.61}$$

where N_{sim} is the number of simulated regional data and $L_{kur}^{[m]}$ is the regional average L-kurtosis for the *m*-th simulated region. The standard deviation of L_{kur}^{R}, σ_4, is calculated as follows (Hosking and Wallis, 2005):

$$\sigma_4 = \left[(N_{sim} - 1)^{-1} \left\{ \sum_{m=1}^{N_{sim}} \left(L_{kur}^{[m]} - L_{kur}^{R} \right)^2 - N_{sim} B_4^2 \right\} \right]^{1/2} \tag{3.62}$$

When Z^{DIST} is about zero, the candidate distribution is the most suitable distribution for the homogeneous region. The acceptable range of this measure is $|Z^{DIST}| \leq 1.64$ at 90% significance level (Hosking and Wallis, 2005).

Furthermore, plotting the L-moment ratio diagram lead to interpret how close is the regional average L-moment ratios and the theoretical curves of the candidate distributions. As a result of this comparison, the best fit distribution could be decided visually and used as a preliminary remark in particular besides the goodness-of-fit measure.

3.3.6. Accuracy of Quantile Estimates

Let *N* be the number of stations in a region and each station-*i* has data sets of observed data Q_{ij} $(j = 1, \dots, n_j)$, sample size of n_j, and the quantile functions of the frequency distribution, $Q_i(F)$. The essential assumption of the index-flood method is that the frequency distribution of all stations in the same homogeneous region is identical and differ only in a site-specific scale factor, known as index-flood. The quantile of non-exceedance probability *F* at station-*i* is calculated as follows (Hosking and Wallis, 2005):

$$Q_i(F) = \mu_i q(F), \quad i = 1, \dots, N. \tag{3.63}$$

in which μ_i is the index-flood and $q(F)$ is a dimensionless regional quantile function (i.e. regional growth curve). Mostly, the scaling factor of index-flood is estimated by calculating the sample mean of data series at station-*i* (Stedinger, 1983; Lettenmaier and Potter, 1985).

The evaluation of the quantile estimates is conducted by utilizing Monte Carlo simulation. As detailed in Hosking and Wallis (2005), while creating simulated regions, they have to reflect the same characteristics with the real data, such as the same number of stations, observation length, regional average L-moment ratios, heterogeneity, intersite dependence, etc. In the simulations, the regional growth curves and the estimation of quantiles for different return periods are calculated. Next, the relative root mean square error (RRMSE) is to be determined (Hosking and Wallis, 2005):

$$RRMSE_i^F = \left[M^{-1} \sum_{m=1}^{M} \left\{ \frac{\hat{Q}_i^{[m]} - Q_i(F)}{Q_i(F)} \right\}^2 \right]^{1/2} \tag{3.64}$$

where $\hat{Q}_i^{[m]}$ is the estimation of quantile for nonexceedance probability *F* at the *m*-th repetition over *M* number of repetitions (generally 1,000 or 10,000) at station-*i*. The regional average RRMSE of the estimated quantile is obtained from:

$$RRMSE_R^F = N^{-1} \sum_{i=1}^{N} RRMSE_i^F \tag{3.65}$$

3.4. Hydrological Modelling

The main aim of hydrological modelling is to obtain runoff hydrographs and for different return periods considering extreme precipitation events to supply inputs to the hydrodynamic model. The upstream inflows to the hydraulic model is estimated by developing rainfall-runoff models due to the streamflow data scarcity in the catchments of Kanlıköy and Gönyeli Ponds.

3.4.1. Representative Hyetographs

The representative hyetographs for different return periods can be used as temporal distribution of extreme precipitation events. In order to estimate the runoff hydrographs, creation of such hyetographs is a prerequisite. In this study, firstly, the hourly precipitation data of representative stations (Lefkoşa Station and Alevkaya Station) are analysed and the percentages of the total precipitation quantity during 24-hour period is obtained. For each two-hour period, a percentage of total precipitation is determined. The precipitation pattern of each station is then determined. Herein, only the events which are greater than 10 mm are considered during the analysis and the hyetograph of the flood day is saved as the design hyetograph.

Finally, the average of the percentage distribution of these stations are taken to determine the final hyetograph which represent the precipitation characteristics of the study area. Therefore, the effect of the mountainous and flat regions on the precipitation characteristics are reflected. For generating different representative hyetographs corresponding to various return periods, the results from the regional frequency analysis of daily precipitation series are used. These daily values are distributed based on the percentages and the final design hyetographs are formed.

3.4.2. The Hydrologic Modelling System (HEC-HMS)

The Hydrologic Modelling System, HEC-HMS model is employed to simulate rainfall-runoff processes (USACE, 2001) through two basic components, basin model and meteorological model. The basin model can be defined as the physical representation of a catchment by defining the precipitation loss methods, such as Green-Ampt, initial and constant losses, SCS CN, etc.; transformation of rainfall to runoff methods, such as Clark's unit hydrograph, SCS unit hydrograph, Snyder's unit hydrograph, etc.; and baseflow separation methods, such as recession curve, non-linear Boussinesq reservoir, etc. Besides, the meteorological model needs the meteorological properties, such as precipitation, evapotranspiration, temperature, etc., or directly specified hyetograph.

The following methods are preferred to form the components of the rainfall-runoff model for the study area. Main factors for selecting these methods are suitability and limitations of the methods and data sets considering the properties of the catchments.

3.4.2.1. SCS Curve Number Method

The Soil Conservation Service (SCS) curve number (CN) (SCS, 1972) is a widely-used method to compute losses of precipitation. Due to its simplicity and providing good results even in complex catchments, SCS CN method is used to estimate precipitation excess as follows (Singh and Seth, 1984):

$$P_e = \frac{(P - I_a)^2}{(P - I_a) + S} \tag{3.66}$$

where P_e is the accumulated precipitation excess at time *t*; P is the accumulated rainfall depth at time *t*; I_a is the initial abstraction; and S is the potential maximum retention. The SCS provides an empirical relation between the I_a and S as:

$$I_a = 0.2S \tag{3.67}$$

Then, the expression of P_e becomes:

$$P_e = \frac{(P - 0.2S)^2}{P + 0.8S} \tag{3.68}$$

The maximum potential retention has a relationship with watershed characteristics in terms of curve number as follows:

$$S = \frac{25400}{CN} - 254 \tag{3.69}$$

Here, CN is determined according to the land use and soil properties of catchment. The SCS categorized soils into four hydrological soil groups from A (low runoff potential) to D (high runoff potential) based on the soil textures (SCS, 1986). Also,

land use groups are defined by SCS to represent the permeability. Moreover, for the catchments which have a different soil groups and land covers, a composite CN could be calculated as follows:

$$CN_{composite} = \frac{\sum(A_{c_i} CN_i)}{\sum A_{c_i}} \tag{3.70}$$

where CN_i is the curve number for subdivision *i* and A_{c_i} is the area of subdivision *i*.

3.4.2.2. SCS Unit Hydrograph Method

The Soil Conservation Service Unit Hydrograph method (Mishra and Singh, 2013) is used to estimate the runoff hydrographs in ungauged catchments. The unit hydrograph (UH) peak discharge in m^3/s is calculated from:

$$Q_p = \frac{2.08 A_c}{t_p} \tag{3.71}$$

where, A_c is the catchment drainage area (km^2); and t_p is the time to peak (hr) which is computed from:

$$t_p = \frac{t_r}{2} + t_l \tag{3.72}$$

where t_r is the duration of excess rainfall (hr) and t_l is the catchment lag time (hr) which is expressed as:

$$t_l = \frac{L^{0.8}(S+1)^{0.7}}{1900 S_h^{0.5}} \tag{3.73}$$

where L is the length of main stream channel (ft), S is the the potential maximum retention (inch), and S_h is the average catchment land slope (%).

3.4.3. Reservoir Routing

When analysing the propagation of flood wave in a reservoir, the continuity equation in system is considered with the flow equation in outlet (Basha, 1994). Therefore, the basic continuity equation can be expressed as:

$$\frac{dS}{dt} = I(t) - Q(t) \tag{3.74}$$

where dS/dt is the rate of storage (S) change, $I(t)$ and $Q(t)$ is the inflow and outflow hydrographs, respectively. Herein, $I(t)$ is generally known as a function of time. However, subsequent S and $Q(t)$ values are unknown. Therefore, $dS = A(h)dh$ is defined as a differential storage at any h water level in reservoir in which the reservoir surface area, $A(h)$, can be obtained from the relation of elevation-area-volume. Then, outflow can be given as the function of h for spillways and the bottom outlet and the new continuity equation becomes (Yanmaz, 2018):

$$\frac{dh}{dt} = \frac{I(t) - Q(h)}{A(h)} = f(h,t) \tag{3.75}$$

Since a first order non-linear ordinary differential equation is formed, numerical solutions must be applied to solve it, such as the Euler method used in this study. Therefore, according to the Euler solution technique, based on the known initial water surface level of h_n, the water surface level, h_{n+1}, at the following time level of $t_n + \Delta t$ is calculated from (Yanmaz, 2018):

$$h_{n+1} = h_n + \Delta t * f(h_n, t_n) \tag{3.76}$$

3.5. Digital Elevation Model (DEM)

As presented by Aronoff (1989), a geographical information system (GIS) acts as a tool to analyze, save, demonstrate, modify, and generate spatially varying data sets. Digital elevation model (DEM) is used, particularly in topography representation, by

GIS tools to calculate some essential parameters which are required in hydrological and hydraulic models, such as flow directions, sinks, flow accumulation, slope, drainage line definition, and definition of sub-catchments (Vaze et al., 2010). In DEM, the data are stored in raster format where each cell represents one numerical value of elevation (O'Callaghan and Mark, 1984). Moreover, the hydrological or hydraulic modelling of complex urban environment is a challenging issue (Schubert and Sanders, 2012). Therefore, a high resolution DEM with large amount of raster data is needed to develop accurate models in terms of containing the impacts of terrain surfaces to the flow properties, such as roads and buildings. However, such data sets lead to increase the computational time as well. Moreover, in urban modelling, instead of DEM which is referring to natural surface elevations, digital terrain model (DTM) is preferred which additionally include the roads, trees, buildings, etc. (Meesuk et al., 2014). ESRI's ArcGIS software is used in this study to execute hydrological analysis by using tools, named as the Spatial Analyst and Arc Hydro.

3.5.1. Quality Control of DEM

There are several reasons to cause errors in DEM, such as scarcity of ground measurements, record length, interpolation techniques, and human errors in measurements (Burrough, 1986; Wise, 1988). Thus, likewise other spatial data sets, DEM also requires the quality control analysis to create a reliable model for floodplains. In this context, spatial and statistical assessment of DEM should be performed because the quality of DEM is mainly based on the data source.

As a first step, spatial interpolation techniques are used in order to express the point data on the spatial basis and create a 3D surface. The commonly used interpolation techniques employed in this study are as follows: Inverse Distance Weighting (IDW), Natural Neighbour, Topo to Raster, Triangulated Irregular Network (TIN), Spline, and Spherical Kriging.

Inverse Distance Weighting is an interpolation technique, which is used to estimate the unknown cell values with the help of known sample points. Estimated values are

the function of the distance and magnitude of neighboring points, and the increase in distance reduces the significance and impact on the cell to be estimated. Additionally, this technique should be used in dense sampling data points which are well distributed over the local surface (Childs, 2004).

Natural Neighbour uses the weighted average of neighboring points. It detects the nearest subset of known points for unknown point and assigns weights relied on proportionate areas in order to estimate a value (Sibson, 1981). It works well with clustered data points (Childs, 2004) and other regularly and irregularly spaced data (Watson, 1992; Sambridge et al., 1995).

Topo to Raster, also known as ANUDEM technique, is introduced by Hutchinson (1988) to develop hydrologically correct DEM with constraints to ensure natural drainage surface and retain ridgelines and streams through the input data. Its algorithm is based on an iterative finite distance method and requires input of points, polylines, or polygons data. Particularly, it is developed to work well with contour data (Childs, 2004).

TIN is a technique of surface representation by triangulating a set of points. Points with their known elevations become the nodes and they are connected to each other to form a series of triangles. Generally, the interpolation is performed among these nodes by satisfying the Delaunay triangulation criterion (no vertex inside of the circumcircles of the triangles) to obtain continuous surface (Watson, 1992).

In Spline interpolation technique, the estimation of unknown values are carried out by using a mathematical function to minimize the total surface curvature. Therefore, a smooth surface is obtained considering that generated surface passes exactly through the data points (Childs, 2004).

Kriging technique employs a geostatistical approach that produces a surface based on the elevations of data points (Caruso and Quarta, 1998). Closely located data tend to be more effective than the data located far from the unknown point. Therefore, it seems similar to IDW technique. However, in Kriging, the interpolation does not only

rely on the distance, but also it is the function of spatial autocorrelation among the data points. In this study, one of the most commonly used techniques of spherical kriging, which enable to fit a curve to the semivariance data in semivariogram is selected for the creation of the surface.

Prior to hydrological analysis, interpolated DEMs require understanding the response and physical characteristics of the basin. Therefore, pre-processing of DEM is generally carried out by using Arc Hydro tool of ArcGIS software in order to perform fill sinks, flow direction, flow accumulation, stream definition, stream segmentation, and catchment delineation (Maidment and Morehouse, 2002). Briefly, the definitions of these steps are given in Table 3.2.

Table 3.2. Definition of Steps in Pre-processing of DEM (Maidment and Morehouse, 2002)

Step	Definition
Fill sinks	To modify depression cells which are surrounded by the higher elevated cells
Flow direction	To determine the flow direction of each grid among the eight possible cell options
Flow accumulation	To compute the accumulated number of cells which drains to target cell
Stream definition	To define a stream network based on the predefined cell value
Stream segmentation	To characterize stream segments
Watershed delineation	To identify sub-catchments relied on stream segment

In the statistical assessment carried out in this thesis, the data of road elevations, fieldwork measurements, and contours are used to generate six different DEMs with the same spatial resolution of 3 m by 3 m. Here, all data measurements are assumed as correct and randomly selected 80% of this data are used for generating the DEMs. The 20% of data are separated for the validation of estimates. In order to assess the accuracy of the interpolation techniques, mean absolute error (MAE), mean square error (MSE), mean absolute percentage error (MAPE), and root mean square error (RMSE) are employed. These four statistics are given as follows where Z_{data} and Z_{est} are the actual elevations and estimated elevations, respectively, with n number of data (Quattrochi et al., 2017):

$$MAE = \frac{1}{n}\sum_{t=1}^{n}|Z_{data} - Z_{est}| \quad (3.77)$$

$$MSE = \frac{1}{n}\sum_{t=1}^{n}(Z_{data} - Z_{est})^2 \quad (3.78)$$

$$MAPE = \frac{100\%}{n}\sum_{t=1}^{n}\left|\frac{Z_{data} - Z_{est}}{Z_{data}}\right| \quad (3.79)$$

and $RMSE$ is calculated by using Equation 3.1.

3.5.2. Creation of DTM

Generally, in a floodplain of an urban area, overland flow transports on the roads through the buildings, which affect the flow direction. For this reason, accurate representation of roads and buildings are necessary to obtain reliable results of flood extent, flow velocities, and flow depths. Due to the data limitation in buildings' heights, representation of the buildings is carried out by defining the buildings' footprints as polygons and excluding them from the study area. Therefore, when water flows on the floodplain, buildings act like a solid object and let water to pass around them.

The topographical maps of 1: 25,000 and 1: 5,000 scales are used to create the DTMs of Kanlıköy and Gönyeli pond catchments and the urbanized regions, respectively. For the representation of roads, the point measurements taken from municipalities are used. After determination of the most appropriate interpolation technique for the study area, raster data with rectangular grid representation is created to represent the 2D surface of the floodplain. Then, the erroneous elevations and sinks are detected and altered based on the raster analysis and expert knowledge on the topography of the study area. At the end, the DTM surface is formed with 3 m grid for easier application and modification processes of hydrodynamic modelling. Besides, by using the DEM

of pond catchments, the catchment area, average catchment slope, percent of imperviousness, and the longest flow path are computed by the application of pre-processing of DEM. These inputs are provided for the rainfall-runoff modelling of HEC-HMS.

CHAPTER 4

HYDRAULIC METHODOLOGY

This chapter explains the methodologies employed by MIKE 11, MIKE 21, and MIKE FLOOD softwares for hydraulic modelling, model development steps of the study area and the remedial structural measures for flood protection of Nicosia.

4.1. Theoretical Background

In hydraulic modelling, the fluid motion can be represented by solving the governing equations developed by employing continuity and equations of motion, also known as Navier-Stokes equations. However, fluids in motion which are under the effect of gravity and pressure, are difficult to represent mathematically in hydrodynamics. Therefore, the experiments, field observations, and simplifications are required (Jordaan and Bell, 2009). The Saint-Venant equations become simpler form of Navier-Stokes equations to apply in numerical models considering several assumptions and the software like SOBEK, HEC-RAS, and MIKE simulate the hydrodynamic flow by solving these equations. In this study, a software developed by Danish Hydraulic Institute, called as MIKE FLOOD is used to execute the hydraulic modelling. MIKE 11 for 1D river model and MIKE 21 for 2D surface model are combined through the interface of MIKE FLOOD to maximize the simulation efficiency in terms of accurate simulation results and less computational time.

The simulation of fluid motion is carried out by solving the continuity and the Navier-Stokes equations. The continuity equation is as follows (Shames, 2003):

$$\frac{\partial \rho}{\partial t}+\frac{\partial u}{\partial x}+\frac{\partial v}{\partial y}+\frac{\partial w}{\partial z}=0 \tag{4.1}$$

where ρ is the density of fluid, u, v, and w are depth-averaged velocity components in x-direction, y-direction, and z-direction, respectively. In Cartesian coordinates (x, y, z), the Navier-Stokes equations are given as:

$$\rho g+\frac{\partial \sigma_{xx}}{\partial x}+\frac{\partial \tau_{yx}}{\partial y}+\frac{\partial \tau_{zx}}{\partial z}=\rho\left(\frac{\partial u}{\partial t}+u\frac{\partial u}{\partial x}+v\frac{\partial u}{\partial y}+w\frac{\partial u}{\partial z}\right) \tag{4.2}$$

$$\rho g+\frac{\partial \tau_{xy}}{\partial x}+\frac{\partial \sigma_{yy}}{\partial y}+\frac{\partial \tau_{zy}}{\partial z}=\rho\left(\frac{\partial v}{\partial t}+u\frac{\partial v}{\partial x}+v\frac{\partial v}{\partial y}+w\frac{\partial v}{\partial z}\right) \tag{4.3}$$

$$\rho g+\frac{\partial \tau_{xz}}{\partial x}+\frac{\partial \tau_{yz}}{\partial y}+\frac{\partial \sigma_{zz}}{\partial z}=\rho\left(\frac{\partial w}{\partial t}+u\frac{\partial w}{\partial x}+v\frac{\partial w}{\partial y}+w\frac{\partial w}{\partial z}\right) \tag{4.4}$$

where g is the gravitational acceleration, σ is the normal stress and τ is the shear stress. The stresses related to deformation rates for an incompressible fluid are given as:

$$\sigma_{xx}=-p+2\mu\frac{\partial u}{\partial x} \qquad \sigma_{yy}=-p+2\mu\frac{\partial v}{\partial y} \qquad \sigma_{zz}=-p+2\mu\frac{\partial w}{\partial z} \tag{4.5}$$

$$\tau_{xy}=\tau_{yx}=\mu\left(\frac{\partial u}{\partial y}+\frac{\partial v}{\partial x}\right) \tag{4.6}$$

$$\tau_{yz}=\tau_{zy}=\mu\left(\frac{\partial v}{\partial z}+\frac{\partial w}{\partial y}\right) \tag{4.7}$$

$$\tau_{zx}=\tau_{xz}=\mu\left(\frac{\partial w}{\partial x}+\frac{\partial u}{\partial z}\right) \tag{4.8}$$

in which p is the fluid pressure and μ is the dynamic viscosity. Substituting equations 4.5-4.8 into 4.2-4.4, the Navier-Stokes equations are formed as:

$$\rho\left(\frac{\partial u}{\partial t}+u\frac{\partial u}{\partial x}+v\frac{\partial u}{\partial y}+w\frac{\partial u}{\partial z}\right)=-\frac{\partial p}{\partial x}+\rho g+\mu\left(\frac{\partial^2 u}{\partial x^2}+\frac{\partial^2 u}{\partial y^2}+\frac{\partial^2 u}{\partial z^2}\right) \quad (4.9)$$

$$\rho\left(\frac{\partial v}{\partial t}+u\frac{\partial v}{\partial x}+v\frac{\partial v}{\partial y}+w\frac{\partial v}{\partial z}\right)=-\frac{\partial p}{\partial y}+\rho g+\mu\left(\frac{\partial^2 v}{\partial x^2}+\frac{\partial^2 v}{\partial y^2}+\frac{\partial^2 v}{\partial z^2}\right) \quad (4.10)$$

$$\rho\left(\frac{\partial w}{\partial t}+u\frac{\partial w}{\partial x}+v\frac{\partial w}{\partial y}+w\frac{\partial w}{\partial z}\right)=-\frac{\partial p}{\partial z}+\rho g+\mu\left(\frac{\partial^2 w}{\partial x^2}+\frac{\partial^2 w}{\partial y^2}+\frac{\partial^2 w}{\partial z^2}\right) \quad (4.11)$$

In order to represent the overland flow in floodplain, the simplified form of the equations above for 2D modelling will be discussed in Section 4.1.2.

4.1.1. 1D Modelling

Based on the conservation of mass and momentum, the Saint Venant equations can be used to estimate the water levels and discharge values through the river with the upstream and downstream boundary conditions (Chanson, 2004). The Saint-Venant equations relying on the assumptions of small bed slope, depth averaged flow velocities, and the hydrostatic pressure are given as:

$$\frac{\partial A_{CS}}{\partial t}+\frac{\partial Q}{\partial x}=0 \quad (4.12)$$

$$\frac{\partial Q}{\partial x}+\frac{\partial}{\partial x}(uQ)+gA_{CS}\left(\frac{\partial h}{\partial x}-S_0\right)+gAS_f=0 \quad (4.13)$$

where A_{CS} is the cross-sectional flow area, Q is the discharge, S_0 is the channel bed slope, and S_f is the friction slope. In MIKE 11 which is used in this study to simulate 1D flow, the vertically integrated equations of conservation of mass and momentum or Saint-Venant equations are solved depending on some assumptions: incompressible

and homogeneous water, small bottom slope, large wave lengths compared to water depth, and subcritical flow conditions. The basic equations in MIKE 11 are as follows:

$$\frac{\partial A_{CS}}{\partial t} + \frac{\partial Q}{\partial x} = q \tag{4.14}$$

$$\frac{\partial Q}{\partial t} + \frac{\partial \left(\alpha \frac{Q^2}{A_{CS}}\right)}{\partial x} + gA\frac{\partial h}{\partial x} + \frac{gQ|Q|}{C^2 A_{CS} R_h} = 0 \tag{4.15}$$

where α is the momentum correction coefficient, C is the Chezy's resistance coefficient, and R_h is the hydraulic radius.

The solutions of both equations are found at each time step along the defined river geometry by transforming the equations into implicit finite difference equations. Therefore, the six-point Abbott numerical scheme (Figure 4.1) including a computational grid and alternating *Q*- (discharge) and *h*-points (water level) is used to solve the continuity and momentum equations (DHI, 2011).

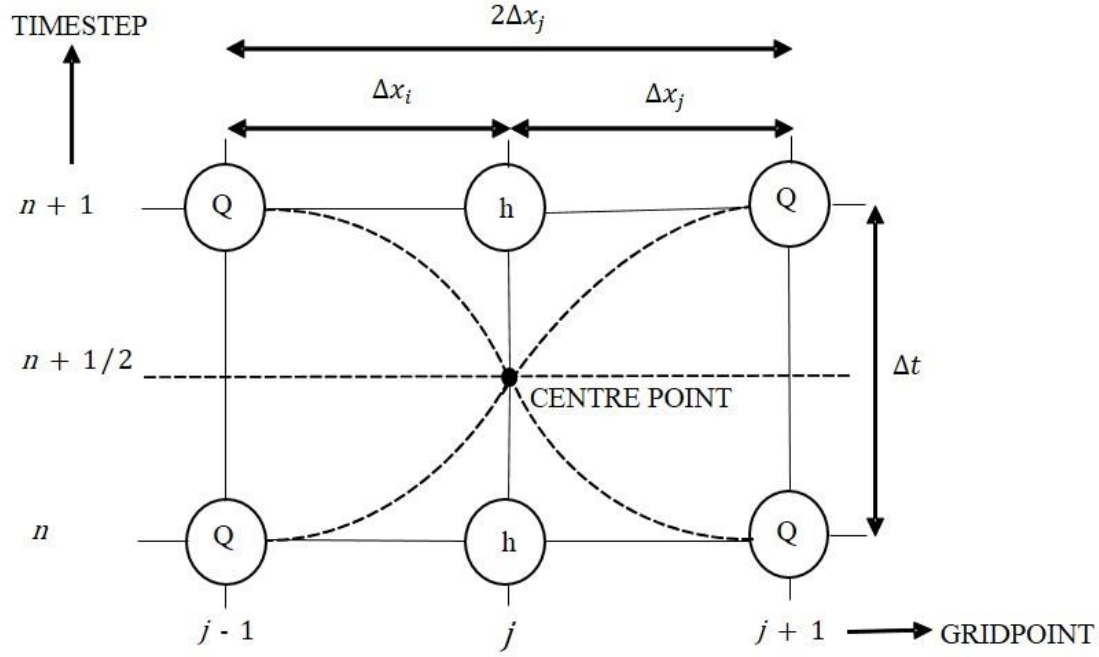

Figure 4.1. Centred 6-point Abbott scheme (DHI, 2011)

4.1.2. 2D Modelling

In order to describe the overland flow, 2D Saint-Venant equations can be used as:

$$\frac{\partial h}{\partial t}+\frac{\partial (hu)}{\partial x}+\frac{\partial (hv)}{\partial y}=0 \tag{4.16}$$

$$\frac{\partial (hu)}{\partial t}+\frac{\partial (huu)}{\partial x}+\frac{\partial (hvu)}{\partial y}=\frac{\partial (hT_{xx})}{\partial x}+\frac{\partial (hT_{xy})}{\partial y}-gh\frac{\partial z}{\partial x}-\frac{\tau_{hx}}{\rho} \tag{4.17}$$

$$\frac{\partial (hv)}{\partial t}+\frac{\partial (huv)}{\partial x}+\frac{\partial (hvv)}{\partial y}=\frac{\partial (hT_{xy})}{\partial x}+\frac{\partial (hT_{yy})}{\partial y}-gh\frac{\partial z}{\partial x}-\frac{\tau_{hy}}{\rho} \tag{4.18}$$

where h is the depth of flow, u and v are the depth-averaged velocity components in the *x*- and *y*-directions, respectively, and T_{xx}, T_{xy}, and T_{yy} are the depth-averaged turbulent stresses, τ_{hx} and τ_{hy} are the bed shear stresses, and *z* is the water surface elevation.

In MIKE 21, the conservation of mass and momentum equations are integrated over depth (vertical space) to represent the flow rate and water level variations. The conservation of mass equation is stated as follows (DHI, 2017):

$$\frac{\partial \zeta}{\partial t}+\frac{\partial p}{\partial x}+\frac{\partial q}{\partial y}=q \tag{4.19}$$

The conservation of momentum in *x*-direction is presented as:

$$\frac{\partial p}{\partial t}+\frac{\partial}{\partial x}\left(\frac{p^2}{h}\right)+\frac{\partial}{\partial y}\left(\frac{pq}{h}\right)+gh\frac{\partial \zeta}{\partial x}+\frac{gp\sqrt{p^2+q^2}}{C^2h^2}$$
$$-\frac{1}{\rho_w}\left[\frac{\partial}{\partial x}(h\tau_{xx})+\frac{\partial}{\partial y}(h\tau_{xy})\right]-\Omega_q-fVV_x+\frac{h}{\rho_w}\frac{\partial}{\partial x}(p_a)=0 \tag{4.20}$$

The conservation of momentum in *y*-direction is given as:

$$\frac{\partial q}{\partial t}+\frac{\partial}{\partial y}\left(\frac{q^2}{h}\right)+\frac{\partial}{\partial x}\left(\frac{pq}{h}\right)+gh\frac{\partial \zeta}{\partial y}+\frac{gq\sqrt{p^2+q^2}}{C^2h^2}$$

$$-\frac{1}{\rho_w}\left[\frac{\partial}{\partial y}(h\tau_{yy})+\frac{\partial}{\partial x}(h\tau_{xy})\right]-\Omega_q-fVV_y+\frac{h}{\rho_w}\frac{\partial}{\partial y}(p_a)=0 \quad (4.21)$$

where ζ is the surface elevation, *t* is time; p and q are the flux densities in *x*- and *y*-direction, h is the water depth, g is the acceleration due to gravity, C is the Chezy resistance coefficient, Ω is the Coriolis parameter, V, V_x, and V_y are the wind velocity and components in *x*- and *y*-direction, f is the wind friction factor, ρ_w is the density of water, p_a is the atmospheric pressure, and τ_{xx}, τ_{yy}, τ_{xy} are the components of effective shear stress.

In MIKE 21, the Alternating Direction Implicit (ADI) technique is used to integrate the equations for the conservation of mass and momentum both in a time and space (DHI, 2017). The equations are solved by applying implicit finite difference methods in a staggered grid in x-y space as demonstrated in Figure 4.2.

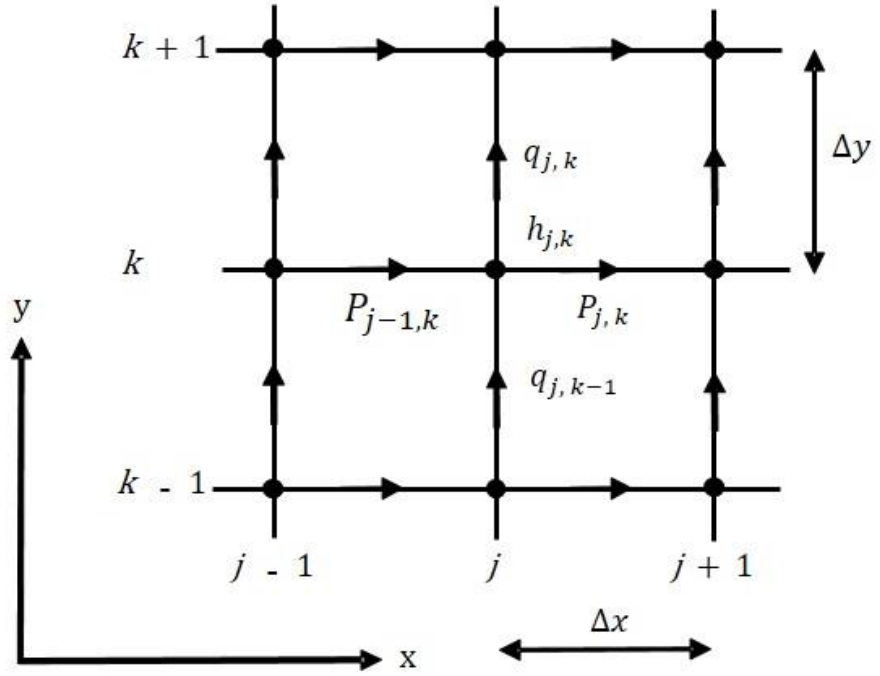

Figure 4.2. Finite difference grid used in the application of the conservation of mass and momentum equations (DHI, 2017)

A Double Sweep (DS) algorithm is used to resolve the equation matrices, which result for each direction and each individual grid. As shown in Figure 4.3, time centering of the three basic equations are solved in one-dimensional sweeps (x-and y- sweeps) and the best approximation is obtained when two sweeps come together at $n + 1/2$.

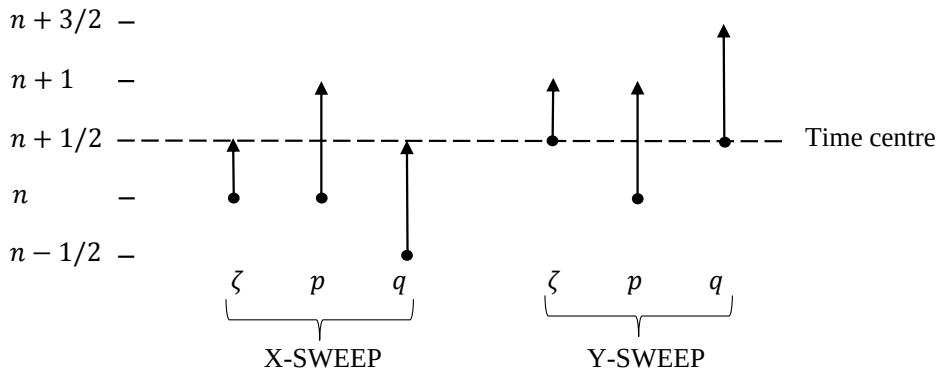

Figure 4.3. Time centering in double sweep algorithm in MIKE 21 (DHI, 2017)

4.1.3. 1D/2D Modelling

Coupling of the 1D river model with the 2D surface model is carried out by using MIKE FLOOD software for this study. The left and the right banks of the 1D model determine the location of lateral links based on the banks of cross-sections in river model as shown in Figure 4.4 and the cell values of the bathymetry in 2D model are used to detect the levee height. When the flow overflows the banks, this phenomenon is represented by using the specified weir equation.

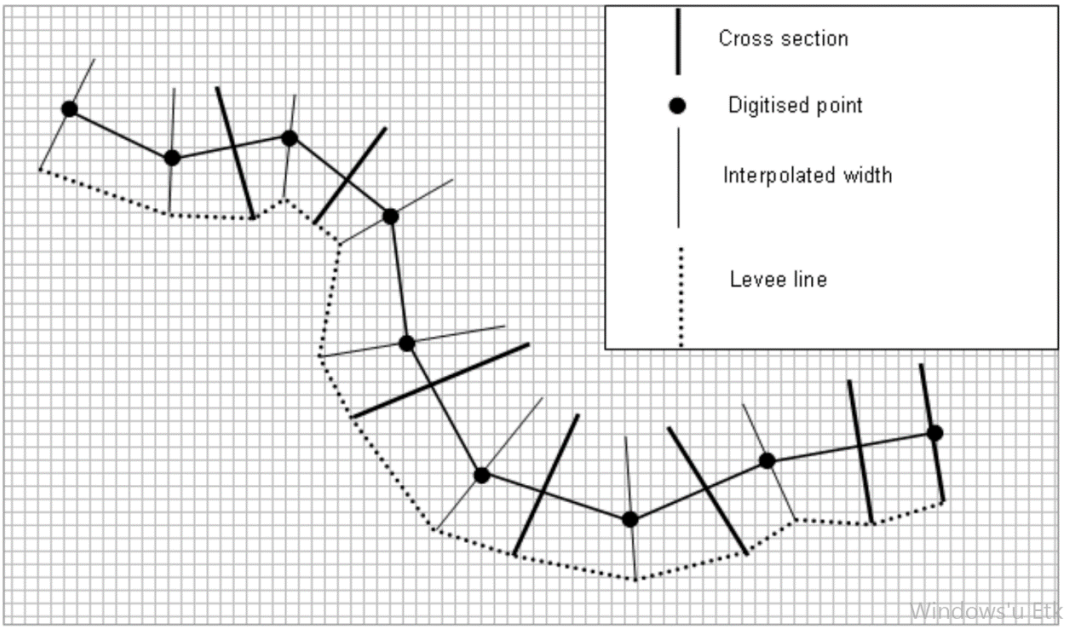

Figure 4.4. Definition of lateral linkage line (DHI, 2017)

The flow transfer to the surface model by enabling the division of lateral link into the many weir substructures. According to the MIKE 11 h-points and the closest MIKE 21 cells, the interpolated water levels are taken as the substructures as given in Figure 4.5.

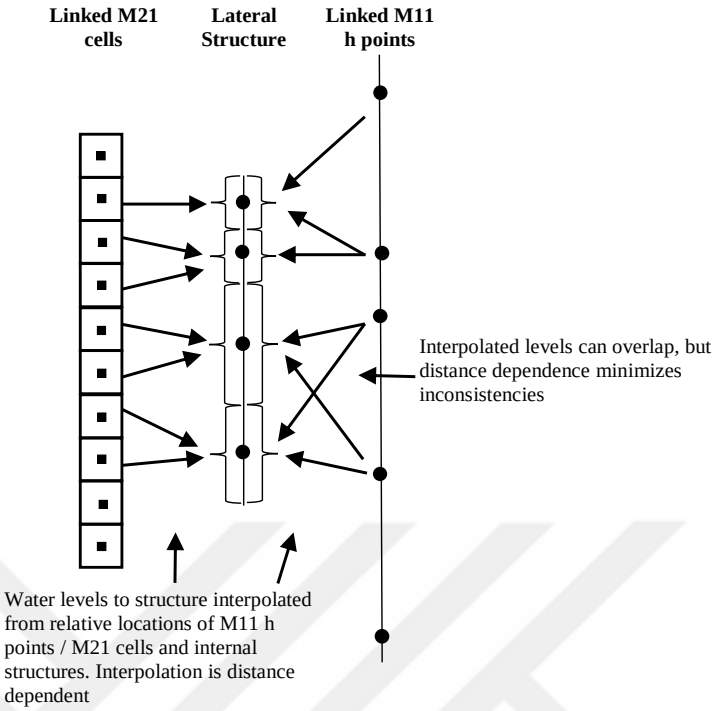

Figure 4.5. Subdivision of lateral link and interpolated water levels (DHI, 2017)

The Courant-Friedrichs-Lewy number (CFL) is a criterion to ensure the stability of a 2D model (DHI, 2017) which may lead to instabilities when it exceeds unity. CFL is expressed as follows (Shames, 2003):

$$CFL = c\frac{\Delta t}{\Delta x} \tag{4.22}$$

where Δt is the time step, Δx is the grid spacing, and c is the celerity. For shallow water, the celerity is calculated as (Shames, 2003):

$$c = \sqrt{gh} \tag{4.23}$$

where g is gravitational acceleration and h is the depth of flow.

4.2. The Model Development

In this section, development of 1D and 2D modelling of Nicosia is presented in detail with the selected parameters and methods.

4.2.1. MIKE 11 Model of Nicosia

4.2.1.1. The River Network

In MIKE 11, river network is created by identifying two branches, the main creek starting from just downstream of Kanlıköy Pond and reaches to the outlet of the study area with a total length of 13.6 km and another creek starting from just downstream of Gönyeli Pond with 5.9 km reach length and connecting to the main creek at the chainage of 11.4 km. First, these creeks are digitized by importing the routes as shape files from ArcGIS software. Since the coordinate system is defined, entering only the first and the last points of branches enable to perform automatical digitizing of creeks. Then, all predefined cross-sections at certain chainages appear automatically on the river network as shown in Figure 4.6.

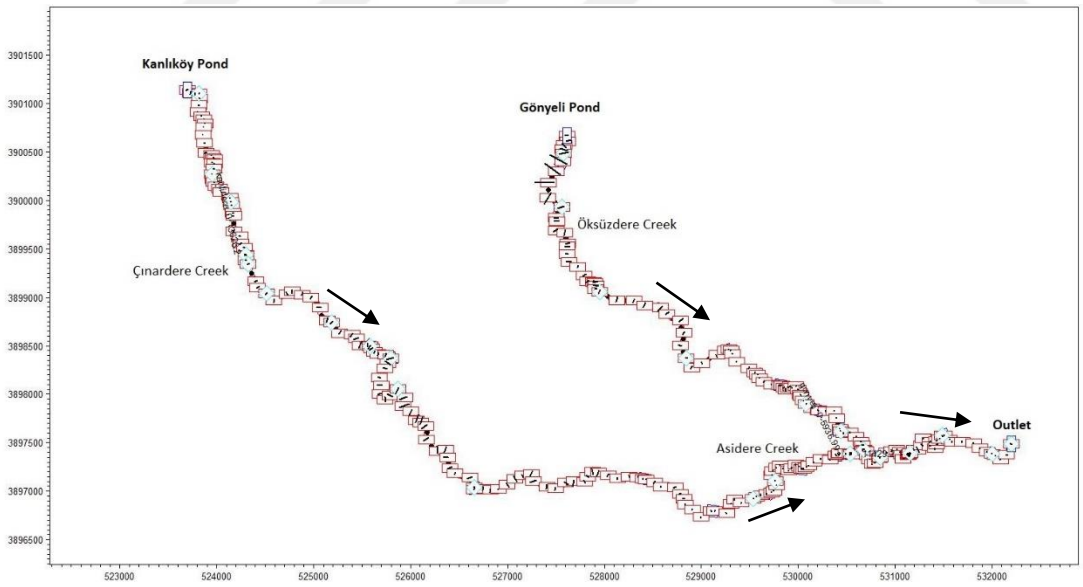

Figure 4.6. River network of MIKE 11

Moreover, hydraulic structures are also added to the river network by this editor. In the study area, there are 24 structures including two primary bridges that crosses the main roads from Nicosia to Güzelyurt and from Nicosia to Girne. In MIKE 11, the bridges are modelled as the combination of a culvert and a weir as illustrated in Figure 4.7. Therefore, when the flow passes under the bridge, it is modelled by considering the phenomena of flow of water through culverts and when the water level reaches the high chord of the bridge deck and overtop it, it is modelled by using the weir flow equations.

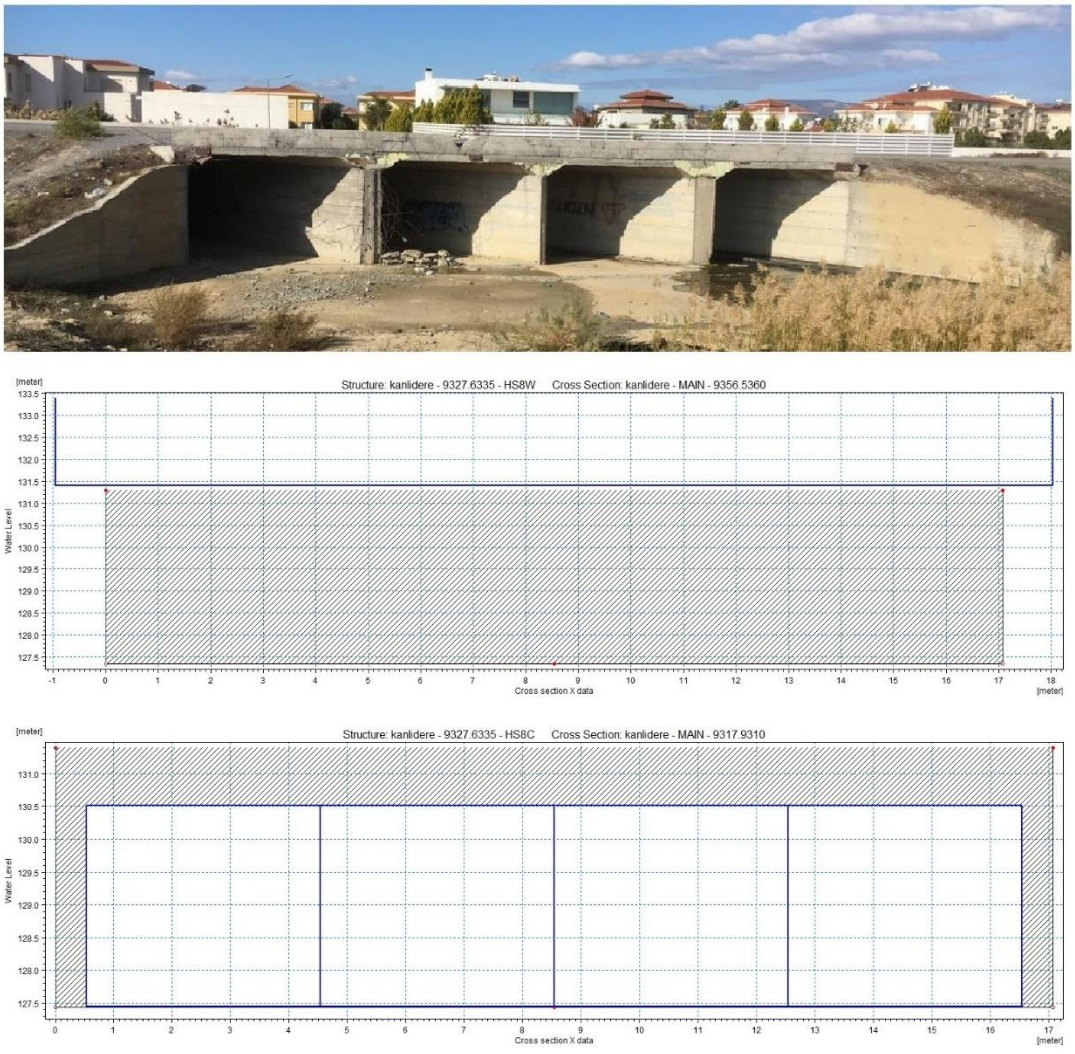

Figure 4.7. A bridge in the study area with the representation of weir and culvert in MIKE 11

4.2.1.2. The Cross-sections

A total of 269 cross-sections on Çınardere, Asidere, and Öksüzdere creeks were collected by the author in a three-month period with a spacing of 30 m to 100 m intervals between cross-sections (Figure 4.8). The average interval of cross-sections was arranged to catch important details along the creeks. In addition, by using the collected raw data, the cross-sections were created and modified in MIKE 11 Cross-section Editor tool (Figure 4.9) in order to better represent the profiles of creeks.

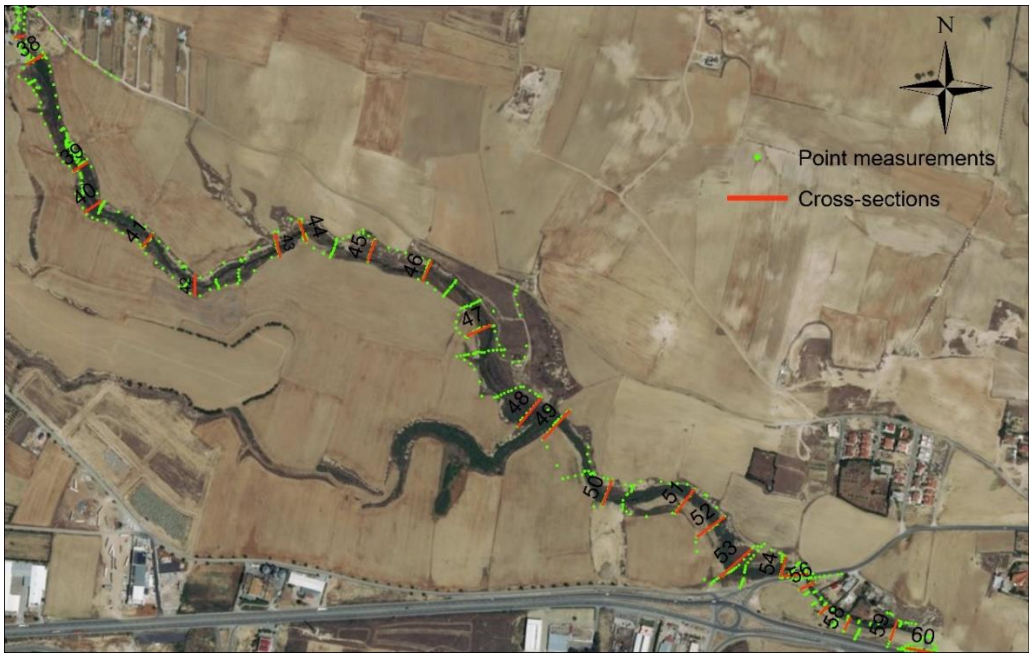

Figure 4.8. Surveying of cross-sections

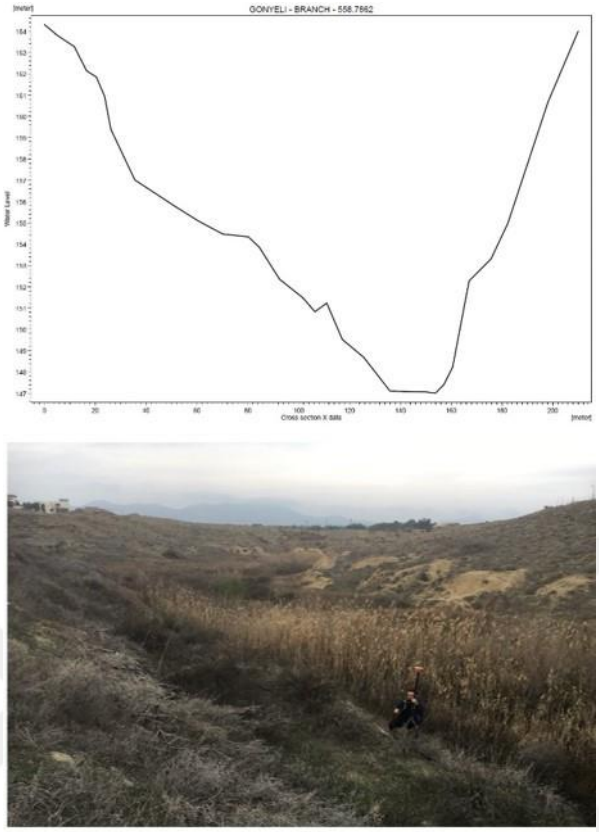

Figure 4.9. Cross-section view from MIKE 11 cross-section editor

4.2.1.3. The Boundary Data

In the model, there are two upstream and one downstream boundary conditions for the floodplain. As mentioned before, for the upstream catchments of ponds, the run-off hydrographs were synthetically generated by utilizing the hydrological models of HEC-HMS. Then, these hydrographs were routed in the pond reservoirs and the inputs were provided for the MIKE 11 model. As given in Figure 4.10, the hydrographs of 2010 flood day for the outlet of Kanlıköy and Gönyeli ponds were used as upstream boundary conditions. Besides, hydrographs of different return periods were also obtained and used as model inputs while executing various scenarios, which will be discussed in the following sections.

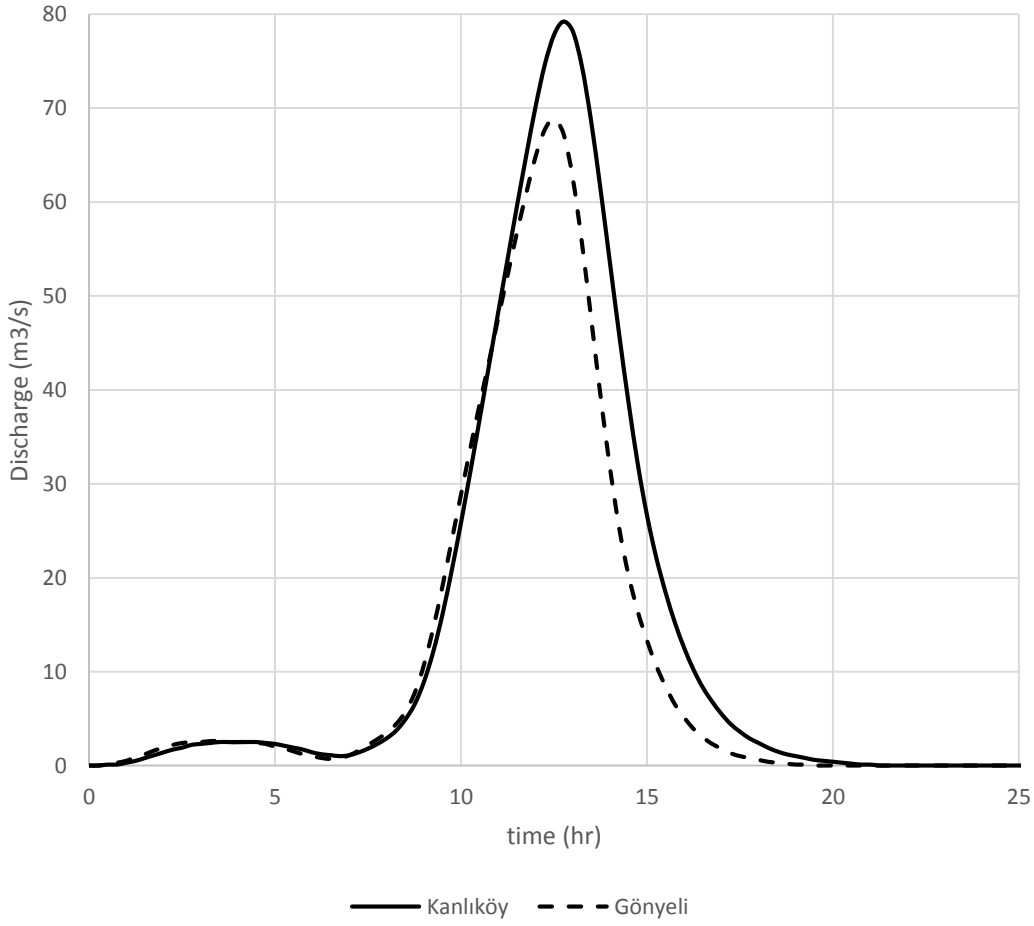

Figure 4.10. Hydrographs from Kanlıköy and Gönyeli ponds as boundary data to MIKE 11

Moreover, as a downstream boundary condition, Q-h boundary at the chainage of 1,3626.17 meters of the main creek was applied to conduct the relation of water surface elevation with discharge as shown in Figure 4.11. In MIKE 11 model, this relation was automatically calculated considering the Manning formula using the local features with the bed slope of 0.0085, $n = 0.08$, and geometrical properties of cross-section at the last chainage.

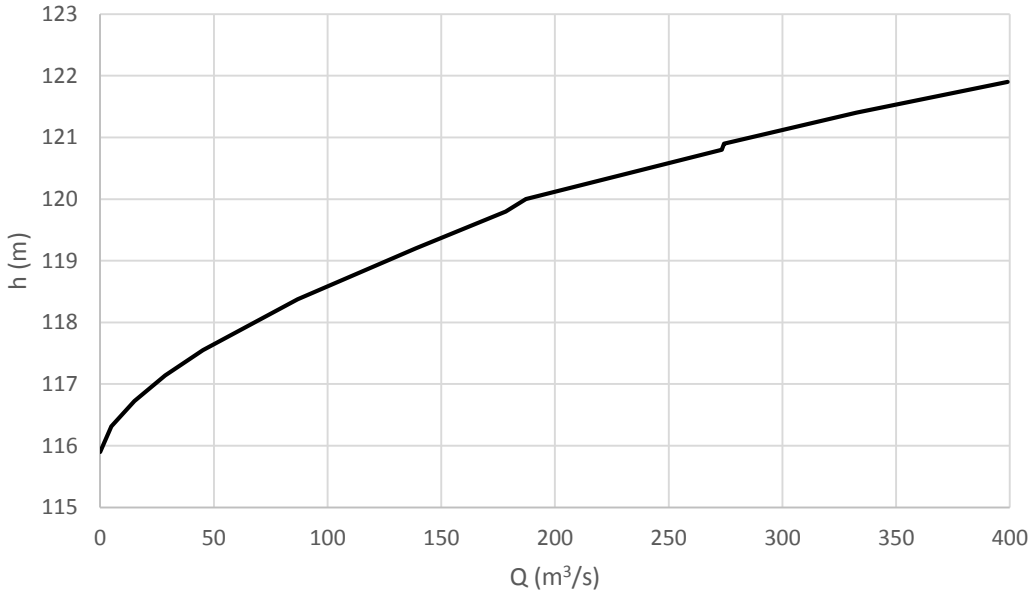

Figure 4.11. Q-h boundary data at the last chainage of main creek

4.2.1.4. The Hydrodynamic (HD) Parameters

In HD parameter editor, several parameters and some methods are provided to use in hydrodynamic simulation. For instance, wave approximation is defined as high order fully dynamics and Manning's roughness coefficients are used for reflecting the bed resistance.

Determination of roughness characteristics based on the soil types and land covers is one of the most crucial issues in hydraulic modelling. Therefore, for reliable estimation of roughness, the following factors should be considered: bed material, degree of irregularity, variations in channel cross-section, obstructions in channel, vegetation condition of bed and banks, and degree of channel meandering (McCuen, 1998). In this study, Manning's roughness coefficient (n) is preferred which is commonly used coefficient to represent the effects of channel or floodplain resistance to the flow. Particularly, in the cases of lack of observations, the selection of Manning's coefficients has to be based on the literature. It has been observed that

realistic estimations of coefficients lead to successful results in practice and this relies on the good assessment and experience on the terrain (Yanmaz, 2002). As noted before, all the cross-sections and the majority of floodplain were surveyed by the author and this experience was valuable for the selection of Manning's coefficients.

In order to evaluate the channel roughness, the approach proposed by Cowan (1956) is used which takes into consideration different factors of channels mentioned above. Herein, the Manning's n value can be calculated as follows:

$$n = (n_b + n_1 + n_2 + n_3 + n_4)m \tag{4.24}$$

where n_b is the base value for material type or the grain size; n_1 is the modification factor for channel irregularity; n_2 is the modification factor for channel variations; n_3 is the modification factor for obstructions in cross-sections; n_4 is the modification factor for vegetation type and density; and m is the correction factor for meandering channels. The details of the factors including types, validity conditions, and recommended values are given in Table 4.1 and Table 4.2 adopted from Yanmaz (2002).

Table 4.1. Manning's Coefficients for n_b (Lagasse et al., 2001)

Channel Type	D_{50} (mm)	n_b
Sand Channels	0.2	0.012
	0.3	0.017
	0.4	0.020
	0.5	0.022
	0.6	0.023
	0.8	0.025
	1.0	0.026
Stable Channels		
Concrete	-	0.012-0.018
Rock	-	0.025
Firm earth	-	0.025-0.032
Coarse sand	1-2	0.026-0.035
Fine gravel	-	0.024
Gravel	2-64	0.028-0.035
Coarse gravel	-	0.026
Cobble	64-256	0.030-0.050
Boulder	>256	0.040-0.070

Table 4.2. Modification Factors for Manning's Coefficient (Lagasse et al., 2001)

n_i	Validity Conditions	Value	Notes
n_1	Smooth	0	Smooth channel
	Minor	0.001-0.005	Slightly eroded banks
	Moderate	0.006-0.010	Moderately eroded bed and bank
	Severe	0.011-0.020	Badly eroded banks
n_2	Uniform	0	Gradually change in cross-section
	Gradual	0.001-0.005	Occasionally change in cross-section
	Severe	0.010-0.015	Frequently change in cross-sections
n_3	Negligible	0-0.004	Obstruction height<5% of cross-sectional area
	Minor	0.005-0.015	Obstruction height<15% of cross-sectional area
	Appreciable	0.020-0.030	Obstruction height≈(15%-50) of cross-sectional area
	Severe	0.040-0.060	Obstruction height>50% of cross-sectional area
n_4	Small	0.002-0.01	y>2*height of vegetation
	Medium	0.01-0.025	y>height of vegetation
	Large	0.025-0.050	y<height of vegetation
	Very large	0.050-0.100	y<0.5*height of vegetation
m	Minor	1.0	Channel sinuosity<1.2
	Appreciable	1.15	1.2≤Channel sinuosity≤1.5
	Severe	1.30	Channel sinuosity>1.5

Herein, the selected Manning's n values along the creeks are listed in Table 4.3. According to the properties of channel bed, the bed material is selected as firm earth for all the creeks in the study area and a single value of $n_b = 0.025$ is applied. For channel irregularity, the modified coefficient varies from $n_1 = 0$ for concrete channels to $n_1 = 0.016$ for the channels with badly eroded banks as shown in Figure 4.12 are used.

Table 4.3. Determined Manning's Coefficients for Creeks

Creek Name	Chainage	n_b	n_1	n_2	n_3	n_4	m	n
Çınardere-Asidere	134.01	0.025	0.003	0.000	0.002	0.006	1	0.036
Çınardere-Asidere	1085.33	0.025	0.003	0.000	0.002	0.038	1	0.068
Çınardere-Asidere	1462.54	0.025	0.003	0.000	0.002	0.018	1	0.048
Çınardere-Asidere	2062.48	0.025	0.008	0.000	0.002	0.038	1	0.073
Çınardere-Asidere	2171.35	0.015	0.000	0.000	0.000	0.002	1	0.017
Çınardere-Asidere	2545.47	0.025	0.008	0.000	0.002	0.038	1	0.073
Çınardere-Asidere	3965.94	0.025	0.008	0.003	0.002	0.018	1	0.056

Table 4.3. (Contd.)

Creek Name	Chainage	n_b	n_1	n_2	n_3	n_4	m	n
Çınardere-Asidere	4230.31	0.025	0.003	0.000	0.000	0.018	1	0.046
Çınardere-Asidere	4923.01	0.025	0.008	0.003	0.002	0.018	1	0.056
Çınardere-Asidere	6448.56	0.025	0.008	0.003	0.002	0.006	1	0.044
Çınardere-Asidere	9863.20	0.025	0.008	0.003	0.002	0.018	1	0.056
Çınardere-Asidere	10211.81	0.015	0.000	0.000	0.002	0.006	1	0.023
Çınardere-Asidere	11265.71	0.025	0.003	0.003	0.002	0.018	1	0.051
Çınardere-Asidere	11717.88	0.015	0.000	0.000	0.002	0.006	1	0.023
Çınardere-Asidere	12127.29	0.025	0.008	0.000	0.002	0.018	1	0.053
Çınardere-Asidere	12709.01	0.025	0.003	0.003	0.002	0.038	1	0.071
Çınardere-Asidere	13283.07	0.025	0.003	0.003	0.002	0.018	1	0.051
Çınardere-Asidere	13626.17	0.025	0.003	0.000	0.002	0.018	1	0.048
Öksüzdere	204.31	0.025	0.016	0.000	0.025	0.018	1	0.083
Öksüzdere	885.68	0.025	0.016	0.000	0.002	0.018	1	0.060
Öksüzdere	2048.55	0.025	0.008	0.000	0.002	0.018	1	0.053
Öksüzdere	3423.34	0.025	0.003	0.003	0.002	0.018	1	0.051
Öksüzdere	5067.60	0.025	0.003	0.003	0.002	0.038	1	0.071
Öksüzdere	5593.77	0.015	0.000	0.000	0.000	0.002	1	0.017
Öksüzdere	5936.99	0.025	0.003	0.000	0.002	0.038	1	0.068

Figure 4.12. Examples for smooth and eroded channels

In addition, variation of cross-sections which lead to energy losses are assessed by n_2 and for the studied creeks, gradually ($n_2 = 0$) and occasionally ($n_2 = 0.003$) changes are generally observed. Obstructions are mostly located in creeks except in some concrete canals ($n_3 = 0$), but the majority of them only block small part of the channels, which is less than 5% of whole cross-sectional area ($n_3 = 0.002$). Moreover, vegetation was mainly dense in all creeks which may cause water levels as well as flood inundation extent to increase. Therefore, n_4 modification factor are chosen up to 0.038 for great amount of vegetation and $n_4 = 0.006$ for almost clean channels as demonstrated in Figure 4.13. The degree of meandering is not considered as a must factor for the creeks ($m = 1$) due to almost straight channel alignment. The final values of Manning's coefficients are calculated and given in Table 4.1.

Figure 4.13. Examples for small and very large amount of vegetation in the creeks

4.2.1.5. Simulation

Within the simulation editor of MIKE 11, all physical and hydrological inputs are combined by hydrodynamic model to conduct the 1D simulation of the study area. In MIKE 11 Nicosia model, the simulation period is taken as the same period of hydrographs to observe the flood inundation while design hydrographs are propogated along the channels. Furthermore, the time step of simulation (Δt) is selected as 1 second for both 1D and 2D MIKE models to satisfy the stability condition.

4.2.2. MIKE 21 Model of Nicosia

4.2.2.1. Mesh Generation

Mesh generator offers several tools to create and modify the 2D bathymetry of the study area. The main aim is to represent the whole study area with triangular elements to perform interpolation. In this context, the bathymetry generation could be divided into two parts: the generation of meshes and interpolation of the bathymetry. In this study, flexible mesh approach which provides flexibility due to the non-orthogonal triangular construction is used to model the surface of floodplain.

Formation of bathymetry layer is one of the most time-consuming issue for 2D modelling. Mesh Generator tool in MIKE 21 was used to represent the topography and surface features of floodplain. In addition, while creating a bathymetry with unstructured meshes for this study, these steps were followed: determination of model borders, importing polylines representing the location of creek banks, importing polygons representing the buildings' footprints, importing scatter data of DTM, generation, analysis and smoothening of meshes, interpolation of the node values, and exporting the final mesh.

As a first step, the boundaries of the domain area are decided depending on the focus area, previously performed test simulations, and the location of open boundaries. Unnecessary regions in domain area lead to increase the mesh elements as well as computational time. Therefore, preliminary test simulations by using the hydrographs

with greater peak discharges are carried out to have an opinion about the maximum possible flood extent. Then, the boundaries of domain are modified to reduce the area and obtain acceptable simulation time. Moreover, in order to avoid the artificial effects of boundaries, the focused area is extended at the points of open boundaries. Thus, when the flood wave reached to the ends of the domain, it accumulated there without affecting the propagation in the interested area.

Since the geometry of channels are defined in 1D Model of MIKE 11, a polygon representing the creek outline according to the widths of the cross-sections along the creek is excluded from the domain. Therefore, the calculations of 1D modelling are kept only in MIKE 11. For these, the polylines representing the location of creek banks are imported from ArcGIS to Mesh Generator and modified to form polygons. Then, these polygons are defined as "exclude from mesh" to prevent the formation of meshes in this area as shown in Figure 4.14.

Moreover, the buildings' footprints obtained from Land Registry Office of Northern Cyprus as AutoCAD file are converted to polygons in ArcGIS. Then, a set of simplifications are carried out to obtain simple representation of buildings for smoothening the mesh and reducing the computational time. Since it is difficult to deal with the polygons of buildings in Mesh Generator tool, ArcGIS is used for these applications. First, the buildings are simplified by removing small polygons out of the study area. Later on, in order to prevent the formation of small meshes between the buildings which are located too close to each other, dissolve, unify, simplify buildings, and aggregate tools were employed in ArcGIS. Therefore, some of them merge to form a single building and the polygon areas are reduced to increase the gap between them as shown in Figure 4.15. In addition, 4726 polygons of buildings are converted to xyz file to easily transfer into the Mesh Generator. Similar with creeks, these polygons are also assigned as "exclude from mesh" and act as solid boundaries to keep water out of the polygons.

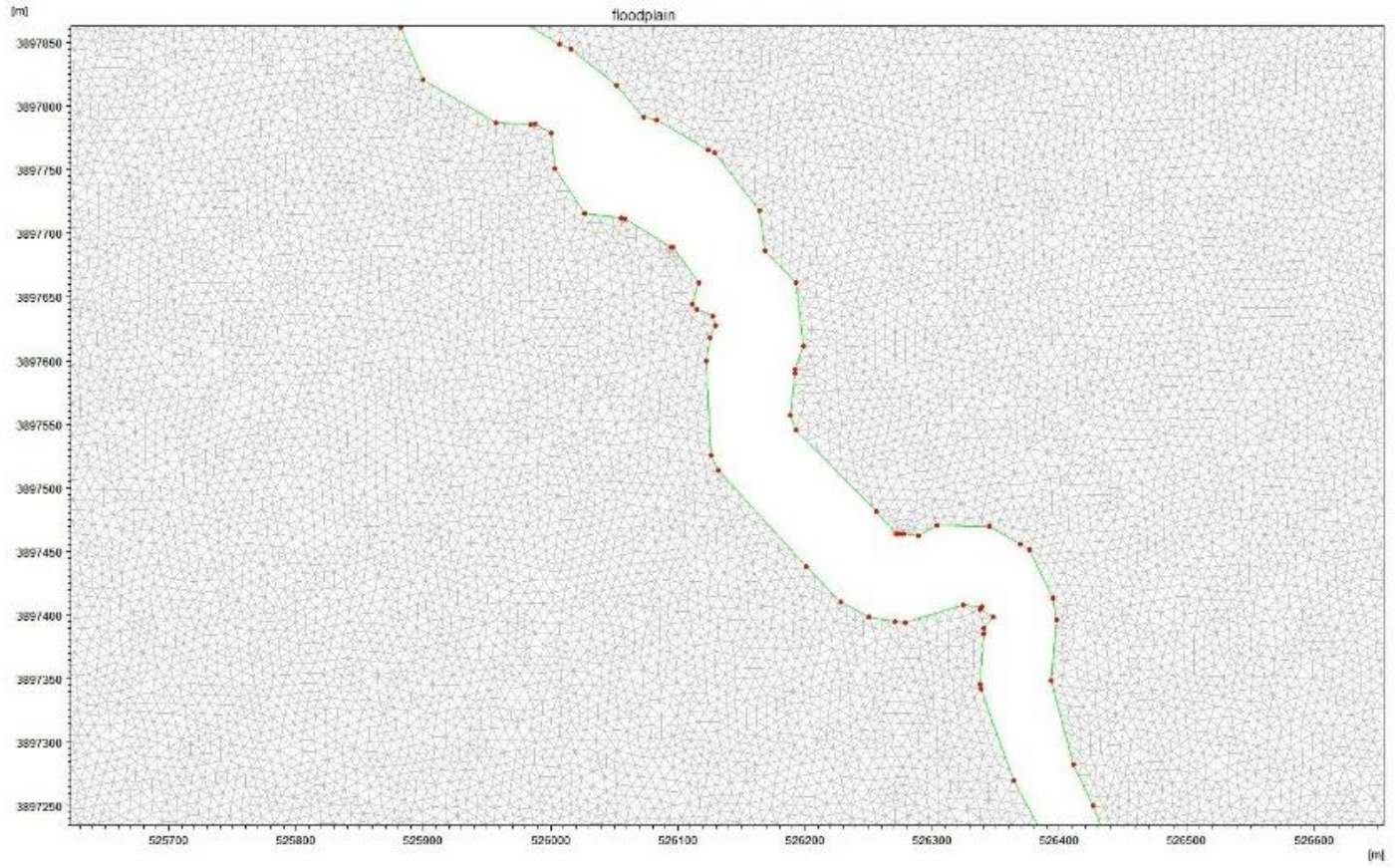

Figure 4.14. Creek outline excluded from mesh

Figure 4.15. Simplification of buildings' footprints

Using the appropriate mesh density is also important in 2D modelling. Particularly, in urban areas, the minimum grid cell size depends on the shortest length between the urban structures like the distance between the buildings (Fewtrell et al., 2008). Therefore, while simulating urban areas, the mesh size must be defined finer than the simulations in rural areas. Moreover, according to the Horritt and Bates (2001), mesh density should be constructed correctly to reflect the storage effects near the channel, which affect the flood routing behavior as well. Furthermore, since the study area is reduced to the mainly focused area considering the maximum probable flood extent, only one mesh size is decided instead of dividing floodplain into different zones. Also, most of the regions in floodplain have a similar situation that the buildings were densely located near the creeks.

As mentioned before, the polygons representing creeks and buildings are removed from the mesh and the remaining part of focused area is assigned to have maximum element area of 40 m^2. This is decided after applying different alternatives, such as 10 m^2, 20 m^2, and 60 m^2. Herein, the CPU of the computer comes out as a major factor. Fundamentally, the maximum element size is selected to represent floodplain at finer scale as possible with the acceptable running time.

The Mesh Generator also offers some other control options, such as smallest allowable angle and maximum allowable nodes. In this study, the angle is selected as 28°. Smaller angles could cause small triangles that negatively affect the stability in terms of CFL number. The elements with small angles are automatically detected and manually modified to contribute to the running time of the simulation in particular. Besides, due to the complex topography in urbanized areas, the maximum allowable nodes is chosen as 10,000,000 to let the tool create many elements with nodes.

Digital terrain model of the focused area which is developed as a raster data is converted to xyz format and imported to Mesh Generator as a set of scatter data. Based on 2,339,694 scatter points and the specified parameters, the meshes are generated as illustrated in Figure 4.16. Total number of 3,004,841 elements and 1,547,243 nodes are obtained for the modelling of the floodplain. Then, the elements are assessed by using "Analyse Mesh" option, which take into account the smallest time step, based on the water level and the water depth and the smallest area and angle based on CFL number. Considering the results of the mesh analyses, the modification is manually executed, but not for all problematic elements due to high amount. Instead, smoothing option is employed for several iterations. At the moment to begin the simulation, in some parts of the floodplain particularly in gaps between the buildings and the closely located vertices, some element areas are detected as too small, e.g. 0.1 m^2. Nevertheless, no more modification is considered due to reasonably constructed mesh.

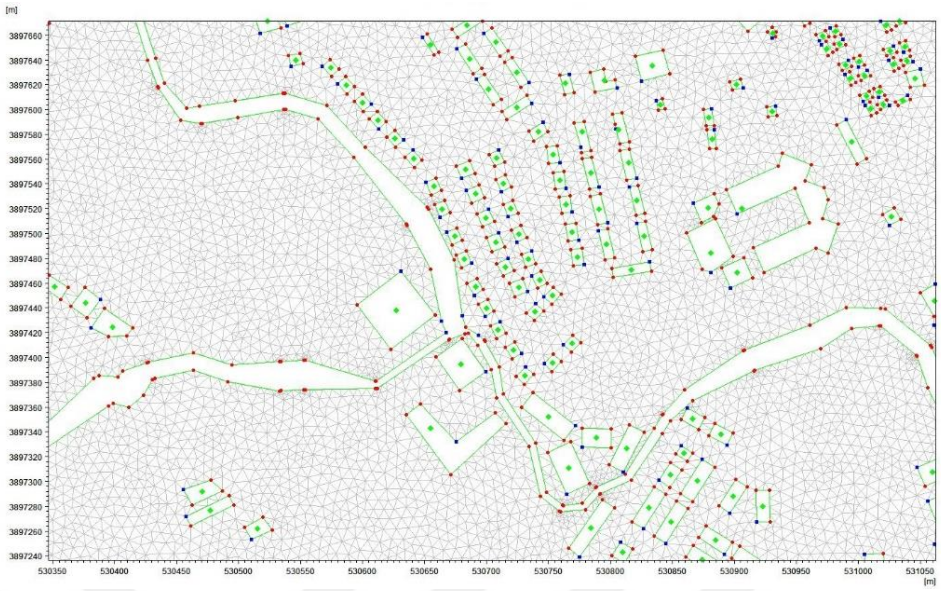

Figure 4.16. A view of floodplain by mesh

Finally, the interpolation is carried out with the scatter data points by using a natural neighbor interpolation technique, which is one of the two possible options in Mesh Generator tool. The bathymetry is obtained as given in Figure 4.17 and exported to be used as an input for MIKE 21 modelling.

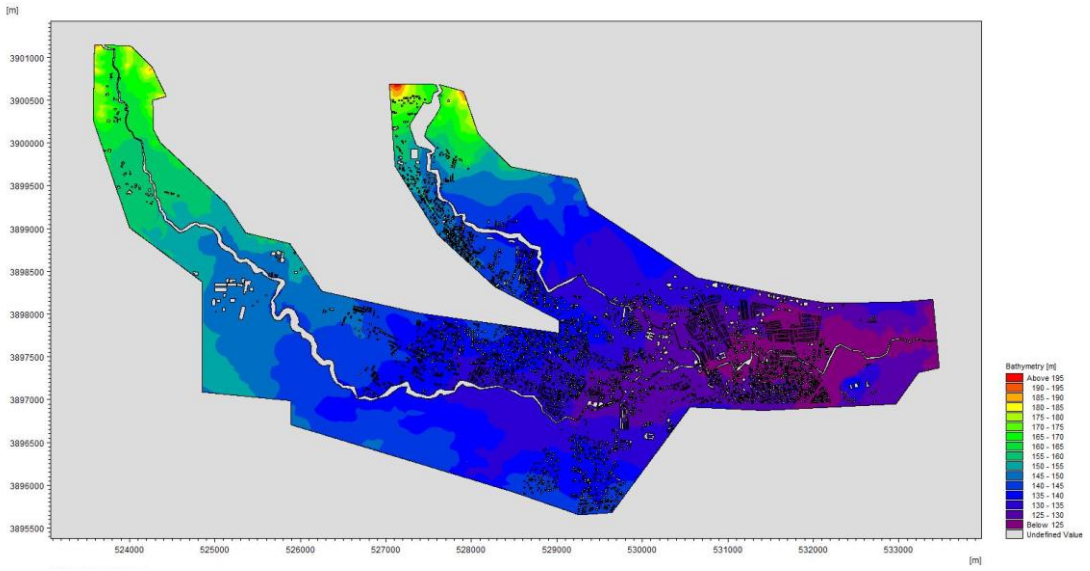

Figure 4.17. Bathymetry of the focused area

4.2.2.2. Floodplain Resistance

The floodplain resistance is described by Manning's roughness coefficient for certain land cover types in MIKE 21. Three land cover types including roads, residential areas, and cultivated areas are defined for the study area of Nicosia and in order to reflect their roughness characteristics, the Manning's coefficients are assigned as displayed in Table 4.4. In addition, since the representation of the buildings and the creeks are executed through the modification of meshes, there is no need to assign any roughness value.

Table 4.4 Manning's Coefficients Corresponding to Different Land Covers.

Land Cover	Manning's Coefficient, n
Roads	0.013
Residential area	0.080
Cultivated area	0.040

4.2.2.3. 2D Simulation

In the simulation of coupling the 1D model with 2D model, the time step defined in MIKE 21 is mainly considered which allows the user to apply a range of minimum to maximum time step values. As mentioned before, the stability of the model is controlled by CFL number, which has a parameter of time step. In this study, the maximum time step is selected as 1 second and the minimum time step is decided as 0.001 seconds to overcome the stability by reducing CFL values. Moreover, drying depth, flooding depth, and wetting depth values are entered to the model as 0.005 m, 0.01 m, and 0.02 m, respectively.

4.2.3. MIKE FLOOD Model of Nicosia

In MIKE FLOOD, the combination of 1D river model and 2D surface model is conducted by defining the lateral links. In this study, the location of these links are determined based on the coordinates of the crests of left and right banks in cross-sections as shown in Figure 4.18. For representing the overbanking flow, the parameters of weir flow equation are used as default. Therefore, when cross-section

overbanks, this lateral flow to the floodplain is modelled by using the weir flow approach.

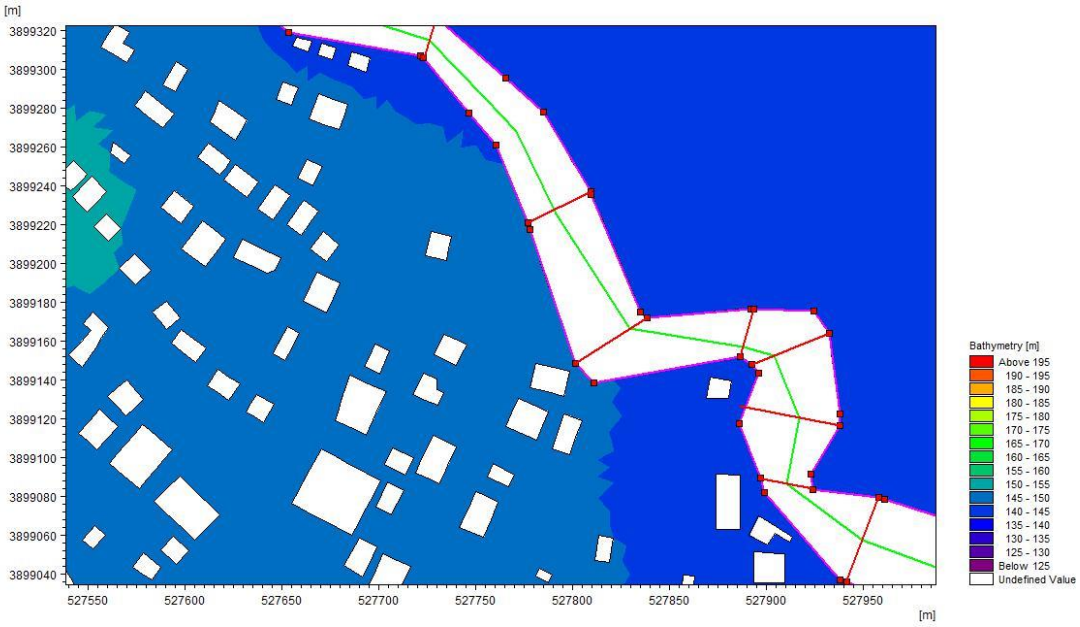

Figure 4.18. Lateral links defined in MIKE FLOOD model

4.3. Calibration of Model

Model calibration is required to modify the model parameters and achieve the best match with the observed events. According to Hall et al. (2005), the channel roughness is the most effective parameter in 1D modeling for calibration. For 2D model, floodplain roughness values and mesh density are used in calibration processes (Horritt and Bates, 2001; Pappenberger et al., 2006). In addition, Pappenberger et al. (2007) stated that the hydraulic structures have great impact on the model results. Also, rather than applying global calibration of model, focusing only the area of special interest and localizing the calibration procedure could provide more accurate simulation results (Pappenberger et al., 2007).

In this study, the Manning's roughness coefficients of river channels and floodplain is selected as the calibration parameters. However, due to the lack of stream gauging station and flow depths measurements in the study area, inundation extent map of 2010 flooding event is only taken as reference in calibration process. This map is developed by the personal communication with the relevant people from the Nicosia Turkish Municipality, Gönyeli Municipality, and Civil Defence of TRNC who are assigned in the rescue efforts personally during the flood day. Moreover, since the measured flow data or taken aerial photographs of flood area are not available, unfortunately the validation of the simulations are not possible.

Moreover, in order to assess the spatial goodness-of-fit of flood extent maps between the generated map from MIKE FLOOD model and the observed one, relative error (RE) and F-statistics (F) are used. Here, relative error can be calculated as follows:

$$RE = \frac{|A_{obs} - A_{est}|}{A_{obs}} \tag{4.25}$$

where A_{obs} is the inundated area of observed flood extent map of 2010 flood event and A_{est} is the estimated flood inundation area of MIKE FLOOD. Besides, the F-statistics is defined as:

$$F = \left(\frac{A_{overlap}}{A_{obs} + A_{est} - A_{overlap}}\right) \times 100\% \tag{4.26}$$

in which $A_{overlap}$ refers to the overlapping areas of observed and modelled flood extent maps.

4.4. Remedial Alternatives for Flood Protection of Nicosia

In order to propose the most appropriate solutions to the flood inundation problem of town of Gönyeli and the city of Nicosia, several alternatives are examined. In Alternative 1, the current condition of study area is modelled and the calibrated model is executed based on the observed flood inundation map of 2010 flood. The

Alternative 2 comprises the dredging of Kanlıköy Pond reservoir by 2 m and raising the embankment and spillway crests elevations. In Alternative 3, implementation of a nearby upstream pond in Kanlıköy to store great amount of water and decrease the peak discharge of inflow to the existing pond is assessed. The Alternative 4 includes the successive dredging of 3 m, 5 m and 7 m of reservoir bed and raising the crest elevations of embankment and spillway for Gönyeli Pond. In Alternative 5, the combination of the best structural measures with creek restoration is evaluated and proposed as the final solution for the flood events of 500-year return period.

CHAPTER 5

DESCRIPTION OF THE STUDY AREA

This chapter describes the topographic, climatic, and soil properties of the study area including Gönyeli town and Nicosia city in Northern Cyprus. Besides, relevant meteorological and topographical data are also introduced.

5.1. Characteristics of the Study Area

The study area covers the floodplains of Öksüzdere Creek, Çınarderesi Creek, and Asidere Creek which pass through the town of Gönyeli and the metropolitan part of the capital city Nicosia and the catchments of the Kanlıköy and Gönyeli ponds (Figure 5.1). The area is located in Middle Mesaoria Plain between the Kyrenia Mountains range in the north and the United Nations buffer zone in the south. It lies between the latitude of 35°11’29’’N to 35°14’43’’N and the longitude of 33°14’39’’E to 33°21’43’’E. The elevation of the floodplain varies in a range of nearly 117.5 m to 210 m.

Figure 5.1. Location of study area (inside of red box shows the floodplains and white outlined areas represent the pond catchments)

The branches of Kanlıdere River, Öksüzdere Creek with a total length of 5.9 km and 13.6 km long main channel of the network consisting of Çınardere Creek and Asidere Creek are considered as the river network of the study area. These creeks are ephemeral creeks, the same as the majority in Cyprus, which has no flow during the year except the rainy winter periods or after sufficient rainfall to generate runoff.

Besides, in the upper part of the study area, there are two ponds, named as Kanlıköy Pond and Gönyeli Pond which are also analysed by conducting a hydrological modelling to provide inputs to the hydrodynamic model within the scope of this study. The catchments of these ponds extend to the top hills of the Kyrenia Mountain Range which have suddenly rising slopes from the plains. The elevation varies from 175 m up to 850 m in Kanlıköy Pond catchment; and from 167 m to 930 m in Gönyeli Pond catchment.

Kanlıköy Pond is located on Çınarderesi Creek just upstream of Kanlıköy village. The aim is to provide water for irrigation of the plains by the villagers. The height of the embankment is 12.36 m from the thalweg and the crest length is 297 m with 6 m top and 70 m base thicknesses (Figure 5.2). It has reservoir volume of about one million m^3 and 110 m^3/s spillway capacity (Konteatis, 1974).

Gönyeli Pond was constructed on Öksüzedere Creek to store water and supply for the irrigation purposes at the upstream of Gönyeli town. The embankment is 16 m high from the thalweg and has a crest length of 196 m with 5 m top thickness and 90 m base thickness. The reservoir capacity of the pond is nearly one million m^3 and its spillway can evacuate water with its maximum capacity of 170 m^3/s (Figure 5.3) (Konteatis, 1974).

Figure 5.2. Location of the reservoir of Kanlıköy Pond

Figure 5.3. Location of the reservoir of Gönyeli Pond

5.2. Climatic Conditions of the Study Area

Due to the geographic location of Cyprus at the eastern Mediterranean Sea, the island is affected by the typical Mediterranean climate regime. In winter, the weather is generally mild with limited rainfall and in summer, it has hot and dry weather conditions (Michaelides et al., 2009).

The island of Cyprus has a complex topography, consisting of the Kyrenia Mountains Range, lying parallel to the northern coastline, Mesaoria Plain, low-lying plain at the center of the island, Karpass Peninsula, and the Troodos Mountains, covering the majority of the South-western region of the Southern Cyprus. For this reason, the local meteorological characteristics including precipitation patterns differ greatly. Besides, precipitation is affected by the movement of moist maritime flows towards to north, mostly taking place at the high elevated regions (Kostopoulou and Jones, 2007). Also, precipitation in winter is strongly associated with cyclogenesis in the region (Pinto et al., 1999).

In Northern Cyprus, the mean annual precipitation has a minimum value of nearly 260 mm in the Western Mesaoria Plain and the maximum value of nearly 550 mm at the Kyrenia Mountains. The whole study area, i.e. including the pond catchments, receives annual mean precipitation of approximately 300 mm at the low-lying areas and 470 mm at the mountainous part. In order to represent the plain and hilly part of the study area, the stations of Lefkoşa and Alevkaya are considered, respectively.

In Lefkoşa Station, the long-term average of annual total precipitation is calculated as 306.6 mm. As illustrated in Figure 3.4, one of the peak values are 439.2 mm, 452.2 mm, and 551.7 mm in water years of 2009-2010, 2001-2002, and 2002-2003, respectively. On the other hand, the annually recorded lowest precipitation is observed in 2007-2008 as 99.5 mm.

In Alevkaya Station, the overall mean of total precipitation series is found as 485.2 mm. The highest values of 704.2 mm, 717.7 mm, and 766.1 mm were recorded in 1991-1992, 2012-2013, and 2009-2010 water years, respectively. Besides, the minimum value of the series is detected as 148 mm in 2007-2008 (Figure 5.4).

During the observation period in Lefkoşa and Alevkaya stations, mainly the highest amount of precipitation is recorded in winter seasons. The driest period ranges from June to September. Conversely, the wettest month is December for the study area. The maximum monthly average precipitation is 55.4 mm in December, 50.5 mm in January, and 44 mm in February for Lefkoşa Station; 95.2 mm in December, 86 mm in January, and 77.5 mm in February for Alevkaya Station (Figure 5.5).

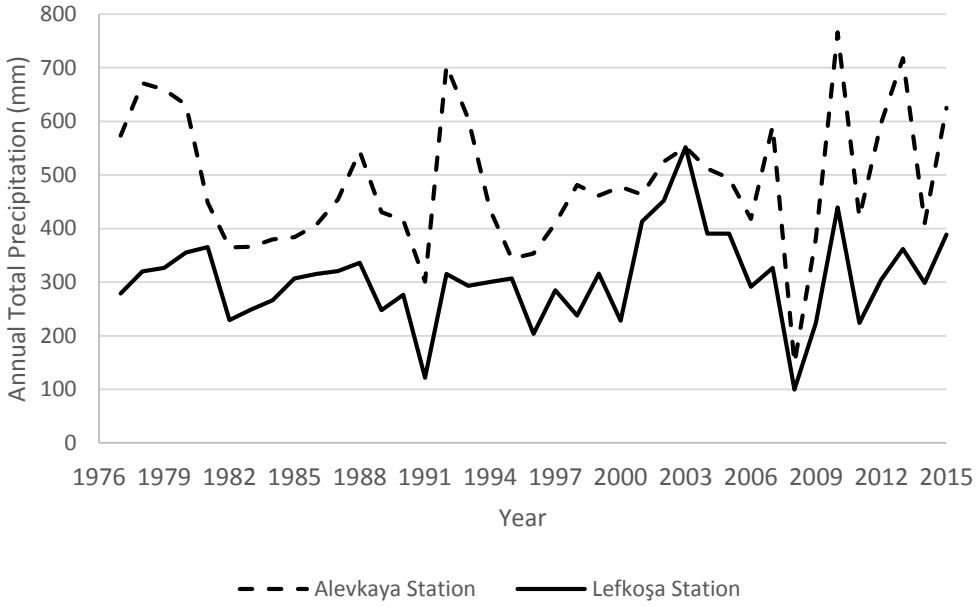

Figure 5.4. Annual total precipitation of Lefkoşa and Alevkaya stations between 1976-1977 and 2014-2015 water years

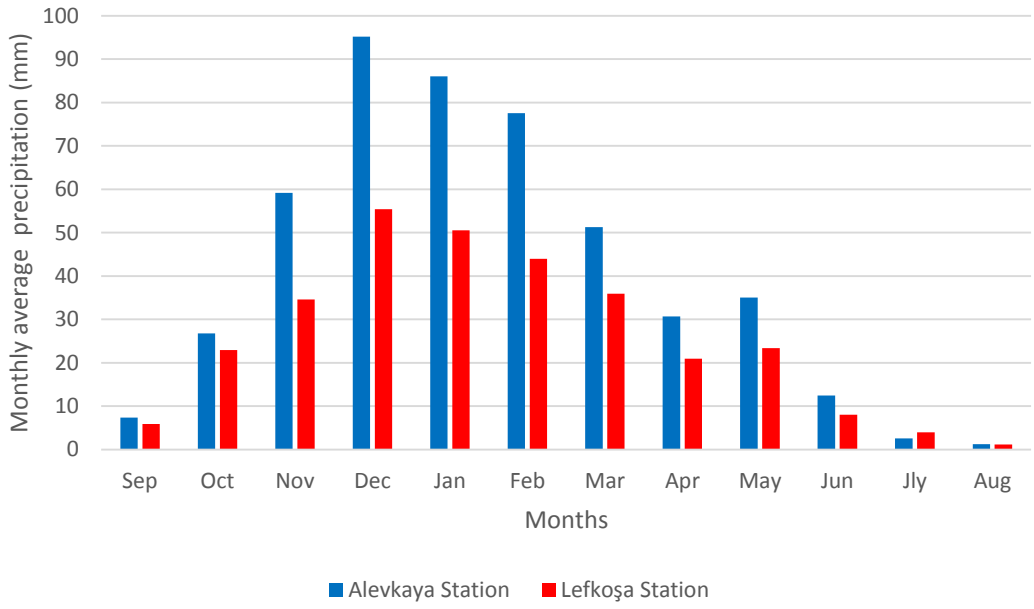

Figure 5.5. Monthly average precipitation of Lefkoşa and Alevkaya stations between 1976-1977 and 2014-2015 water years

The most remarkable flooding event of the recent decade occurred on 26 February, 2010 in the water year of 2009-2010 when Alevkaya Station recorded the highest total annual precipitation value ever and Lefkoşa Station observed the third highest value in their record periods. Moreover, as demonstrated in Figure 5.5, since the monthly average precipitation in February is 44 mm for Lefkoşa Station and 77.5 mm for Alevkaya Station, in 2009-2010 water year, February monthly precipitation values are recorded as 125.6 mm and 247.2 mm for Lefkoşa and Alevkaya stations, respectively. Furthermore, based on the observed data on 26 February, 2010, the daily precipitation over Lefkoşa and Alevkaya stations are detected as 63 mm and 80 mm, respectively.

5.3. Soil and Land Cover

Analyzing the soil data is a must while conducting a flood management study which is directly related with the behavior of soil properties. For instance, if a catchment has a majority of soil pattern having high infiltration capacity or pervious soil structure, the probability of flooding will reduce. The soil permeability and the rock type under the ground have a strong impact on observed runoff in a catchment (Kalantari et al., 2014).

In order to analyze and better understand the characteristics of soil series in the study area, a soil map is obtained from the Agricultural Office in Northern Cyprus (Figure 5.6). This map is generated by Dinç et al. (2000) based on the detailed soil survey to develop an agricultural master plan. In this context, a set of 109 soil series are identified and named unique to Northern Cyprus. Generally, silty clay loam, sandy clay loam, clay loam and loamy texture are the soils that predominate the country. From the viewpoint of flood management, the soil types mostly have a low and moderate hydraulic conductivity and infiltration rates across the country (Dinç et al., 2000).

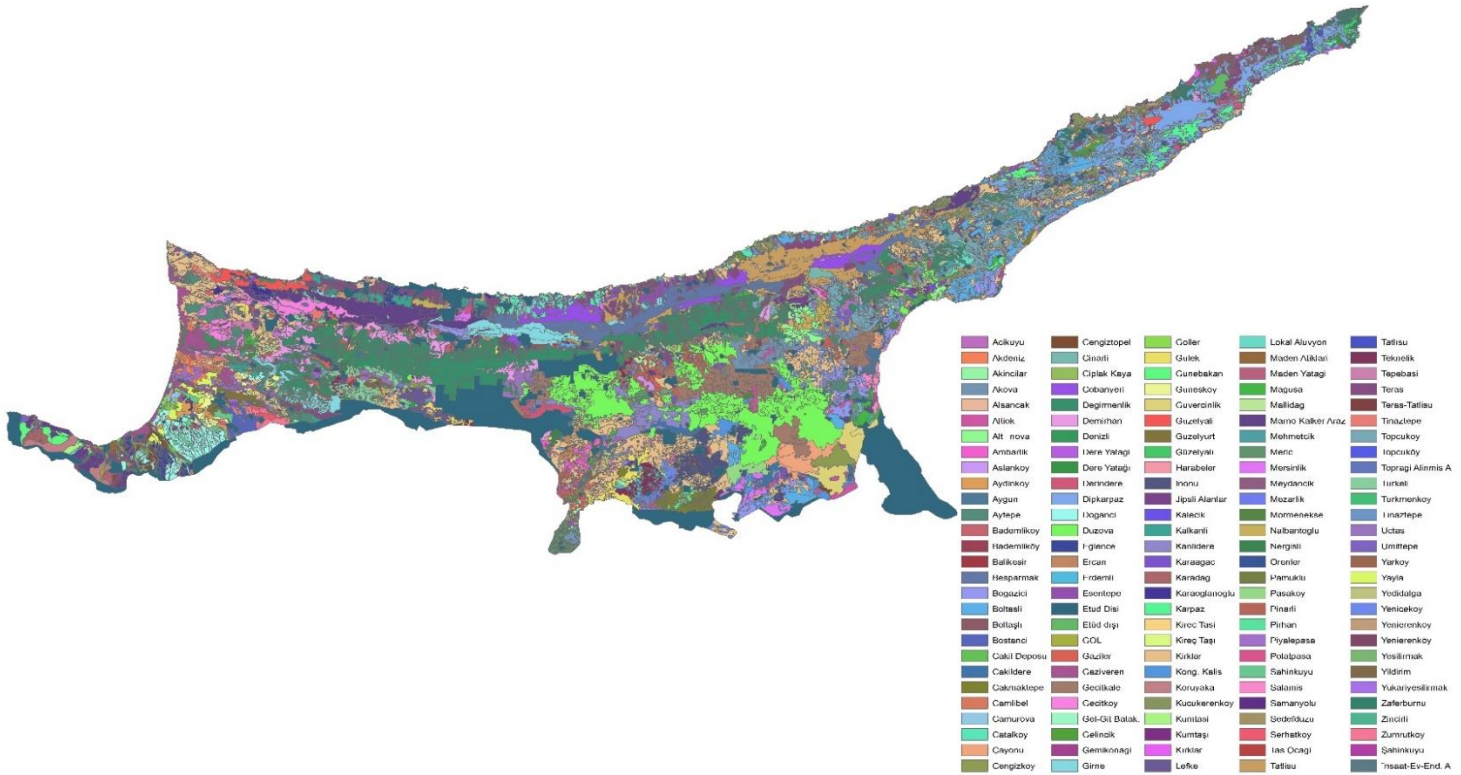

Figure 5.6. Soil map of Northern Cyprus

For this study, the soil properties are necessary for determination of the infiltration parameters for the modelling phase. The soil details of the pond catchments are extracted from the soil map of Northern Cyprus prepared by Dinç et al. (2000). In Figure 5.7, the distribution of different soil types is illustrated. Majority of soil types in catchments are Değirmenlik (43%), Demirhan (16%), and Marno-Kalker (18%) for Kanlıköy Pond catchment; Değirmenlik (43%), Boğaziçi (14%), and Demirhan (12%) for Gönyeli Pond catchment.

Değirmenlik soil series has the widest spreading area which are formed on the Miocene limestone clay storage with 26,390 ha area, approximately 7.88% of Northern Cyprus (Dinç et al., 2000). All profiles are clay textured and very calcareous. The clay content is generally 24% near the surface and increases up to 42% (Dinç et al., 2000). Besides, the clay textures of the other soil types vary in a range of 19%-32% in Demirhan, 19%-45% in Marno-Kalker, and 34%-36% in Boğaziçi soil series. In this regard, while developing the hydrological models of the Kanlıköy and Gönyeli pond catchments, having such type of soils should be considered to better reflect the complex rainfall-runoff process, particularly in parameter selection. Because, the clayey soils have high runoff potential which lead to increase the amount of flood volume and the probability of flooding events.

Changes in land cover due to urbanization, deforestation, and agricultural facilities cause the severe and frequent floods (Tollan, 2002). Therefore, in order to transfer the impact of land cover on the model, modelling of floodplain is required. For the floodplains of the study area, the land use is classified into five categories: buildings, cultivated area, residential area, roads, and creek (Figure 5.8). The focused region mostly consists of urbanized area due to the existence of Gönyeli town and Nicosia city. The majority of cultivated areas are located in the North-western part of the region around the village of Kanlıköy and upstream of the creeks. Also, this information will be used to determine the Manning roughness coefficients of floodplain by assigning a reasonable value to each land cover while executing hydrodynamic modelling.

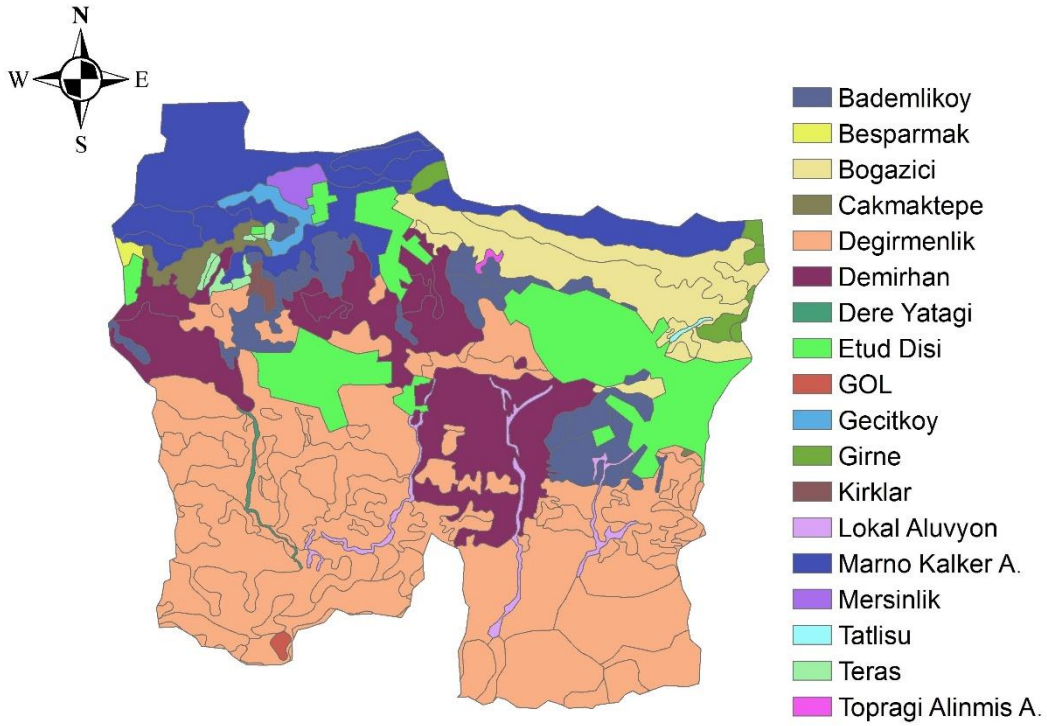

Figure 5.7. Soil map of the catchments of Kanlıköy and Gönyeli ponds

Figure 5.8. Land cover of floodplains in the study area

5.4. The Data Sets

This section gives information about the available data sets of precipitation, topography, soil and executed fieldworks to obtain geometric characteristics of cross-sections and water level measurements in Kanlıköy and Gönyeli ponds.

5.4.1. Precipitation Data

The daily precipitation, totals of 37 precipitation stations are provided from the Meteorological Office of Northern Cyprus and used to conduct a study for the assessment of extreme precipitation events and hydrological modelling of the study area. As shown in Figure 5.9, these stations are uniformly distributed throughout the northern part of Cyprus which cover a total study area of 3,355 km^2 from the Karpass Peninsula in the northeast to Morphou (Güzelyurt) Bay in the west, the Kyrenia Mountains lying along the northern coastline with average annual precipitation total of 550 mm, and the Mesaoria Plain at the center of the island stretching from Morphou Bay in the west and Famagusta (Gazimağusa) Bay in the east with a mean annual precipitation of 260 mm. Therefore, all critical regions of Northern Cyprus could be reflected in terms of local climatic conditions.

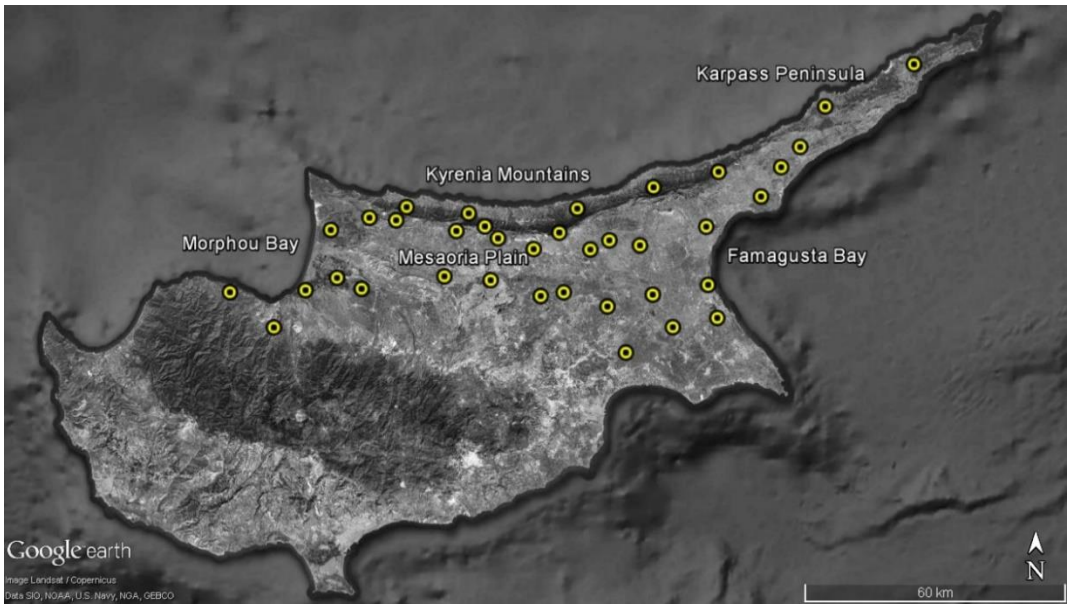

Figure 5.9. Locations of precipitation stations

The data series of 37 stations with different record lengths have observation periods including some missing parts spanning from 1976 to 2015 (Table 5.1). The 11 out of 37 stations have 39-year recording period from 1976-1977 to 2014-2015, 23 of 37 stations record the 37-year data from 1978-1979 to 2014-2015, one station has a 31-year record from 1984-1985 to 2014-2015, and two stations observe 28-year data from 1987-1988 to 2014-2015.

Table 5.1. Geographical Coordinates and Missing Data Percentages of Precipitation Stations

Stations	Latitude (◦)	Longitude (◦)	Elevation (m)	% of missing data
Akdeniz	35.29972	32.965	277	9
Alayköy	35.18472	33.25667	166	0
Alevkaya	35.28583	33.53472	623	0
Beyarmudu	35.047159	33.69582	87	9.5
Beylerbeyi	35.29729	33.354036	225	0.9
Bogaz	35.28825	33.28484	300	0
Çamlibel	35.31611	33.07056	89	0
Çayırova	35.349489	34.031298	67	3.6
Çayönü	35.109444	33.808348	11	0.6
Değirmenlik	35.25276	33.472181	168	0
Dörtyol	35.17889	33.75861	54	0
Ercan	35.15917	33.50194	119	0
Esentepe	35.33273	33.578518	183	0
Gazimağusa	35.13639	33.93556	10	1.8
Gaziveren	35.17306	32.92194	19	0.2
Geçitkale	35.23333	33.72861	45	0
Girne	35.34194	33.33139	10	0
Gönendere	35.26983	33.656601	81	6.3
Güzelyurt	35.18889	32.98194	52	0
İskele	35.28611	33.88444	39	0
Kantara	35.40056	33.91361	480	0
Karpaz	35.59889	34.37917	136	0
Kozanköy	35.30643	33.127067	247	0
Lapta	35.33575	33.163364	168	0.5
Lefke	35.09664	32.84091	129	0
Lefkoşa	35.19639	33.35194	134	0
Margo	35.16701	33.545259	110	23.4
Mehmetçik	35.42222	34.07833	99	0
Salamis	35.180802	33.897344	6	0
Serdarlı	35.25183	33.610235	111	0.2
Taşkent	35.273698	33.385963	341	2.6
Tatlısu	35.3741	33.764034	200	2.9
Vadili	35.138689	33.651608	54	9.2
Yenierenköy	35.53556	34.18944	123	0
Yeşilırmak	35.16639	32.73694	20	8.8
Ziyamet	35.453501	34.124509	82	0
Zümrütköy	35.17444	33.04917	129	0

While executing hydrological studies, particularly to employ the rainfall-runoff simulations, use of precipitation data at a fine scale (e.g. hourly) as input is required (Choi et al., 2008). Therefore, hourly precipitation data of Lefkoşa and Alevkaya stations are obtained from the Meteorological Office for the study area. These data sets are collected over the period of January 2007 and August 2015 and are used for determining the design hyetographs for the hydrological modelling. Moreover, when analyzing the hourly data series of representative stations, 33.2 mm/hr for Lefkoşa Station and 61.4 mm/hr for Alevkaya Station are detected as the most intense precipitation events at hourly scale.

5.4.2. Topographic Data sets

Topographic data sets including elevation data employ as the main source to represent the river geometry and floodplains. In flood modelling, realistic representation of floodplains involving roads, buildings, embankments, etc., is required for 2D modelling part in particular. Besides, the accuracy of model results relies on the type and source of data and the interpolation techniques used in DEM development (Tennakoon, 2004).

5.4.2.1. Available Topographic Data

For this study, topographic maps which are commonly used data for digital elevation model (DEM) generation are obtained from the Mapping Office of Northern Cyprus. The digitized forms of topographic maps in a scale of 1:25,000 and 1:5,000 which have the contour intervals of 5 m and 2.5 m, respectively, are available for the study area. Moreover, the elevation of the roads based on the ground survey are obtained from the Nicosia Turkish Municipality and Gönyeli Municipality. Also, the Land Registry Office of Northern Cyprus provides the buildings footprints. Then, all available data sets are transferred into a geographical information system software, named as ArcGIS in order to produce the DEM.

5.4.2.2. Fieldwork Data

The remaining required data sets including the geometry of the creeks, dimensions of hydraulic structures, and the bathymetry of ponds for hydrological and hydraulic modeling are collected by conducting fieldworks. In creek cross-section survey, detailed 269 cross-sections with an average width of 100 m are surveyed by the author of this thesis along the creeks in the study area (see Figure 5.10). The total length of nearly 20 km-long creeks with a varying cross-section interval of 30 m to 100 m (example in Figure 5.11) are measured by using the device of global navigation satellite system (GNSS). The GNSS device with real time kinematics (RTK) technology comprise of one stationary device to receive data from satellites and one mobile instrument to collect data as shown in Figure 5.12. The stored data consisting of latitude, longitude, and elevation could have errors up to 3 cm in the horizontal direction and 2 cm in the vertical direction.

Besides, a total of 24 hydraulic structures comprising culverts and bridges which are located along the creeks are measured in detail to determine the dimensions of openings, decks, piers, and embankments (see Figure 5.13). The author has carried out all these measurements in a period from October 2017 to December 2017.

Figure 5.10. Cross-section examples in the study area

Figure 5.11. Example of collected data along the Çınardere Creek

Figure 5.12. GNSS device

Figure 5.13. Example of bridge and culvert in the study area

In addition, in order to determine the bathymetry of Kanlıköy and Gönyeli ponds, the flow depths at different observation points are manually measured (Figure 5.14). The coordinates of readings are provided by using GNSS device (Figure 5.12). The recorded information is used in hydrological model in the reservoir routing calculations.

Figure 5.14. Application of water level measurements

The results and discussion of hydrological and hydraulic modelling are introduced in the following chapters.

CHAPTER 6

RESULTS AND DISCUSSION OF HYDROLOGICAL MODELLING

In this chapter, the results of hydrological modelling including a set of quality control approaches, trend analysis, regional frequency analysis, rainfall-runoff simulations, and DEM formation of floodplains are presented and discussed.

6.1. Quality Control and Trend Analysis

6.1.1. Application of Quality Control Procedure

In the data set of 37 precipitation stations, 15 stations had different amount of missing records in their observation periods. As discussed in Hidalgo-Munoz et al. (2011), these missing values affected the results while analyzing the precipitation events in climatic studies and must be completed. However, it was difficult to refer to any agreed method for estimating missing values. After reviewing the literature and detailed analysis of existing data sets, the stations having more than 10% missing data were decided to be removed from the study. In this regard, only Margo Station with 23.4% of missing data was excluded prior to the application of quality control procedure.

As given in Table 6.1, the appropriate estimation methods corresponding to the optimum radius values are determined based on the lowest RMSE values which are varying from 2.15 mm to 5.43 mm. Following the estimation procedure, at each step the radius was increased and new neighboring stations were included in calculation process of missing data. Utilizing the data of added stations may increase or decrease the RMSE depending on the physical characteristics of data. Moreover, the estimates of all possible combinations were not so different from each other in terms of

calculated RMSE except the method of nearest neighbor. NN demonstrated relatively poor performance in estimation of missing values compared to the other methods in the meaning of higher RMSE values. The majority of the missing data estimation was conducted by the methods of NR, CCW, and MNR-T. Consequently, the missing periods of 14 precipitation stations were completed by the appropriate methods with corresponding neighboring stations in the optimum radius and 36 stations with completed daily precipitation series were created for further analysis in quality checks.

Table 6.1. Percent Missing Data, Descriptive Statistics and RMSE Values for the Best Methods and the Corresponding Number of Neighboring Stations within the Optimum Radius

Stations	% of missing data	Mean (mm)	Standard Deviation (mm)	RMSE (mm)	Number of Neighboring Stations	Optimum Radius (km)	Best Method
Akdeniz	9.0	1.04	4.25	3.06	7	25.0	MNR-T
Beyarmudu	9.5	0.93	4.51	3.00	8	25.0	NR
Beylerbeyi	0.9	1.35	6.52	4.47	12	25.0	MNR-T
Çayırova	3.6	1.08	5.19	3.23	4	15.0	NR
Çayönu	0.6	1.10	6.29	5.43	5	15.0	CCW
Gazimağusa	1.8	0.92	4.38	3.16	7	25.0	IDW
Gaziveren	0.2	0.75	3.11	2.15	4	15.0	NR
Gönendere	6.3	0.89	3.75	3.01	9	22.5	NR
Lapta	0.5	1.49	7.24	4.44	3	12.5	CCW
Serdarlı	0.2	0.90	4.17	2.89	6	15.0	NR
Taşkent	2.6	1.28	5.90	4.01	14	25.0	MNR-T
Tatlısu	2.9	1.30	5.90	4.24	6	22.5	CCW
Vadili	9.2	0.80	4.14	2.60	8	17.5	MNR-T
Yeşilırmak	8.8	1.00	4.06	3.20	3	25.0	CCW

Any precipitation value greater than 508 mm or repeating values at least seven times was detected which implied that there was no unreasonable value in precipitation series. For example, the maximum daily record for all stations was 215 mm (in Girne Station) which was less than the half of the upper limit in fix range test.

In order to determine the outliers in precipitation series, three different approaches were followed: checking for the gross errors in annual maximum daily series,

identifying the discordant stations in a region by using annual total precipitation series, and assessing the monthly precipitation series by calculating the threshold values for each month and replacing outliers with them. First of all, the discordancy measure (D_i) was calculated for each annual maximum daily series by assuming that Northern Cyprus is a homogeneous region as a whole. In the first trial, D_i was found as 3.66 for Mehmetçik Station and this value was greater than the critical value ($D_{cr} = 3$) which was determined for a number of stations more than 15 in a region by Hosking and Wallis (2005). In addition, Mehmetçik Station has the largest L_{skew} and L_{kur} values and one of the highest L_{CV} value among the precipitation stations as shown in Figure 6.1. Such these big L-moment ratios could lead to high discordancy measure due to the effect of erroneous values. When examined in detail, the series of Mehmetçik Station is compared with the neighboring stations of Çayırova and Ziyamet which are located 8.3 and 6.14 km far, respectively (Figure 6.2). Herein, 390 mm precipitation in a day was recorded on 7th November, 2005 which was relatively high checking against the two surrounding stations in those days. Therefore, this value was marked as erroneous and altered by following the same procedure of completing missing periods as previously mentioned. After modification of Mehmetçik Station, this step was repeated as a second trial due to the reason that changing in regional average L-moment ratios in a region leaded to new discordancy measures for all stations. Then in the second trial, Boğaz Station with $D_i = 3.49$, the largest L_{CV} and L_{skew} values, and one of the highest value of L_{kur} are computed as shown in Figure 6.3. On 13th February, 2012, 306.9 mm daily precipitation in Boğaz Station is thought to be errorneous data after comparing to the surrounding stations of Girne and Beylerbeyi as shown in Figure 6.4. Similarly, the correction was done and the process was repeated as a third trial. Finally, all the stations with the values of $D_i < 3$ are obtained as given in Table 6.2 which implies that there is no gross errors in the series of precipitation stations in a region.

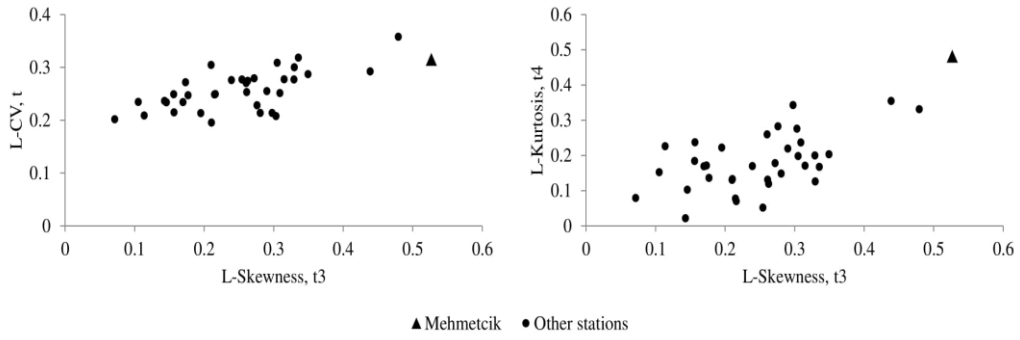

Figure 6.1. L-moment ratios of coefficient of variation versus coefficient of skewness and coefficient of kurtosis versus coefficient of skewness plots of annual maximum daily series in the first trial

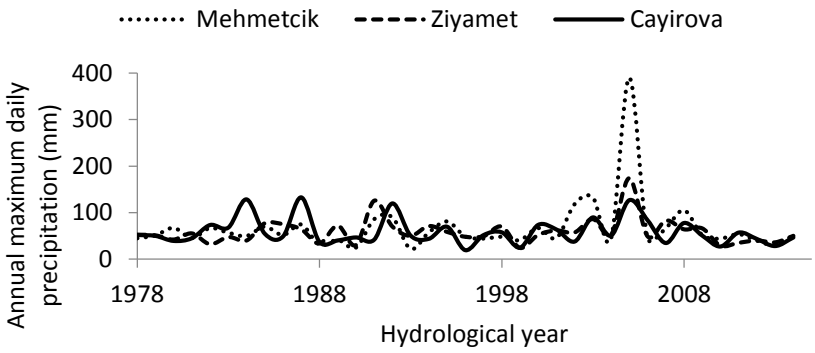

Figure 6.2. Annual maximum daily precipitation series of Mehmetçik, Ziyamet, and Cayırova stations

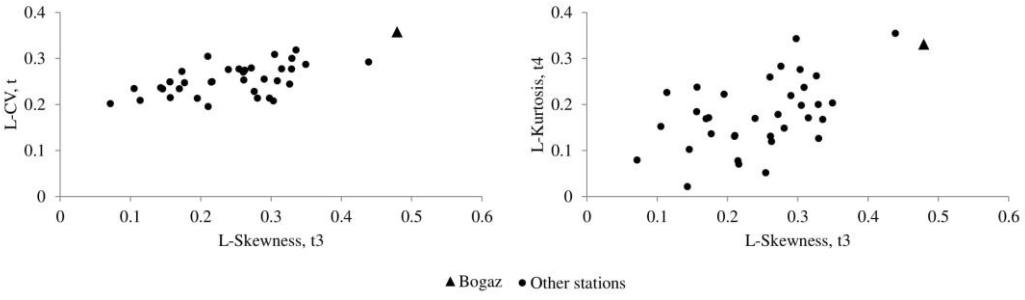

Figure 6.3. L-moment ratios of coefficient of variation versus coefficient of skewness and coefficient of kurtosis versus coefficient of skewness plots of annual maximum daily series in the first trial in the second trial

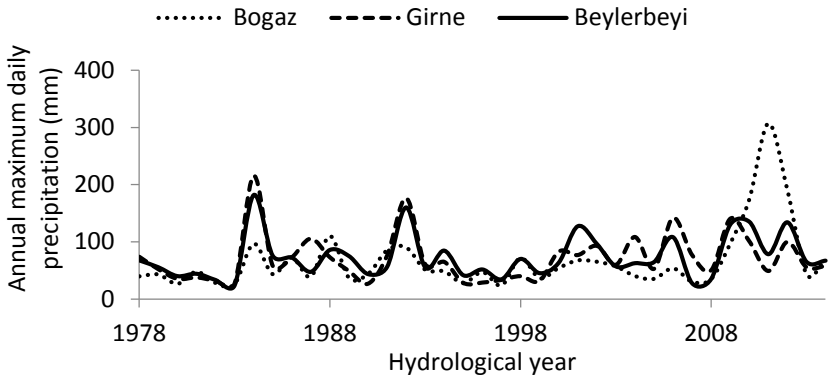

Figure 6.4. Annual maximum daily precipitation series of Boğaz, Girne, and Beylerbeyi stations

Table 6.2. Discordancy Measures Calculated in Each Trial

Precipitation Stations	First Trial D_i	Second Trial D_i	Third Trial D_i
Akdeniz	0.64	0.72	0.76
Camlibel	0.34	0.34	0.35
Lapta	1.13	1.12	1.16
Girne	0.74	0.81	1.04
Beylerbeyi	0.14	0.15	0.20
Bogaz	2.67	**3.49**	0.98
Tatlisu	0.89	0.89	0.89
Kantara	0.63	0.61	0.63
Esentepe	0.43	0.52	0.58
Guzelyurt	0.28	0.31	0.36
Gaziveren	0.38	0.38	0.37
Lefke	1.01	1.01	1.03
Yesilirmak	0.99	1.03	1.23
Ercan	0.33	0.33	0.34
Serdarli	1.27	1.30	1.31
Degirmenlik	0.57	0.70	0.84
Gecitkale	1.66	1.64	1.87
Gonendere	0.25	0.27	0.28
Vadili	1.16	1.17	1.17
Beyarmudu	1.18	1.41	1.69
Cayirova	0.10	0.13	0.15
İskele	0.23	0.24	0.27
Mehmetcik	**3.66**	0.69	0.71
Gazimagusa	2.02	1.93	2.03
Salamis	0.74	0.84	0.88
Alevkaya	0.38	0.37	0.36
Zumrutkoy	1.37	2.01	2.53
Alaykoy	0.28	0.33	0.35
Lefkosa	1.78	1.78	1.78
Ziyamet	0.73	0.82	0.83
Karpaz	0.43	0.49	0.58

Table 6.2 (Contd.)

Precipitation Stations	First Trial D_i	Second Trial D_i	Third Trial D_i
Yenierenkoy	1.83	2.05	2.07
Dortyol	1.76	1.75	1.75
Taskent	1.28	1.37	1.34
Kozankoy	1.59	1.56	1.66
Cayonu	1.12	1.43	1.61

Note: Bold value represents the values exceeding the critical value of D_i

Afterwards, the same procedure was conducted for the series of total annual precipitation to detect the discordant stations. As illustrated in Figure 6.5, the L-moment ratios of Çayönü, Serdarlı, and Yeşilırmak stations differ from the whole group of values and marked as discordant. However, the elimination of these stations from the study was left after the application of homogeneity tests, because the same data sets will also be used for the homogeneity analysis.

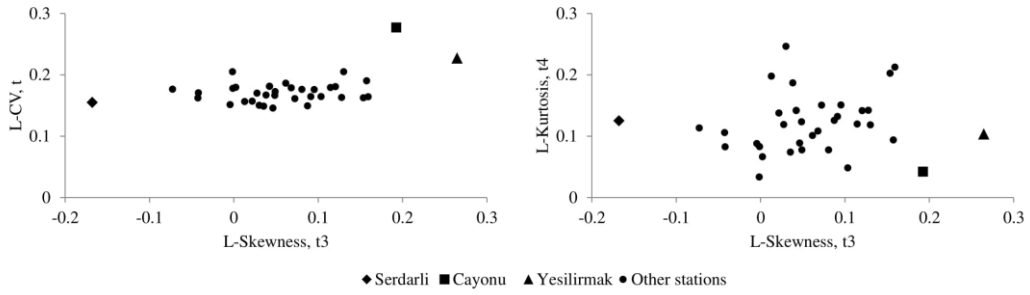

Figure 6.5. L-moment ratios of coefficient of variation versus coefficient of skewness and coefficient of kurtosis versus coefficient of skewness plots of total annual precipitation series for Serdarlı, Çayönü, and Yeşilırmak stations

Furthermore, detection of outliers for each month was executed by replacing the values which were greater than certain thresholds. In this context, monthly total precipitation series aggregated by daily series are assessed, and as displayed in Figure 6.6, the total amount of outliers in seasons are found as 65.2% in summer, 24.2% in autumn, 7.4% in spring, and 3.2% in winter. For monthly scale, the majority of outliers was distributed as 25.1% in July, 22.7% in August, 20.1% in September, and 17.4% in June. The other months had relatively less amount of outliers. Generally, summer

and early autumn are dry spells in terms of mostly no precipitation events in Northern Cyprus. For this reason, the majority of data consist of many zero values which lead to lower values of P_{out}. If any precipitation event occurred particularly due to isolated thunderstorms in this period, they naturally become outliers and need to be replaced by a unique P_{out} value.

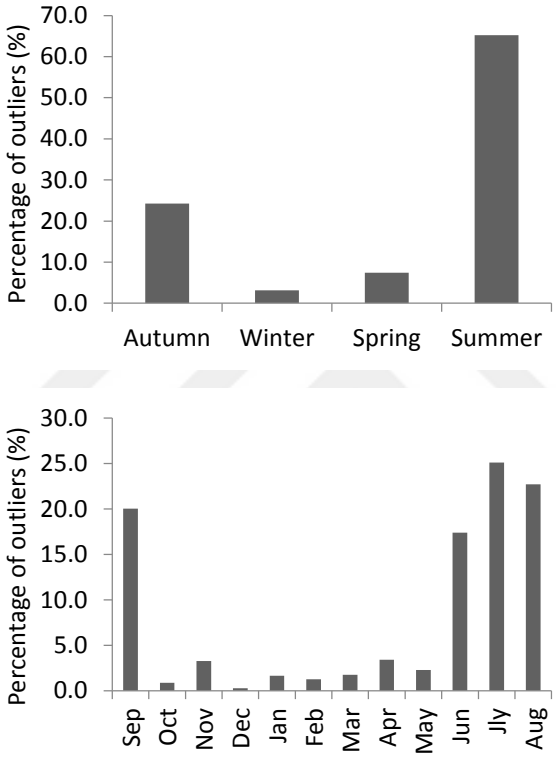

Figure 6.6. The outlier percentage distribution in monthly and seasonal scale

6.1.2. Homogeneity Assessment

The homogeneity assessment was conducted by following the two-step approach of Wijngaard et al. (2003). The results of the homogeneity test methods for the testing variables, given as the total annual precipitation, monthly maximum precipitation, and annual wet days are listed in Table 6.3. Firstly, one of the testing variables of the total

annual precipitation series were assessed by applying absolute homogeneity tests. Based on the results, Yeşilırmak and Tatlısu stations were flagged as suspect and Çayönü Station was found as doubtful.

According to the test results of Yeşilırmak Station, the null hypothesis at the 5% level was rejected for SNHT, Buishand range test, and Von Neumann ratio test. In the water year of 2007-2008, the break point was appointed. In Tatlısu station, three homogeneity tests of SNHT, Pettitt test, and Von Neumann ratio test rejected the null hypothesis at the 5% significance level and the break year was found at 1983-1984. In Çayönü Station, two out of four tests (Buishand range test and Von Neumann test) were significant and the break point was detected at 1999-2000.

By using the monthly maximum precipitation series as a testing variable, Çayönü Station was flagged as doubtful. The Buishand range test and the Von Neumann ratio test rejected the null hypothesis at the 5% level and the break year was found at 1999-2000. On the other hand, when the homogeneity of the stations is checked by using the testing variable of annual wet days, all the series were marked as useful as given in Table 6.3.

While analyzing the homogeneity of the seasonal total precipitation, the steps were separately repeated for the total precipitation in autumn, winter, spring, and summer, respectively. As illustrated in Table 6.4, no series are found as inhomogeneous by using the autumn, spring, and summer totals. However, Yeşilırmak and Çayönü stations were classified as doubtful when the series of winter totals were in use. In Yeşilırmak Station, the SNHT and the Von Neumann test were significant at the 5% level and the break year was observed at 2007-2008. In Çayönü Station, the Buishand range test and the Von Neumann test rejected the null hypothesis and determined the inhomogeneity at 1999-2000.

Table 6.3. Absolute Homogeneity Test Results for the Variables of Total Annual Precipitation, Monthly Maximum Precipitation and Annual Wet Days in Tatlısu, Yeşilırmak and Çayönu Stations

		Total annual precipitation			Monthly maximum precipitation			Annual wet days		
Station	Test Name	Test Statistics	Breakpoint	Result	Test Statistics	Breakpoint	Result	Test Statistic	Breakpoint	Result
Tatlısu	SNHT	9.30	1983-84	R	5.86	1993-94	F	2.89	2013-14	F
	Buishand	1.40	1983-84	F	1.30	1993-94	F	1.11	1988-89	F
	Pettitt	176	1983-84	R	144	1993-94	F	94	1989-90	F
	V. Neumann	1.41	-	R	1.76	-	F	1.59	-	F
Yeşilırmak	SNHT	16.19	2007-08	R	5.80	2007-08	F	9.28	2007-08	R
	Buishand	1.58	2007-08	R	0.96	2007-08	F	1.48	2008-09	F
	Pettitt	156	2007-08	F	130	2007-08	F	140	2007-08	F
	V. Neumann	1.18	-	R	1.41	-	R	1.73	-	F
Çayönü	SNHT	6.14	1999-00	F	4.16	1999-00	F	1.15	1992-93	F
	Buishand	1.81	1999-00	R	1.51	1999-00	R	0.90	2007-08	F
	Pettitt	101	1999-00	F	81	1999-00	F	55	2007-08	F
	V. Neumann	1.18	-	R	1.38	-	R	2.26	-	F

Note: R and F stand for reject and fail to reject the null hypothesis, respectively.

Table 6.4. Absolute Homogeneity Test Results for the Variables of Seasonal Total Precipitation in Tatlısu, Yeşilırmak and Çayönü Stations

		Autumn total precipitation			Winter total precipitation			Spring total precipitation		
Station	Test Name	Test Statistics	Breakpoint	Result	Test Statistics	Breakpoint	Result	Test Statistic	Breakpoint	Result
Tatlısu	SNHT	5.23	1983-84	F	3.6	1983-84	F	3.53	2009-10	F
	Buishand	1.01	1984-85	F	1.21	1997-98	F	0.77	1985-86	F
	Pettitt	138	1983-84	F	124	1997-98	F	94	2009-10	F
	V. Neumann	2.31	-	F	1.5	-	F	1.86	-	F
Yeşilırmak	SNHT	8.43	2006-07	R	10.79	2007-08	R	8.79	2006-07	R
	Buishand	1.08	2007-08	F	1.31	2007-08	F	1.27	2007-08	F
	Pettitt	115	2008-09	F	150	2007-08	F	146	2006-07	F
	V. Neumann	1.91	-	F	1.37	-	R	1.85	-	F
Çayönü	SNHT	1.70	2011-12	F	4.9	1999-00	F	3.17	2000-01	F
	Buishand	0.97	2009-10	F	1.59	1999-00	R	1.08	2000-01	F
	Pettitt	37	2011-12	F	103	1999-00	F	60	2000-01	F
	V. Neumann	2.01	-	F	1.25	-	R	2.17	-	F

Note: R and F stand for reject and fail to reject the null hypothesis, respectively.

The results obtained from the variables of annual total precipitation and winter total precipitation were both agreed that Yeşilırmak and Çayönü stations had inhomogeneous series and the detected break years were also consistent with each other. As a final decision, Yeşilırmak, Çayönü, and Tatlısu stations were eliminated from the data set and the remaining 33 homogeneous precipitation stations were selected to pass the next step for the trend analysis of extreme precipitation indices. Additionally, all these detected inhomogeneities should be validated by using historical metadata for each station. However, this is not possible due to the missing information for this study area.

6.1.3. Trend Analysis of Extreme Precipitation Indices

The majority of the higher values in extreme precipitation indices was distributed along the north coastal strip and on the Kyrenia Mountains in particular. On the contrary, the lower values covered the low-lying region of Mesaoria Plain. This spatial allocation was consistent with the mean annual precipitation series.

Prior to the trend analysis of precipitation indices, the first step was to perform the autocorrelation analysis for the annual and seasonal index series of precipitation stations. In order to control the serial independence, the null hypothesis of no serial dependence was investigated based on the formed 95% confidence interval according to the different sample sizes. The series with the lag-1 autocorrelation coefficients (r_1) in the interval were passed to the trend analysis stage, otherwise, the prewhitening was required before applying trend tests.

By using the annual series, 13 out of 231 calculated r_1 values are found as significant in terms of both positive and negative serial correlation as listed in Table 6.5. In Boğaz Station, the series of R95p index had the maximum r_1 value of 0.425 and in Lefkoşa Station, the minimum value was computed as -0.398 which were all significant at the 5% significance level. A small amount of significant r_1 with 7, 13, and 5 out of 231 were obtained in autumn, winter, and spring, respectively. In addition, 67% of all coefficients were detected as positively correlated. The 18% of the significant

correlations in the autumn was positive serial correlation. This ratio was 81% in winter and 52% in spring.

The existance of positive serial correlation in series lead to increase the probability of the incorrect rejection of the true null hypothesis of trendless series. Therefore, previously determined series were prewhitened and then, they were tested by the Mann-Kendall method. For instance, in Beyarmudu Station, an upward significant trend with $Z_s = 2.331$ was indicated by using the annual series of R20mm. After applying the prewhitening, Z_s statistic was decreased to 1.650 which implies the insignificant trend. Likewise, the prewhitened series of the R95pTOT annual series in Alevkaya Station and the R95pTOT winter series in İskele Station were prevented the erroneous decision about the significant trends and the results were changed as insignificant trends. Generally, the total number and the percentages of increasing or decreasing trends of indices are listed in Table 6.6. The information about the significant trends were also included.

Table 6.5. The results of Autocorrelation Analysis of Extreme Indices on Annual Scale

Stations	RR1	PRCPTOT	SDII	R20mm	RX1day	R95p	R95pTOT
Akdeniz	-0.140	-0.009	0.164	0.104	0.047	-0.012	-0.141
Camlibel	0.079	0.033	0.011	-0.099	-0.147	-0.045	-0.081
Lapta	0.053	0.146	0.241	-0.037	0.273	0.249	0.246
Girne	0.088	-0.009	0.043	-0.094	-0.008	0.063	**0.366**
Beylerbeyi	-0.059	-0.006	0.021	-0.015	0.005	0.058	0.035
Bogaz	0.267	0.170	**0.292**	0.041	0.203	**0.425**	0.242
Kantara	0.123	0.089	**0.342**	0.161	0.214	0.217	0.071
Esentepe	0.042	0.151	0.007	0.106	0.030	0.129	-0.068
Guzelyurt	0.024	-0.013	-0.155	0.000	-0.275	-0.147	-0.110
Gaziveren	-0.056	-0.070	-0.151	-0.021	-0.182	-0.070	0.031
Lefke	-0.073	0.148	0.045	0.227	-0.026	0.080	-0.078
Ercan	0.106	0.220	0.147	-0.163	-0.025	-0.008	-0.049
Serdarli	0.122	0.096	0.017	-0.078	-0.023	-0.045	-0.146
Degirmenlik	0.168	0.195	0.151	-0.056	0.051	**0.323**	0.067
Gecitkale	0.287	0.128	-0.126	0.056	-0.218	0.012	0.008
Gonendere	**0.338**	0.198	0.163	-0.011	0.088	0.213	0.215

Note: Bold value represents the significant serial correlation at the 5% level.

Table 6.5 (Contd.)

Stations	RR1	PRCPTOT	SDII	R20mm	RX1day	R95p	R95pTOT
Vadili	0.122	0.194	0.226	0.181	0.125	0.213	0.065
Beyarmudu	0.178	0.025	0.214	**0.294**	0.012	-0.005	0.097
Cayirova	0.109	0.003	**0.327**	0.122	-0.091	-0.216	-0.261
İskele	0.012	0.059	0.215	**0.385**	-0.062	0.016	0.044
Mehmetcik	0.171	0.107	0.065	0.108	-0.014	-0.031	-0.2
Gazimagusa	0.082	0.24	0.248	0.202	0.014	-0.012	-0.103
Salamis	0.091	0.056	0.253	-0.017	0.205	0.084	0.185
Alevkaya	-0.016	0.133	0.285	0.028	0.245	0.169	**0.34**
Zumrutkoy	0.013	0.014	-0.061	0.066	-0.137	-0.017	0.075
Alayköy	0.032	0.097	0.007	0.217	0.071	0.086	0.182
Lefkosa	0.024	0.272	0.251	**0.376**	-0.023	0.029	**-0.398**
Ziyamet	0.232	-0.119	0.082	-0.121	-0.076	-0.108	0.025
Karpaz	0.17	0.009	**0.325**	-0.062	0.093	0.119	0.113
Yenierenköy	-0.142	0.079	0.199	0.237	-0.063	0.089	0.055
Dortyol	0.225	0.196	0.119	0.011	-0.015	0.166	-0.054
Taskent	-0.028	-0.046	-0.085	0.094	0.002	-0.089	0.082
Kozankoy	0.058	0.016	0.036	-0.165	-0.122	-0.038	-0.109

Note: Bold value represents the significant serial correlation at the 5% level.

Table 6.6. The Total Number and Percentage of Increasing or Decreasing Trends in Precipitation Indices

Time scale	Index	IT	IT%	Sig (IT)	Sig (IT)%	DT	DT%	Sig (DT)	Sig (DT)%
Annual	RR1	21	63.6	2	10	12	36.4	1	8
	PRCPTOT	25	75.8	0	0	8	24.2	0	0
	SDII	23	69.7	2	9	10	30.3	0	0
	R20mm	25	75.8	1	4	8	24.2	0	0
	RX1day	24	72.7	1	4	9	27.3	0	0
	R95p	30	90.9	1	3	3	9.1	0	0
	R95pTOT	29	87.9	2	7	4	12.1	0	0
Autumn	RR1	23	69.7	0	0	10	30.3	0	0
	PRCPTOT	21	63.6	0	0	12	36.4	0	0
	SDII	14	42.4	0	0	19	57.6	1	5
	R20mm	24	72.7	1	4	9	27.3	0	0
	RX1day	14	42.4	0	0	19	57.6	0	0
	R95p	13	39.4	0	0	20	60.6	0	0
	R95pTOT	15	45.5	0	0	18	54.5	1	6
Winter	RR1	20	60.6	0	0	13	39.4	0	0
	PRCPTOT	24	72.7	0	0	9	27.3	0	0
	SDII	24	72.7	0	0	9	27.3	0	0
	R20mm	23	69.7	0	0	10	30.3	0	0
	RX1day	29	87.9	0	0	4	12.1	0	0
	R95p	32	97.0	0	0	1	3.0	0	0
	R95pTOT	28	84.8	3	11	5	15.2	0	0
Spring	RR1	14	42.4	0	0	19	57.6	1	5
	PRCPTOT	19	57.6	0	0	14	42.4	1	7
	SDII	17	51.5	1	6	16	48.5	0	0
	R20mm	19	57.6	2	11	14	42.4	0	0
	RX1day	18	54.5	1	6	15	45.5	0	0
	R95p	18	54.5	2	11	15	45.5	0	0
	R95pTOT	22	66.7	0	0	11	33.3	0	0

Note: IT, Sig (IT), DT, and Sig (DT) stand for increasing trend, significant increasing trend, decreasing trend, and significant decreasing trend, respectively.

6.1.3.1. Annual Trends

In Table 6.7, the Mann-Kendall trend test results on annual scale are shown. Generally, increasing trends with 77% of the stations dominated Northern Cyprus but only 4.3% of the stations exhibited significant trends at the 5% level. The R95p index had the maximum number of increasing trends in nearly 91% of stations. However, as shown in Table 6.7, only in Alevkaya Station the trend is significant with $Z_s = 2.141$. In Çamlıbel and Vadili stations, the RR1 index had significant upward trends with Sen's slopes of 0.464 day/year and 1.978 day/year, respectively. Moreover, Ziyamet Station

was detected as the one which observed the highest number of significant decreasing trends in a region. For PRCPTOT index, 75.8% of the stations had upward trends, but no one was significant. For SDII index, 69.7% of the stations demonstrated increasing trends. Herein, Gönendere, Beyarmudu and Dörtyol stations with Z_s values of 2.298, 2.008, and 2.030, respectively, showed significantly positive trends. Zümrütköy Station was the only one having statistically significant positive trend for R20mm with the Sen's slope of 0.0038 day/year among the 75.8% of series. For RX1day index, 72.7% of the stations were found as insignificant increasing trends and only in Gönendere Station, the trend was significantly positive. Girne and Beylerbeyi stations which are located very close to each other exhibited significant upward trends for R95pTOT index. The remaining stations had insignificant positive trends and there is no any detected decreasing trend.

The results revealed that in Northern Cyprus, the trends had a varying behavior in terms of a mix characteristics of increasing and decreasing and they were mainly insignificant. This pattern is consistent with the other studies, such as Kostopoulou and Jones (2005) for the Mediterranean, Zhang et al. (2005) for the Middle East, and other regions (e.g. Fan et al., 2012). Similarly, a mix pattern of trends were indicated in globally investigated studies as well (e.g. Easterling et al., 2000; Frich et al., 2002). Moreover, Alexander et al. (2006) presented that mostly the trends were insignificant by using the data on global scale which was in line with the findings of this study. As supported by Donat et al. (2013), the variability of annually calculated extreme indices did not show any spatial distribution regularly and the direction or magnitude of trends varied from one station to another independently. Donat et al. (2013) also stated that the trends were generally insignificant. Klein Tank and Können (2003) used the data sets in Europe and presented random trends as well as in nearby stations. Furthermore, according to Hadjinicolaou et al. (2011) the extreme indices consist of RX1day and SDII demonstrated insignificant upward trends for the future in Cyprus based on the projections carried out by six regional climate models. This result was validated by 70% of stations in the northern part of Cyprus. Moreover, Seyhun and Akıntuğ (2013)

exhibited insignificant trends for the total annual precipitation series of 20 stations in Northern Cyprus. When all results were analyzed, this finding was consistent with the results particularly for PRCPTOT index which was defined as the total annual precipitation in wet days.

6.1.3.2. Seasonal Trends

It is clear that there is no significant trend in autumn for the indices of RX1day, PRCPTOT, RR1, and R95p as illustrated in Table 6.6 and Table 6.8. In the RR1 and PRCPTOT indices, 69.7% and 63.6% of series showed insignificant upward trends, respectively. In Lefke Station, positive significant trend was detected for the R20mm index at 1% significance level. Besides, 58% of the stations indicated downward trends involving the indices of the R95p, RX1day, SDII, and R95pTOT. Among these, the SDII index series of Vadili Station and R95pTOT index series of Lefkoşa Station exhibited significant decreasing trends at 5% level. Additionally, Seyhun and Akıntuğ (2013) presented that there were significantly increasing trends in autumn rainfall for Çamlıbel and Lefke station at the 10% significance level. This finding was supported by the results particularly for the PRCPTOT index.

As shown in Table 6.9, positive trends are observed in approximately 77% of stations for the extreme precipitation indices in winter season. However, only the R95pTOT index is found as significant for the stations of Ercan at 5% level, Serdarlı at 1% level, and Vadili at 5% level as given in Table 6.9. All these stations were located in the Mesaoria Plain. In addition, except in Kozanköy Station, insignificant increasing trends were detected for the index of R95p in all other stations.

While examining the trends in spring period, the number of increasing and decreasing trends are almost the same (Table 6.10). In the RR1 index, the downward trends in 57.6% of stations were found and only Gönendere Station with significant trend at 5% level was detected. Also, in the same station, the positive significant trends were observed for the indices of the SDII at 1% level and R20mm, RX1day, R95p at 5% level. Moreover, in Gönendere and Beyarmudu stations, the increasing significant

trends were obtained at 5% level for R20mm index. The insignificant downward trends were found in 42.4% of the stations for the index of PRCPTOT and one significant trend at 5% level was obtained at Yenierenköy Station. This finding was consistent with those of Seyhun and Akıntuğ (2013) which revealed the significant trend for Yenierenköy Station by testing the total rainfall series in spring.

In this study, summer season was decided to be eliminated from the investigation of seasonal trends due to the undefined indices. Because the climate of Cyprus has characteristics of very hot and long dry spells in summer which lead to stations to have almost all data with zero values and undefined index values.

6.2. Regional Frequency Analysis

6.2.1. Preliminary Data Screening

Beforehand two stations named as Taşkent and Kozanköy were excluded from the study due to their relatively shorter observations periods. Substantially, the underlying reason was the limitation of applying some time series clustering approaches for the series with different lengths. In addition, previously determined inhomogeneous series of Tatlısu, Yeşilırmak, and Çayönü stations were also omitted for the regional frequency analysis due to having no historical metadata. According to the results of trend analysis, Gönendere Station had the statistically significant trend for the annual maximum daily series or in other words, RX1day index. Therefore, this station was also not considered for the further analyses. Finally, the 30 stations with quality-controlled, complete, and homogeneous series were validated for the assumptions of frequency analysis in terms of serial independency and stationarity. As mentioned before, all these stations were checked against the serial correlation and stationarity by applying the lag-1 autocorrelation coefficient and a nonparametric Mann-Kendall test, respectively.

As recommended by Hosking and Wallis (2005), preliminary data screening is conducted by calculating discordancy measure (D_i) under the assumption of all stations are in the same homogeneous region. Herein, none of the precipitation series

had a discordancy test statistic greater than the critical value ($D_{cr} = 3$) for 30 stations which means that there is discordant station in the group.

6.2.2. Formation of Homogeneous Regions

In order to identify the homogeneous regions, several time series clustering approaches were applied to the annual maximum precipitation series besides the classical approach of using the meteorological and physical characteristics of stations. Firstly, conventional approach was carried out by determining four clustering variables, named as latitude, longitude, elevation, and mean annual precipitation in order to properly reflect the features of hydrological regions. Besides, the optimum number of regions were determined by calculating 30 indices of NbClust R-package developed by Charrad et al. (2014). The best number of regions were found as three based on the results applying the majority rule. Then, as recommended by Hosking and Wallis (2005), the Hierarchical Ward's method was employed to form the clusters depending on the distance matrix calculated by the Euclidean distance. Regarding this, the clusters were constructed as follows: first cluster (Sub-region 1) including the 9 precipitation stations located around the Kyrenia Mountains; second cluster (Sub-region 2) covering the area of Mesaoria Plain with 16 stations; and third cluster (Sub-region 3) consisting of 5 stations in the Karpass Peninsula. Next, the heterogeneity test was applied to each sub-region and all of three sub-regions were declared as acceptably homogeneous. On the other hand, this time discordancy measure was calculated by considering the sub-regions separately homogeneous. According to the results, in Sub-region 1, Kantara Station was detected as discordant and as suggested by Hosking and Wallis (2005), manual refinement was executed by transferring this station from Sub-region 1 to Sub-region 3 consistent with the characteristics of the region like elevation and mean annual precipitation. After the relocation, checking of discordancy measure was repeated and no discordancy was detected.

Table 6.7. The Results of Mann-Kendall Test of Extreme Indices on Annual Scale

Indices	Akdeniz	Çamlıbel	Lapta	Girne	Beylerbeyi	Boğaz	Kantara	Esentepe	Güzelyurt	Gaziveren	Lefke
RR1	0.210	**2.566**	0.629	-0.485	0.354	0.642	-0.997	1.853	0.512	0.525	1.153
PRCPTOT	0.615	1.949	0.432	-0.078	0.615	0.798	0.772	0.968	0.667	1.190	1.543
SDII	0.693	0.562	0.405	0.562	-0.013	0.101	1.022	-0.435	0.092	0.850	1.452
R20mm	1.141	1.806	0.894	-0.053	0.264	0.934	0.463	0.122	1.284	1.147	1.334
RX1day	0.497	0.824	0.013	1.439	1.609	1.270	0.222	0.907	0.484	1.295	1.557
R95p	0.262	1.792	0.641	1.321	1.949	1.056	0.576	1.053	0.772	1.347	1.609
R95pTOT	0.013	1.112	0.379	**2.275**	**2.289**	1.258	0.170	1.403	1.295	1.609	0.693
Indices	Ercan	Serdarlı	Değirmenlik	Geçitkale	Gönendere	Vadili	Beyarmudu	Çayırova	İskele	Mehmetçik	Gazimağusa
RR1	0.184	0.555	0.378	-0.157	-0.754	**1.978**	0.788	1.193	-0.131	1.192	0.485
PRCPTOT	0.968	0.578	0.981	0.275	0.871	0.131	1.645	1.164	-0.065	1.321	1.164
SDII	1.583	-0.704	0.880	0.405	**2.298**	-1.517	**2.008**	0.480	-0.013	0.144	1.347
R20mm	1.352	0.832	0.738	-0.385	1.155	-0.159	1.650	0.598	0.541	0.765	0.027
RX1day	0.955	0.352	-0.013	-0.510	**2.542**	0.811	1.573	-0.602	-0.144	-0.196	1.779
R95p	0.641	0.855	1.033	0.170	0.968	1.321	1.597	0.288	0.065	1.073	1.334
R95pTOT	-0.667	0.277	0.352	-0.536	0.774	1.687	0.556	-1.164	0.065	0.248	1.321
Indices	Salamis	Alevkaya	Zümrütköy	Alayköy	Lefkoşa	Ziyamet	Karpaz	Yenierenköy	Dörtyol	Taşkent	Kozanköy
RR1	-0.061	0.969	1.257	-1.469	1.432	**-2.177**	-1.624	-0.367	-1.952	1.567	-0.732
PRCPTOT	-0.774	0.750	1.491	-0.536	0.387	-0.301	0.001	-0.745	-0.232	0.612	-0.170
SDII	-0.919	-0.145	0.484	0.955	-0.001	1.112	0.858	-0.719	**2.030**	-0.771	0.340
R20mm	-0.467	-0.639	**2.196**	-0.978	0.605	0.463	0.316	-1.281	0.520	0.439	-0.172
RX1day	-0.811	0.617	1.073	1.047	0.23	-0.144	0.550	0.118	1.172	-0.435	-0.034
R95p	-0.181	**2.141**	1.779	0.392	0.726	0.157	0.183	-0.523	0.422	0.494	-0.408
R95pTOT	0.847	1.106	1.949	1.399	0.402	0.641	0.353	0.484	1.866	0.178	-0.170

Note: Bold values represent the significant trends at the 5% level.

Table 6.8. The Results of Mann-Kendall Test of Extreme Indices in Autumn

Indices	Akdeniz	Çamlıbel	Lapta	Girne	Beylerbeyi	Boğaz	Kantara	Esentepe	Güzelyurt	Gaziveren	Lefke
RR1	0.434	1.825	0.907	-0.092	0.830	1.404	-0.586	0.912	0.066	0.553	0.857
PRCPTOT	0.759	1.884	0.523	0.379	-0.092	0.726	0.039	1.790	-0.249	0.052	1.779
SDII	0.405	0.327	-0.366	-0.039	-1.216	0.097	0.510	1.790	-0.615	-0.353	0.680
R20mm	0.960	1.024	0.696	0.097	0.068	-0.260	0.482	1.908	0.249	0.724	**2.900**
RX1day	1.033	1.780	0.497	-0.183	-0.641	0.060	-0.327	1.452	-0.589	0.105	1.348
R95p	1.033	1.780	0.432	-0.183	-0.641	-0.085	-0.001	1.524	-0.589	0.052	1.348
R95pTOT	0.065	0.013	-0.510	0.144	-0.824	-1.403	-0.719	0.097	0.092	0.144	0.078
Indices	Ercan	Serdarlı	Değirmenlik	Geçitkale	Gönendere	Vadili	Beyarmudu	Çayırova	İskele	Mehmetçik	Gazimağusa
RR1	0.767	1.090	1.568	1.636	-0.220	1.762	0.998	0.527	0.164	1.146	1.306
PRCPTOT	0.275	0.603	1.270	0.039	0.544	-0.327	0.254	-0.536	-0.749	0.222	0.706
SDII	0.368	-0.855	0.876	-1.921	0.603	**-2.370**	-0.022	-0.955	-0.722	-0.536	0.419
R20mm	0.564	0.174	0.967	-0.749	0.078	-0.983	1.378	-0.582	-0.770	0.739	0.713
RX1day	0.497	-0.038	1.572	-0.680	0.303	-0.510	0.230	-1.020	-0.497	-0.013	1.151
R95p	0.497	-0.038	1.572	-0.680	0.085	-0.510	0.230	-0.732	-0.497	-0.379	1.151
R95pTOT	-1.478	-1.257	-0.405	-1.504	-0.327	0.392	-0.690	-1.216	-0.536	-0.562	0.667
Indices	Salamis	Alevkaya	Zümrütköy	Alayköy	Lefkoşa	Ziyamet	Karpaz	Yenierenköy	Dörtyol	Taşkent	Kozanköy
RR1	-0.244	1.142	0.541	-0.540	1.621	-1.472	-0.725	-0.420	-1.152	1.369	-1.093
PRCPTOT	-0.799	0.363	0.523	-0.445	0.206	-0.484	-0.876	-1.347	-1.103	0.494	-0.136
SDII	-0.557	-0.830	0.275	-0.368	-0.805	0.719	-1.033	-1.373	0.099	-0.217	0.034
R20mm	-1.414	0.368	1.525	0.120	0.054	0.420	-0.513	-1.215	-1.067	0.021	0.730
RX1day	-1.234	-0.690	0.929	-0.393	-0.181	-0.458	-1.269	-1.256	-1.131	0.316	-0.001
R95p	-1.234	-0.278	0.824	-0.393	-0.181	-0.236	-1.269	-1.583	-1.131	0.356	-0.323
R95pTOT	0.145	-1.403	0.118	0.196	**-1.984**	1.164	-0.327	-0.222	0.199	-0.494	0.646

Note: Bold values represent the significant trends at the 5% level. Both bold and underlined values represent the significant trends at the 1% level.

Table 6.9. The Results of Mann-Kendall Test of Extreme Indices in Winter

Indices	Akdeniz	Çamlıbel	Lapta	Girne	Beylerbeyi	Boğaz	Kantara	Esentepe	Güzelyurt	Gaziveren	Lefke
RR1	-0.039	1.467	0.559	0.499	0.643	0.528	-0.669	1.455	1.050	0.787	0.184
PRCPTOT	0.432	1.007	0.123	0.092	0.615	0.823	-0.379	0.145	0.654	0.706	0.745
SDII	0.536	0.432	0.353	0.327	0.405	0.508	0.615	-0.194	0.013	1.007	0.955
R20mm	0.693	0.916	0.741	-0.001	0.463	0.984	-0.191	-0.184	-0.480	1.179	0.439
RX1day	-0.327	0.079	0.504	1.505	1.661	1.065	0.510	0.581	-0.026	0.824	0.275
R95p	0.275	0.458	0.286	0.785	1.583	1.150	0.445	1.246	0.536	1.530	0.379
R95pTOT	0.065	-0.275	-0.432	1.216	1.478	0.750	0.641	1.306	-0.013	1.426	-0.484
Indices	Ercan	Serdarlı	Değirmenlik	Geçitkale	Gönendere	Vadili	Beyarmudu	Çayırova	İskele	Mehmetçik	Gazimağusa
RR1	-0.118	0.731	-0.731	-0.669	-0.101	0.865	0.461	0.813	-0.171	0.682	-0.105
PRCPTOT	0.772	-0.176	0.226	-0.196	0.218	0.065	0.968	0.798	0.065	0.589	0.667
SDII	1.609	-0.566	0.427	0.955	0.992	-0.301	1.427	0.667	0.536	1.007	1.086
R20mm	1.376	0.915	0.245	0.228	0.485	0.149	1.156	1.541	0.586	0.320	-0.160
RX1day	1.217	0.641	0.226	0.379	1.271	0.916	1.767	0.876	1.517	1.649	1.360
R95p	1.753	1.823	0.204	0.536	1.077	1.178	1.512	1.112	1.334	1.334	0.562
R95pTOT	**2.158**	**3.017**	0.251	1.609	1.476	**2.080**	1.403	1.138	1.294	1.426	0.432
Indices	Salamis	Alevkaya	Zümrütköy	Alayköy	Lefkoşa	Ziyamet	Karpaz	Yenierenköy	Dörtyol	Taşkent	Kozanköy
RR1	-0.146	0.061	1.193	-0.919	0.485	-0.551	-0.027	0.656	-0.533	0.951	0.188
PRCPTOT	-0.484	0.001	0.275	-0.013	-0.315	-0.001	0.196	-0.013	0.204	0.375	-0.238
SDII	-0.121	0.363	-0.353	1.138	-1.306	0.902	1.086	-0.222	1.335	-0.178	-0.544
R20mm	0.509	-0.839	0.832	-0.970	-0.230	0.464	0.530	0.602	0.382	-0.201	-0.397
RX1day	0.593	0.036	0.353	1.007	-0.085	1.165	1.624	0.746	0.641	0.356	-0.816
R95p	0.266	0.169	1.020	0.366	0.151	0.929	0.785	0.379	0.926	0.533	-0.884
R95pTOT	1.790	0.145	1.609	1.216	1.185	1.661	1.792	1.059	1.076	1.087	-0.816

Note: Bold values represent the significant trends at the 5% level. Both bold and underlined values represent the significant trends at the 1% level.

Table 6.10. The Results of Mann-Kendall Test of Extreme Indices in Spring

Indices	Akdeniz	Çamlıbel	Lapta	Girne	Beylerbeyi	Boğaz	Kantara	Esentepe	Güzelyurt	Gaziveren	Lefke
RR1	-0.210	1.024	0.342	-1.078	-0.763	-0.583	-0.039	0.341	-0.263	-0.158	0.407
PRCPTOT	-0.458	1.007	0.170	-1.256	-0.902	-0.363	0.863	-0.194	0.445	-0.615	1.099
SDII	-1.076	-0.422	-0.558	-0.602	-0.353	-0.435	1.269	-0.435	0.432	-0.248	0.445
R20mm	1.299	1.250	0.543	-0.100	-0.086	0.329	1.482	-1.418	1.636	-0.800	0.319
RX1day	-0.039	0.157	0.275	-0.039	0.667	0.290	0.942	-0.290	-0.026	-0.262	0.576
R95p	0.001	0.170	0.196	-0.249	0.667	0.097	0.785	-0.678	-0.026	-0.340	0.445
R95pTOT	-0.144	-1.138	0.196	0.772	1.242	0.702	0.013	0.097	-0.301	0.379	0.078
Indices	Ercan	Serdarlı	Değirmenlik	Geçitkale	Gönendere	Vadili	Beyarmudu	Çayırova	İskele	Mehmetçik	Gazimağusa
RR1	0.132	-0.013	0.417	-0.223	**-2.300**	1.261	0.693	0.801	-0.329	0.961	-0.671
PRCPTOT	0.065	0.226	0.855	0.772	1.185	0.458	1.379	0.772	-0.065	0.248	-0.262
SDII	0.445	0.578	0.440	1.242	**2.782**	-0.772	1.694	-0.262	-0.641	-0.170	-0.092
R20mm	-0.085	1.277	0.781	-0.589	**2.567**	0.529	**2.522**	-0.946	-0.405	0.395	1.131
RX1day	-0.041	0.340	0.780	-0.065	**2.130**	0.249	1.368	-0.432	-0.824	0.837	-0.484
R95p	-0.041	0.629	0.805	-0.065	**2.130**	0.589	1.392	-0.432	-0.719	0.837	-0.589
R95pTOT	-0.118	0.063	0.226	-1.583	1.006	-0.536	0.726	-0.745	-0.615	0.177	0.772
Indices	Salamis	Alevkaya	Zümrütköy	Alayköy	Lefkoşa	Ziyamet	Karpaz	Yenierenköy	Dörtyol	Taşkent	Kozanköy
RR1	0.170	0.316	0.841	-0.554	-1.084	-1.024	-0.736	-0.814	-1.817	0.675	-0.307
PRCPTOT	-0.375	-0.194	1.844	-0.013	0.581	-0.157	-0.248	**-2.001**	0.001	0.968	0.544
SDII	-0.750	-0.750	0.929	0.118	0.847	0.693	0.536	-1.452	1.430	0.494	0.393
R20mm	-0.300	-1.245	-0.400	-0.320	1.082	0.522	0.014	-1.451	1.061	1.525	-0.130
RX1day	-0.484	-0.133	1.715	-0.065	0.544	0.196	-0.105	-1.505	0.627	1.067	0.238
R95p	-0.484	-0.133	**1.977**	-0.065	0.544	0.196	-0.222	-1.558	0.627	1.067	-0.272
R95pTOT	-0.048	0.484	1.164	0.013	0.363	0.589	0.353	-0.222	1.893	0.257	-0.476

Note: Bold values represent the significant trends at the 5% level. Both bold and underlined values represent the significant trends at the 1% level.

Secondly, nine different time series clustering approaches were adapted to regional frequency analysis for obtaining homogeneous regions more accurately. These approaches involving shape-based, feature-based, and model-based methods were used with the data sets of monthly total precipitation series. Since there are several other time series clustering methods reported in literature, some trials were also executed different from the mentioned methods. However, the final clustering results were not reasonable with respect to hydrological aspect. Therefore, the analyses were carried out with at least physically possible clusters. The applicable methods were employed by utilizing TSclust R-package of Montero and Vilar (2014).

In shape-based approaches, the Ward's method forms the clusters based on the similarity measures of the Euclidean (EUCL), Manhattan (MAN), and Dynamic Time Warping (DTW) which directly use the monthly precipitation data. The results of clustering in three methods are the same with each other and with the conventional approach as well (Table 6.11). Herein, it needs to be emphasized that these methods generated the clusters of conventional approach directly without refinement.

In feature-based approaches of discrete wavelet transform (DWT), correlation-based (COR), and symbolic aggregate approximation (SAX), the series was transformed to feature vector to reduce their dimensions. Therefore, Ward's method was applied to the vectors rather than using the high dimensional raw data. According to the final clusters shown in Table 6.11, COR offers five sub-regions with almost equally distributed number of stations for each cluster. DWT and SAX showed close results with three sub-regions and two of three clusters had relatively greater number of stations.

In model-based approaches, Piccolo distance (AR.PIC), Maharaj distance (AR.MAH), and Cepstral-based distance (LPC.Cep) were embedded in Ward's method to cluster the series based on the parameters of the fitted model. As listed in Table 6.11, all model-based approaches agree to divide the region into two sub-regions. But, the stations located in clusters were different in all three methods. However, the same

probability distributions were proposed as best fit distributions for the sub-regions. Therefore, totally seven different candidate clustering cases were generated for analyzing in detail.

All sub-regions of candidate clustering were evaluated by using the heterogeneity measure and the result showed that these sub-regions were acceptably homogeneous with validating criterion of $H < 1$. Then, in order to determine the best fitted distribution for each sub-region among the candidate distributions of PE3, GNO, GLO, GEV and GPA, the goodness-of-fit measure (Z^{DIST}) was calculated. If a distribution satisfied the condition of $Z^{DIST} \leq 1.64$, it was called as acceptable fit for a certain region. Here, more than one distribution can satisfy this criterion as well. In that case, the best option become the best fit which have the closest Z^{DIST} statistic value to zero (Hosking and Wallis, 2005). In addition to this, visual evaluation of best fit was carried out by plotting L-moment ratio diagrams. Besides, several simulations were generated by applying all the alternative best fit distributions to the sub-regions. After 1,000 number of Monte Carlo realizations, a best fit distribution was decided considering the lowest RRMSE values of regional growth curves for larger return periods. The best fit results are given in Table 6.11 with goodness-of-fit statistics and the heterogeneity measures. In about the half of the candidate sub-regions, PE3 was found as the most appropriate distribution (9 of 20), then GLO was decided in 6 of 20 sub-regions, GNO in 4 of 20, and GEV was only selected to describe one sub-region.

For the assessment of uncertainty in clustering approaches, the jackknife validation procedure was employed with the performance evaluation indices of AB, RB, RMSE, RRMSE, and NASH for different return periods. The recommended Log-Pearson Type III (LP3) was used to perform local frequency analysis and its results were also validated by the Kolmogorov-Simirnov test at all significance levels. The results of the jackknife procedure in terms of comparing local and regional frequency results based on different candidate clustering are listed in Table 6.12. As expected, the performance indices had small values in lower return periods or in other words, more precise quantile estimates.

Table 6.11. Results of Clustering Approaches, Heterogeneity Measures, and Goodness-of-fit Tests for 30 Precipitation Stations in Northern Cyprus Region

				Candidate distributions					Best fit
Method (distance measure)	Sub-region	Number of stations	H	GLO	GEV	GNO	PE3	GPA	
Conventional (EUCL) Shape-based (EUCL, MAN, DTW)	1	8	-0.37	2.56	**1.33**	**0.70**	**-0.42**	-1.79	PE3
	2	16	0.45	**1.20**	**-0.49**	**-1.16**	-2.41	-4.63	GNO
	3	6	-0.65	**-1.29**	-1.97	-2.45	-3.30	-3.78	GLO
Feature-based (COR)	1	5	-0.07	**1.32**	**0.39**	**-0.06**	**-0.88**	-1.95	PE3
	2	7	0.38	1.66	**0.28**	**-0.10**	**-0.86**	2.96	PE3
	3	6	-0.65	-1.30	-1.97	-2.45	-3.29	-3.79	GLO
	4	6	-1.44	2.13	1.36	0.66	-0.56	-0.81	PE3
	5	6	-0.99	-0.02	-1.16	-1.44	-2.01	-3.80	GNO
Feature-based (DWT)	1	11	0.07	**1.54**	**0.28**	**-0.42**	-1.65	-2.97	GNO
	2	12	0.09	**0.09**	**-1.20**	-1.79	-2.86	-4.40	GEV
	3	7	-0.43	**1.29**	**0.14**	**-0.35**	**-1.25**	-2.70	PE3
Feature-based (SAX)	1	11	-1.28	2.43	**1.24**	**0.41**	**-1.05**	-1.96	PE3
	2	13	-0.44	**1.15**	**-0.65**	**-1.13**	-2.08	-4.87	GNO
	3	6	-0.65	**-1.25**	-1.90	-2.37	-3.20	-3.67	GLO
Model-based (AR.PIC)	1	12	-1.28	2.70	**1.43**	**0.57**	**-0.94**	-1.94	PE3
	2	18	-1.00	**-0.02**	-1.70	-2.33	-3.50	-5.79	GLO
Model-based (AR.MAH)	1	15	-1.81	2.27	**0.96**	**0.03**	**-1.60**	-2.55	PE3
	2	15	-1.38	**0.03**	-1.65	-2.14	-3.13	-5.60	GLO
Model-based (LPC.Cep)	1	12	-1.3	2.73	**1.46**	**0.6**	**-0.91**	-1.91	PE3
	2	18	-1	**-0.04**	-1.72	-2.35	-3.53	-5.82	GLO

Note: Bold value represents the candidate distributions which meet the criterion of the goodness-of-fit statistic.

COR feature-based time series clustering approach mostly demonstrated the best performance in terms of least biased results. As illustrated in Table 6.12, the AB index has a range from 2.78 mm to 35.98 mm which are smaller than the conventional approach. In RB index, the results of the clustering methods were negative which meant that the regional frequency analysis overestimated the results of the local frequency analysis. For instance, while analyzing extreme precipitation events, using the homogeneous sub-regions and frequency distributions of COR instead of conventional approach brought in better estimations by decreasing the RB index of larger return periods, such as in 100-year from -0.97% to 0.60%; in 200-year from -1.67% to 0.81%; and in 500-year from -6.01% to -2.20 %.

With respect to RMSE and RRMSE indices, again COR demonstrated the top success by having lower values of indices in general. When compared to conventional approach, RMSE reduced from a range of 3.79 mm to 52.12 mm to the range of 3.52 mm to 44.59 mm. Besides, the RRMSE values in larger return periods decreased from 16.19% to 13.53% in 100-year; from 20.63% to 17.78% in 200-year; and from 27.43% to 24.10% in 500-year.

According to NASH index, the acceptable range was between 0 and 1 for which value of 1 represented the best match. Similarly, COR had the highest accuracy with varying NASH values from 0.97 in 10-year to 0.48 in 500-year return period. To summarize, COR clustering appeared as the best performing approach compared to conventional and other time series clustering approaches. Particularly, the estimation improvement for the larger return periods was contributed to the extreme precipitation analysis. Therefore, the final homogeneous regions are formed based on the results of COR as shown in Figure 6.7 including the sub-regions and precipitation stations listed in Table 6.13.

As mentioned in Bagnall and Janacek (2005), decision of the most appropriate clustering approaches is strongly related with the basic purpose of performing clustering. For instance, DWT and SAX which lead to decrease the dimension of series

by extracting a number of coefficients as features generally used for investigating the similarity of series in terms of periodicities. However, while using long time series, model-based approaches are more suitable (Wang et al., 2006). On the other hand, such approaches can fail to group data if the clusters are so close to each other (Mitsa, 2010). Likewise, in this study, model-based approaches showed poor performance of clustering precipitation series.

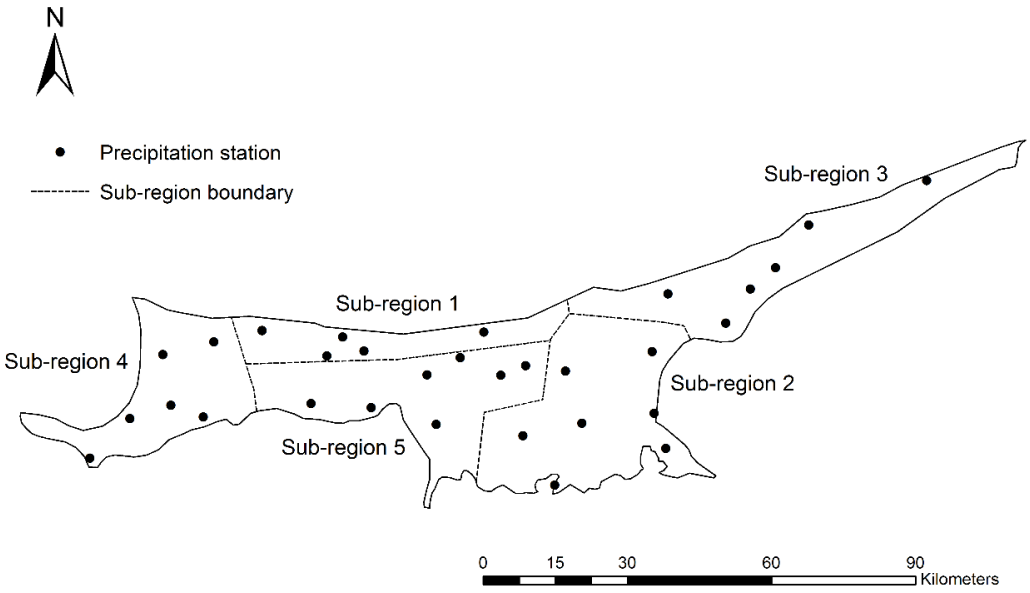

Figure 6.7. The final homogeneous regions

Since the main objective is to group of stations following the same pattern during the observation period, correlation-based approach, COR, was the most appropriate method in delineation of Northern Cyprus into five homogeneous sub-regions. In Nikolakis (2008), the whole island of Cyprus was delineated into four regions by applying factor analysis to the monthly mean rainfall series. The regions covering Northern Cyprus were consistent with the sub-regions of COR excluding eastern part of the Mesaoria Plain or Sub-region 2. It must be noted that the data sets and recording periods of Nikolakis (2008) and this study are different from each other.

Table 6.12. The Results of Performance Evaluation Indices Jack-knife Validation Procedure for Each Clustering Alternative

Error Type	Return period (year)	Clustering method						
		Conventional, EUCL, MAN, DTW	COR	DWT	SAX	AR.PIC	AR.MAH	LPC.Cep
AB (mm)	10	3.17	**2.78**	3.19	2.86	3.05	2.79	3.01
	50	11.88	**9.89**	12.64	10.31	10.71	10.32	10.56
	100	18.72	**15.71**	19.13	17.09	16.66	17.08	16.57
	200	27.82	**23.65**	27.34	26.07	25.24	26.12	25.11
	500	41.67	**35.98**	37.61	39.04	41.06	39.22	40.80
RB (%)	10	-0.29	-0.73	-0.57	-0.55	0.39	**-0.17**	0.37
	50	-0.54	0.22	-0.80	**-0.07**	-0.92	-0.48	-0.90
	100	-0.97	0.60	-0.94	**-0.01**	-2.36	-1.08	-2.32
	200	-1.67	0.81	-1.14	**-0.15**	-4.42	-2.09	-4.40
	500	-6.01	**-2.20**	-4.43	-3.69	-11.25	-7.13	-11.21
RMSE (mm)	10	3.79	**3.52**	3.76	3.60	4.00	3.62	3.98
	50	14.58	**11.85**	14.84	12.80	13.13	12.91	13.10
	100	23.09	**19.45**	22.59	20.59	21.05	20.89	21.01
	200	34.61	**30.15**	32.47	31.47	32.08	31.99	31.98
	500	52.12	**44.59**	45.35	48.36	48.77	48.93	48.67

Note: Bold value represents the best performing statistics.

Table 6.12 (Contd.)

Error Type	Return period (year)	Clustering method						
		Conventional, EUCL, MAN, DTW	COR	DWT	SAX	AR.PIC	AR.MAH	LPC.Cep
RRMSE (%)	10	4.69	**4.21**	4.55	4.27	4.56	4.25	4.30
	50	12.16	9.85	12.53	9.95	10.66	9.48	**8.23**
	100	16.19	**13.53**	16.50	13.65	15.39	13.74	15.12
	200	20.63	**17.78**	20.67	17.88	21.19	18.91	21.08
	500	27.43	**24.10**	26.29	24.30	30.94	27.05	30.61
NASH	10	**0.97**	**0.97**	**0.97**	**0.97**	0.96	**0.97**	0.96
	50	0.78	**0.87**	0.76	0.83	0.82	0.85	0.83
	100	0.61	**0.73**	0.59	0.70	0.63	0.69	0.64
	200	0.40	**0.59**	0.35	0.53	0.29	0.39	0.31
	500	0.21	**0.48**	0.10	0.38	-0.19	-0.08	-0.12

Note: Bold value represents the best performing statistics.

Table 6.13. Characteristics of Precipitation Stations in Each Homogeneous Sub-Regions

Sub-region	Stations	Latitude (◦)	Longitude (◦)	Elevation (m)	MAP (mm)
1	Lapta	35.335754	33.163364	168	531.2
	Girne	35.34194	33.33139	10	466.6
	Beylerbeyi	35.297294	33.354036	225	483.6
	Bogaz	35.288252	33.28484	300	400.5
	Esentepe	35.332728	33.578518	183	432.9
2	Gecitkale	35.23333	33.72861	45	323.9
	Vadili	35.138689	33.651608	54	284.7
	Beyarmudu	35.047159	33.69582	87	333.2
	Gazimagusa	35.13639	33.93556	10	327.4
	Salamis	35.180802	33.897344	6	313.9
	Dortyol	35.17889	33.75861	54	268.9
	Iskele	35.28611	33.88444	39	330.3
3	Cayirova	35.349489	34.031298	67	381.4
	Mehmetcik	35.42222	34.07833	99	405.3
	Ziyamet	35.453501	34.124509	82	419.7
	Karpaz	35.59889	34.37917	136	489.5
	Yenierenkoy	35.53556	34.18944	123	444.1
	Kantara	35.40056	33.91361	480	546.7
4	Akdeniz	35.29972	32.965	89	377.0
	Camlibel	35.31611	33.07056	277	446.3
	Guzelyurt	35.18889	32.98194	52	277.8
	Gaziveren	35.17306	32.92194	19	264.8
	Lefke	35.096638	32.84091	129	301.2
	Zumrutkoy	35.17444	33.04917	129	277.6
5	Ercan	35.15917	33.50194	119	303.4
	Serdarli	35.251828	33.610235	111	316.4
	Degirmenlik	35.252756	33.472181	168	324.0
	Alevkaya	35.28583	33.53472	623	469.6
	Alaykoy	35.18472	33.25667	166	277.2
	Lefkosa	35.19639	33.35194	134	300.4

6.2.3. Goodness-of-Fit and Assessment of Estimates

The final homogeneous sub-regions were decided based on the result of COR clustering method. Therefore, as given in Table 6.11, the probability distribution of Sub-region 1, Sub-region 2 and Sub-region 4 is determined as PE3 whereas GLO for

Sub-region 3, and GNO for Sub-region 5 are proposed. At the same time, L-moment ratio diagrams which illustrate L_{skew} and L_{kur} ratios calculated for each station and sub-region are supported the selection of distributions as shown in Figure 6.8. Finally, the dimensionless regional growth curves specific to each sub-region were obtained relying on the selected distributions.

In order to evaluate the accuracy of the estimates, RMSE and error bounds of the quantile estimates were calculated and compared by using the simulated and actual data sets. Here, the simulated data was generated to mimic the actual data for each sub-region by employing Monte Carlo simulation procedure. In this study, 10,000 realizations are created in simulation and after the repeated process, RMSE and 90% error bounds of estimated regional growth curves (Figure 6.9) are obtained. When the results were examined, the uncertainty in quantile estimation of larger return periods was increased. For example, for the return periods less than 100-year, the RMSE values had a range of 0.014 to 0.269 throughout the all study region. Additionally, the RMSE value calculated in Sub-region 3 differed compared to other regions and found as 0.696 with wide error bounds for 500-year return period. This leads to questionable quantile estimates. The reason could be the changes of precipitation characteristics of the region particularly in larger return periods. Therefore, more data sets should be included into the region to increase the observation length and the number of stations for achieving reliable estimates.

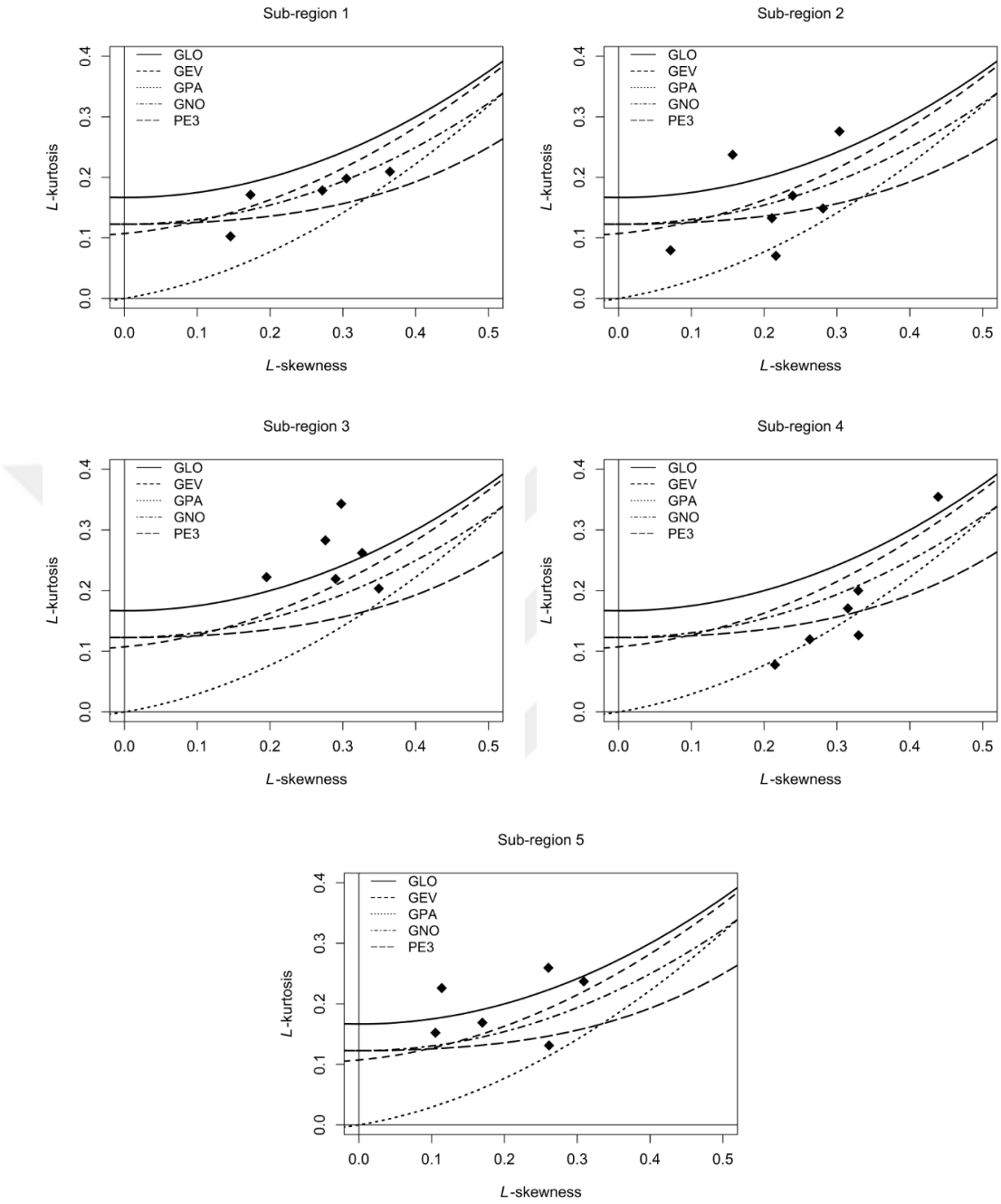

Figure 6.8. L-moment ratio diagrams for each homogeneous sub-region

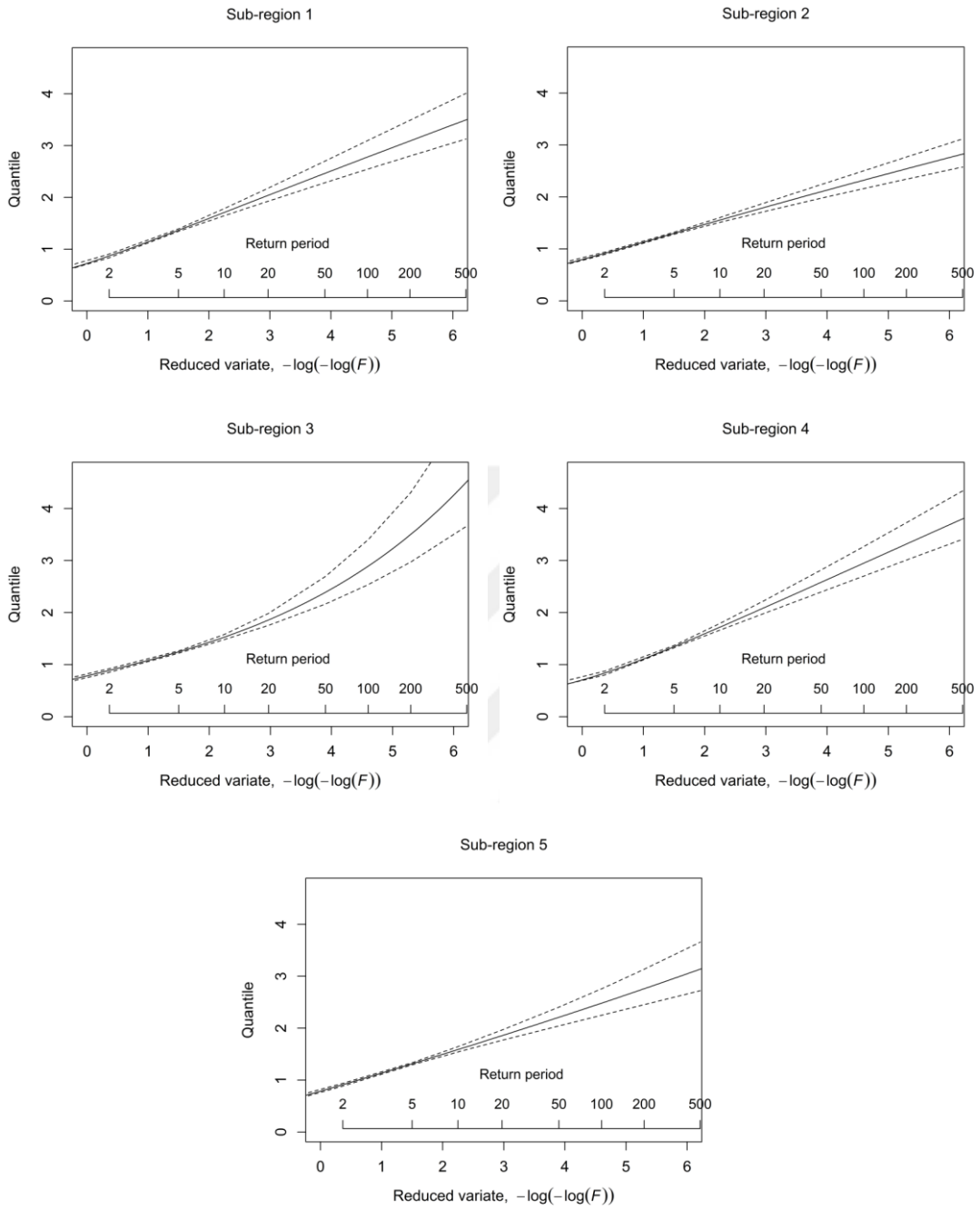

Figure 6.9. Sub-regions' regional growth curves and 90% error bounds

As summarized in Table 6.14, the maximum daily precipitation estimates for different return periods are carried out in 30 precipitation stations based on the regional growth curves for each sub-region and estimation of index-flood for each station. In Table 6.14, the estimates based on the conventional approach is also shared in parenthesis with the estimated based on the COR time series clustering method. Here, because the same stations and distribution was determined for Sub-region 3 in both conventional and COR approach, the estimations of maximum daily precipitation values became the same. Moreover, the maximum estimations were found for the stations covering the Sub-region 3 in the Karpass Peninsula of Northern Cyprus. This region also had the maximum annual precipitation totals as well. The stations located around the Kyrenia Mountains were marked with the higher estimates. The rest of the stations in other homogeneous sub-regions had relatively lower estimates but still high enough to cause flooding events when considering the past events. Extreme precipitation estimates exhibit spatial distribution, e.g have a tendency to increase from the central region of island (e.g. Mesaoria Plain) towards the north coast (e.g. Kyrenia Mountains and Karpass Peninsula). Likewise, mean annual precipitation series in line with the maximum daily precipitation series have the similar spatial characteristics.

Table 6.14. The Annual Maximum Daily Estimates for Different Return Periods Based on Conventional and COR Clustering Approaches

	Non-exceedance probability (Return period)							
	0.5	0.8	0.9	0.95	0.98	0.99	0.995	0.998
Stations	2 year	5 year	10year	20 year	50 year	100 year	200 year	500 year
Akdeniz	35.3	56.7	72.5	88.2	108.8	124.4	139.8	160.3
	(36.8)	(57.1)	(71.3)	(85.0)	(102.5)	(115.6)	(128.5)	(145.4)
Alaykoy	32.8	47.3	57.2	66.8	79.5	89.3	99.3	112.9
	(32.3)	(47.0)	(57.4)	(67.8)	(82.1)	(93.2)	(104.9)	(121.0)
Alevkaya	61.2	88.2	106.6	124.5	148.3	166.5	185.1	210.5
	(58.5)	(90.9)	(113.5)	(135.2)	(163.2)	(184.0)	(204.5)	(231.4)
Beyarmudu	44.7	63.6	76.1	87.9	102.8	113.7	124.4	138.2
	(44.0)	(63.9)	(78.0)	(92.3)	(111.6)	(126.8)	(142.6)	(164.5)
Beylerbeyi	63.4	99.5	124.5	148.6	179.5	202.5	225.1	254.7
	(63.5)	(98.7)	(123.2)	(146.8)	(177.2)	(199.8)	(222.1)	(251.2)
Bogaz	53.6	84.1	105.2	125.5	151.7	171.0	190.2	215.1
	(53.7)	(83.4)	(104.1)	(124.0)	(149.7)	(168.8)	(187.6)	(212.2)
Camlibel	45.3	72.6	92.9	113	139.4	159.3	179.1	205.2
	(47.1)	(73.1)	(91.3)	(108.8)	(131.3)	(148)	(164.5)	(186.1)

Table 6.14 (Contd.)

	Non-exceedance probability (Return period)							
	0.5	0.8	0.9	0.95	0.98	0.99	0.995	0.998
Stations	2 year	5 year	10year	20 year	50 year	100 year	200 year	500 year
Cayirova	52.9	74.0	90.9	110.4	142.1	171.8	208.0	268.3
	(52.9)	(74.0)	(90.9)	(110.4)	(142.1)	(171.8)	(208.0)	(268.3)
Degirmenlik	46.4	66.9	80.8	94.4	112.4	126.2	140.3	159.5
	(45.7)	(66.4)	(81.1)	(95.9)	(116.0)	(131.8)	(148.2)	(171.1)
Dortyol	37.5	53.3	63.8	73.6	86.1	95.3	104.2	115.8
	(36.8)	(53.5)	(65.4)	(77.3)	(93.5)	(106.2)	(119.5)	(137.9)
Ercan	39.5	56.9	68.8	80.4	95.7	107.5	119.5	135.8
	(38.9)	(56.5)	(69.1)	(81.6)	(98.8)	(112.2)	(126.2)	(145.6)
Esentepe	49.4	77.5	97.0	115.8	139.8	157.7	175.3	198.4
	(49.5)	(76.9)	(96.0)	(114.4)	(138.0)	(155.6)	(173.0)	(195.7)
Gazimagusa	43.9	62.5	74.8	86.3	101.0	111.7	122.2	135.8
	(43.2)	(62.7)	(76.6)	(90.6)	(109.6)	(124.5)	(140.1)	(161.6)
Gaziveren	25.9	41.6	53.2	64.7	79.9	91.3	102.6	117.6
	(27.8)	(40.4)	(49.3)	(58.3)	(70.5)	(80.2)	(90.2)	(104.0)
Gecitkale	41.1	58.4	69.9	80.7	94.4	104.4	114.2	126.9
	(40.4)	(58.6)	(71.6)	(84.7)	(102.5)	(116.4)	(130.9)	(151.1)
Girne	62.3	97.8	122.4	146.1	176.5	199.0	221.3	250.4
	(62.4)	(97.0)	(121.1)	(144.3)	(174.2)	(196.4)	(218.3)	(246.9)
Guzelyurt	29.8	47.8	61.2	74.4	91.8	104.9	118.0	135.2
	(31.9)	(46.4)	(56.7)	(67.0)	(81.1)	(92.1)	(103.6)	(119.6)
Iskele	48.0	68.2	81.6	94.2	110.1	121.8	133.3	148.1
	(47.1)	(68.4)	(83.6)	(98.9)	(119.6)	(135.9)	(152.8)	(176.3)
Kantara	60.4	84.5	103.9	126.1	162.3	196.3	237.6	306.5
	(60.4)	(84.5)	(103.9)	(126.1)	(162.3)	(196.3)	(237.6)	(306.5)
Karpaz	54.2	75.8	93.1	113.1	145.5	176.0	213.1	274.8
	(54.2)	(75.8)	(93.1)	(113.1)	(145.5)	(176.0)	(213.1)	(274.8)
Lapta	64.4	101.1	126.5	150.9	182.3	205.6	228.6	258.6
	(64.5)	(100.2)	(125.1)	(149.1)	(179.9)	(202.9)	(225.5)	(255.1)
Lefke	32.1	51.6	66	80.2	99.0	113.1	127.2	145.7
	(34.4)	(50.0)	(61.1)	(72.3)	(87.4)	(99.3)	(111.7)	(128.9)
Lefkosa	37.8	54.5	65.8	76.9	91.5	102.8	114.3	129.9
	(37.2)	(54.1)	(66.1)	(78.1)	(94.5)	(107.3)	(120.7)	(139.3)
Mehmetcik	54.2	75.9	93.2	113.2	145.6	176.1	213.2	275.0
	(54.2)	(75.9)	(93.2)	(113.2)	(145.6)	(176.1)	(213.2)	(275.0)
Salamis	42.6	60.5	72.4	83.7	97.8	108.2	118.4	131.6
	(41.8)	(60.8)	(74.3)	(87.8)	(106.2)	(120.7)	(135.7)	(156.6)
Serdarli	41.6	59.9	72.4	84.6	100.7	113.1	125.8	143.0
	(40.9)	(59.5)	(72.7)	(85.9)	(104.0)	(118.1)	(132.9)	(153.3)
Vadili	35.7	50.8	60.7	70.1	82.0	90.7	99.2	110.3
	(35.1)	(51.0)	(62.3)	(73.6)	(89.0)	(101.2)	(113.8)	(131.3)
Yenierenkoy	53.2	74.4	91.4	111.0	142.8	172.8	209.2	269.8
	(53.2)	(74.4)	(91.4)	(111.0)	(142.8)	(172.8)	(209.2)	(269.8)
Ziyamet	52.3	73.2	89.9	109.2	140.5	169.9	205.7	265.3
	(52.3)	(73.2)	(89.9)	(109.2)	(140.5)	(169.9)	(205.7)	(265.3)
Zumrutkoy	31.1	49.8	63.7	77.5	95.6	109.3	122.9	140.8
	(33.3)	(48.3)	(59.1)	(69.8)	(84.5)	(96.0)	(108.0)	(124.6)

6.3. Hydrological Modelling

In hydrological modelling, the upstream catchments of Kanlıköy and Gönyeli ponds were mainly examined to provide input hydrographs to hydraulic model of the town of Gönyeli and the city of Nicosia which covers the main settlement areas.

6.3.1. Design Hyetographs

In order to determine the design hyetograph, Alevkaya Station for reflecting the mountainous areas and Lefkoşa Station for the low-lying urban area were chosen as the representative stations. As mentioned before, these stations were located in the same homogeneous sub-region, named as Sub-region 5 which covers the whole study area. When analysing the heavy precipitation events greater than 10 mm daily depth in hourly data of Lefkoşa Station, the average precipitation depth was found as 20.2 mm with mean duration of 14 hours. Also, Alevkaya Station had an average 26.6 mm daily total and 10.7 hours average precipitation duration. Moreover, the pattern of heavy precipitation events has a distribution as shown in Figure 6.10. Generally, in the first 6, 12, and 18 hours of precipitation event, 63%, 86.4%, and 94.9% of total daily precipitation were observed as an average.

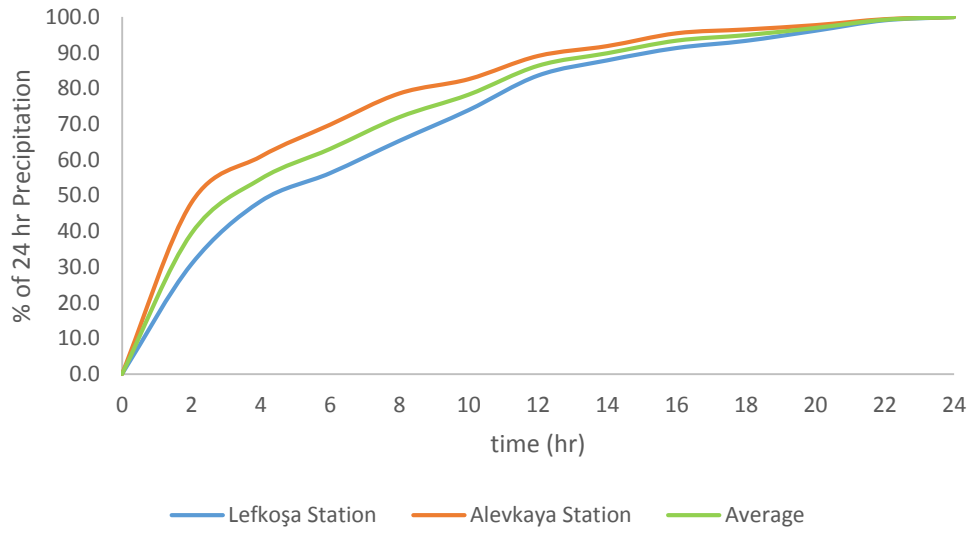

Figure 6.10. Daily precipitation distribution of Lefkoşa Station, Alevkaya Station, and average of both stations

Besides, in flood day of 26th of February, 2010, 63 mm and 80 mm of daily precipitation were recorded in Lefkoşa and Alevkaya stations, respectively. The observed hyetographs of the flood day in Lefkoşa and Alevkaya stations are illustrated in Figure 6.11 and Figure 6.12, respectively. The peak intensities in hyetographs were found as 20.8 mm/hr in Lefkoşa Station after the 12 hours of the beginning of precipitation event. In Alevkaya Station, 30.6 mm/hr intensity is observed after 10 hours. Actually, this distribution does not match with the general characteristics of heavy precipitation events as given in Figure 6.10. For instance, in the first 10 hours, 78.3% of precipitation had already observed.

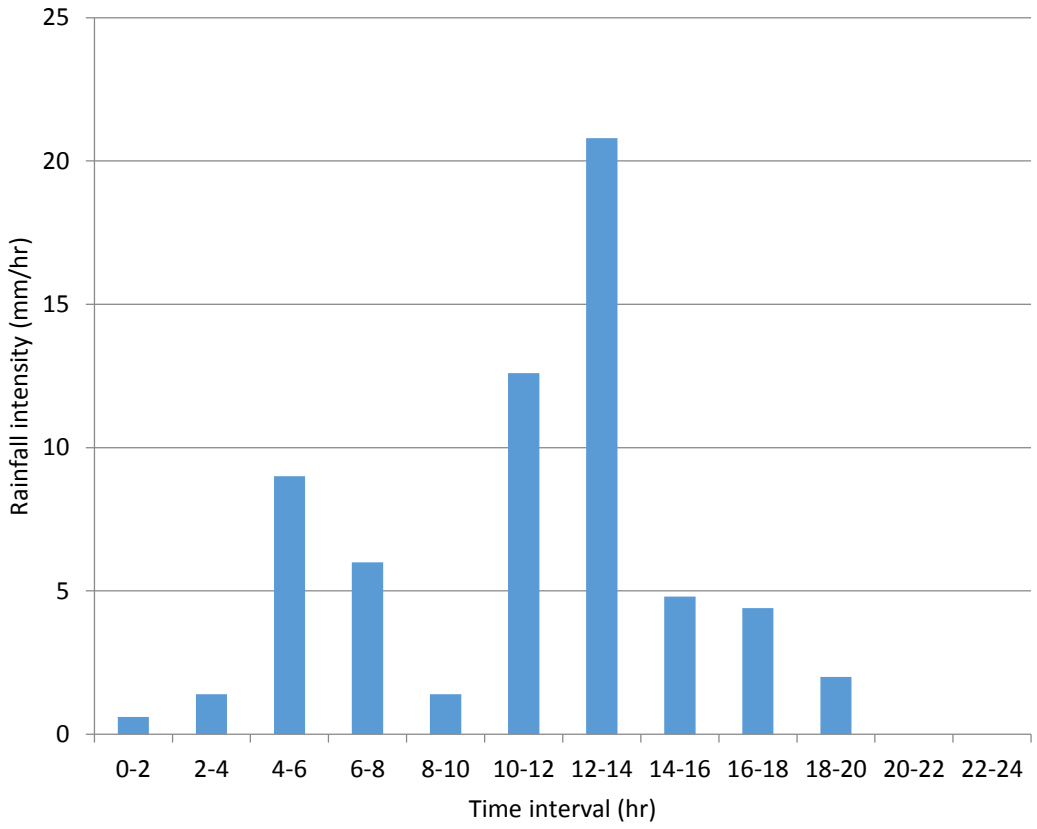

Figure 6.11. The hyetograph of flood day observed in Lefkoşa Station

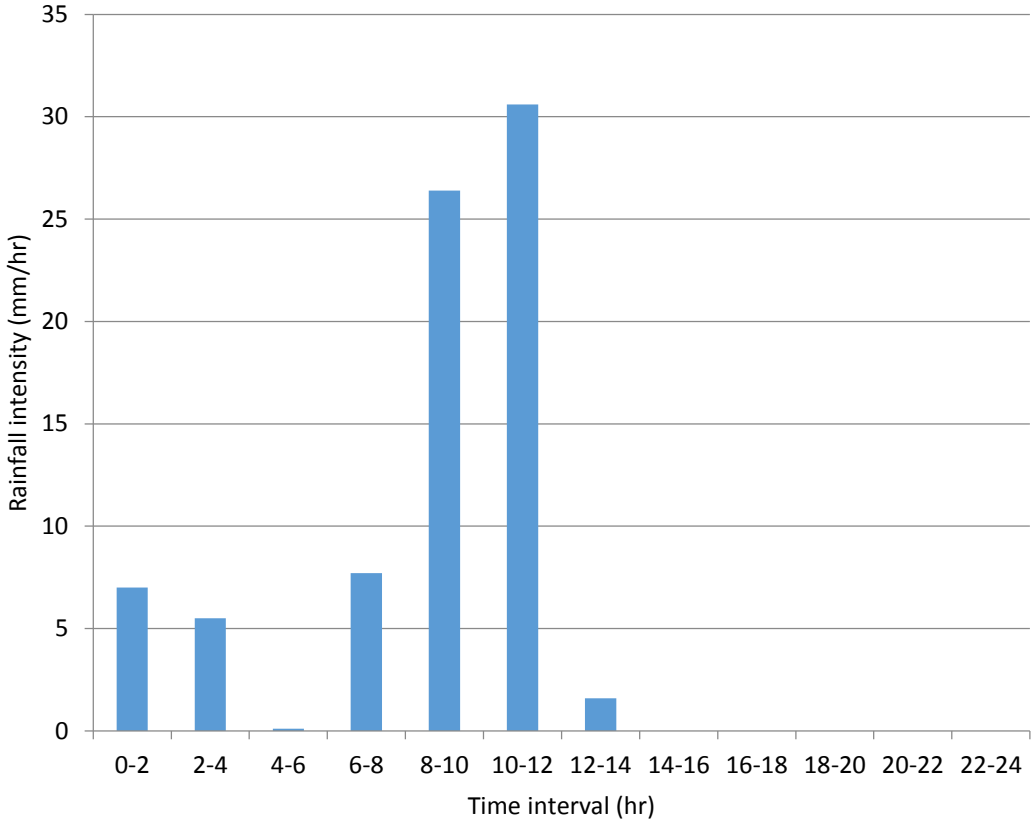

Figure 6.12. The hyetograph of flood day observed in Alevkaya Station

For the most extreme cases of (i.e. up to 500-year return period), the hyetographs were generated based on the estimations of regional frequency analysis for the maximum daily precipitation and average daily precipitation distribution. To be on safer side, the estimates of Alevkaya Station were considered while distributing daily amount through the pattern. The hyetographs for 100, 200, and 500-year return periods are illustrated in Figure 6.13.

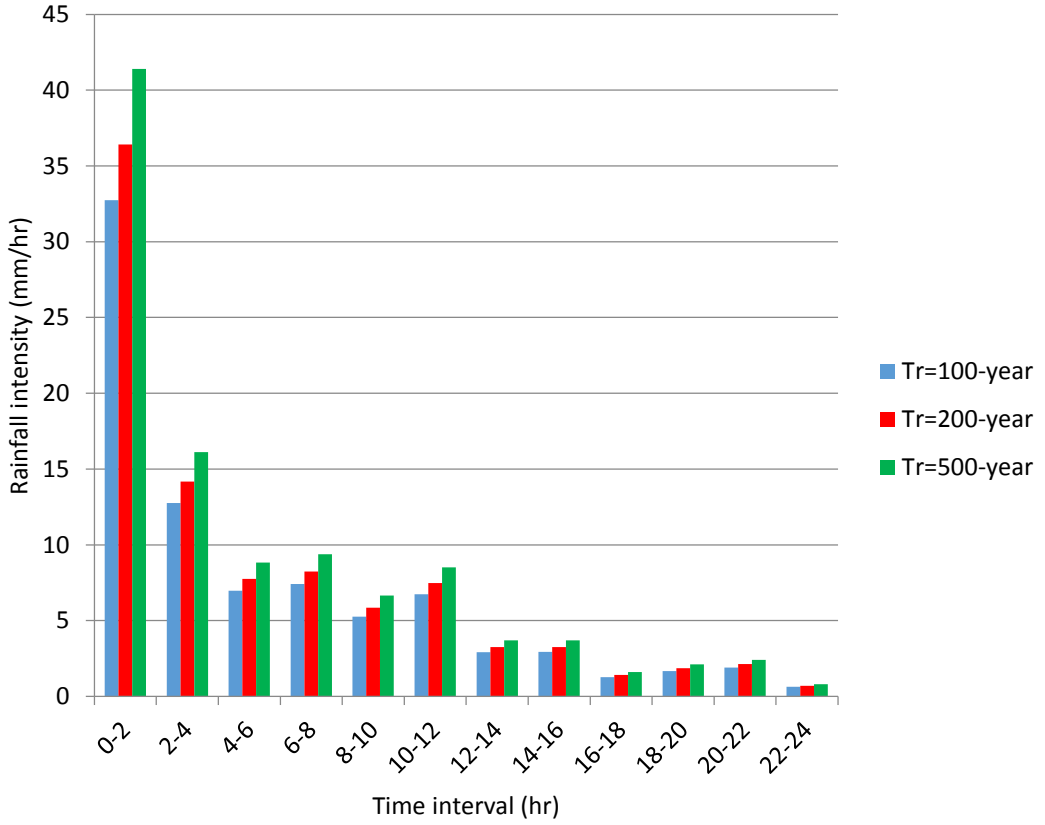

Figure 6.13. The hyetograph of estimated storms with return periods of 500-year, 200-year, and 100-year

6.3.2. Generation of Run-off Hydrographs

6.3.2.1. Pre-Processing of Pond Catchments

The outflow hydrographs of Kanlıköy and Gönyeli ponds were used as inflow to the system, which was the mainly interested area of urbanized region. Since there was no any streamflow gauging station on the creeks, these hydrographs had to be generated synthetically. For this reason, SCS Unit Hydrograph method was used to obtain unit hydrographs based on the physical characteristics of relevant catchments. Priorly, pre-procession of catchments was required to reach depressionless DEM by applying a set of procedures as follows: fill the sinks, flow direction and flow accumulation, stream

definition, and definition of sub-catchments. Therefore, the Spatial Analyst and Arc Hydro tools of ArcGIS were used to extract some parameters of catchments, which were needed for the hydrological analysis.

First, as shown in Figure 6.14, DEM is created for Kanlıköy and Gönyeli pond catchments by using the 1: 25,000 and 1: 5,000 topographical maps. Then, one of the common problems of existence of sink cells was filled to increase the accuracy of determination of flow directions. By utilizing the elevations of cells, the flow direction as shown in Figure 6.15 are determined to represent the water flow directions and possible paths on the surface. Then, the flow accumulation was calculated relied on the flow direction properties and determined the number of cells discharging into each cell. Furthermore, possible drainage lines are detected by using the stream definition and stream segmentation functions of Arc Hydro tool as demonstrated in Figure 6.16. To conclude the pre-processing of DEM section, the pond catchments are formed based on the pour points located at the outlet of the ponds and the catchments are defined as given in Figure 6.14.

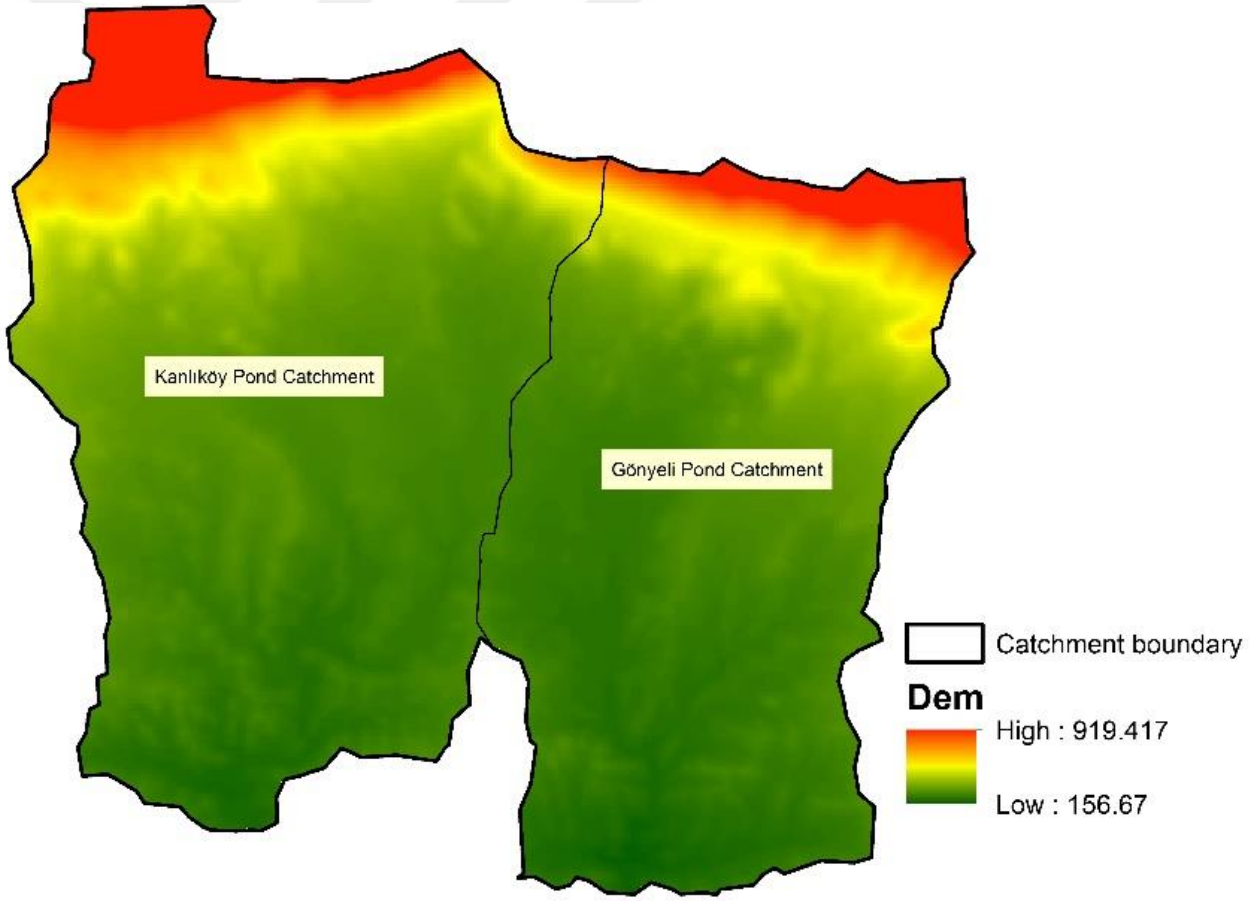

Figure 6.14. Kanlıköy and Gönyeli pond catchments

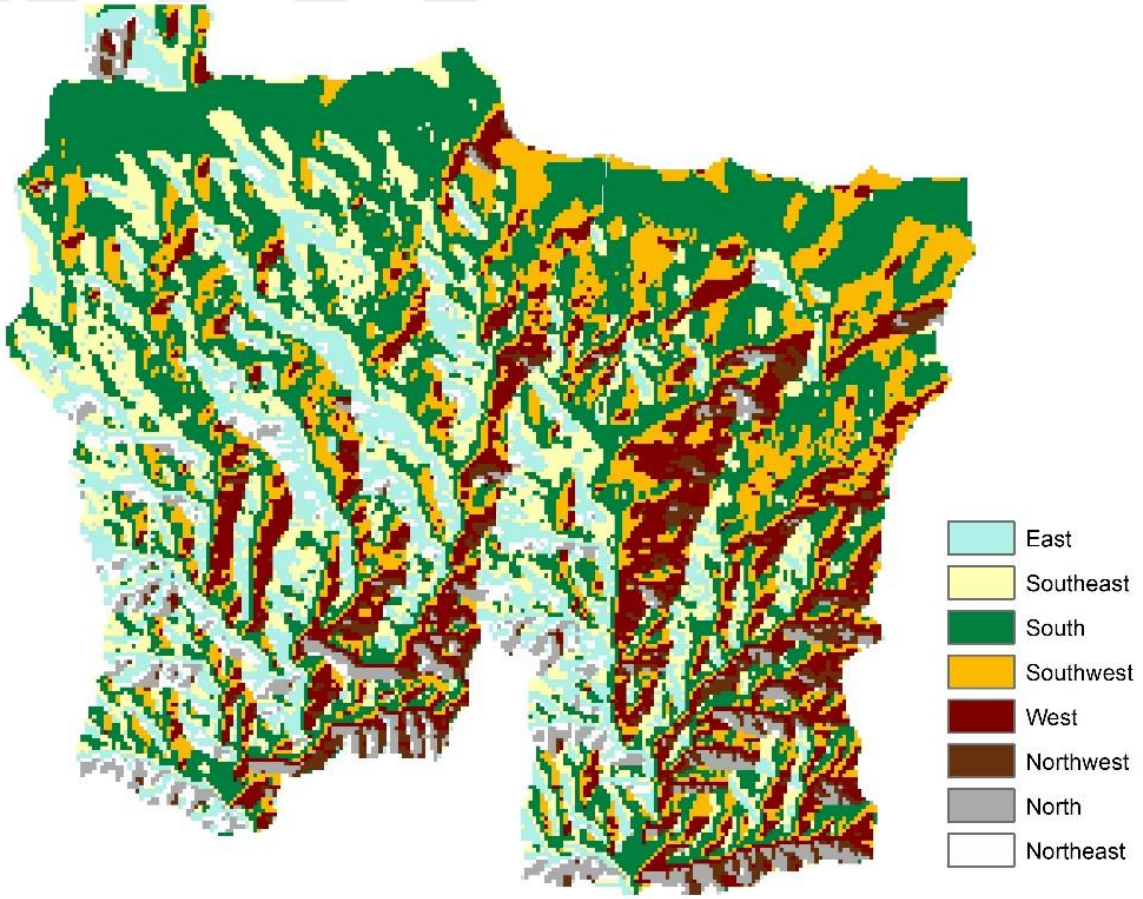

Figure 6.15. Flow direction map of Kanlıköy and Gönyeli pond catchments

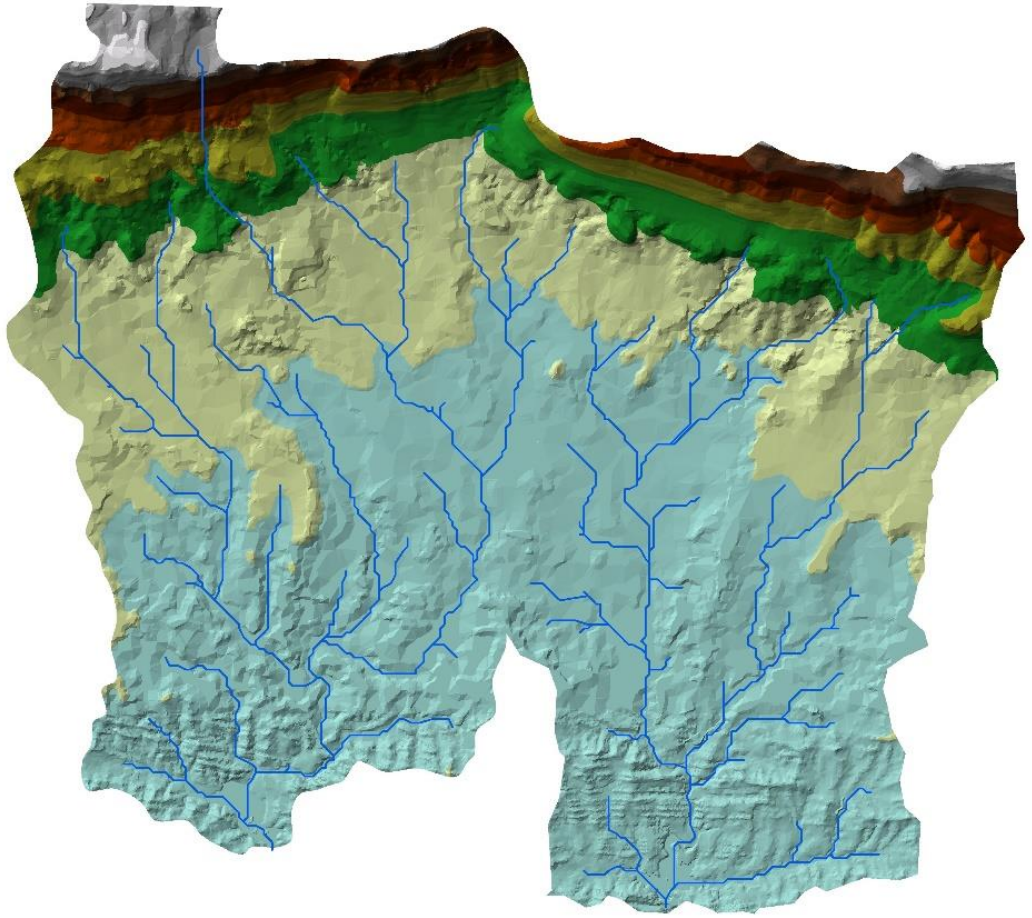

Figure 6.16. Drainage lines in Kanlıköy and Gönyeli pond catchments

6.3.2.2. HEC-HMS Model of Pond Catchments

To generate the run-off hydrographs, a composite CN was determined based on the soil map and land cover. Due to the soil texture of high clay content in the pond catchments, the hydrologic soil types were determined as Group C for the soil type of Bademliköy and Group D for the soil types of Marno-Kalker, Demirhan, Değirmenlik, and Boğaziçi, which cover almost the whole region. Other physical parameters for employing SCS UH method are calculated by using ArcGIS and summarized in Table 6.15.

Table 6.15. Parameters Used in SCS Unit Hydrograph Method

Parameter	Kanlıköy Pond Catchment	Gönyeli Pond Catchment
CN	80.4	81
L (ft)	45275.6	31824.2
S	2.4	2.3
S_h (%)	13.1	12.0
t_l (hr)	1.83	1.42
A (km^2)	32.1	25.5
t_r (hr)	2	2
t_p (hr)	2.83	2.42
Q_p (m^3/s)	23.58	21.96

In this study, two-hour duration unit hydrographs (UH_2) are generated for the catchments as illustrated in Figure 6.17. By using these unit hydrographs, the direct runoff hydrographs as inflow to the ponds were generated via HEC-HMS for different return periods and flood day. In Table 6.16, the peak discharge values of inflows regarding the different return periods in Kanlıköy and Gönyeli ponds are listed. Since the peak discharge values in Kanlıköy and Gönyeli ponds are computed as 79.2 m^3/s and 68.8 m^3/s, respectively, the return period of 2010 flood is approximately found as 35 years from Figure 6.18.

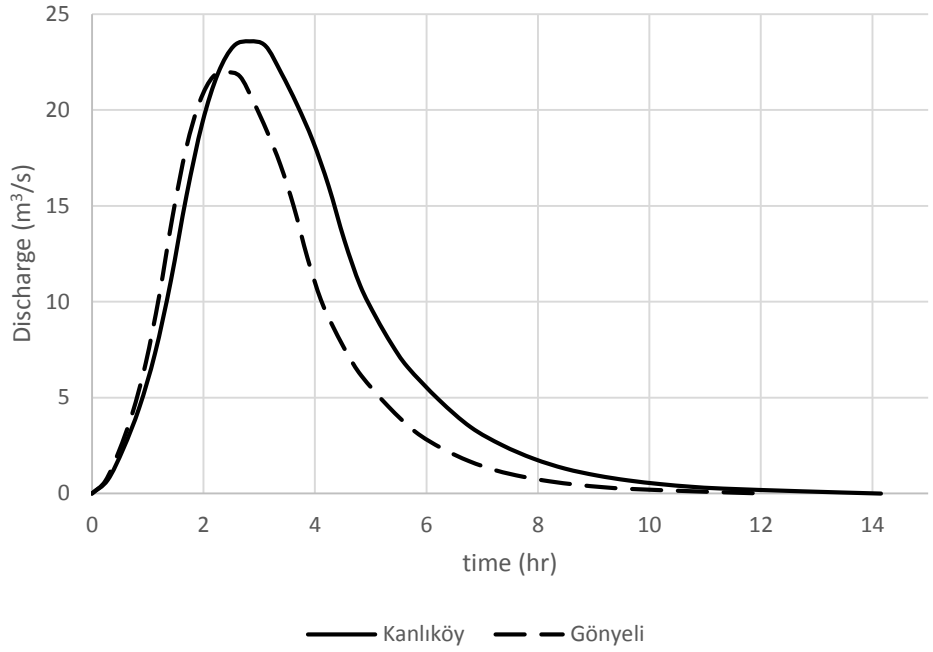

Figure 6.17. UH2 of Kanlıköy and Gönyeli pond catchments

Table 6.16. Calculated Inflow Peak Discharges into Kanlıköy and Gönyeli Ponds Corresponding to Different Return Periods

Return Period (years)	Q_{peak} in Kanlıköy Pond (m^3/s)	Q_{peak} in Gönyeli Pond (m^3/s)
2	18.1	15.8
5	37.0	32.8
10	52.1	46.2
20	68.3	60.8
50	90.7	81.0
100	109.2	97.3
200	128.0	114.1
500	155.5	138.4

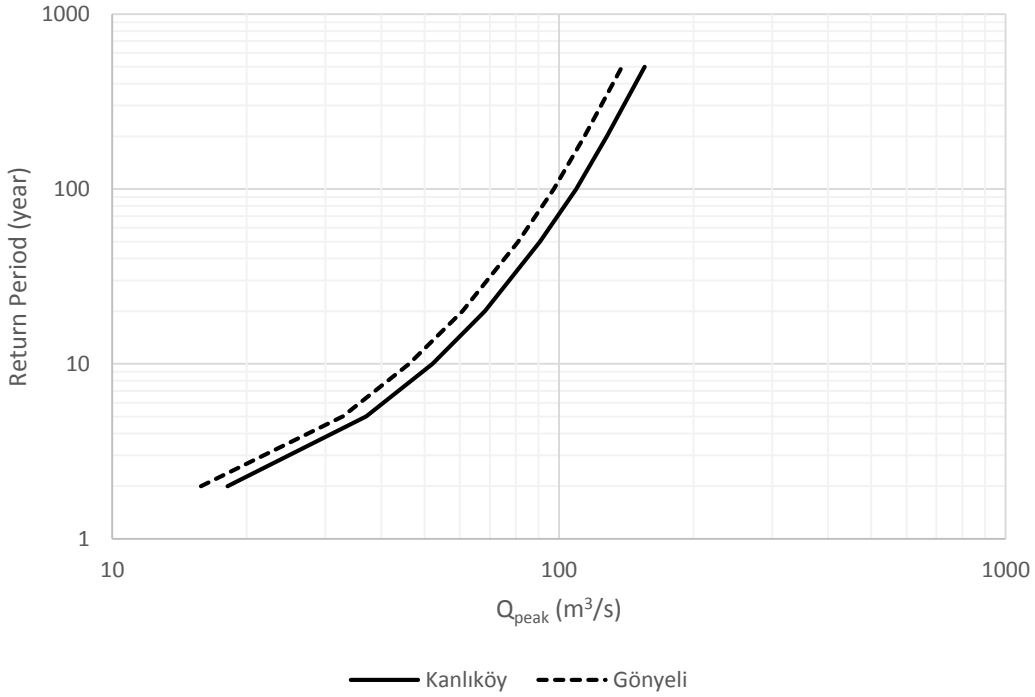

Figure 6.18. Qpeak values corresponding to different return periods of inflows in Kanlıköy and Gönyeli ponds

6.3.3. DEM Formation of Floodplain

In the formation of DEM, six different interpolation techniques were employed to generate the surface of the floodplain by using the contours digitized from topographical maps, ground point measurements, and the points obtained by the author from fieldworks. The spatial resolution was decided as 3 m for all methods and the extent of DEMs were limited according to the maximum possible flood extent in the floodplain. The final surfaces generated by IDW, Natural Neighbor, Topo to Raster, TIN, Spline, and Spherical Kriging techniques are illustrated in Figure 6.19. Herein, randomly selected and uniformly distributed data sets, which consist of 80% of data, were used in creation process.

Quality control of final DEMs were executed by applying some statistics and visual assessment of surfaces. In statistical analysis, previously observed 20% of data are compared with the interpolated values through the statistics of mean absolute error (MAE), mean square error (MSE), mean absolute percentage error (MAPE), and root mean square error (RMSE) and the results are listed in Table 6.17.

a) Inverse Distance Weighting

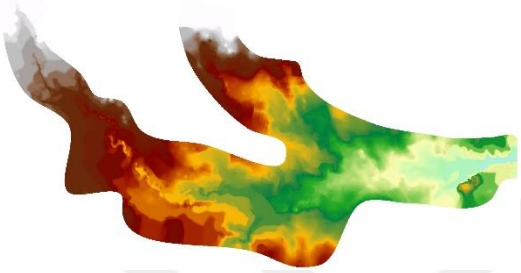

b) Natural Neighbor

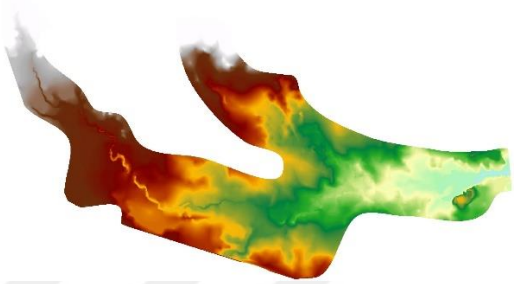

c) Topo to raster

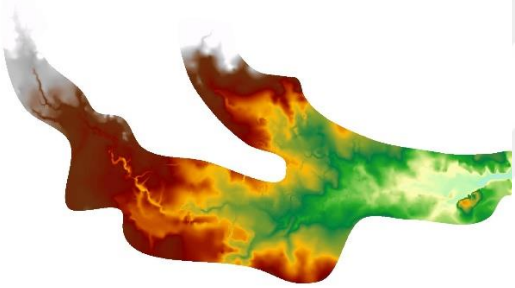

d) TIN

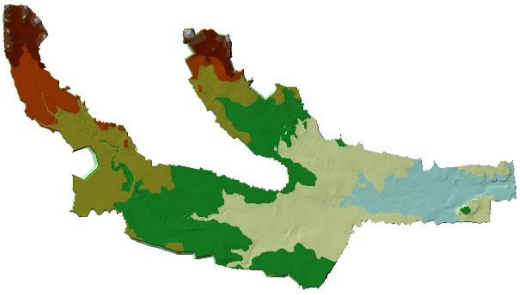

e) Spline

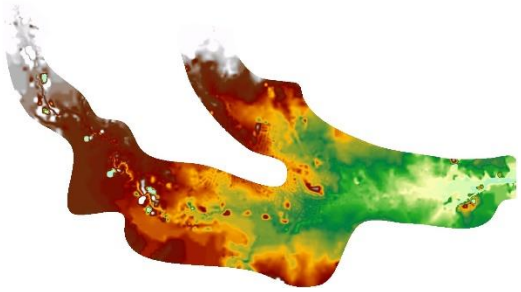

f) Spherical Kriging

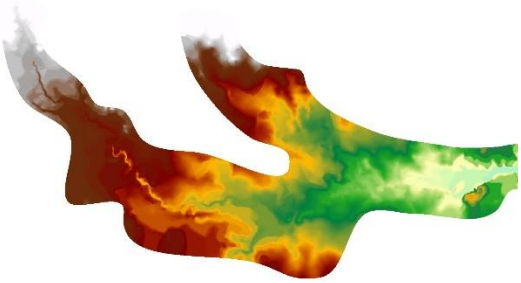

Figure 6.19. DEMs of different interpolation techniques

Table 6.17. Statistical Analysis Results of Observed and Estimated Measurements of Different Interpolation Techniques

Interpolation Technique	MAE	MSE	MAPE	RMSE
Inverse Distance Weighting	0.24	0.29	0.17	0.53
Natural Neighbor	0.16	0.12	0.11	0.35
Topo to Raster	0.19	0.18	0.13	0.43
Triangulated Irregular Network	0.38	11.57	0.26	3.40
Spline	0.18	0.42	0.12	0.65
Spherical Kriging	0.16	0.16	0.11	0.40

The results indicated that all interpolation techniques, except TIN, created DEMs with high accuracy and they differed by a narrow margin in terms of statistical analyses. The DEM created by Natural Neighbor is the most suitable technique for the floodplain with the lowest values of MAE, MSE, MAPE, and RMSE. In terms of MAE and MAPE, there was no distinction between Natural Neighbor and Spherical Kriging. However, MSE and RMSE suggested Natural Neighbor performed much close to the real observations. In addition, Inverse Distance Weighting, Topo to Raster, and Spline techniques revealed sufficient results compared to Natural Neighbor in the range of 0.18-0.24 for MAE, 0.18-0.42 for MSE, 0.12%-0.17% for MAPE, and 0.43-0.65 for RMSE. On the other hand, it was clear that TIN was insufficient to represent the surface with these data sets. Unlike rural areas, urbanized regions have more detailed topography and more observations may be required to increase the performance of interpolation for TIN surface.

In spatial analysis of DEMs, Spline interpolation technique appeared as the worst surface of the floodplain. Particularly, the areas with no data points, this technique failed to make correct estimations to represent the real topography. Therefore, as shown in Figure 6.19, some parts of the DEM become erroneous. When the errors were deeply investigated, it was found that generally the inaccurately estimated values were located in the areas, which had sparse data sets or discontinuities in data distribution.

As a general conclusion of statistical and spatial assessments, Natural Neighbor DEM was decided as the most appropriate model for the 2D modelling of the study area. Then, the sinks were removed and the hydrologically improved DEM raster was obtained with 3 m spatial resolution.

CHAPTER 7

RESULTS AND DISCUSSION OF HYDRAULIC MODELLING

In this section, the results of hydraulic modelling with the inputs including physical and hydrological characteristics of catchments are presented. In addition, several remedial alternatives consisting of dredging of pond reservoirs, raising the crest elevations of embankments and spillways, and new upstream pond were evaluated for the flood inundation problem of Nicosia. Furthermore, beside the conditions of current case, the hydrographs with 500-year return period are considered for the flood protection of Nicosia, because such densely populated cities are recommended to be protected against the events of high return periods, such as 500 years (Yanmaz, 2018). The all five remedial alternatives with different cases are listed in Table 7.1 in which K_d and K_s are the crest elevations of pond embankment and its spillway, respectively.

Table 7.1. Remedial Alternatives for Different Cases

Alternative	Case	Details
1	Current case	Assessment of MIKE FLOOD model for 2010 flood event
2	Current case with $K_d = 175.4$ m $K_s = 173.9$ m	Assessment of Kanlıköy Pond
	2 m dredging with existing K_d and K_s	
	2 m dredging $K_d = 177$ m $K_s = 175$ m	
	2 m dredging $K_d = 178$ m $K_s = 176$ m	
3	$K_d = 190$ m $K_s = 187$ m	New upstream pond in Kanlıköy
	$K_d = 193$ m $K_s = 190$ m	
	$K_d = 196$ m $K_s = 193$ m	

Table 7.1 (Contd.)

Alternative	Case	Details
4	Current case with $K_d = 168$ m $K_s = 165$ m	Assessment of Gönyeli Pond
	3 m dredging with existing K_d and K_s	
	3 m dredging $K_d = 169$ m $K_s = 167$ m	
	5 m dredging with existing K_d and K_s	
	5 m dredging $K_d = 170$ m $K_s = 168$ m	
	7 m dredging with existing K_d and K_s	
	7 m dredging $K_d = 171$ m $K_s = 168.5$ m	
5	Final solution	Implementation of upstream pond in Kanlıköy and 7 m dredging of Gönyeli Pond with $K_d = 171$ m and $K_s = 168.5$ m and using reasonably smaller Manning's roughness coefficients

As a preliminary assessment, it was not possible to control incoming flows to the existing ponds in the upstream by a possible lateral diversion canal overlying the existing ponds due to lack of available storage area at the upstream reaches. On the other hand, transmission of flood volumes from one pond to the other was also not possible due to relatively smaller reservoir volumes of the ponds. Furthermore, Gönyeli Pond was located at lower altitude than that of Kanlıköy. Hence, gravity transmission from Gönyeli Pond to Kanlıköy Pond was not possible. It was also not possible to convey floodwaters of Kanlıköy Pond to Gönyeli Pond because of lower reservoir capacity of Gönyeli Pond. Therefore, various possible alternatives were evaluated considering the locations of the nearby settlements, existing roads, and new roads under planning stage.

7.1. Alternative 1 (Current Case)

At first in the assessment of current case, based on successive trials using 1D modelling approach, the capacity of the creeks is analyzed and both ponds are expected to release at most 4.5 m^3/s which do not cause downstream inundation as shown in Figure 7.1 and Figure 7.2. Therefore, any remedial measure that discharges more than this limiting value was considered to be inappropriate.

In order to evaluate the storage capacities of existing ponds at different water levels, area-elevation and volume-elevation relationships were derived utilizing the DEM and bathymetric measurements in the ponds. Therefore, the alternatives could be discussed by conducting reservoir routing for realistic results. Moreover, based on the personal communications with the water affairs office of Northern Cyprus, the pond reservoirs were observed almost full just before 2010 flood day due to heavy storms already started in previous days. For this reason, in Alternative 1, the reservoir routing was not taken into account while modelling and calibrating the model of current case.

For Kanlıköy Pond, the contour lines with 1-meter interval and corresponding volumes are calculated in ArcGIS and the curves of area-elevation and volume-elevation are given in Figure 7.3 and Figure 7.4, respectively. Therefore, the relation was derived for Kanlıköy Pond with $R^2 = 0.997$ as follows:

$$A(h) = -7.2h^6 + 301.8h^5 - 4891.8h^4 + 38184h^3 - 143622h^2 + 259277h + 9351.3 \quad (7.1)$$

where h is the water depth measured from the thalveg of the reservoir bed in m and A is area enclosed by the given depth in m^2.

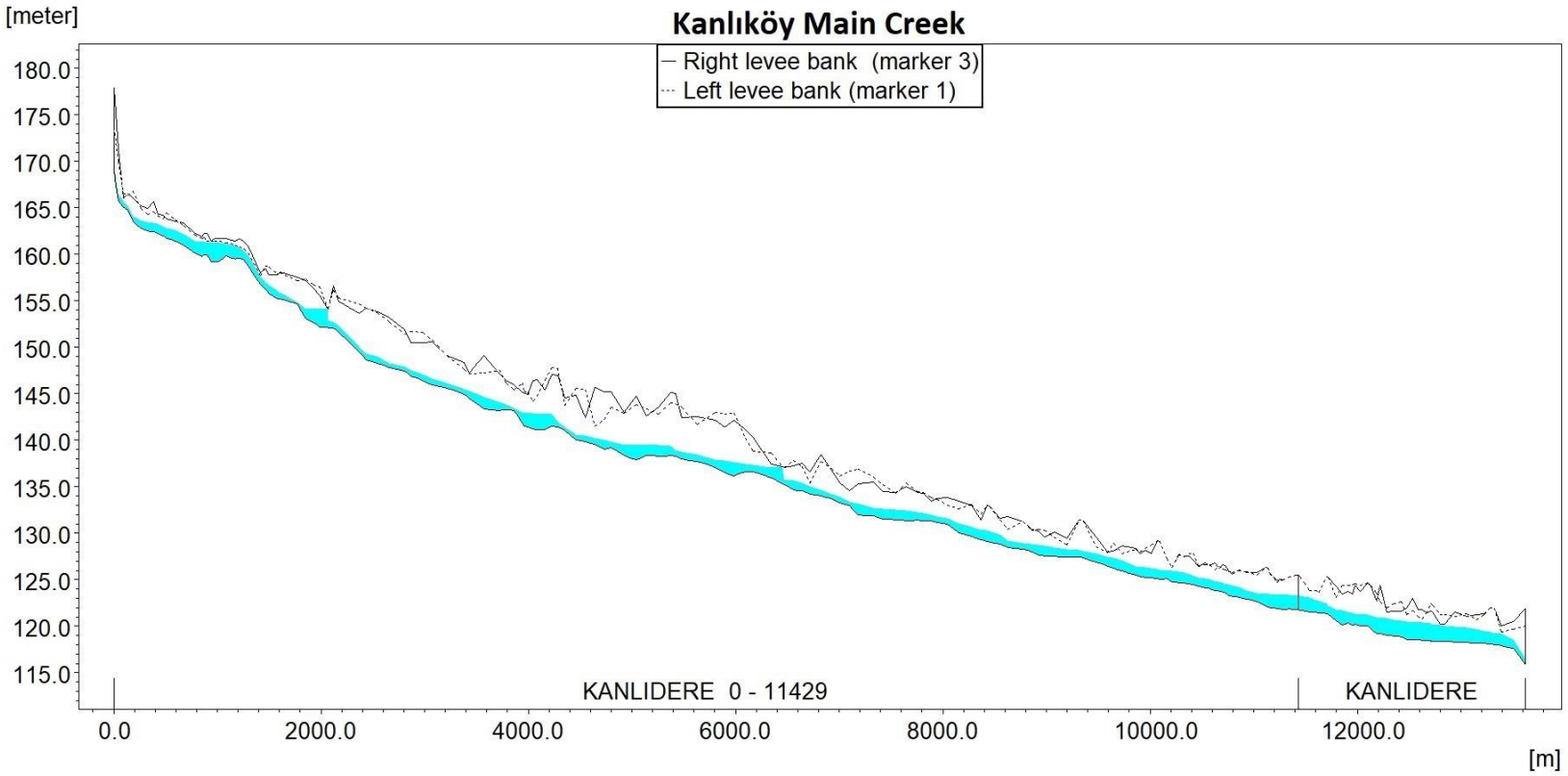

Figure 7.1. The maximum water level in Kanlıköy main creek when the discharges of 4.5 m3/s was released by Kanlıköy and Gönyeli ponds

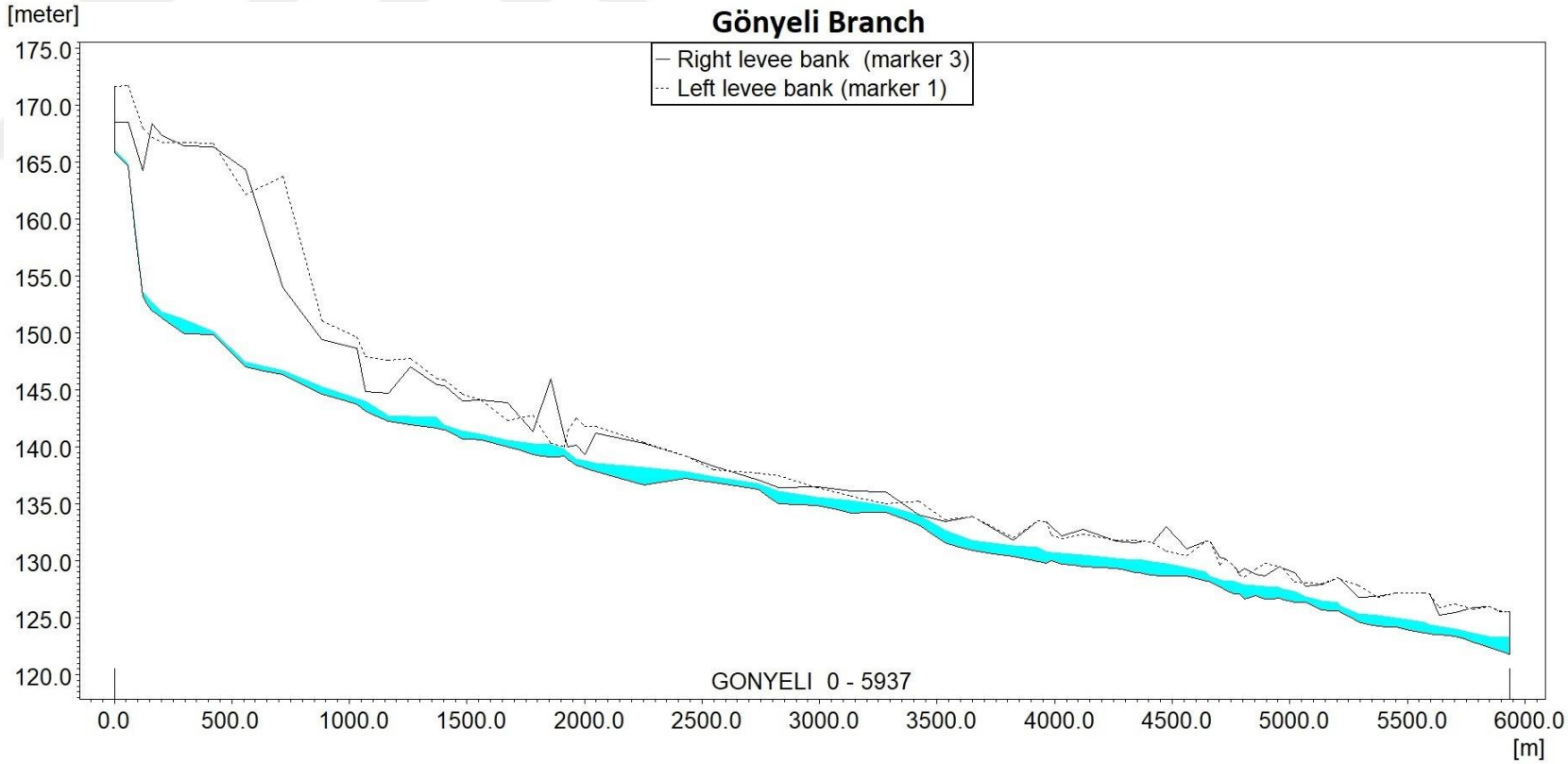

Figure 7.2. The maximum water level in Gönyeli branch when the discharges of 4.5 m3/s was released by Gönyeli ponds

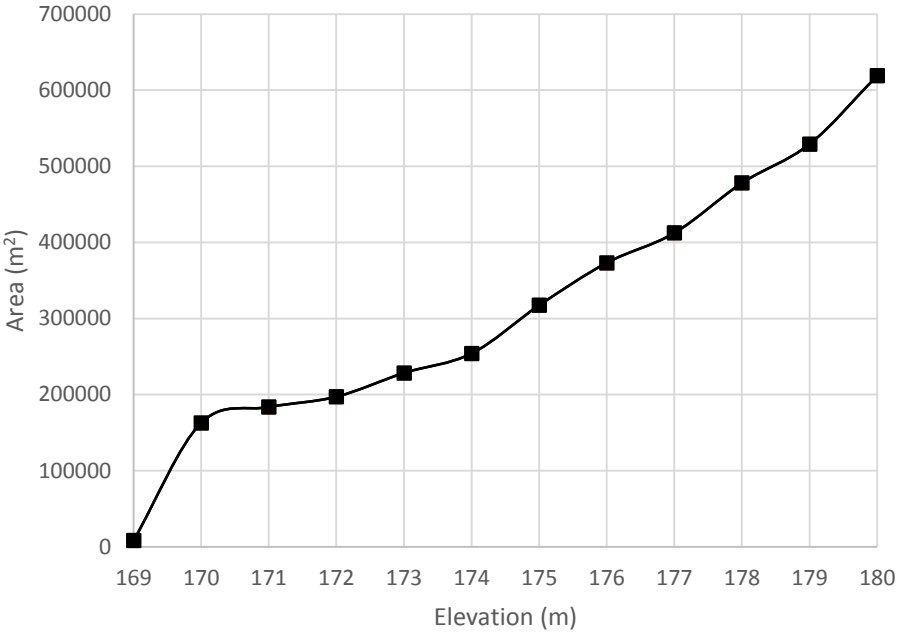

Figure 7.3. Area-elevation relation for Kanlıköy Pond in current case

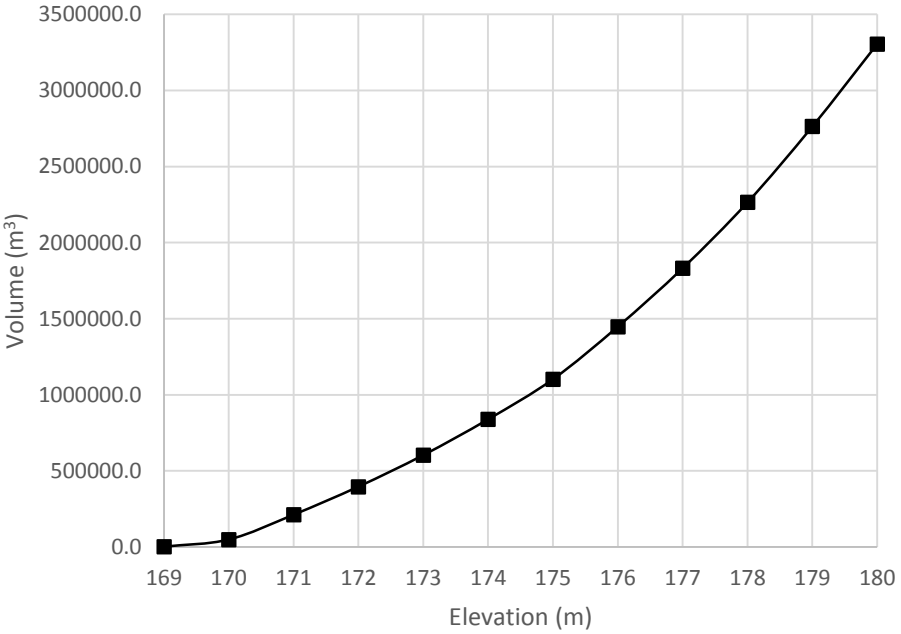

Figure 7.4. Volume-elevation relation for Kanlıköy Pond in current case

For Gönyeli Pond, the water surface area and the corresponding volume stored in reservoir are also computed in ArcGIS and the area-elevation and the volume-elevation curves are provided in Figure 7.5 and Figure 7.6, respectively. In this regard, the water surface area (A) as a function of the water depth (h) was computed with $R^2 = 0.998$ as follows:

$$A(h) = -1.0167h^6 + 98.393h^5 - 1978.1h^4 + 16862h^3 - 67278h^2 + 127214h + 66538 \quad (7.2)$$

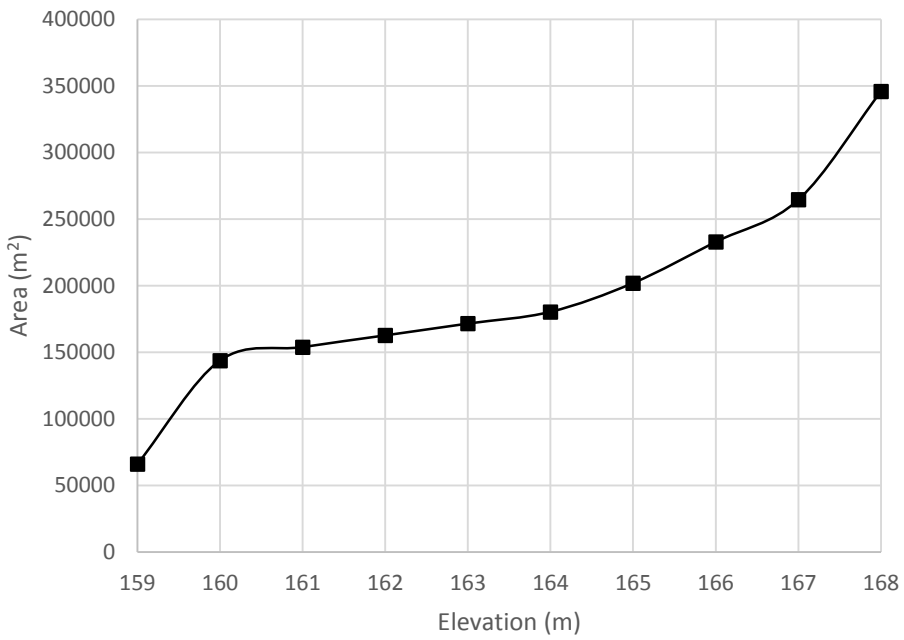

Figure 7.5. Elevation-area relation for Gönyeli Pond in current case

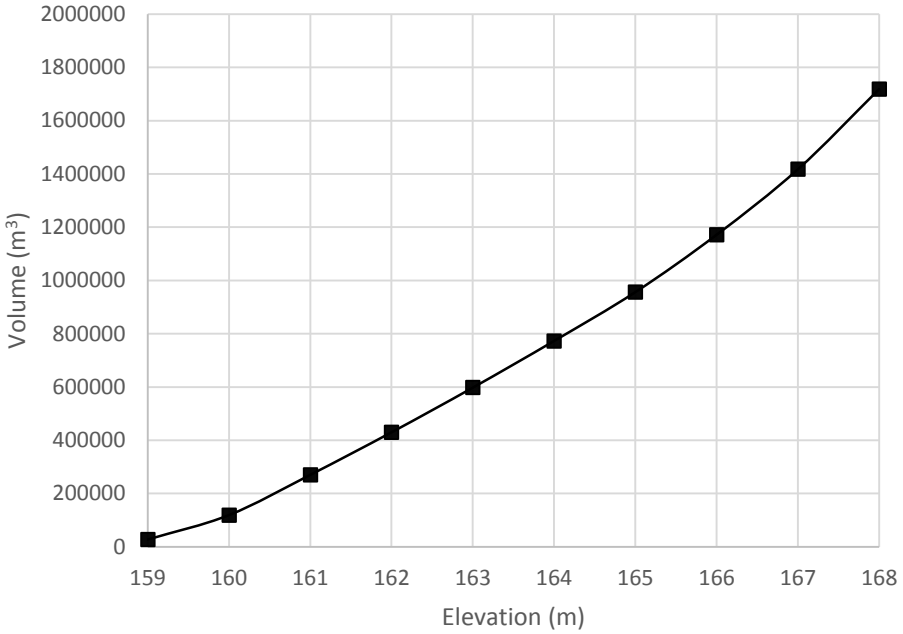

Figure 7.6. Elevation-volume relationship of Gönyeli Pond in current case

In order to obtain 1D/2D modelling of the focused study area, the calibration was conducted by comparing the observed flood extent map with the MIKE FLOOD model. In the first trial, the flood extent map was generated based on the selected physical and hydrological parameters from literature and the hydrographs from the hydrological modelling. Due to the high level of knowledge and experience about the topography as well as the rainfall-runoff response of the study area, close match of flood extent map was developed.

Then, in calibration process, the channel roughness values were not altered because, in MIKE 11 model, 26 different Manning's roughness values were assigned to represent the sections with different roughness characteristics based on one-to-one observations of the author. Only the Manning's roughness coefficients of floodplains were modified locally to obtain the final model. These modifications were carried out in residential areas by changing Manning's n-value from 0.08 to 0.02 for underestimated areas and from 0.08 to 0.2 for overestimated areas. The resultant flood

extent maps of observed 2010 flood event, uncalibrated model, and calibrated model are shown in Figure 7.7.

As clearly seen from Figure 7.8, even in uncalibrated model performs too close flood extent map estimates for the rural region of the study area, which is not required any modification on the floodplain roughness values. On the other hand, in Figure 7.9, mainly the majority of inundated areas are matched, but in some parts, such as exit area of village of Yenikent at the southwestern part, the greatest difference is detected for the uncalibrated model. These areas were tried to be modified by decreasing and increasing the local roughness coefficients.

According to the results of flood extent estimates in terms of RE and F-statistics as given in Table 7.2, even uncalibrated model has low RE value and high F-statistics as 0.15 and 81.06%, respectively. In addition, after the local modifications of floodplain roughness values, the calibrated model reached lower RE values to only 0.01. The spatial goodness-of-fit by means of F-statistics showed that calibrated model had over 93% agreement with the observed flood extent. Consequently, the calibrated model was decided as the final model and used for the further analyses of different alternatives.

Table 7.2. Comparison of the Flood Extent of Uncalibrated and Calibrated Models with 2010 Observation Map

	Area (km^2)		Fitness	
Models	Observed	Modelled	RE	F (%)
Uncalibrated model	2.22	1.89	0.15	81.06
Calibrated model	2.22	2.20	0.01	93.86

Figure 7.7. The boundaries of maximum flood extent maps of 2010 flood event (red line), calibrated model (green line), and uncalibrated model (blue line)

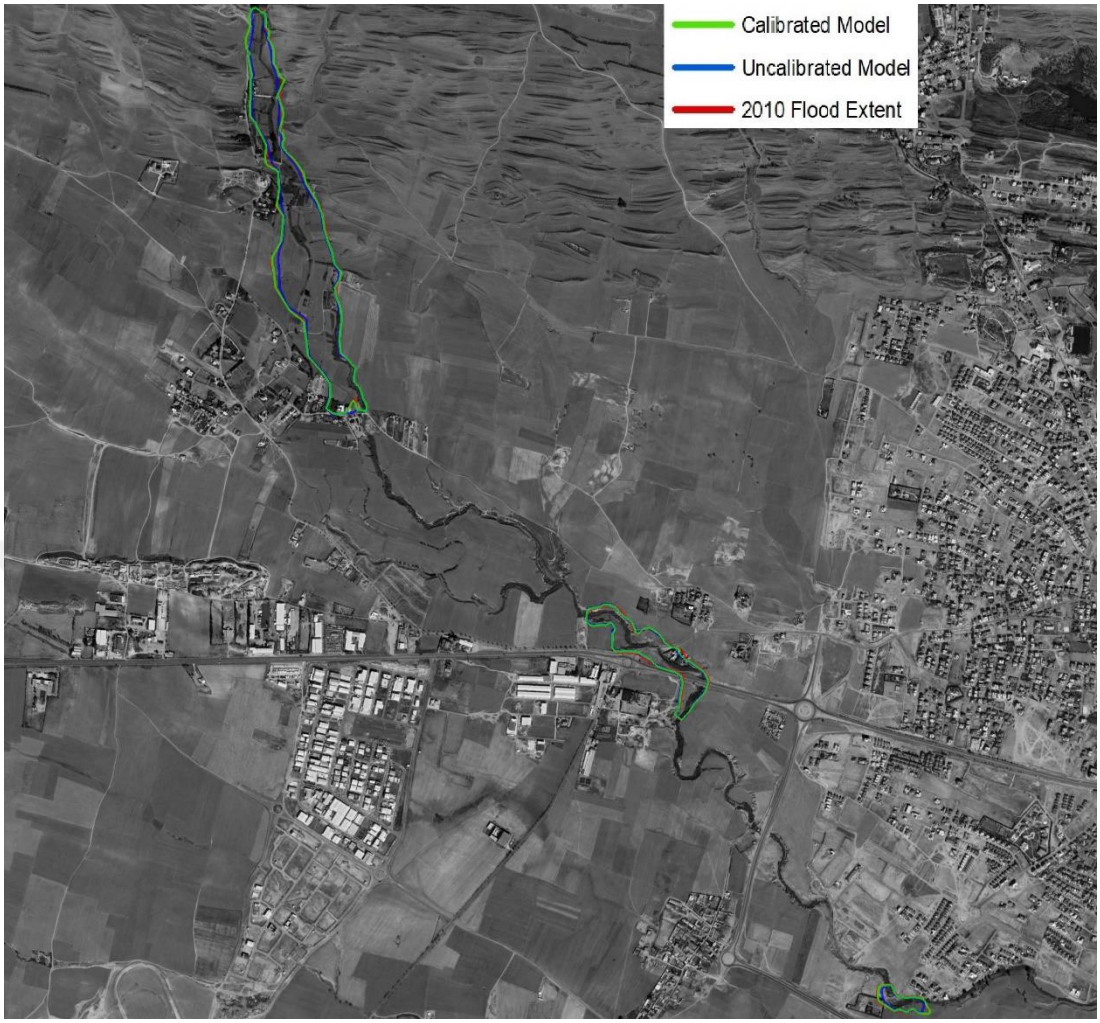

Figure 7.8. Rural part of the study area

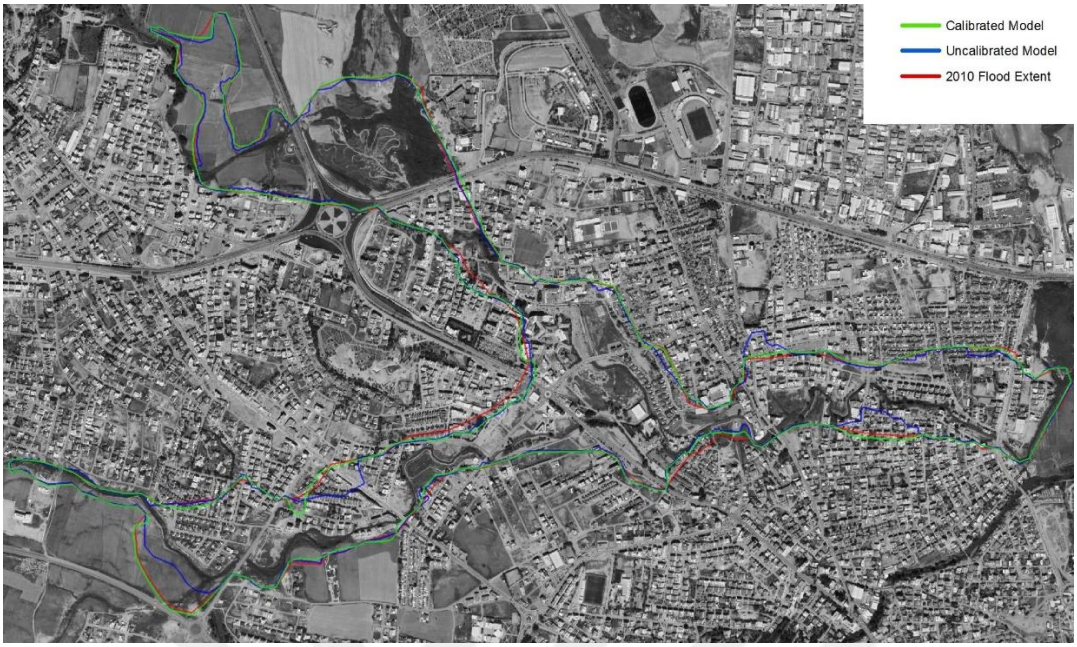

Figure 7.9. Urbanized part of the study area

MIKE 11 provides longitudinal views of main creek from Kanlıköy Pond and a branch from Gönyeli Pond for 2010 flood day as shown in Figure 7.10 and Figure 7.11, respectively. When analyzing the results, the cross-sections located at the just downstream of Kanlıköy Pond and at the main settlement areas of Nicosia were overtopped. After the maximum discharge entered the creek from the first cross-section, it was transferred along the 13.6 km long creek and observed about 2.5 hours later at the last cross-section. On the other hand, for the branch of Gönyeli, the main problem was at the downstream of the creek. From the outlet of the Gönyeli Pond to the exit of the town of Gönyeli, there was no serious inundation problem due to high capacity of the creek. The peak discharge arrived at the last cross-section in almost 1.5 hours later.

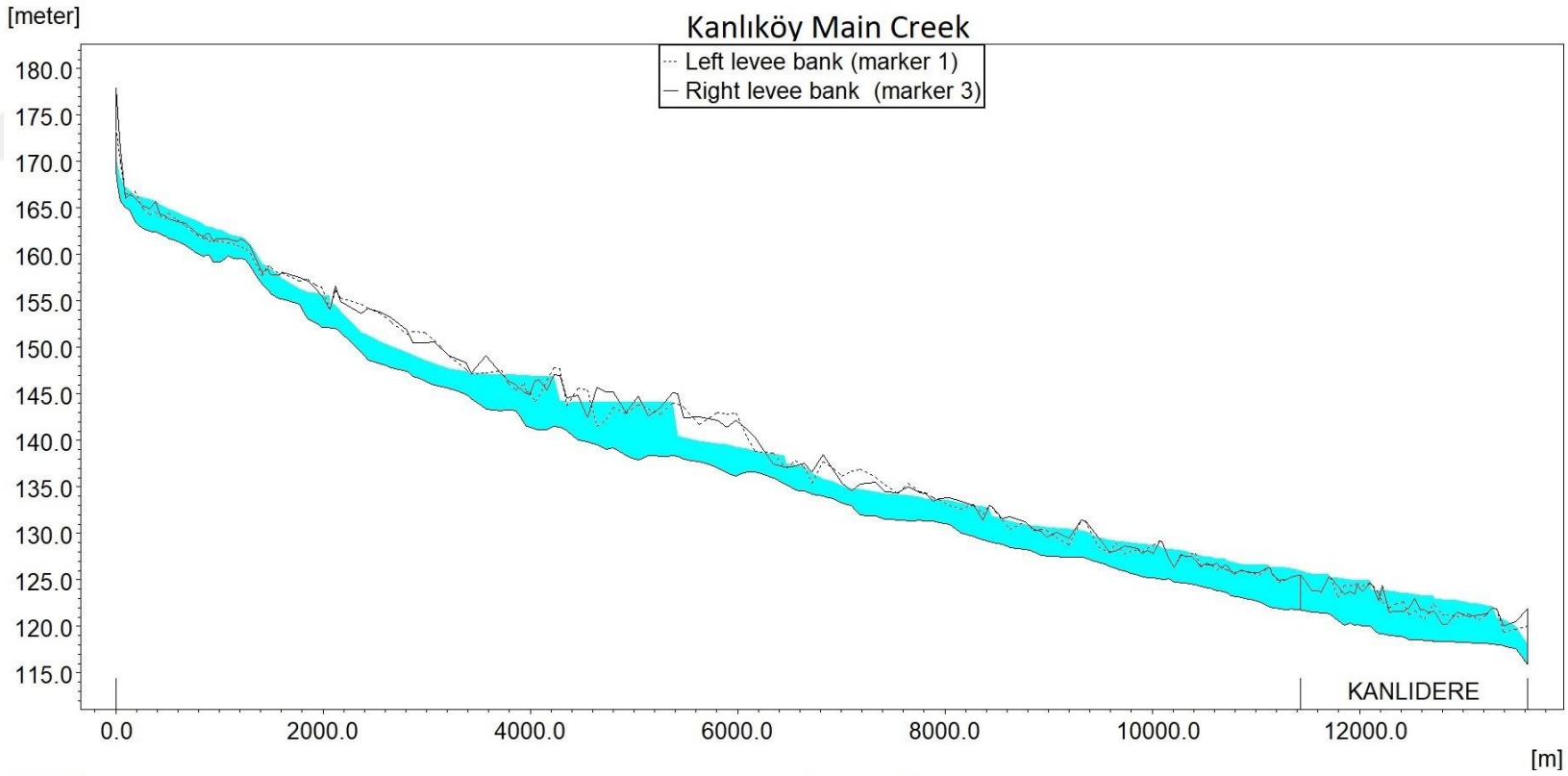

Figure 7.10. The longitudinal views of main creek of Kanlıköy in flood day

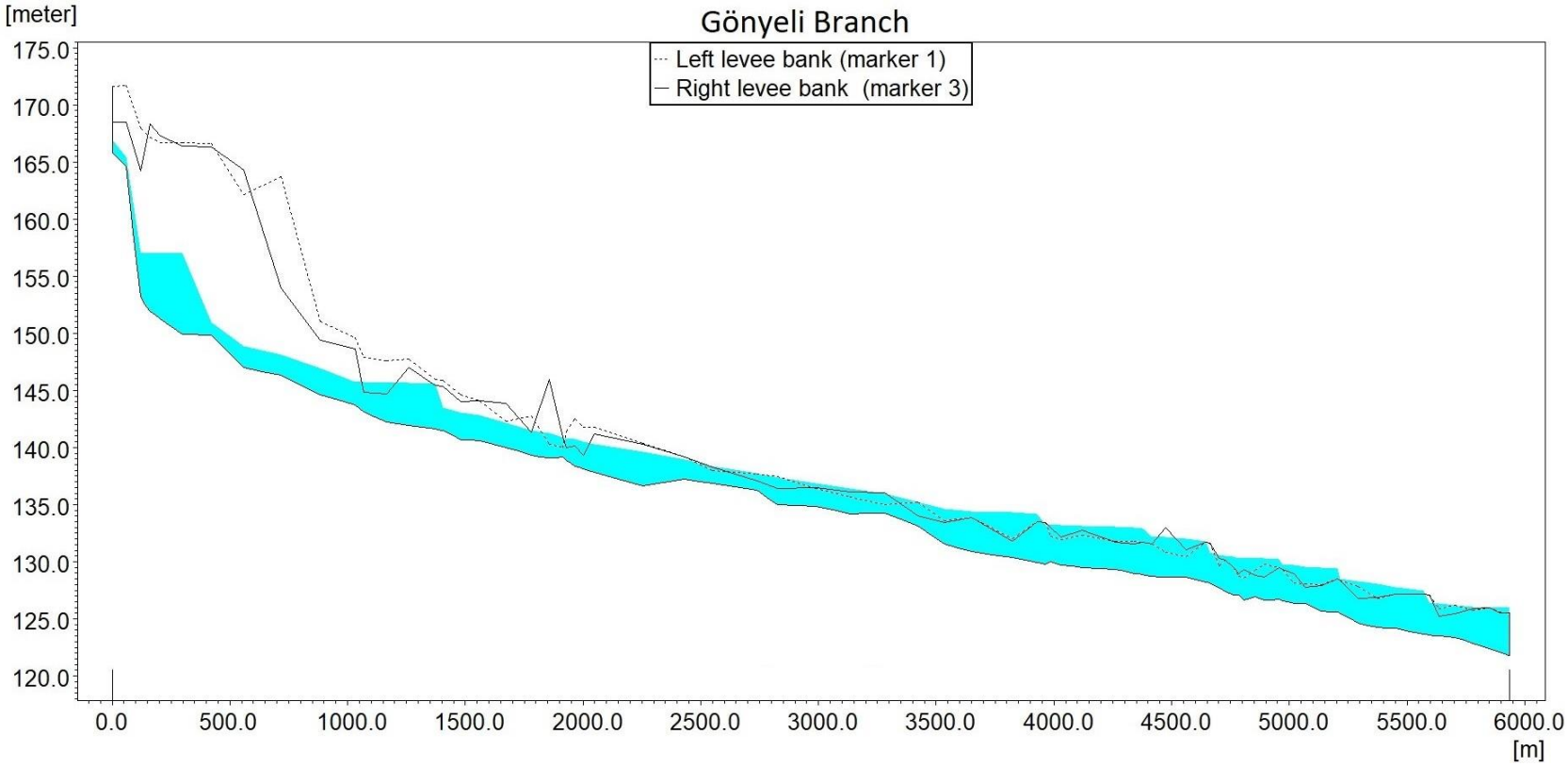

Figure 7.11. The longitudinal views of branch of Gönyeli in flood day

In order to conduct a detailed analysis of inundation areas, the results of 2D model were investigated. As can be seen from Figure 7.12, the location of a joint point of branch of Gönyeli to the main creek is the most hazardous region of the city. Moreover, the location of the main hospital of the country, named as Burhan Nalbantoğlu Hospital, a high school of Levent College, and the dense settlements around the creek made this area as the one of the most critical points in the study area.

Other inundated areas in the study area consisting of the main settlement regions at the western and eastern part of Nicosia, the busiest intersection of Gönyeli roundabout, and the downstream of Kanlıköy Pond are demonstrated in Figure 7.13. The majority of the creeks passing through these areas had a dense vegetation and obstructions, which lead to decrease the velocity and increase the flow depths in the creeks. Besides, the low banks also cause easier overbanking in some places, e.g. in the village of Kanlıköy and near the exit part of Gönyeli town as shown in Figure 7.14. Therefore, the discharge of 4.5 m^3/s was adequate to cause flooding particularly first in these cross-sections. Moreover, according to the flood extent map of the simulation, 797 buildings were affected under 2.22 km^2 inundated area. When population and urbanization growths are taken into account, in a new flooding event, this number could dramatically raise in the future. Furthermore, 12 out of 25 hydraulic structures that were added to the river network was detected as insufficient to drain flood flow. Therefore, their dimensions and capacities should be assessed in detail to mitigate the extent of local inundation.

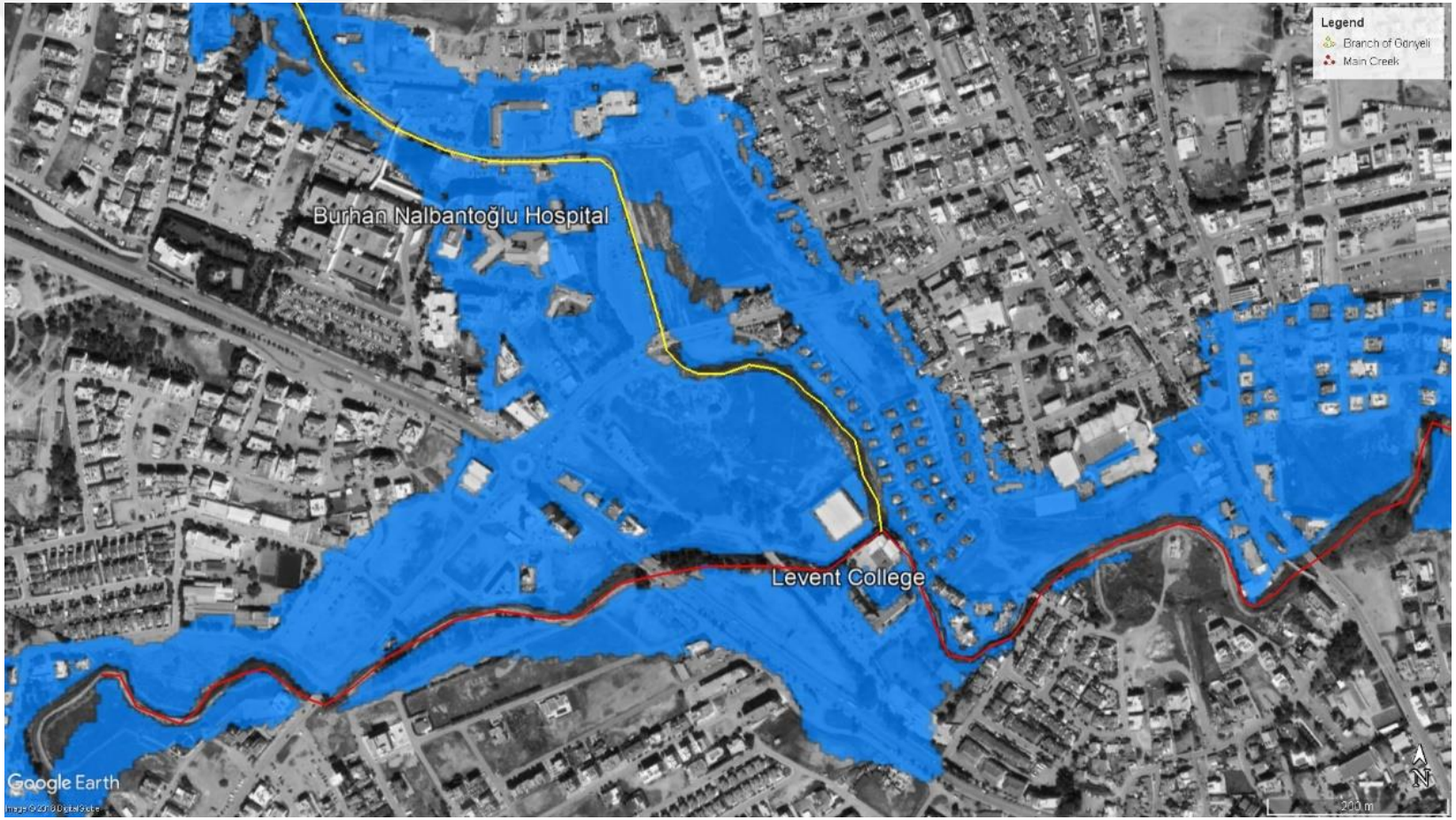

Figure 7.12. A joint point of the branch of Gönyeli to the main creek of Kanlıköy

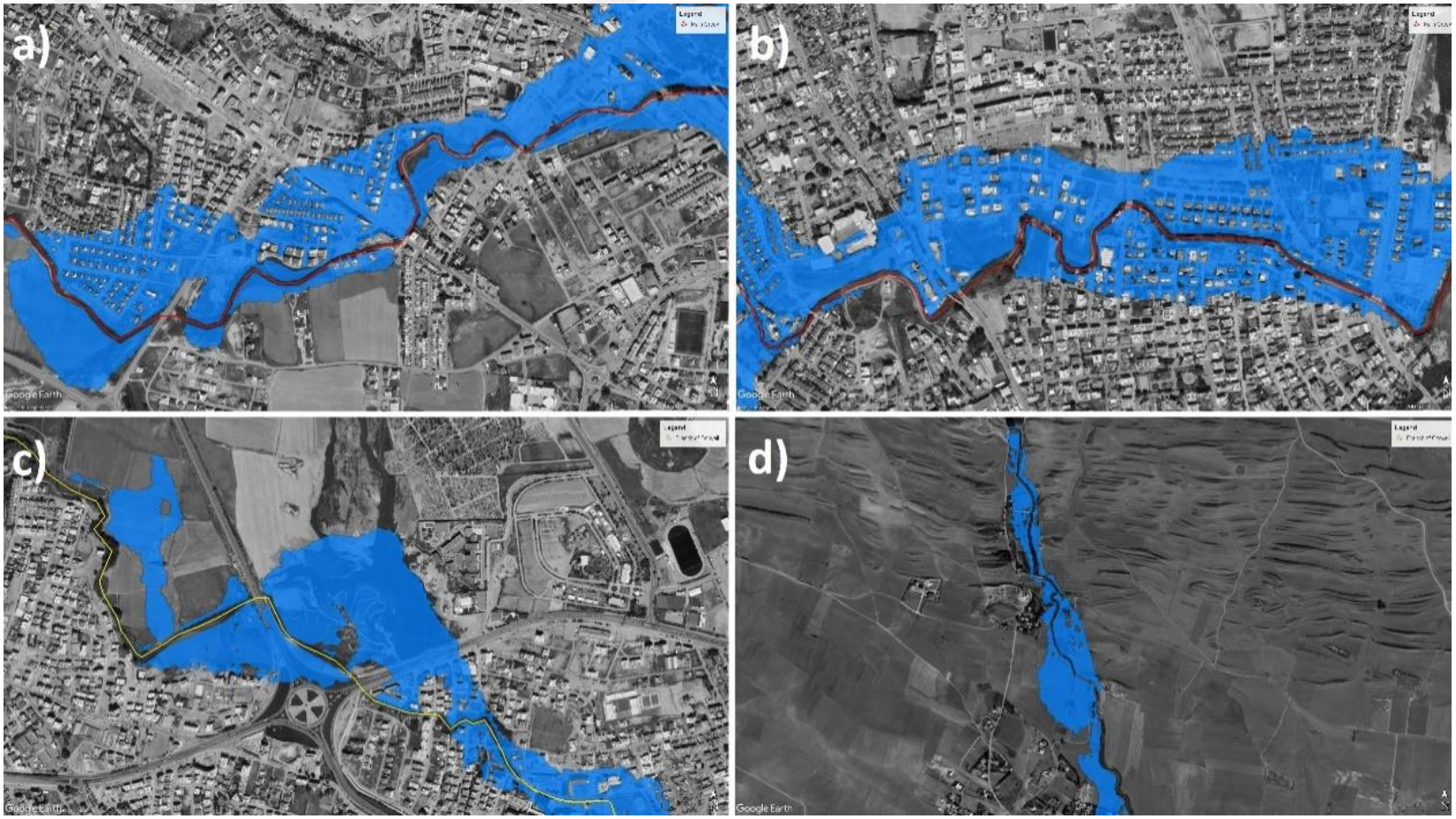

Figure 7.13. Inundated areas in the study area including a) western part of Nicosia; b) eastern part of Nicosia; c) Gönyeli roundabout; d) downstream of Kanlıköy pond

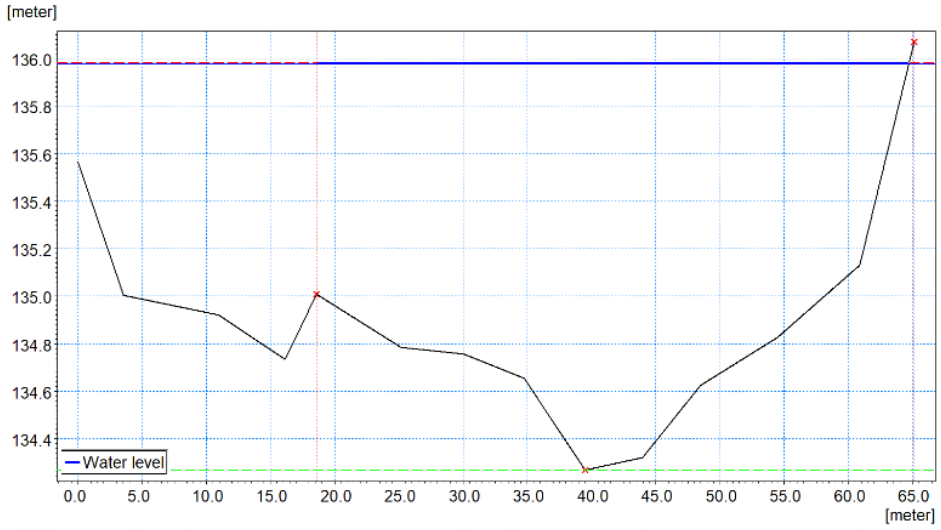

Figure 7.14. The cross-section located at the chainage of 3279.7 m on the Gönyeli branch

In Figure 7.15, the map of total flow depths in focused areas for the simulated 2010 flood event are displayed. Particularly, high flow depths near the settlements were very hazardous with regard to human lives and must be urgently interfered to protect such areas of top priority. Unfortunately, the main settlement areas and other public places (e.g. schools) were in great danger. In this context, not only assessment of flow depths, but also the flow velocities affected the intensity of flood. As illustrated in Figure 7.16, higher flow velocities are observed at the inner part of the cities and they must be carefully evaluated by considering both the flow depth and velocity. As stated in Jonkman and Penning-Rowsell (2008), depth-velocity product of a range from 0.6 m^2/s to 2 m^2/s was the critical ratio for standing in flows according to the available studies. Moreover, McBean et al. (1988) indicated that flow with 1 m depth and 3 m/s velocity could create a force exceeding the design capacity of a typical residential wall. In this regard, knowing the flow characteristics in the floodplain is valuable to avoid of human loss in particular during the flooding.

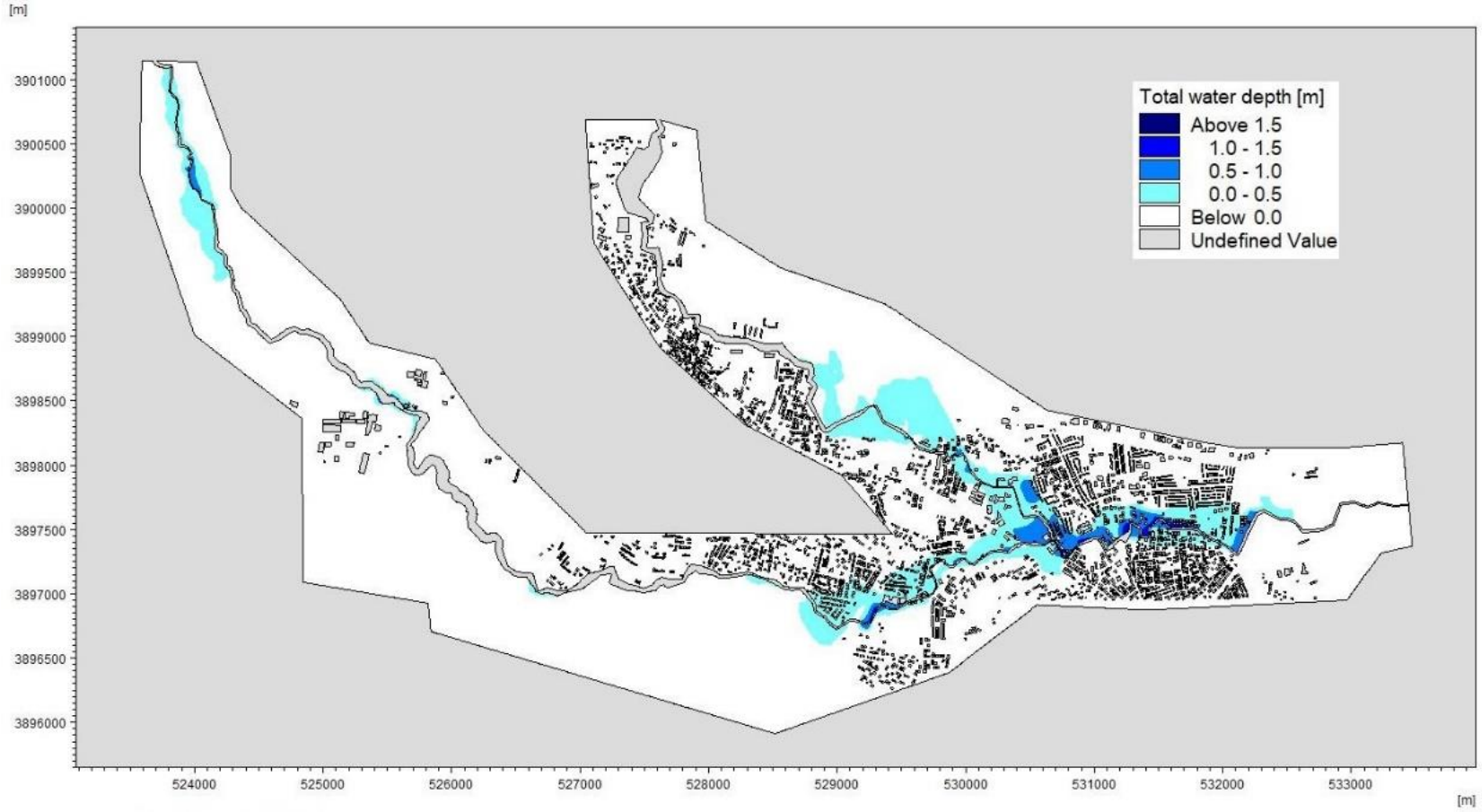

Figure 7.15. Flow depths of simulated 2010 flood

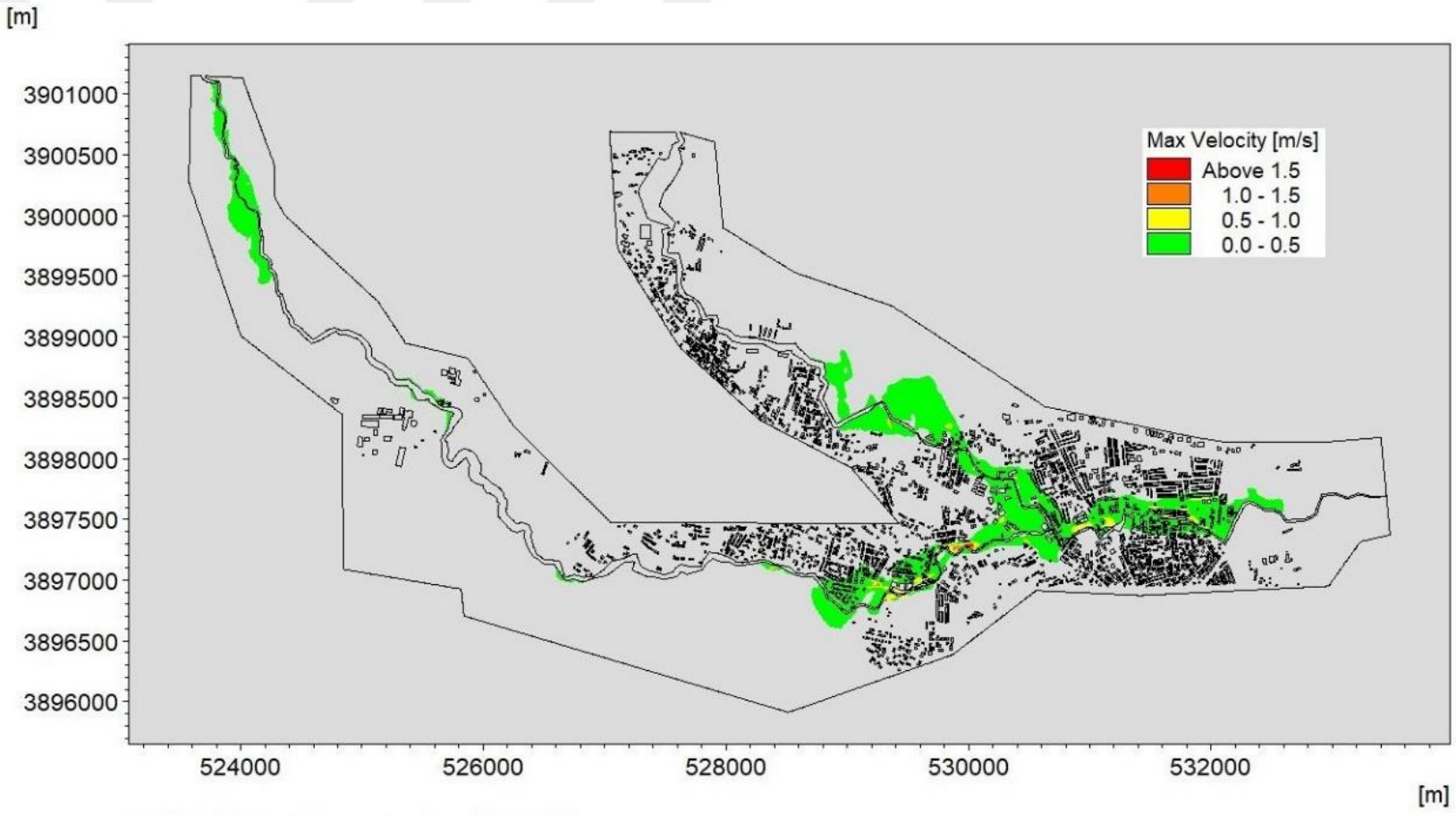

Figure 7.16. Maximum velocity map of simulated 2010 flood

7.2. Alternative 2 (Assessment of Kanlıköy Pond)

Kanlıköy Pond has an embankment and a spillway with the crest elevations of $K_d = 175.4$ m and $K_s = 173.9$ m, respectively. In the first trial, the current case was assessed by applying a 500-year inflow hydrograph. As given in Figure 7.17, the outflow hydrograph with a peak discharge of 121.2 m^3/s is obtained which caused serious downstream inundation.

Secondly, the reservoir bed of Kanlıköy Pond was decided to be dredged by 2 m with the same K_d and K_s values. This time the peak discharge of the outflow hydrograph is reduced to 113.5 m^3/s as illustrated in Figure 7.17, which still could lead to a large area under water.

In the third trial, the reservoir was dredged by 2 m and K_d and K_s values were raised to 177 m and 175 m, respectively. The maximum discharge becomes as 95.8 m^3/s as exhibited in Figure 7.17 and it is big enough to cause serious downstream inundation.

Another trial was employed to dredge the reservoir by 2 m and increase the crest elevations to $K_d = 178$ m, and $K_s = 176$ m. This change has a limited impact on the outflow hydrograph and the maximum discharge is decreased to 79.8 m^3/s as shown in Figure 7.17.

It should be noted that in the implementations of dredging or raising the hydraulic structures, new area-elevation relationship was derived while applying reservoir routing by considering the lowest elevation of reservoir bed and K_d value.

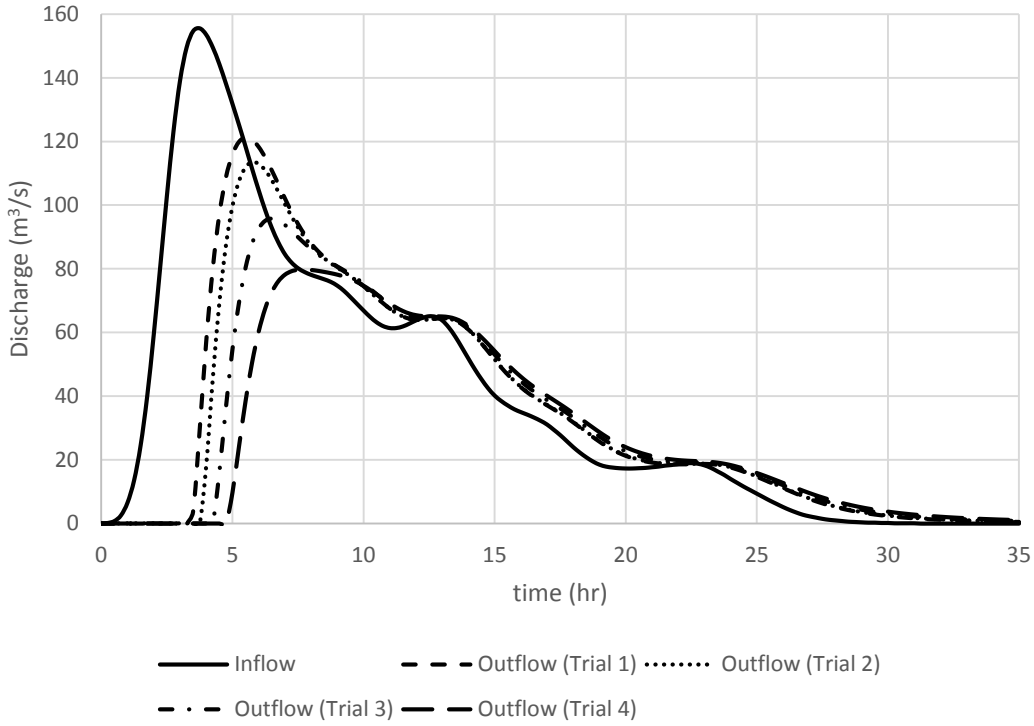

Figure 7.17. Inflow hydrograph of Q500 and outflow hydrograph of different trials in Kanlıköy Pond

7.3. Alternative 3 (New Upstream Pond in Kanlıköy)

In this alternative, implementation of a nearby upstream pond in Kanlıköy was evaluated to keep the most of the volume of water and release a limited amount. In order to determine the most appropriate location, the stream network in the pond catchment is identified and the location on the branch, which has a high storage potential, is selected based on the suitable topographic and environmental conditions as shown in Figure 7.18. In addition, having no settlement around it gives flexibility in the selection of the pond site

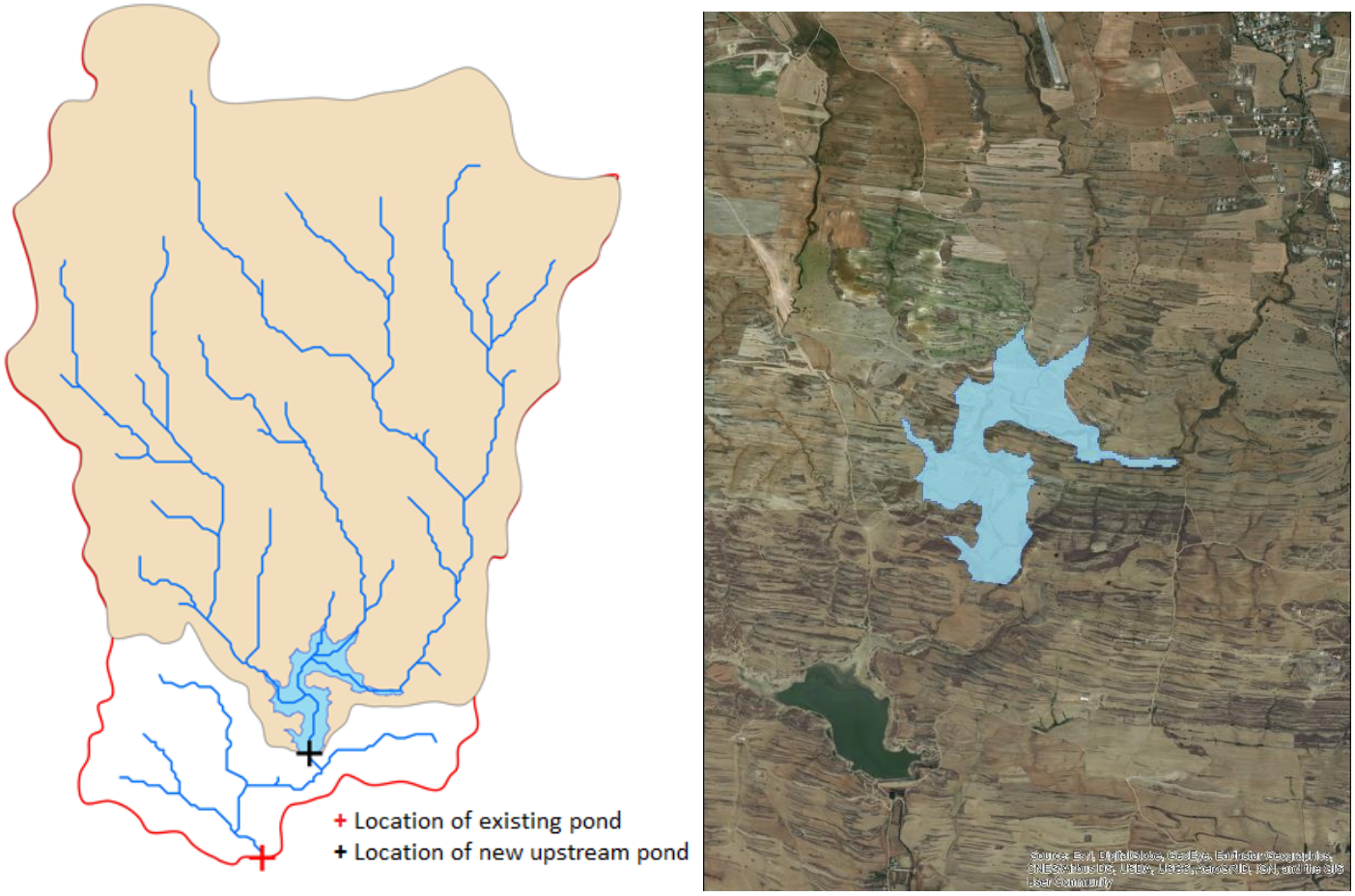

Figure 7.18. Location of existing and new upstream pond

The area-elevation (Figure 7.19) and volume-elevation (Figure 7.20) curves are generated in order to examine the efficiency of the upstream pond which has an ability to save vast amount of volume of water before entering the current Kanlıköy Pond. The relation of the water surface area (A) and water depth (h) from the thalweg in the reservoir was obtained with $R^2 = 0.996$ as follows:

$$A(h) = 12.58h^6 - 414.99h^5 + 5028.3h^4 - 27117h^3 + 64174h^2 - 40296h + 11814 \quad (7.3)$$

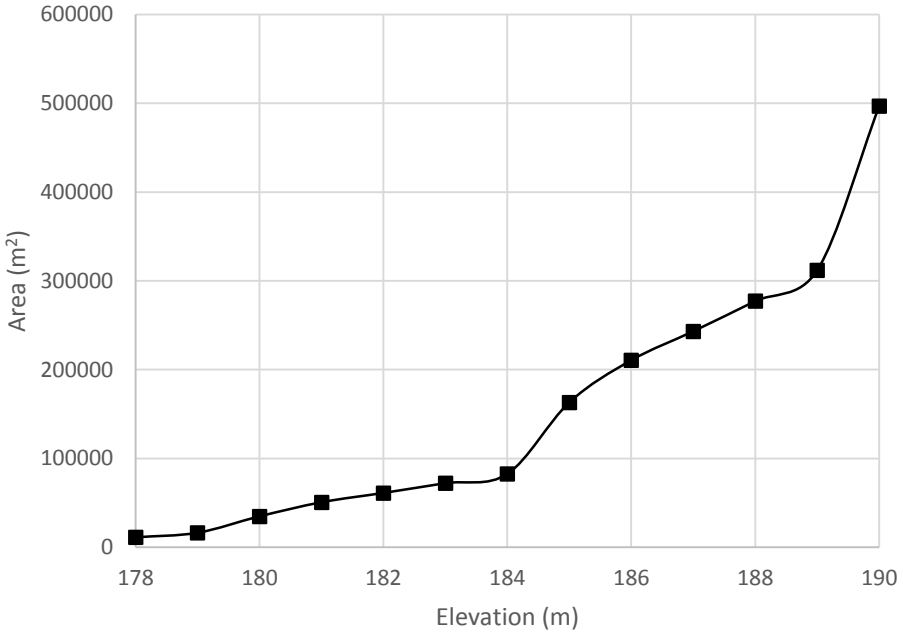

Figure 7.19. Area-elevation relation for upstream pond in Kanlıköy

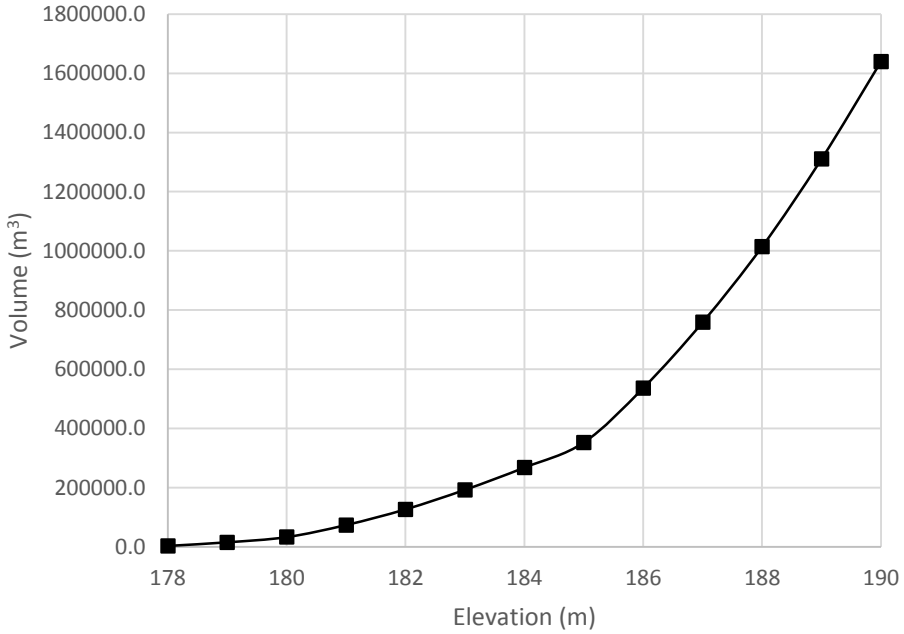

Figure 7.20. Volume-elevation relation for upstream pond in Kanlıköy

In the first trial, this alternative was analyzed for 500-year hydrograph for the assumptions of doing nothing to existing Kanlıköy Pond and considering an upstream pond with $K_d = 190$ m and $K_s = 187$ m. This implementation reduces the peak discharge of inflow hydrograph to the existing pond from 155.5 m^3/s to 128.4 m^3/s and the flow hydrograph at the outlet of the Kanlıköy Pond is found with the maximum discharge of 94.5 m^3/s as shown in Figure 7.21. This hydrograph could cause a serious inundation in the study area. Therefore, in the second trial, upstream pond properties were altered as $K_d = 193$ m and $K_s = 190$ m. In the present condition, the inflow to the Kanlıköy Pond had a peak discharge of 75.9 m^3/s and only a slight decrease was detected as 70.4 m^3/s. Finally, the pond was considered to have $K_d = 196$ m and $K_s = 193$ m, which was reasonable relied on the topographical properties. In the third trial, the maximum discharge of inflow to Kanlıköy Pond was calculated as 8.3 m^3/s and at the outlet, only a small hydrograph with the peak discharge of 3.2 m^3/s was obtained. Fortunately, this value was less than the critical value of 4.5 m^3/s and this

alternative was decided as the final solution for the Kanlıköy and the main creek of the study area. The summary of the outflows through the spillway of existing Kanlıköy Pond is displayed in Figure 7.21. Since both ponds are very close to each other, no reduction is considered in the inflow hydrograph entering the upstream pond.

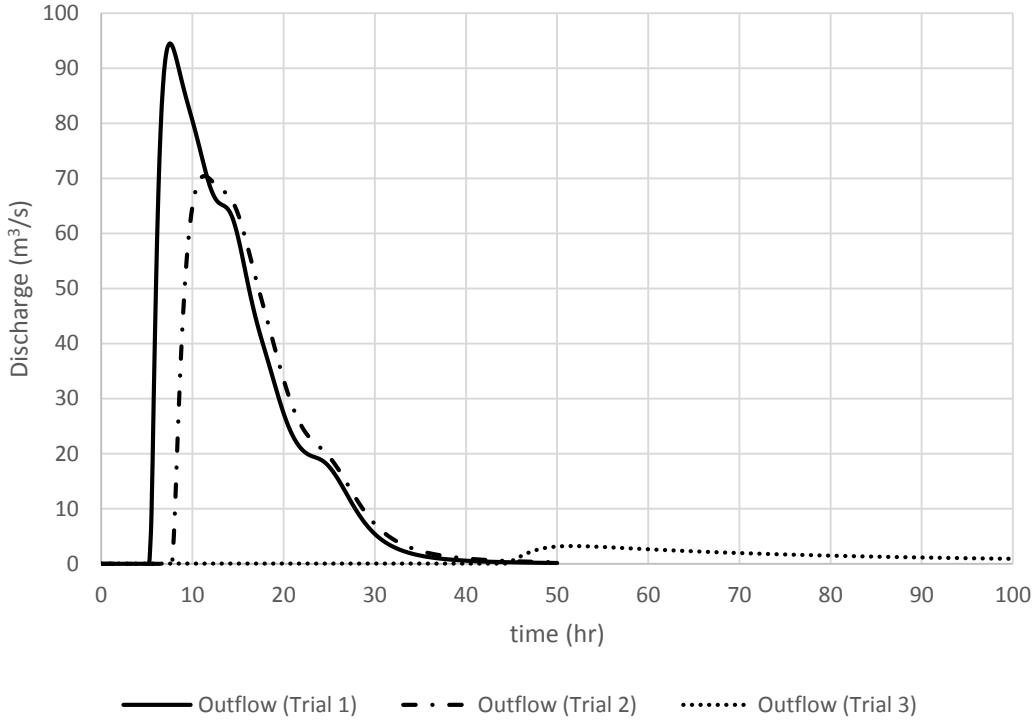

Figure 7.21. The outflow hydrographs observed at the outlet of the existing Kanlıköy Pond

7.4. Alternative 4 (Assessment of Gönyeli Pond)

In Alternative 4, the contribution of Gönyeli Pond catchment to the focused study area was examined by executing several trials of dredging and raising the crest elevations of the embankment and the spillway. Therefore, for the application of reservoir routing, the area-elevation relationship (Figure 7.22) is derived by using the contours of topographical maps and ground measurements in fieldworks.

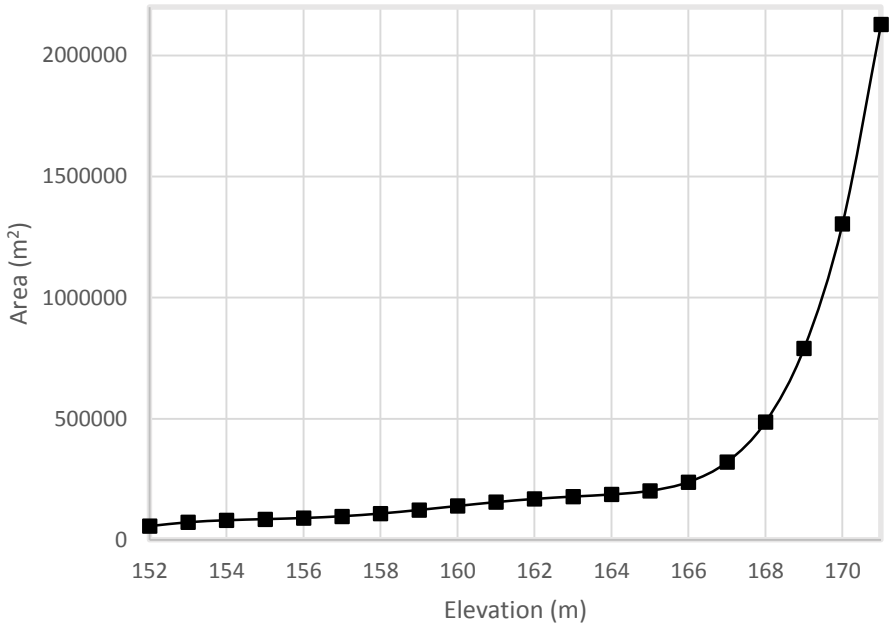

Figure 7.22. Area-elevation relation of Gönyeli Pond

In the first trial, the current case of Gönyeli Pond with $K_d = 168$ m and $K_s = 165$ m was employed with respect to the hydrograph of 500-year return period. The inflow having a peak discharge of 138.4 m^3/s was lowered to 111.5 m^3/s. However, this caused a serious inundation for the downstream side.

In the second trial, reservoir bed of Gönyeli Pond was dredged by 3 m with the same values of K_d and K_s. The outflow hydrograph with the maximum discharge of 96.5 m^3/s was obtained, which was not adequate to protect the study area. The third trial included both reservoir bed dredging of 3 m with the modified values of $K_d = 169$ m and $K_s = 167$ m and the peak discharge of 64.7 m^3/s was calculated at the outlet.

In Trial 4, the reservoir bed is dredged by 5 m and the current values of K_d and K_s are used. This time, the maximum discharge was found as 84.8 m^3/s. Therefore, in addition to the bed dredging of 5 m, the modification of $K_d = 170$ m and $K_s = 168$ was applied as Trial 5. The peak discharge was reduced to 55.1 m^3/s but still it is not sufficient to protect the downstream from flooding.

In Trial 6, the reservoir bed dredging by 7 m with the current values of K_d and K_s were assessed. The peak discharge of inflow was decreased to 62.8 m^3/s, which was still high for protecting the downstream inundation. Therefore, the altered values of $K_d = 171$ m and $K_s = 168.5$ m with 7 m dredging was considered in the last trial. Since the settlement density was high around the reservoir lake of Gönyeli Pond, the selected crest elevations were the limit values. Finally, this implementation reduces the maximum discharge to 32.9 m^3/s and this trial was accepted as the final solution for Gönyeli Pond.

Consequently, the results of several trials are given in Figure 7.23. As shown before, the final solution for Gönyeli Pond lowers the peak of the inflow of 500-year from 138.4 m^3/s to 32.9 m^3/s. However, this decrease in attenuation is still not protected the whole study area.

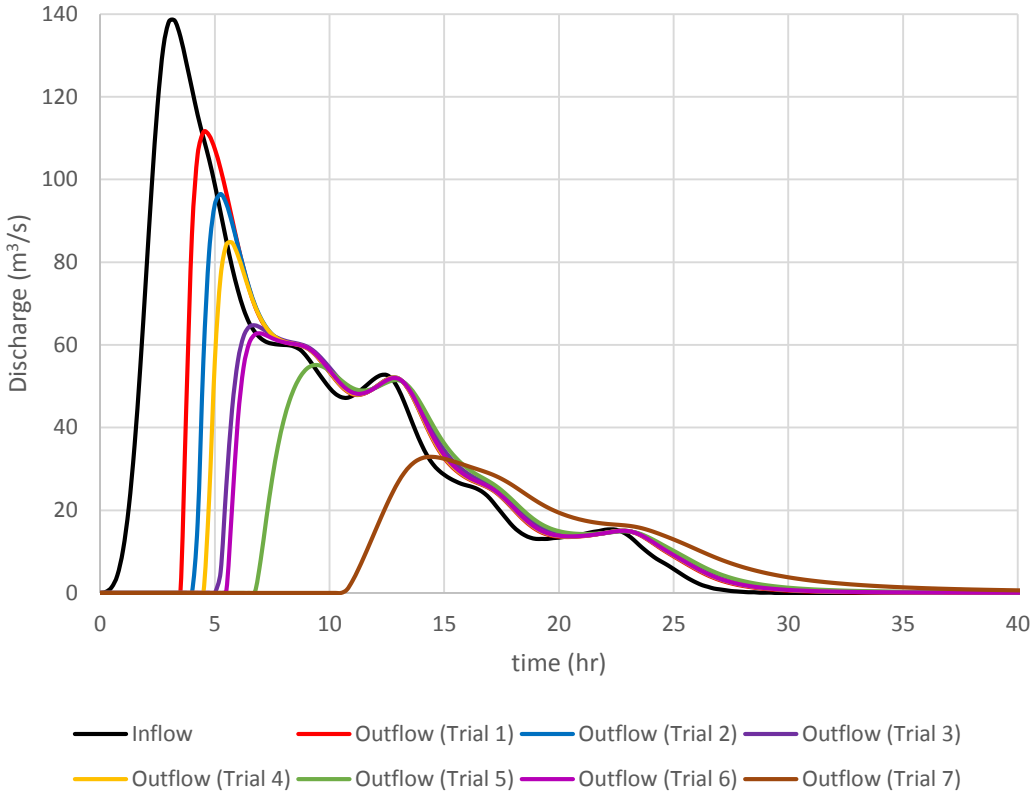

Figure 7.23. Summary of the results of the trials for Gönyeli Pond

7.5. Alternative 5 (Assessment of Final Solution)

Final solutions for Kanlıköy and Gönyeli ponds are combined and tested by using MIKE FLOOD model. When the 500-year runoff hydrographs enter to the modified system of Nicosia, the flood inundation extent is obtained as shown in Figure 7.24. As discussed before, this proposed solution reduces the flood peaks to a certain level and almost whole Nicosia was protected against the event of 500-year return period. As seen in Figure 7.24, only limited areas including the lower elevations of Gönyeli roundabout and a few buildings are affected.

Moreover, based on the inspection of the inundation map to be obtained using the above solutions, Manning's roughness coefficients were decreased a bit to cause rapid transmission of the flood waves with smaller flow depths. For the cross-sections where

possible, the Manning's values were reduced to 0.025 in terms of restoration of earth channels. The flood inundation map of this application is given in Figure 7.25. In such case, small inundation of shallow water in Gönyeli roundabout was observed. Besides, the inundated area covering the buildings at the downstream part of city was protected by the contribution of creek restoration.

Moreover, the final solution with reasonably smaller Manning's roughness coefficients was repeated for Q_{200}. After the reservoir routing of inflows for 200-year return period, the outflow hydrographs at the outlet of Kanlıköy and Gönyeli ponds were used as upstream boundary conditions to MIKE 11 model. According to the simulation result, no overbanking flow is detected along the creeks as displayed in Figure 7.26 and Figure 7.27. Therefore, the flooding events having a return period of 200-years or less will not result in inundation for the city of Nicosia after the implementation of final proposed measures.

Figure 7.24. Flood extend obtained by applying the final solution of Kanlıköy and Gönyeli ponds

Figure 7.25. Flood extend obtained by applying the final solution of Kanlıköy and Gönyeli ponds with reasonably smaller Manning's coefficient

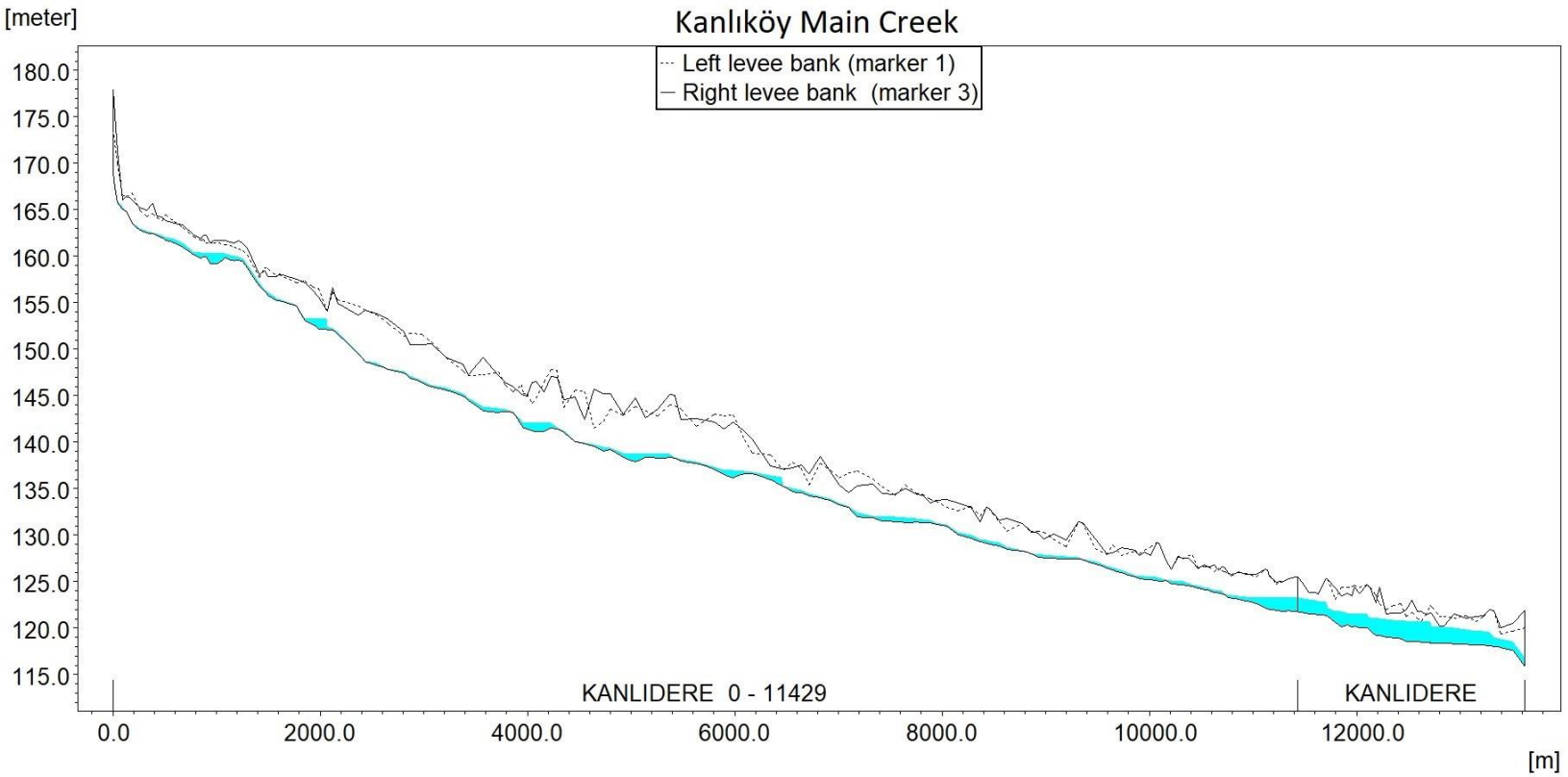

Figure 7.26. The result of 1D modelling of final solution with smaller roughness values for Q200 in the main creek of Kanlıköy

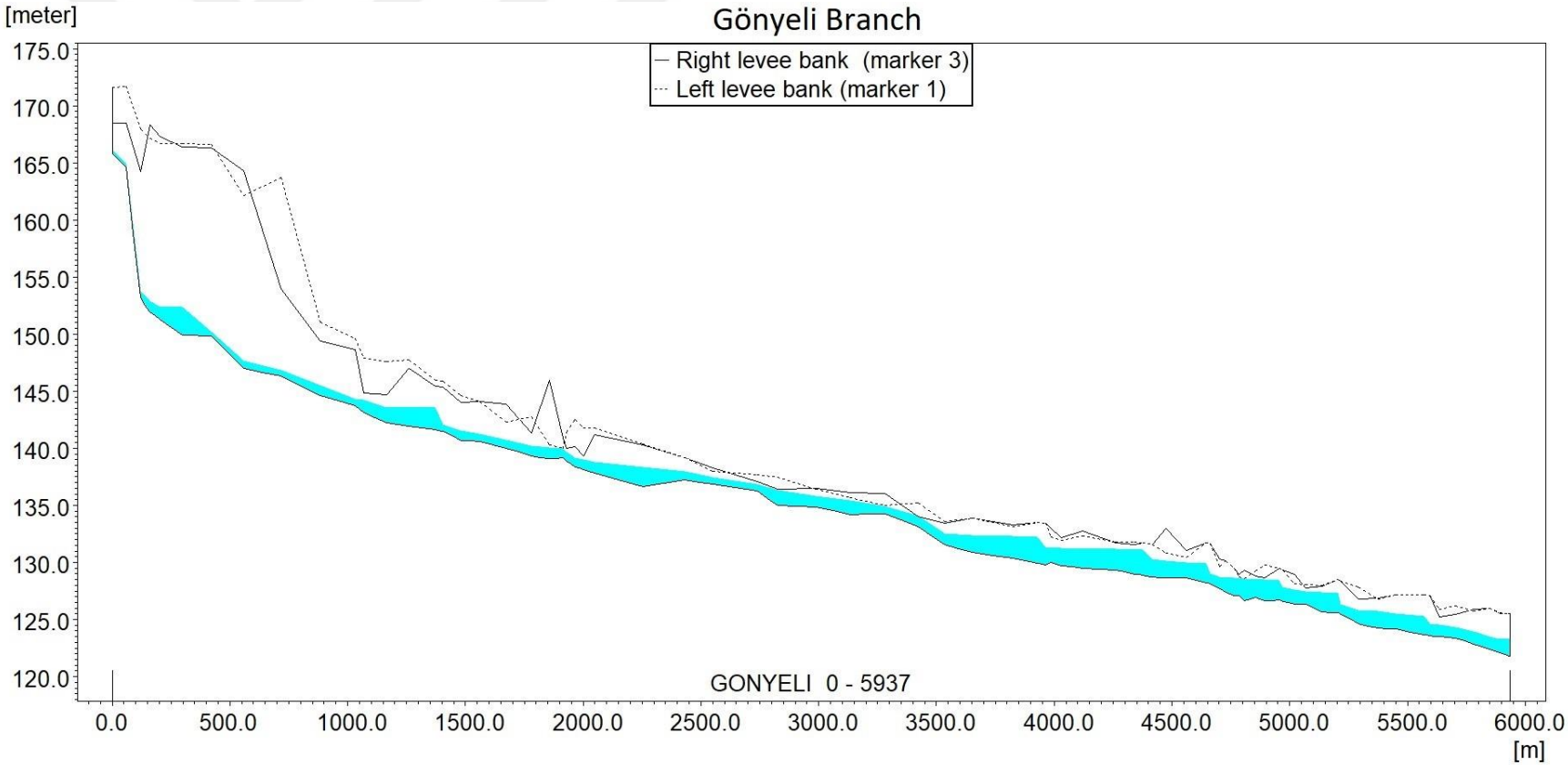

Figure 7.27. The result of 1D modelling of final solution with smaller roughness values for Q200 in the branch of Gönyeli

As a concluding remark, it can be said that the city of Nicosia will be protected with the proposed structural measures up to Q_{500} flood. Additional recommendations including a set of non-structural measures are provided in the next chapter.

CHAPTER 8

CONCLUSIONS AND RECOMMENDATIONS

8.1. Conclusions

In this research, flood management was conducted to protect the capital city of Nicosia against the flooding by proposing remedial structural measures. In this context, the flood modelling including both hydrological and hydraulic analyses was carried out to understand the rainfall-runoff response of the study area and implement hydraulic modelling to examine the current service level of hydraulic structures as well as considering new structural measures to mitigate the extent of flood inundation against the events of larger return periods.

In hydrological modelling, at first, 37 precipitation stations for the period of 1976-2015 were assessed across Northern Cyprus. To ensure the reliability of data series, a set of procedures consisting of estimating the missing data, quality controls, and four absolute homogeneity tests were executed. The series of 33 out of 37 stations were determined as completed, quality-controlled, and homogeneous based on the results of tests. Furthermore, in order to identify homogeneous regions of Northern Cyprus, time series clustering approaches were proposed as the contribution to the regional frequency analysis. Thus, the robust regional estimations of annual maximum daily values were achieved particularly for larger return periods. Moreover, these estimates were used to obtain the design hyetographs relied on the precipitation patterns of the stations of Lefkoşa and Alevkaya, which were assumed to represent the precipitation characteristics of the basin.

Kanlıköy and Gönyeli ponds were located at the upstream of the urbanized part of the study area and their contribution to the flood management was crucial in terms of decreasing the flood peaks before entering the main settlement part of the city. Therefore, HEC-HMS models of pond catchments were developed to simulate the hydrological processes and generate unit hydrographs due to lack of stream gauging stations in the study area. The input data required for executing SCS Unit Hydrograph approach via HEC-HMS were derived by using the data of precipitation, soil features, land covers, and topography. After generation of inflow hydrographs to the ponds, reservoir routing was employed based on the derived relations of area-elevation and volume-elevation curves of ponds to obtain outflow hydrographs which were used as boundary conditions for hydrodynamic model.

Since the accurate representation of floodplain topography was essential for realistic results of flood model, the digital elevation models by using different interpolation techniques were statistically and spatially assessed. According to the results, natural neighbor method was found as the most appropriate technique for the interpolation of the floodplain for this study. In addition, the main challenging task was the adaptation of topographical data sets from different sources and coordinate systems.

In order to model the 2010 flood event, the coupling of 1D MIKE 11 and 2D MIKE 21 was employed by MIKE FLOOD, which provided dynamically flow exchanges between models. Therefore, 1D model simulating the channel flow through the hydraulic structures and 2D model simulating the flow on the floodplain were developed and based on the observed flood inundation map of 2010 event, it was calibrated by using locally changing Manning's roughness coefficients for floodplain resistance. The calibrated model showed promising results with approximately 94% similarity according to the calculated spatial goodness-of-fit statistics.

Consequently, five alternatives were discussed for the flood protection of Nicosia. These alternatives included current case of Kanlıköy and Gönyeli ponds, dredging and raising the crest elevations of Kanlıköy Pond, implementation of a nearby upstream

pond in Kanlıköy, dredging and rasing of the crest elevations for Gönyeli Pond, and implementation of combined final solutions for Kanlıköy and Gönyeli ponds by also considering reasonably smaller Manning's roughness coefficients for the creeks as reflecting possible channel restoration studies. According to the flood extent maps, the majority of the study area except some small areas for the events of 500-year return periods and whole study area for the events of less than and equal to 200-year return periods were protected after the application of the final solutions.

8.2. Recommendations to the Govermental Agencies

- Automatic recording precipitation stations should be located throughout the Northern Cyprus to record the precipitation depths in smaller time intervals. Therefore, precise information on daily distribution of precipitation and the intensity-duration-frequency curves can be created by the relevant public institutions and used for water resources projects.
- Streamflow gauging stations are urgently needed particularly on the creeks passing through the major cities of the country. One of the main responsibilities of the relevant public institutions is to collect and supply data as in the case of the developed countries for management and planning studies.
- Developing digital elevation model by using both the ground measurements and high resolution remote sensing techniques, such as LiDAR is required for the realistic representation of complex urbanized areas and more reliable and detailed results for flood modelling.
- By using the appropriate methods considering the biological aspects as well, the restoration of creeks must be executed. Therefore, rapid transmission of flood waves with smaller flow depth will contribute to the drainage systems in terms of decreasing of flood inundation depths.
- Besides the structural measures proposed in this study, also nonstructural measures should be considered, such as increasing the awareness about the flash floods particularly in schools, developing policies about the flood risk

management, informing the people especially living near the creeks about the preparedness and adaptation issues, providing early warning systems to warn people on time and evacuate, if necessary, etc.

- Upon implementation of the aforementioned structural measures, recording precipitation and streamflow gauges are recommended to be placed in Kanlıköy and Gönyeli basins at critical locations.

8.3. Recomendations for Further Research

- Performing nonstationary regional frequency analysis enable to utilize more precipitation stations which do not satisfy the assumption of stationarity and leads to obtain more accurate estimates for extreme events.
- Development of flood hazard maps to detect the risky zones of the city is required for the city planning and informing the local people.
- Economic analyses of flood management measures have to be assessed in decision-making process.
- By using different flood modelling software, such as SOBEK and TUFLOW, the results of this study can be verified and discussed for the study area. The practicality in terms of the required parameters and capabilities of the models can also be examined.

REFERENCES

Abbott, M. B., Bathurst, J. C., Cunge, J. A., O'Connell, P. E., and Rasmussen, J. (1986). "An introduction to the European Hydrological System—Systeme Hydrologique Europeen, "SHE", 1: History and philosophy of a physically-based, distributed modelling system." *Journal of Hydrology,* 87(1-2), 45-59.

Abderrezzak, K. E. K., Paquier, A., and Mignot, E. (2009). "Modelling flash flood propagation in urban areas using a two-dimensional numerical model." *Natural Hazards,* 50(3), 433-460.

Afshari, S., Tavakoly, A. A., Rajib, M. A., Zheng, X., Follum, M. L., Omranian, E., and Fekete, B. M. (2018). "Comparison of new generation low-complexity flood inundation mapping tools with a hydrodynamic model." *Journal of Hydrology,* 556, 539-556.

Aghabozorgi, S., Seyed Shirkhorshidi, A., and Ying Wah, T. (2015). "Time-series clustering: A decade review." *Information Systems,* 53, 16–38. doi.org/10.1016/j.is.2015.04.007.

Ahmad, M. M., Ghumman, A. R., and Ahmad, S. (2009). "Estimation of Clark's instantaneous unit hydrograph parameters and development of direct surface runoff hydrograph." *Water Resources Management,* 23(12), 2417–2435. Doi: 10.1007/ s11269-008-9388-8.

Alexander, L. V., et al. (2006). "Global observed changes in daily climate extremes of temperature and precipitation." *Journal of Geophysical Research: Atmospheres,* 111(D5), 1-22. Doi: 10.1029/2005JD006290.

Alexandersson, H. (1986). "A homogeneity test applied to precipitation data." *Journal of Climatology,* 6(6), 661–675.

Ali, A. M., Solomatine, D. P., and Di Baldassarre, G. (2015). "Assessing the impact of different sources of topographic data on 1-D hydraulic modelling of floods." *Hydrology and Earth System Sciences,* 19(1), 631-643.

Alobaidi, M. H., Marpu, P. R., Ouarda, T. B., and Chebana, F. (2015). "Regional frequency analysis at ungauged sites using a two-stage resampling generalized ensemble framework." *Advances in Water Resources,* 84, 103–111.

Apel, H., Aronica, G. T., Kreibich, H., and Thieken, A. H. (2007). "Evaluation of different modelling strategies for flood risk assessment in urban areas." *Proceedings of the Congress-international Association for Hydraulic Reserach* 32(1), 121.

Arduino, G., Reggiani, P., and Todini, E., (2005). "Recent advances in flood forecasting and flood risk assessment." *Hydrology and Earth System Sciences Discussions,* 9(4), 280–284.

Arnbjerg-Nielsen, K. (2012). "Quantification of climate change effects on extreme precipitation used for high resolution hydrologic design." *Urban Water Journal*, 9(2), 57–65.

Aronoff, S. (1989). *Geographic Information Systems: A Management Perspective*. Geocarto International. https://doi.org/10.1080/10106048909354237

ASCE. (1996). *Hydrology Handbook,* 2nd Ed., New York.

Bagnall, A. and Janacek, G. (2005). "Clustering time series with clipped data." *Machine Learning*, 58(2-3), 151-178.

Ballesteros, J. A., Eguibar, M., Bodoque, J. M., Díez- Herrero, A., Stoffel, M., and Gutiérrez- Pérez, I. (2011). "Estimating flash flood discharge in an ungauged mountain catchment with 2D hydraulic models and dendrogeomorphic palaeostage indicators." *Hydrological Processes*, 25(6), 970-979.

Bardossy, A. and Pegram, G. (2014). "Infilling missing precipitation records-A comparison of a new copula-based method with other techniques." *Journal of Hydrology*, 519, 1162–1170.

Barnett, V., and Lewis, T. (1994). *Outliers in Statistical Data*, 3rd Ed., Wiley, Chichester, U.K.

Basha, H. A. (1994). "Nonlinear reservoir routing: particular analytical solution." *Journal of Hydraulic Engineering*, 120(5), 624-632.

Bates, P. D. and De Roo, A. P. J. (2000). "A simple raster-based model for flood inundation simulation." *Journal of Hydrology*, 236(1-2), 54–77.

Bayazit, M. and Onoz, B. (2007). "To prewhiten or not to prewhiten in trend analysis?" *Hydrological Sciences Journal*, 52(4), 611-624.

Berndt, D. and Clifford, J. (1994). "Using dynamic time warping to find patterns in time series." *AAAI-94 Workshop on Knowledge Discovery in Databases, AAAI*, Palo Alto, CA, 359–370.

Bezak, N., Šraj, M., and Mikoš, M. (2016). "Copula-based IDF curves and empirical rainfall thresholds for flash floods and rainfall-induced landslides." *Journal of Hydrology*, 541, 272-284.

Bhandari, M., Nyaupane, N., Mote, S. R., Kalra, A., and Ahmad, S. (2017). "2D Unsteady Flow Routing and Flood Inundation Mapping for Lower Region of Brazos River Watershed." *Proceedings of the World Environmental and Water Resources Congress*, 292-303.

Bharath, R. and Srinivas, V. V. (2015). "Regionalization of extreme rainfall in India." *International Journal of Climatology*, 35(6), 1142-1156.

Bhaskar, N. R. and O'Connor, C. A. (1989). "Comparison of method of residuals and cluster analysis for flood regionalization." *Journal of Water Resources Planning and Management*, 115(6), 793-808.

Bingham, C. and Nelson, L. S. (1981). "An approximation for the distribution of the von Neumann ratio." *Technometrics*, 23(3), 285-288.

Bladé, E., Gómez-Valentín, M., Dolz, J., Aragón-Hernández, J. L., Corestein, G., and Sánchez-Juny, M. (2012). "Integration of 1D and 2D finite volume schemes for computations of water flow in natural channels." *Advances in Water Resources*, 42, 17-29.

Blöschl, G. (2006). *Rainfall-runoff Modeling of Ungauged Catchments*. Encyclopedia of hydrological sciences.

Bolle, A., et al. 2006. "Hydraulic modelling of the two-directional interaction between sewer and river systems." *Prococeedings of the Urban Drainage Modelling and Water Sensitive Urban Design*, Monash Univ., Melbourne, Australia.

Bonsal, B. R., Cuell, C., Wheaton, E., Sauchyn, D. J., and Barrow, E. (2017). "An assessment of historical and projected future hydro- climatic variability and extremes over southern watersheds in the Canadian Prairies." *International Journal of Climatology*, 37(10), 3934-3948.

Bothale, R. V. and Katpatal, Y. B. (2015). "Trends and anomalies in extreme climate indices and influence of El Niño and La Niña over Pranhita catchment in Godavari Basin, India." *Journal of Hydrologic Engineering*, 21(2), 05015023.

Brunner, G. W. (2002). *HEC-RAS river analysis system: User's manual*. US Army Corps of Engineers, Institute for Water Resources, Hydrologic Engineering Center.

Brunner G. W. (2014) *Combined 1D and 2D modelling with HEC-RAS*. USACE.

Budiyono, Y., Aerts, J., Brinkman, J., Marfai, M. A., and Ward, P. (2015). "Flood risk assessment for delta mega-cities: a case study of Jakarta." *Natural Hazards*, 75(1), 389-413.

Buishand, T. A. (1982). “Some methods for testing the homogeneity of rainfall records.” *Journal of Hydrology*, 58(1-2), 11–27.

Burby, R. J. (2001). “Flood insurance and floodplain management: the US experience.” *Global Environmental Change Part B: Environmental Hazards*, 3(3), 111-122.

Burn, D. H. (2014). “A framework for regional estimation of intensity–duration–frequency (IDF) curves.” *Hydrological Processes*, 28(14), 4209–4218.

Burn, D. H. (1989). “Cluster analysis as applied to regional flood frequency.” *Journal of Water Resources Planning and Management*, 115(5), 567-582.

Burrough, P. A. (1986). *Principles of Geographical Information Systems for Land Resources Assessment*. Geocarto International.

Caruso, C. and Quarta, F. (1998). “Interpolation methods comparison.” *Computers and Mathematics with Applications*, 35(12), 109-126.

Casale, R., and Margottini, C. (1999). *Floods and Landslides: Integrated Risk Assessment: Integrated Risk Assessment; with 30 Tables*. Springer Science and Business Media.

Castellarin, A., Burn, D., and Brath, A. (2001). “Assessing the effectiveness of hydrological similarity measures for flood frequency analysis.” *Journal of Hydrology*, 241(3–4), 270–285.

Chanson, H. (2004). *Hydraulics of Open Channel Flow: An Introduction*. Elsevier.

Charalambous, K., Bruggeman, A., Bakirtzis, N., and Lange, M. A. (2016). “Historical flooding of the Pedieos River in Nicosia, Cyprus.” *Water History*, 8(2), 191-207.

Charrad, M., Ghazzali, N., Boiteau, V., and Niknafs, A. (2014). “NbClust: An R package for determining the relevant number of clusters in a data set.” *Journal of Statistical Software*, 61(6), 1–36.

Chatterjee, C., Förster, S., and Bronstert, A. (2008). “Comparison of hydrodynamic models of different complexities to model floods with emergency storage areas.” *Hydrological Processes: An International Journal*, 22(24), 4695-4709.

Chebana, F., Charron, C., Ouarda, T. B., and Martel, B. (2014). “Regional frequency analysis at ungauged sites with the generalized additive model.” *Journal of Hydrometeorology*, 15(6), 2418-2428.

Chiang, S. M., Tsay, T. K., and Nix, S. J. (2002). "Hydrologic regionalization of watersheds. I: Methodology development." *Journal of Water Resources Planning and Management*, 128(1), 3–11.

Childs, C. (2004). *Interpolating surfaces in ArcGIS spatial analyst*. ArcUser, 3235, 569. https://www.esri.com/news/arcuser/0704/files/interpolating.pdf

Choi, J., Socolofsky, S. A., and Olivera, F. (2008). "Hourly disaggregation of daily rainfall in Texas using measured hourly precipitation at other locations." *Journal of Hydrologic Engineering*, 13(6), 476-487.

Cobby, D. M., Mason, D. C., Horritt, M. S., and Bates, P. D. (2003). "Two-dimensional hydraulic flood modelling using a finite-element mesh decomposed according to vegetation and topographic features derived from airborne scanning laser altimetry." *Hydrological Processes*, 17(10), 1979-2000.

Conrad, V., and Pollak, C. (1950). *Methods in Climatology*, Harvard University Press, Cambridge, MA.

Cook, A. and Merwade, V. (2009). "Effect of topographic data, geometric configuration and modeling approach on flood inundation mapping." *Journal of Hydrology*, 377(1-2), 131-142.

Corduas, M. (2011). "Clustering streamflow time series for regional classification." *Journal of Hydrology*, 407(1-4), 73–80.

Cowan, W. L. (1956). "Estimating hydraulic roughness coefficients." *Agricultural Engineering*, 37(7), 473-475.

CRED/EM-DAT data, *Centre for research on the epidemiology of disasters (CRED)-international disaster database (EM-DAT),* Available online at: http://www.emdat.be/database (Verified 29 July 2018)

Dalrymple, T. (1960). "Flood frequency analysis." Water Supply Paper No. 1543-A, U.S. Geological Survey, Reston, VA, 80.

Daupras, F., Antoine, J. M., Becerra, S., and Peltier, A. (2015). "Analysis of the robustness of the French flood warning system: A study based on the 2009 flood of the Garonne River." *Natural Hazards*, 75(1), 215-241.

David, E., Erlich, M., and Masson, A. (2009). *Benefits of 2D modelling approach for urban flood management*, CRC Press.

Deltares, 2017. *SOBEK Suite*, Deltares.

DHI (2000). *MIKE-21, User guide*, Danish Hydraulic Institute.

DHI, (2011). *A Modelling System for Rivers and Channels. Reference Manual*. DHI Water and Environment, Denmark.

DHI, (2017). *MIKE 21 Flow model and MIKE 21 Flood Screening Tool. Hydrodynamic Module. Scientific Documentation*. DHI Water and Environment, Denmark.

DHI, (2009). *MIKE FLOOD: 1D-2D Modelling User Manual*. MIKE by DHI.

DHI. (1997). *MIKE11 GIS Reference and User Manual*. Danish Hydraulic Institute: Horsholm, Denmark.

Di Baldassarre, G. (2012). *Floods in a Changing Climate: Inundation Modelling* (Vol. 3). Cambridge University Press.

Dijkman, J. (2007). *A Dutch Perspective on Coastal Louisiana Flood Risk Reduction and Landscape Stabilization*. Work (p. 185). London.

Dinç, U., et al. (2000). *Kuzey Kıbrıs Türk Cumhuriyeti Detaylı Toprak Etüd ve Haritalama Projesi*. Cilt-I KKTC Tarım ve Orman Bakanlığı, Çukurova Üniversitesi Ziraat Fakültesi Toprak Bölümü Bilimsel ve Teknik İşbirliği, 648.

Donat, M. G., et al. (2013). "Updated analyses of temperature and precipitation extreme indices since the beginning of the twentieth century: The HadEX2 dataset." *Journal of Geophysical Research: Atmospheres*, 118(5), 2098-2118.

Dookie, N., Chadee, X. T., and Clarke, R. M. (2018). "Trends in extreme temperature and precipitation indices for the Caribbean small islands: Trinidad and Tobago." *Theoretical and Applied Climatology*, 1-14.

Durre, I., Menne, M. J., Gleason, B. E., Houston, T. G., and Vose, R. S. (2010). "Comprehensive automated quality assurance of daily surface observations." *Journal of Applied Meteorology and Climatology*, 49(8), 1615–1633.

Eischeid, J. K., Pasteris, P. A., Diaz, H. F., Plantico, M. S., and Lott, N. J. (2000). "Creating a serially complete, national daily time series of temperature and precipitation for the western United States." *Journal of Applied Meteorology*, 39(9), 1580–1591.

European Climate Assessment and Dataset. (2017). "Indices of extremes." ⟨http://eca.knmi.nl/indicesextremes⟩ (Feb. 26, 2017).

Fan, X., Wang, Q., and Wang, M. (2012). “Changes in temperature and precipitation extremes during 1959–2008 in Shanxi, China.” *Theoretical and Applied Climatology*, 109(1-2), 283-303.

Feng, S., Hu, Q., and Qian, W. (2004). “Quality control of daily meteorological data in China, 1951–2000: A new dataset.” *International Journal of Climatology: A Journal of the Royal Meteorological Society*, 24(7), 853–870.

Fernandes, E. H., Dyer, K. R., and Niencheski, L. F. H. (2001). “Calibration and validation of the TELEMAC-2D model to the Patos Lagoon (Brazil).” *Journal of Coastal Research*, 34, 470-488.

Fewtrell, T. J., Bates, P. D., Horritt, M., and Hunter, N. M. (2008). “Evaluating the effect of scale in flood inundation modelling in urban environments.” *Hydrological Processes: An International Journal*, 22(26), 5107-5118.

Fleming, G. (2002). “How can we learn to live with rivers? The findings of the Institution of Civil Engineers Presidential Commission on flood-risk management.” *Philosophical Transactions of the Royal Society of London A: Mathematical, Physical and Engineering Sciences*, 360(1796), 1527-1530.

Frank, E., Ostan, A., Coccato, M., and Stelling, G. S. (2001). “Use of an integrated one dimensional-two dimensional hydraulic modelling approach for flood hazard and risk mapping.” *WIT Transactions on Ecology and the Environment*, 50, 99-108.

Frich, P., Alexander, L. V., Della-Marta, P. M., Gleason, B., Haylock, M., Tank, A. K., and Peterson, T. (2002). “Observed coherent changes in climatic extremes during the second half of the twentieth century.” *Climate research*, 19(3), 193-212.

Gaile, G. L. and Willmott, C. (2013). *Spatial statistics and models* (Vol. 40). Springer Science & Business Media.

Ganoulis, J. (2003). “Risk- based floodplain management: A case study from Greece.” *International Journal of River Basin Management*, 1(1), 41-47.

Gao, Z., Long, D., Tang, G., Zeng, C., Huang, J., and Hong, Y. (2017). “Assessing the potential of satellite-based precipitation estimates for flood frequency analysis in ungauged or poorly gauged tributaries of China’s Yangtze River basin.” *Journal of Hydrology*, 550, 478-496.

Gilbert, R. O. (1987). *Statistical Methods for Environmental Pollution Monitoring*. John Wiley and Sons.

Gilles D. W. (2010) *Application of Numerical Models for Improvement of Flood Preparedness*. Master's thesis, University of Iowa.

Gilles, D., and Moore, M. (2010). "Review of hydraulic flood modeling software used in Belgium, The Netherlands, and The United Kingdom." *International Perspectives in Water Resources Management*, Iowa City, IA.

Golay, X., Kollias, S., Stoll, G., Meier, D., Valavanis, A., and Boesiger, P. (1998). "A new correlation-based fuzzy logic clustering algorithm for FMRI." *Magnetic Resonance in Medicine*, 40(2), 249–260.

Golian, S., Saghafian, B., Elmi, M., and Maknoon, R. (2011). "Probabilistic rainfall thresholds for flood forecasting: evaluating different methodologies for modelling rainfall spatial correlation (or dependence)." *Hydrological Processes*, 25(13), 2046-2055.

González-Rouco, J. F., Jiménez, J. L., Quesada, V., and Valero, F. (2001). "Quality control and homogeneity of precipitation data in the southwest of Europe." *Journal of Climate*, 14(5), 964–978.

Griffiths, G. M., Salinger, M. J., and Leleu, I. (2003). "Trends in extreme daily rainfall across the South Pacific and relationship to the South Pacific Convergence Zone." *International Journal of Climatology: A Journal of the Royal Meteorological Society*, 23(8), 847–869.

Gullett, D.W., Vincent, L. and Sajecki, P.J.F. (1990). *Testing for Homogeneity in Temperature Time Series at Canadian Climate Stations*, CCC Report No. 90-4, Atmospheric Environment Service, Downsview, Ontario.

Guse, B., Thieken, A. H., Castellarin, A., and Merz, B. (2010). "Deriving probabilistic regional envelope curves with two pooling methods." *Journal of Hydrology*, 380(1-2), 14-26.

Hadjinicolaou, P., Giannakopoulos, C., Zerefos, C., Lange, M. A., Pashiardis, S., and Lelieveld, J. (2011). "Mid-21st century climate and weather extremes in Cyprus as projected by six regional climate models." *Regional Environmental Change*, 11(3), 441-457.

Hailegeorgis, T. T. and Alfredsen, K. (2017). "Regional flood frequency analysis and prediction in ungauged basins including estimation of major uncertainties for mid-Norway." *Journal of Hydrology: Regional Studies*, 9, 104-126.

Hailegeorgis, T. T., Thorolfsson, S. T., and Alfredsen, K. (2013). "Regional frequency analysis of extreme precipitation with consideration to uncertainties to update IDF curves for the city of Trondheim." *Journal of Hydrology*, 498, 305–318.

Hall, J. W., Tarantola, S., Bates, P. D., and Horritt, M. S. (2005). "Distributed sensitivity analysis of flood inundation model calibration." *Journal of Hydraulic Engineering*, 131(2), 117-126.

Heino, R. (1994). *Climate in Finland during the Period of Meteorological Observations*, Finnish Meteorological Institute Contributions.

Hesselink, A. W., Stelling, G. S., Kwadijk, J. C., and Middelkoop, H. (2003). "Inundation of a Dutch river polder, sensitivity analysis of a physically based inundation model using historic data." *Water Resources Research*, 39(9), 1234. Doi: 10.1029/2002WR001334.

Hidalgo-Munoz, J. M., Argüeso, D., Gámiz-Fortis, S. R., Esteban-Parra, M. J., and Castro-Díez, Y. (2011). "Trends of extreme precipitation and associated synoptic patterns over the southern Iberian Peninsula." *Journal of Hydrology*, 409(1-2), 497–511.

Hong-Fa, W. (2012). "Clustering of hydrological time series based on discrete wavelet transform." *Physics Procedia*, 25, 1966–1972.

Horritt, M. S. and Bates, P. D. (2001). "Effects of spatial resolution on a raster based model of flood flow." *Journal of Hydrology*, 253(1-4), 239-249.

Hosking, J. R. (1990). "L-moments: Analysis and estimation of distributions using linear combinations of order statistics." *Journal of the Royal Statistical Society. Series B (Methodological*), 52, 105–124.

Hosking, J. R. M., and Wallis, J. R. (2005). *Regional Frequency Analysis: An Approach Based on L-Moments*, Cambridge University Press, New York.

Howe, J. and White, I. (2004). "Like a fish out of water: The relationship between planning and flood risk management in the UK." *Planning Practice and Research*, 19(4), 415-425.

Hu, K., Ding, P., Wang, Z., and Yang, S. (2009). "A 2D/3D hydrodynamic and sediment transport model for the Yangtze Estuary, China." *Journal of Marine Systems*, 77(1-2), 114-136.

Hunter, N. M., Bates, P. D, Horritt, M. S., and Wilson, M. D. (2007) "Simple spatially-distributed models for predicting flood inundation: A review" *Geomorphology*, 90(3-4), 208-225.

Hutchinson, M. F. (1988). "Calculation of hydrologically sound digital elevation models." *Proceedings of the Third International Symposium on Spatial Data Handling (Vol. 133)*. Sydney: International Geographical Union.

Hydrologic Engineering Center (HEC). (2002). HEC-RAS River Analysis System, User's Manual, Version 3Ð1. US Army Corps of Engineers: Davis, California.

IPCC (Intergovernmental Panel on Climate Change). (2014). *Climate Change 2014- Impacts, Adaptation and Vulnerability: Regional Aspects*, Cambridge University Press, New York.

Isaaks, E. H., and Srivastava, R. M. (1989). *Applied Geostatistics*, Oxford University Press, New York.

Jacobson, C. R., (2011). "Identification and quantification of the hydrological impacts of imperviousness in urban catchments: A review." *Journal of Environmental Management*, 92(6), 1438–1448. doi.org/10.1016/j.jenvman.2011.01.018.

Jarvis, C. H. and Stuart, N. (2001). "A comparison among strategies for interpolating maximum and minimum daily air temperatures. Part II: The interaction between number of guiding variables and the type of interpolation method." *Journal of Applied Meteorology*, 40(6), 1075-1084.

Jonkman, S. N. and Penning- Rowsell, E. (2008). "Human Instability in Flood Flows 1." *JAWRA Journal of the American Water Resources Association*, 44(5), 1208-1218.

Jordaan, J. M., and Bell, A. (Eds.). (2009). *Hydraulic Structure, Equipment and Water Data Acquisition Systems*. Eolss Publishers Company Limited.

Kalantari, Z., Nickman, A., Lyon, S. W., Olofsson, B., and Folkeson, L. (2014). "A method for mapping flood hazard along roads." *Journal of Environmental Management*, 133, 69-77.

Kalpakis, K., Gada, D., and Puttagunta, V. (2001). "Distance measures for effective clustering of ARIMA time-series." *Proceedings of the IEEE International Conference on Data Mining*, IEEE, New York, 273–280.

Karabork, M. C., Kahya, E., and Komuscu, A. U. (2007). "Analysis of Turkish precipitation data: Homogeneity and the Southern Oscillation forcings on frequency distributions." *Hydrological Processes: An International Journal*, 21(23), 3203–3210.

Karamage, F., et al. (2017). "Modeling rainfall-runoff response to land use and land cover change in Rwanda (1990–2016)." *Water*, 9(2), 147. doi.org/10.3390/w9020147.

Katz, R. W. (1999). "Extreme value theory for precipitation: sensitivity analysis for climate change." *Advances in Water Resources*, 23(2), 133-139.

Kaufman, L., and Rousseeuw, P. J. (2009). *Finding Groups in Data: An Introduction to Cluster Analysis* (Vol. 344). John Wiley and Sons.

Kendall, M.G., 1975. *Rank Correlation Methods*. Griffin, London.

Kiedrzyńska, E., Kiedrzyński, M., and Zalewski, M. (2015). "Sustainable floodplain management for flood prevention and water quality improvement." *Natural Hazards*, 76(2), 955-977.

Kileshye Onema, J. M., Taigbenu, A. E. and Ndiritu, J. (2012). "Classification and flow prediction in a data-scarce watershed of the equatorial Nile region." *Hydrology and Earth System Sciences*, 16(5), 1435–1443.

Kim, J. W. and Pachepsky, Y. A. (2010). "Reconstructing missing daily precipitation data using regression trees and artificial neural networks for SWAT streamflow simulation." *Journal of Hydrology*, 394(3-4), 305-314.

Kjeldsen, T. R., Smithers, J. C., and Schulze, R. E. (2002). "Regional flood frequency analysis in the KwaZulu-Natal province, South Africa, using the index-flood method." *Journal of Hydrology*, 255(1-4), 194–211.

Klein Tank, A. M. G. and Können, G. P. (2003). "Trends in indices of daily temperature and precipitation extremes in Europe, 1946-99." *Journal of Climate*, 16(22), 3665–3680.

Klok, E. J., and Klein Tank, A. M. G. (2009). Updated and extended European dataset of daily climate observations. *International Journal of Climatology: A Journal of the Royal Meteorological Society*, 29(8), 1182-1191.

Konteatis, C. A. C. (1974). *Dams of Cyprus*. Water Development Department, Ministry of Agriculture and Natural Resources. Nicosia Cyprus.

Koriche, S. A., Rientjes, T., Haile, A. T., and Bekele, S. (2012). *Remote Sensing Based Hydrological Modelling for Flood Early Warning in the Upper and Middle Awash River Basin*. University of Twente Faculty of Geo-Information and Earth Observation (ITC).

Kostopoulou, E. and Jones, P. D. (2007). "Comprehensive analysis of the climate variability in the eastern Mediterranean. Part I: Map-pattern classification." *International Journal of Climatology*, 27(9), 1189–1214.

Kousky, C. and Kunreuther, H. (2014). "Addressing affordability in the national flood insurance program." *Journal of Extreme Events*, 1(01), 1450001.

Kryžanowski, A., Brilly, M., Rusjan, S., and Schnabl, S. (2014). "Structural flood-protection measures referring to several European case studies." *Natural Hazards and Earth System Sciences*, 14(1), 135-142.

Kumar, R., Goel, N. K., Chatterjee, C., and Nayak, P. C. (2015). "Regional flood frequency analysis using soft computing techniques." *Water Resources Management*, 29(6), 1965-1978.

Kunkel, K. E., Easterling, D. R., Hubbard, K., Redmond, K., Andsager, K., Kruk, M. C., and Spinar, M. L. (2005). "Quality control of pre-1948 cooperative observer network data." *Journal of Atmospheric and Oceanic Technology*, 22(11), 1691-1705.

Kysely, J., Gaal, L., Beranova, R., and Plavcova, E., (2011). "Climate change scenarios of precipitation extremes in Central Europe from ENSEMBLES regional climate models." *Theoretical and Applied Climatology*, 104(3–4), 529–542.

Lagasse, P. F., Zevenbergen, L. W., Schall, J. D., and Clopper, P. E. (2001). *Bridge Scour and Stream Instability Countermeasures*. No: FHWA NHI 01-003, U.S. Department of Transportation, Federal Highway Administration, VA, USA.

Landwehr, J. M., Matalas, N. C., and Wallis, J. R. (1979). "Probability weighted moments compared with some traditional techniques in estimating Gumbel parameters and quantiles." *Water Resources Research*, 15(5), 1055–1064.

Lettenmaier, D. P. and Potter, K. W. (1985). "Testing flood frequency estimation methods using a regional flood generation model." *Water Resources Research*, 21(12), 1903-1914.

Leventis, P. (2005). *Twelve Times in Nicosia: Nicosia, Cyprus, 1192-1570: Topography, Architecture and Urban Experience in A Diversified Capital City*. Cyprus Research Centre.

Li, C., Cheng, X., Li, N., Du, X., Yu, Q., and Kan, G. (2016). "A framework for flood risk analysis and benefit assessment of flood control measures in urban areas." *International Journal of Environmental Research and Public Health*, 13(8), 787. doi.org/10.3390/ijerph13080787.

Liao, T. W. (2005). "Clustering of time series data: A survey." *Pattern Recognition*, 38(11), 1857–1874.

Lin, J., Keogh, E., Wei, L., and Lonardi, S. (2007). "Experiencing SAX: A novel symbolic representation of time series." *Data Mining and Knowledge Discovery*, 15(2), 107–144.

Liu, J., Doan, C. D., Liong, S. Y., Sanders, R., Dao, A. T., and Fewtrell, T. (2015). "Regional frequency analysis of extreme rainfall events in Jakarta." *Natural Hazards*, 75(2), 1075-1104.

Lu, J. Y., Hong, J. H., Su, C. C., Wang, C. Y., and Lai, J. S. (2008). "Field measurements and simulation of bridge scour depth variations during floods." *Journal of Hydraulic Engineering*, 134(6), 810-821.

Maidment, D. R., and Morehouse, S. (2002). *Arc Hydro: GIS for Water Resources* (Vol. 1). ESRI, Inc.

Maharaj, E. A. (2000). "Cluster of time series." *Journal of Classification*, 17(2), 297-314.

Malekinezhad, H. and Zare-Garizi, A. (2014). "Regional frequency analysis of daily rainfall extremes using L-moments approach." *Atmósfera*, 27(4), 411-427.

Mann, H. B. (1945). "Nonparametric tests against trend." Econometrica: *Journal of the Econometric Society*, 13(3), 245-259.

Marengo, J. A., Torres, R. R., and Alves, L. M. (2017). "Drought in Northeast Brazil-past, present, and future." *Theoretical and Applied Climatology*, 129(3-4), 1189-1200.

McBean, E. A., Gorrie, J., Fortin, M., Ding, J., and Monlton, R. (1988). "Adjustment factors for flood damage curves." *Journal of Water Resources Planning and Management*, 114(6), 635-646.

McCuen, R.H. 1998. *Hydrologic Analysis and Design*. Prentice-Hall; Englewood Cliffs, NJ.

Meesuk, V., Vojinovic, Z., Mynett, A. E., and Abdullah, A. F. (2015). "Urban flood modelling combining top-view LiDAR data with ground-view SfM observations." *Advances in Water Resources*, 75, 105-117.

Merz, R. and Blöschl, G. (2005). "Flood frequency regionalization: Spatial proximity vs. catchment attributes." *Journal of Hydrology*, 302(1-4), 283-306.

Michaelides, S. C., Tymvios, F. S., and Michaelidou, T. (2009). "Spatial and temporal characteristics of the annual rainfall frequency distribution in Cyprus." *Atmospheric Research*, 94(4), 606-615.

Miller, R. G. (1964). "A trustworthy jackknife." *The Annals of Mathematical Statistics*, 35(4), 1594–1605.

Mishra, S. K. and Singh, V. P. (2013). *Soil Conservation Service Curve Number (SCS-CN) Methodology* (Vol. 42). Springer Science & Business Media.

Mishra, A., Anand, A., Singh, R., and Raghuwanshi, N. S. (2001). "Hydraulic modeling of Kangsabati main canal for performance assessment." *Journal of Irrigation and Drainage Engineering*, 127(1), 27-34.

Mitsa, T. (2010). *Temporal Data Mining*, Chapman and Hall, Boca Raton, FL.

Montero, P. and Vilar, J. (2014). "TSclust: An R package for time series clustering." *Journal of Statistical Software*, 62(1), 1-43.

Nandalal, K. D. W. (2009). "Use of a hydrodynamic model to forecast floods of Kalu River in Sri Lanka." *Journal of Flood Risk Management*, 2(3), 151-158.

Ngo, L., Madsen, H., and Rosbjerg, D. (2007). "Simulation and optimisation modelling approach for operation of the Hoa Binh reservoir, Vietnam." *Journal of Hydrology*, 336(3-4), 269-281.

Ngongondo, C. S., Xu, C. Y., Tallaksen, L. M., Alemaw, B., and Chirwa, T. (2011). "Regional frequency analysis of rainfall extremes in Southern Malawi using the index rainfall and L-moments approaches." *Stochastic Environmental Research and Risk Assessment*, 25(7), 939-955.

Nikolakis, D. (2008). "A statistical study of precipitation in Cyprus." *Hellenic Journal of Geosciences*, 43, 67-74.

Nied, M., Hundecha, Y., and Merz, B. (2013). "Flood-initiating catchment conditions: a spatio-temporal analysis of large-scale soil moisture patterns in the Elbe River basin." *Hydrology and Earth System Sciences*, 17(4), 1401-1414. doi.org/10.5194/hess-17-1401-2013.

O'Callaghan, J. F. and Mark, D. M. (1984). "The extraction of drainage networks from digital elevation data." *Computer Vision, Graphics, and Image Processing*, 28(3), 323-344.

Ouarda, T. B. M. J., et al. (2008). "Intercomparison of regional flood frequency estimation methods at ungauged sites for a Mexican case study." *Journal of Hydrology*, 348(1-2), 40-58.

Oudin, L., Kay, A., Andréassian, V., and Perrin, C. (2010). "Are seemingly physically similar catchments truly hydrologically similar?" *Water Resources Research*, 46(11). W11558. Doi: 10.1029/2009WR008887.

Panda, D. K., Panigrahi, P., Mohanty, S., Mohanty, R. K., and Sethi, R. R. (2016). "The 20th century transitions in basic and extreme monsoon rainfall indices in India: Comparison of the ETCCDI indices." *Atmospheric Research*, 181, 220-235.

Paparrizos, S. and Maris, F. (2017). "Hydrological simulation of Sperchios River basin in Central Greece using the MIKE SHE model and geographic information systems." *Applied Water Science*, 7(2), 591-599.

Pappenberger, F., Beven, K., Frodsham, K., Romanowicz, R., and Matgen, P. (2007). "Grasping the unavoidable subjectivity in calibration of flood inundation models: A vulnerability weighted approach." *Journal of Hydrology*, 333(2-4), 275-287.

Pappenberger, F., Matgen, P., Beven, K. J., Henry, J. B., and Pfister, L. (2006). "Influence of uncertain boundary conditions and model structure on flood inundation predictions." *Advances in Water Resources*, 29(10), 1430-1449.

Patel, D. P., Ramirez, J. A., Srivastava, P. K., Bray, M., and Han, D. (2017). "Assessment of flood inundation mapping of Surat city by coupled 1D/2D hydrodynamic modeling: a case application of the new HEC-RAS 5." *Natural Hazards*, 89(1), 93-130.

Patro, S., Chatterjee, C., Mohanty, S., Singh, R., and Raghuwanshi, N. S. (2009). "Flood inundation modeling using MIKE FLOOD and remote sensing data." *Journal of the Indian Society of Remote Sensing*, 37(1), 107-118.

Paulhus, J. L. and Kohler, M. A. (1952). "Interpolation of missing precipitation records." *Monthly Weather Review*, 80(8), 129–133.

Pechlivanidis, I. G., et al. (2017). "Analysis of hydrological extremes at different hydro-climatic regimes under present and future conditions." *Climatic Change*, 141(3), 467-481.

Peterson, T. C., et al. (1998). "Homogeneity adjustments of in situ atmospheric climate data: a review." *International Journal of Climatology: A Journal of the Royal Meteorological Society*, 18(13), 1493-1517.

Pettitt, A. N. (1979). "A non-parametric approach to the change-point problem." *Applied Statistics*, 28(2), 126-135.

Phillips, B.C, Tilley, J.R. Yu, S. and de Silva, N. (2005) "Review of Flooding in Prospect Creek, Fairfield", Proceedings, 45th Floodplain Management Authorities Conference, 22-25 February, Narooma.

Piccolo, D. (1990). “A distance measure for classifying ARIMA models.” *Journal of Time Series Analysis*, 11(2), 153–164.

Pinto, J. G., Ulbrich, U., and Speth, P. (1999). “The variability of cyclonic activity in the Mediterranean area in the last 40 years and its impact on precipitation.” *Proceedings of the 1st EGS Plinius Conference*, Bios Publisher, Cosenza, Italy, 29–40.

Potter, K. W. and Faulkner, E. B. (1987). “Catchment response time as a predictor of flood quantiles 1.” *JAWRA Journal of the American Water Resources Association*, 23(5), 857-861.

Prinzio, M. D., Castellarin, A., and Toth, E. (2011). “Data-driven catchment classification: Application to the pub problem.” *Hydrology and Earth System Sciences*, 15(6), 1921–1935.

Prosdocimi, I., Kjeldsen, T. R., and Miller, J. D. (2015). “Detection and attribution of urbanization effect on flood extremes using nonstationary flood- frequency models.” *Water Resources Research*, 51(6), 4244-4262. Doi: 10.1002/2015WR017065.

Quattrochi, D. A., Wentz, E., Lam, N. S. N., and Emerson, C. W. (2017). *Integrating Scale in Remote Sensing and GIS*. CRC Press.

Quirogaa, V. M., Kurea, S., Udoa, K., and Manoa, A. (2016). “Application of 2D numerical simulation for the analysis of the February 2014 Bolivian Amazonia flood: Application of the new HEC-RAS version 5.” *Ribagua*, 3(1), 25-33.

Rahman, M. H., Matin, M. A., and Salma, U. (2017). “Analysis of precipitation data in Bangladesh through hierarchical clustering and multidimensional scaling.” *Theoretical and Applied Climatology*, 1-17.

Rasekh, A., Afshar, A., and Afshar, M. H. (2010). “Risk-cost optimization of hydraulic structures: methodology and case study.” *Water Resources Management*, 24(11), 2833-2851.

Reek, T., Doty, S. R., and Owen, T.W. (1992). “A deterministic approach to the validation of historical daily temperature and precipitation data from the cooperative network.” *Bulletin of the American Meteorological Society*, 73(6), 753–765.

Renard, B. and Lang, M. (2007). “Use of a Gaussian copula for multivariate extreme value analysis: some case studies in hydrology.” *Advances in Water Resources*, 30(4), 897-912.

Ribeiro, S., Caineta, J., and Costa, A. C. (2016). "Review and discussion of homogenisation methods for climate data." *Physics and Chemistry of the Earth*, 94, 167–179.

Rossman, L. A. (2010). *Storm Water Management Model User's Manual, Version 5.0*. Cincinnati: National Risk Management Research Laboratory, Office of Research and Development, US Environmental Protection Agency.

Rouillard, J. J., Ball, T., Heal, K. V., and Reeves, A. D. (2015). "Policy implementation of catchment-scale flood risk management: learning from Scotland and England." *Environmental Science and Policy*, 50, 155-165.

Sadeghi, S. H. R., Jalili, K., and Nikkami, D. (2009). "Land use optimization in watershed scale." *Land Use Policy*, 26(2), 186-193.

Sahin, E., Akintug, B., and Yanmaz, A. M. (2013). "Modeling of Morphou (Guzelyurt) flood and remedial measures." *Teknik Dergi*, 24(3), 6447-6462.

Salas, J. D. (1980). *Applied Modeling of Hydrologic Time Series*. Water Resources Publication.

Sambridge, M., Braun, J., and McQueen, H. (1995). "Geophysical parametrization and interpolation of irregular data using natural neighbours." *Geophysical Journal International*, 122(3), 837-857.

Sampath, D. S., Weerakoon, S. B., and Herath, S. (2015). "HEC-HMS model for runoff simulation in a tropical catchment with intra-basin diversions-case study of the Deduru Oya river basin, Sri Lanka." *Engineer: Journal of the Institution of Engineers, Sri Lanka*, 48(1), 1-9.

Santos, E. B., Lucio, P. S., and Santos, C. M. (2015). "Precipitation regionalization of the Brazilian Amazon." *Atmospheric Science Letters*, 16(3), 185-192.

Satyanarayana, P. and Srinivas, V. V. (2008). "Regional frequency analysis of precipitation using large- scale atmospheric variables." *Journal of Geophysical Research: Atmospheres*, 113, D24110. Doi: 10.1029/2008JD010412.

Savvidou, K., Nicolaides, K. A., Michaelides, S. C., Orphanou, A., Charalambous, M., and Adamou, S. (2008). "A study of the flood events in Cyprus." *Advances in Science and Research*, 2(1), 127-131.

Schick, A. P., Grodek, T., and Lekach, J. (1997). “Sediment management and flood protection of desert towns: effects of small catchments.” *IAHS Publications-Series of Proceedings and Reports-Intern Assoc Hydrological Sciences*, 245, 183-190.

Schubert, J. E. and Sanders, B. F. (2012). “Building treatments for urban flood inundation models and implications for predictive skill and modeling efficiency.” *Advances in Water Resources*, 41, 49-64.

SCS (1972). *National Engineering Handbook, Section 4*. Hydrology, Soil Conservation Service, USDA, U.S. Dept. of Agriculture, Washington

SCS (1986). *Urban Hydrology for Small Watersheds*, USDA.

Sen, P. K. (1968). “Estimates of the regression coefficient based on Kendall's tau.” *Journal of the American Statistical Association*, 63(324), 1379-1389.

Seo, D. J., Krajewski W. F. and Bowles D. S. (1990). “Stochastic interpolation of rainfall data from rain gages and radar using cokriging: 1. Design of experiments.” *Water Resources Research*, 26(3), 469-477.

SEPA (2016) *Natural Flood Management Handbook*. Stirling: Scottish Environment Protection Agency (SEPA).

Sequeiros, O. E., Cantero, M. I., and Garcia, M. H. (2009). “Sediment management by jets and turbidity currents with application to a reservoir for flood and pollution control in Chicago, Illinois.” *Journal of Hydraulic Research*, 47(3), 340-348.

Seyhun, R., and Akintug, B. (2013). “Trend analysis of rainfall in North Cyprus.” *Causes, impacts and solutions to global warming*, I. Dincer, C. O. Colpan, and F. Kadioglu, eds., Springer, New York, 169–181.

Shafer, M. A., Fiebrich, C. A., Arndt, D. S., Fredrickson, S. E., and Hughes, T. W. (2000). “Quality assurance procedures in the Oklahoma Mesonetwork.” *Journal of Atmospheric and Oceanic Technology*, 17(4), 474–494.

Shames, I. H. *Mechanics of Fluids*, (2003). McGraw-Hill, New York, NY, USA.

Shao, J., and Tu, D. (1995). *The Jackknife and Bootstrap*, Springer, New York.

Sibson, R. (1981) *A Brief Description of Natural Neighbour Interpolation*. *In: Interpreting Multivariate Data*, John Wiley and Sons, Ltd, Chichester, 21-36.

Singh, P., Sinha, V. S. P., Vijhani, A., and Pahuja, N. (2018). "Vulnerability assessment of urban road network from urban flood." *International Journal of Disaster Risk Reduction*, 28, 237-250.

Singh, R. D. and S. M. Seth. (1984). Comparison of Unit Hydrograph, CS 7, Technical Report, National Institute of Hydrology.

Sivakumar, B. and Singh, V. P. (2012). "Hydrologic system complexity and nonlinear dynamic concepts for a catchment classification framework." *Hydrology and Earth System Sciences*, 16(11), 4119-4131.

Sivapalan, M., Takeuchi, K., Franks, S. W., Gupta, V. K., Karambiri, H., Lakshmi, V., ... and Oki, T. (2003). "IAHS Decade on predictions in ungauged basins (PUB), 2003-2012: shaping an exciting future for the hydrological sciences." *Hydrological Sciences Journal*, 48(6), 857-880.

Smith, L. C., Turcotte, D. L., and Isacks, B. L. (1998). "Stream flow characterization and feature detection using a discrete wavelet transform." *Hydrological Processes*, 12(2), 233-249.

Smith, L. M. and Winkley, B. R. (1996). "The response of the Lower Mississippi River to river engineering." *Engineering Geology*, 45(1-4), 433-455.

Srikanthan, R. and MacMahon, T. A. (1981). "Log pearson type 3 distribution effect of dependence, distribution parameters and sample size on peak annual flood estimates." *Journal of Hydrology*, 52(1), 149-159.

Stedinger, J. R. (1983). "Estimating a regional flood frequency distribution." *Water Resources Research*, 19(2), 503-510.

Suhaila, J., Sayang, M. D., and Jemain, A. A. (2008). "Revised spatial weighting methods for estimation of missing rainfall data." *Asia-Pacific Journal of Atmospheric Sciences*, 44(2), 93–104.

Syme, W. J., Pinnell, M. G., and Wicks, J. M. (2004). "Modelling flood inundation of urban areas in the UK using 2D/1D hydraulic models." *Proceedings of the 8th National Conference on Hydraulics in Water Engineering*, the Institution of Engineers, Australia.

Şahin, E. A Study on Flood Management Practices for Güzelyurt, (MSc Thesis), Department of Civil Engineering, METU, Ankara, 2012.

Tang, W. Y., Kassim, A. H. M., and Abubakar, S. H. (1996). "Comparative studies of various missing data treatment methods-Malaysian experience." *Atmospheric Research*, 42(1-4), 247–262.

Tarekegn, T. H., Haile, A. T., Rientjes, T., Reggiani, P., and Alkema, D. (2010). "Assessment of an ASTER-generated DEM for 2D hydrodynamic flood modeling." *International Journal of Applied Earth Observation and Geoinformation*, 12(6), 457-465.

Tariq, M. A. U. R. and Van de Giesen, N. (2012). "Floods and flood management in Pakistan." *Physics and Chemistry of the Earth*, 47, 11-20.

Tayanç, M., Dalfes, H. N., Karaca, M., and Yenigun, O. (1998). "A comparative assessment of different methods for detecting inhomogeneities in a Turkish temperature data set." *International Journal of Climatology*, 18(5), 561–578.

Tayefi, V., Lane, S.N., Hardy, R.J., and Yu, D. (2007). "A comparison of one and two dimensional approaches to modelling flood inundation over complex upland floodplains." *Hydrological Processes*, 21(23), 3190-3202.

Teegavarapu, R. S. (2012). *Floods in a Changing Climate: Extreme Precipitation*. Cambridge University Press.

Teegavarapu, R. S. V. and Chandramouli, V. (2005). "Improved weighting methods, deterministic and stochastic data-driven models for estimation of missing precipitation records." *Journal of Hydrology*, 312(1-4), 191–206.

Teng, J., Jakeman, A. J., Vaze, J., Croke, B. F., Dutta, D., and Kim, S. (2017). "Flood inundation modelling: A review of methods, recent advances and uncertainty analysis." *Environmental Modelling and Software*, 90, 201-216.

Tennakoon, K. B. M. (2004). Parameterisation of 2D hydrodynamic models and flood hazard mapping for Naga city, Philippines. Itc.

Thielen, J., Bartholmes, J., Ramos, M. H., and Roo, A. D. (2009). "The European flood alert system–part 1: concept and development." *Hydrology and Earth System Sciences*, 13(2), 125-140.

Timbadiya, P. V., Patel, P. L., and Porey, P. D. (2014). "A 1D–2D coupled hydrodynamic model for river flood prediction in a coastal urban floodplain." *Journal of Hydrologic Engineering*, 20(2), 05014017, 1-18.

Tollan, A. (2002). "Land-use change and floods: what do we need most, research or management?" *Water Science and Technology*, 45(8), 183-190.

Ulke, A., Tayfur, G., and Ozkul, S. (2009). "Predicting suspended sediment loads and missing data for Gediz River, Turkey." *Journal of Hydrologic Engineering*, 14(9), 954-965.

Um, M. J., Kim, Y., Markus, M., and Wuebbles, D. J. (2017). "Modeling nonstationary extreme value distributions with nonlinear functions: an application using multiple precipitation projections for US cities." *Journal of Hydrology*, 552, 396-406.

USACE (U.S. Army Corps of Engineers), 2000. Hydrologic Modeling System. HEC-HMS Technical Reference Manual, CPD-74B, Hydrologic Engineering Center, Davis, California.

Vaze, J., Teng, J., and Spencer, G. (2010). "Impact of DEM accuracy and resolution on topographic indices." *Environmental Modelling and Software*, 25(10), 1086-1098.

Vaze, J., et al. (2013). In: Proceedings of the 20th International Congress on Modelling and Simulation (MODSIM2013). The Australian Water Resource Assessment System (AWRA), Adelaide, Australia.

Vaze, J., et al. (2013). "The Australian Water Resource Assessment Modelling System (AWRA)." *Proceedings of 20th International Congress on Modelling and Simulation*, Adelaide, Australia.

Vicente-Serrano, S. M., Beguería, S., López-Moreno, J. I., García-Vera, M. A., and Stepanek, P. (2010). "A complete daily precipitation database for northeast Spain: Reconstruction, quality control, and homogeneity." *International Journal of Climatology*, 30(8), 1146–1163.

Vincent, L. A. and Mekis, E. (2006). "Changes in daily and extreme temperature and precipitation indices for Canada over the twentieth century." *Atmosphere-Ocean*, 44(2), 177-193.

Visser, H., Petersen, A. C., and Ligtvoet, W. (2014). "On the relation between weather-related disaster impacts, vulnerability and climate change." *Climatic Change*, 125(3-4), 461-477.

Vojinovic, Z., et al. (2016). "Holistic approach to flood risk assessment in areas with cultural heritage: a practical application in Ayutthaya, Thailand." *Natural Hazards*, 81(1), 589-616.

Von Neumann, J. (1941). "Distribution of the ratio of the mean square successive difference to the variance." *The Annals of Mathematical Statistics*, 12(4), 367–395.

Von Storch, H., and Navarra, A. (1995). *Analysis of Climate Variability - Applications of Statistical Techniques*. Springer-Verlag, New York.

Wallis, J. R., Lettenmaier, D. L., and Wood, E. F. (1991). "Daily hydroclimatological data set for the continental United States." *Water Resources Research*, 27(7), 1657–1663.

Wang, X., Smith, K. and Hyndman, R. (2006). "Characteristic-based clustering for time series data." *Data mining and knowledge Discovery*, 13(3), 335-364.

Wang HJ, Chen YN, Xun S, Lai DM, Fan YT, Li Z (2013) Changes in daily climate extremes in the arid area of northwestern China. *Theoritical Applied Climatology*, 112:15–28

Wang, Z., Zeng, Z., Lai, C., Lin, W., Wu, X., and Chen, X. (2017). "A regional frequency analysis of precipitation extremes in Mainland China with fuzzy c-means and L- moments approaches." *International Journal of Climatology*, 37(S1), 429-444.

Ward, J. H. (1963). "Hierarchical groupings to optimize an objective function." *Journal of the American Statistical Association*, 58(301), 236–244.

Watson, D.F., 1992. *Contouring: A Guide to the Analysis and Display of Spatial Data*, Pergamon Press, London.

Waylen, K. A., Holstead, K. L., Colley, K., and Hopkins, J. (2018). "Challenges to enabling and implementing Natural Flood Management in Scotland." *Journal of Flood Risk Management*, 11, S1078-S1089.

Wazneh, H., Chebana, F., and Ouarda, T. B. M. J. (2015). "Delineation of homogeneous regions for regional frequency analysis using statistical depth function." *Journal of Hydrology*, 521, 232–244.

WBM Oceanics (2003) "TUFLOW (and ESTRY) User Manual - GIS Based 2D/1D Hydrodynamic Modelling", User Manual, Brisbane.

Wijngaard, J. B., Klein Tank, A. M. G., and Können, G. P. (2003). "Homogeneity of 20th century European daily temperature and precipitation series." *International Journal of Climatology*, 23(6), 679–692.

Wise, S., (1998), *The Effect of GIS Interpolation Errors on the Use of Digital Elevation Models in Geomorphology, In: Landform Monitoring, Modelling and Analysis*, Edited by S. N. Lane, K. S. Richards and J. H. Chandler, John Wiley and Sons.

WL (2005) *SOBEK – Reference Manual*. Delft Hydraulics, Netherlands.

World Meteorological Organization World Weather/Climate Extremes Archive. (2017). "World weather and climate extremes archive." ⟨https://wmo.asu.edu/⟩ (Feb. 26, 2017).

Yang, T., et al. (2010). "Regional frequency analysis and spatio-temporal pattern characterization of rainfall extremes in the Pearl River Basin, China." *Journal of Hydrology*, 380(3), 386–405.

Yanmaz, A. M. (2002). *Köprü Hidroliği*. ODTÜ Geliştirme Vakfı Yayıncılık.

Yanmaz, A. M. (2018). *Applied Water Resources Engineering*. 5th Edition, Ankara: METU Press.

Yazdi, J., and Neyshabouri, S. S. (2012). Optimal design of flood-control multi-reservoir system on a watershed scale. *Natural Hazards*, 63(2), 629-646.

Yoon, T. H. and Kang, S. K. (2004). "Finite volume model for two-dimensional shallow water flows on unstructured grids." *Journal of Hydraulic Engineering*, 130(7):678–688. Doi: 10.1061/(ASCE)0733-9429(2004)130:7(678).

Zaifoğlu, H. and Akıntuğ, B. (2016): "Remedial Measures for Flood Problems of Nicosia Industrial Area, North Cyprus." *12th International Water Advances in Civil Engineering Conference*, September 21-23, 2016 Istanbul, Turkey.

Zhang, X., et al. (2005). "Trends in Middle East climate extreme indices from 1950 to 2003." *Journal of Geophysical Research: Atmospheres*, 110(D22).

Zhang, H., Ho, T. B., Zhang, Y., and Lin, M. S. (2006). "Unsupervised feature extraction for time series clustering using orthogonal wavelet transform." *Informatica*, 30(3), 305–319.

Zhao, G., Zhai, J., Tian, P., Zhang, L., Mu, X., An, Z., and Han, M. (2018). "Variations in extreme precipitation on the Loess Plateau using a high-resolution dataset and their linkages with atmospheric circulation indices." *Theoretical and Applied Climatology*, 133(3-4), 1235-1247.

CURRICULUM VITAE

PERSONAL INFORMATION

Surname, Name: Zaifoğlu, Hasan
Nationality: Turkish Cypriot
Date and Place of Birth: 13 October 1989, Gazimağusa
Marital Status: Married
Phone: +90 392 661 29 97
Fax: +90 392 661 29 97
Email: zaifogluhasan@hotmail.com

EDUCATION

Degree	Institution	Year of Graduation
PHD	METU Civil Engineering	2018
MS	ITU Hydraulics and Water Resources Engineering	2013
BS	ITU Civil Engineering	2011
High School	Güzelyurt Türk Maarif College, Kıbrıs	2006

WORK EXPERIENCE

Year	Place	Enrollment
2013-2018	Middle East Technical University Northern Cyprus Campus	Teaching Assistant

FOREIGN LANGUAGES

English

PUBLICATIONS

Journal Papers

Zaifoğlu, H., Akıntuğ, B., and Yanmaz, A. M. (2018): "Regional Frequency Analysis of Precipitation Using Time Series Clustering Approaches." *Journal of Hydrologic Engineering*, 23(6), 5584.0001659.

Zaifoğlu, H., Akıntuğ, B., and Yanmaz, A. M. (2017): "Quality Control, Homogeneity, and Trends of Extreme Precipitation Indices in Northern Cyprus." *Journal of Hydrologic Engineering*, 22(12), 05017024.

Conference Papers

Zaifoğlu, H., Akıntuğ, B., and Yanmaz, A. M. (2018): Assessment of Bostanci flood by integrated 1D/2D modelling. *The 5th IAHR Europe Congress*, June 12-14, 2018, Trento, Italy.

Zaifoğlu, H., Akıntuğ, B., and Yanmaz, A. M. (2018): Trend Analysis of Extreme Precipitation Indices for Northern Cyprus. *The 5th IAHR Europe Congress*, June 12-14, 2018, Trento, Italy.

Zaifoğlu, H., Akıntuğ, B., and Yanmaz, A. M. (2018): Quality and Homogeneity Analysis of Precipitation Data in North Cyprus. *13th International Water Advances in Civil Engineering Conference*, September 12-14, 2018 Çeşme-İzmir, Turkey.

Zaifoğlu, H. and Akıntuğ, B. (2016): Remedial Measures for Flood Problems of Nicosia Industrial Area, North Cyprus. *12th International Water Advances in Civil Engineering Conference*, September 21-23, 2016 Istanbul, Turkey. (Full Text)

Zaifoglu, H. and Aksoy, H. (2013): Baseflow Index for Hydrological Watersheds in Eastern Part of Turkey. *International Water Association 5th Eastern European Young and Senior Water Professionals Conference*, June 26-28, 2013 Kiev, Ukraine.

Zaifoglu, H. ve Aksoy, H. (2013): Fırat Havzası için Taban Akışı Tahminleri. *VII. Ulusal Hidroloji Kongresi*, 26-27 Eylül 2013 Isparta, Türkiye.

HOBBIES

Reading, Politics, Football, Cinema, Trekking, Travel